WAVELET ANALYSIS AND DETERMINATION OF THE OPTIMUM PROBABILITY DISTRIBUTION OF HYDROMETEOROLOGICAL TIME SERIES FOR NYANDO RIVER BASIN

BY

JOHN ODONGO SARANGA

A THESIS SUBMITTED TO THE SCHOOL OF ENGINEERING IN PARTIAL FULFILMENT OF THE REQUIREMENTS FOR THE AWARD OF THE DEGREE OF MASTER OF SCIENCE IN WATER ENGINEERING

DEPARTMENT OF CIVIL AND STRUCTURAL ENGINEERING

MOI UNIVERSITY

2022

DECLARATION

Student Declaration

This thesis is my original work and has not been presented for a degree in any other university. No part of this thesis may be reproduced without written permission of the author and/ or Moi University

John Odongo Saranga — November 17, 2022
EC/PGCS/08/11 — Date

Declaration by the Supervisors

This thesis has been submitted for examination with our approval as University Supervisors.

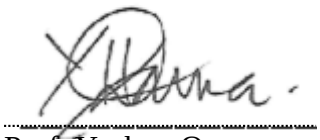

November 21, 2022
Prof. Yashon Ouma — Date
Department of Civil & Structural Engineering
Moi University, Eldoret, Kenya

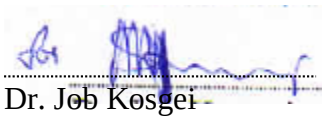

November 21, 2022
Dr. Job Kosgei — Date
Department of Civil & Structural Engineering
Moi University, Eldoret, Kenya

DEDICATION

This research is dedicated to my work colleagues, parents, children, relatives, and friends for encouragement and making steps towards advancing in higher education. Their continuous encouragement, moral and financial support saw me through my academic experience. My late mother, Damaris Awino, and the late father, Haningtone Saranga inspired my life to this outstanding achievement; God bless their work.

ACKNOWLEDGEMENTS

I wish to acknowledge God, the Almighty, for His immense blessings, strength, and endurance that He granted me in the course of my research. All honour and Glory be to Him. My sincere gratitude and appreciation go to my supervisors: Prof. Ouma Yashon and the late Dr. Job Kosgei for their dedication in guiding me to understand this thesis's detailed requirements. God bless them abundantly. I shall forever be grateful to them.

I lastly wish to acknowledge the support and encouragement that I received from my friend Edwin Okama, my work colleague, Eng. Isaac Ngugi and my family members, classmates, and friends. I highly appreciate.

ABSTRACT

Perturbations in hydrologic time series have recently been witnessed in many parts of the world and knowledge of their occurrence is of great socio-economic significance. Various statistical techniques have been used in the past to analyse hydro-climatic series without revealing important frequency information. The main objective of this study was to analyse the trend, periodicity and frequency of the hydrometeorological time series for Nyando River basin. The specific objectives were to: determine trends investigate periodicity and determine the optimum probability distribution in rainfall and streamflow time series. Rainfall data of lengths ranging from of 41 - 100 years were obtained from Water Resources Authority, Kenya Meteorological Department and Finlay Kenya Limited. Streamflow data of lengths ranging from 45 – 60 years were obtained from Water Resources Authority. The datasets were first tested for homogeneity, normality and independence. This study used Wavelet Transform (WT) method in addition to Mann-Kendall (M-K) and Fourier Transform (FT) to investigate the rainfall and streamflow trend and periodicity in the basin. In trend detection, M-K computed the z-statistical values and declared trend or no trend at 95% confidence interval, while WT detected the peaks and disclosed the time-frequency information for the trends. Further, FT and WT techniques were used to estimate the power spectrum and to reveal the periodicities. To obtain the probability distributions, L-moment diagrams were generated to compare the L-skewness verses L-kurtosis relations of different distributions. The closest relationships were further confirmed using goodness-of-fit tests. The M-K results revealed minimal trend in rainfall but showed an overall increasing trend in streamflow. WT revealed overall increasing trends for both rainfall and streamflow. The dominant rainfall and streamflow periodicities were determined at 2-7 years, 2.7-3.3 years, 3.5-4 years, 5.6-6.5 years and 7-8 years. Based on the results, this study concluded that the Nyando River basin rainfall and streamflow exhibited increasing trends with periodic cycles over the last thirty years. Further, the study found that PE3 provides good approximation to the annual maximum floods in the basin. The study recommends that PE3 could be adopted for estimating the return periods of floods in the design of hydraulic structures for the Nyando River basin. Similar studies can be applied in other River basins in Kenya to determine the optimal probability distributions for the analysis of extreme rainfall and streamflow.

TABLE OF CONTENTS

DECLARATION ii
DEDICATION iii
ACKNOWLEDGEMENTS iv
ABSTRACT v
TABLE OF CONTENTS vi
LIST OF TABLES x
LIST OF FIGURES xi
ACRONYMS xiii
CHAPTER ONE 1
BACKGROUND OF THE STUDY 1
1.1 Introduction 1
1.2 Problem Statement 2
1.3 Justification of the Study 3
1.4 Study Objectives 4
1.5 Study Area 5
1.5.1 Location 5
1.5.2 Hydrology 5
1.5.3 Climate 5
1.5.4 Geology and soils 6
1.5.5 Land Use 7
1.5.6 Landforms 7
CHAPTER TWO 8
LITERATURE REVIEW 8
2.1 Introduction 8
2.2 Rainfall Seasons in Kenya 8
2.3 Trend Analysis 9
2.4 Periodicity Detection 11
2.4.1 Fourier Transform in Spectral Analysis 11
2.4.2 Wavelet-based Periodicity Detection 12
2.5 Flood Frequency Analysis using L-moments 14
2.6 Conclusion 15

CHAPTER THREE 17
MATERIALS AND METHODS 17
3.1 Introduction 17
3.2 Data 17
3.3 Methodology 19
3.3.1 Watershed delineation 20
3.3.2 Data Quality Analysis 21
3.3.3 Trend analysis 25
3.3.4 Periodicity analysis of rainfall and streamflow 29
3.3.5 Regional frequency analysis 36
3.4 Summary of Methodology 42
CHAPTER FOUR 43
RESULTS AND DISCUSSIONS 43
4.1 Introduction 43
4.2 Rainfall and streamflow data quality analysis 43
4.2.1 Percentage missing data 43
4.2.2 Rainfall and streamflow data characteristics 43
4.2.3 Results of homogeneity tests 45
4.2.4 Results of normality tests 51
4.2.5 Results of independence tests 58
4.2.6 Summarized results of the data quality analysis 59
4.3 Results of trend analysis 60
4.3.1 Results of Mann-Kendall trend analysis 60
4.3.2 Results of trend analysis using Wavelet transform 70
4.4 Results of periodicity analysis 81
4.4.1 Results of periodicity analysis using spectral technique 81
4.4.2 Results of periodicity analysis using wavelet transform 87
4.5 Comparative Evaluation of Wavelet and Conventional Methods 108
4.6 Results of frequency analysis 109
4.6.1 Discordancy measure (Di) 109
4.6.2 Results of heterogeneity measure (H) 110
4.6.3 Results of cluster analysis 111
4.6.4 Results of distribution selection 114
4.6.5 Results of Goodness-of-fit tests 121

4.6.6 Regional growth curves 122
CHAPTER FIVE 128
CONCLUSIONS AND RECOMMENDATIONS 128
5.1 Conclusions 128
5.2 Recommendations 130
REFERENCES 131
APPENDICES 135
Appendix 1: Simplified Flow Chart for Catchment Delineation 135
Appendix 2: Catchment Delineation 136
Appendix 2A: Digital Elevation Model for Nyando River basin area. 136
Appendix 2B: Flow direction map for Nyando River basin. 136
Appendix 2C: Flow accumulation map for Nyando River basin. 137
Appendix 2D: Strahler stream network for Nyando River basin. 137
Appendix 3A-Rainfall Homogeneity Test Results for Rainfall 138
Appendix 3B- Homogeneity Test Results for Streamflow. 139
Appendix 4: Change point Test Results 141
Appendix 4A: Change point test results for rainfall 141
Appendix 4B: Change point test results for streamflow 147
Appendix 5A: Normality Test Results 157
Appendix 5B: Rainfall normality test results 157
Appendix 5B: Streamflow normality test results 162
Appendix 6A: M-K Results for split rainfall series 166
Appendix 6B: M-K Results for split streamflow series 175
Appendix 7A: Wavelet trend results for rainfall 183
Appendix 7B-Wavelet trend results for streamflow 193
Appendix 8A: Rainfall Spectral Analysis Results 202
Appendix 8B: Streamflow spectral analysis results (periodograms) 204
Appendix 9A: Wavelet rainfall periodicity results 206
Appendix 9B: Streamflow wavelet spectral results 212
Appendix 9C: Cross wavelet results 216
Appendix 9D: Wavelet Coherence 222
Appendix 10A: Rainfall annual maximum series 225
Appendix 10B: Streamflow annual maximum series 226
Appendix 11A: Rainfall growth curves 227

Appendix 11B: Streamflow growth curves 228
Appendix 12: Plagiarism checker certificate.....229

LIST OF TABLES

Table 3.1: Details of the rainfall gauging stations 18
Table 3.2: Details of the streamflow gauging stations 18
Table 3.3: Rainfall time series grouped data 27
Table 3.4: Streamflow time series grouped data 27
Table 4.1: Nyando Annual Rainfall characteristics 44
Table 4.2: Nyando Annual Streamflow characteristics 45
Table 4.3: Rainfall change point results 48
Table 4.4: Streamflow change point results 50
Table 4.5: Results of streamflow independence tests 59
Table 4.6: Z-statistics for MAM sub-series rainfall trend analysis 62
Table 4.7: Z-Statistics for MAM sub-series rainfall trend analysis 63
Table 4.8: Z-statistics for MAM streamflow sub-series trend analysis 67
Table 4.9: Z-statistics for streamflow complete series trend analysis 67
Table 4.10: Summary of rainfall wavelet trend test results 72
Table 4.11: Summary of streamflow wavelet trend test results 76
Table 4.12: Summary results of rainfall spectral analysis 84
Table 4.13: Results of spectral analysis for streamflow 87
Table 4.14: Results of rainfall periodicity analysis using wavelet transform 94
Table 4.15: Results of Streamflow periodicity analysis using wavelet transform 99
Table 4.16: L-Moments and Discordancy values for rainfall stations 110
Table 4.17: L-moments and Discordancy values for streamflow stations 110
Table 4.18: Summary of clusters for Rainfall stations 112
Table 4.19: Summary of cluster for streamflow within Nyando 112
Table 4.20: Goodness -of- fit measure for rainfall distributions 121
Table 4.21: Goodness -of- fit measure for different streamflow 122
Table 4.22: Extreme rainfall events in clusters I and III 124
Table 4.23: Extreme rainfall events in clusters II 124
Table 4.24: Extreme streamflow events in cluster I 126
Table 4.25: Extreme streamflow events II 126
Table 4.26: Extreme streamflow events III 126
Table 4.27: Extreme streamflow events in cluster IV 126

LIST OF FIGURES

Figure 3.1: Summarized Flow Chart on Methodology. 19
Figure 4.1: (b) Homogeneity plots for JJA rainfall.....46
Figure 4.1: (c) Homogeneity plots for OND rainfall. 46
Figure 4.2: (a) Homogeneity plots for MAM streamflow. 49
Figure 4.2: (b) Homogeneity plots for JJA streamflow. 49
Figure 4.2 (c): Homogeneity plots for OND streamflow.....49
Figure 4.3: Normality plot for statistical *p*-values in rainfall. 52
Figure 4.4: (a) Normality plot for MAM rainfall at Finlay.....52
Figure 4.4: (b) Normality plot for JJA rainfall at Finlay. 53
Figure 4.4: (c) Normality plot for OND rainfall at Finlay. 53
Figure 4.5: (a) Normality plot for MAM & OND statistical *p*-values in streamflow..54
Figure 4.5: (b) Normality plot for JJA statistical *p*-values in streamflow. 55
Figure 4.6: (a) Normality plot for MAM streamflow at Nyando station. 56
Figure 4.6: (b) Normality plot for JJA streamflow at Nyando station. 56
Figure 4.7: Independence plots for streamflow. 58
Figure 4.8: (a) Mean MAM rainfall variability at Finlay station. 64
Figure 4.8: (b) Mean JJA rainfall variability at Finlay station. 64
Figure 4.8: (c) Mean OND rainfall variability at Finlay station. 65
Figure 4.9 (a): MAM Mean streamflow variability for Ainamotua.....68
Figure 4.9: (b) JJA Mean streamflow variability for Ainamotua. 68
Figure 4.9: (c) OND Mean streamflow variability for Ainamotua. 69
Figure 4.10: (a) Wavelet--based mean rainfall variability in MAM at Finlay.....73
Figure 4.10(b): Wavelet-based mean rainfall variability in JJA at Finlay. 73
Figure 4.10(c): Wavelet- based mean rainfall variability in OND at Finlay. 74
Figure 4.11: (a) Wavelet-based mean streamflow variability in MAM at Ainamotua. 77
Figure 4.11: (b) Wavelet-based mean stream flow variability in JJA at Ainamotua...78
Figure 4.11: (c) Wavelet-based mean streamflow variability in OND at Ainamotua. 78
Figure 4.12 (a): Rainfall periods at Ahero station 82
Figure 4.12 (b): Rainfall periods at Ahero station 82
Figure 4.12 (c): Rainfall periods at Nandi Tea station.....83
Figure 4.13: (a) Streamflow periods at Mbogo station. 85

Figure 4.13: (b) Streamflow periods at Nyando Kericho station. 86
Figure 4.13: (c) Streamflow periods at Masaita station. 86
Figure 4.14: (a) Wavelet power spectra for rainfall at Finlay. 90
Figure 4.14: (b) Wavelet power spectra for rainfall at Ahero. 91
Figure 4.14: (c) Wavelet power spectra for rainfall at Londiani. 92
Figure 4.15: (a) Wavelet power spectra for streamflow at Nyando 1GD07. 96
Figure 4.15: (b) Wavelet power spectra for streamflow at Tugenon 97
Figure 4.15: (c) Wavelet power spectra for streamflow at Nyando. 98
Figure 4.16 (a): Cross wavelets in November rainfall –OND streamflow. 102
Figure 4.16 (b): Cross wavelets in March rainfall –April streamflow. 103
Figure 4.16 (c): Cross wavelets in April rainfall –MAM streamflow Zone 1 103
Figure 4.17: (a) Wavelet power for zones I & III of OND streamflow. 104
Figure 4.17: (b) Cross wavelet power between zones I & II of OND streamflow. ... 105
Figure 4.18: WTC for OND streamflow zones II & III. 106
Figure 4.19: Cluster dendrogram developed for Nyando Rainfall. 113
Figure 4.20: Cluster dendrogram developed for Nyando streamflow. 114
Figure 4.21: (a) Regional average L-moments for Cluster I rainfall. 115
Figure 4.21: (b) Regional average L-moments for Cluster II rainfall. 115
Figure 4.21: (c) Regional average L-moments for Cluster III rainfall 116
Figure 4.22: (a) Regional average L-moments for cluster I streamflow 118
Figure 4.22: (b) Regional average L-moments for cluster II streamflow 118
Figure 4.22: (c) Regional average L-moments for cluster III streamflow 119
Figure 4.22: (d) Regional average L-moments for cluster IV streamflow 119
Figure 4.23: Rainfall growth curves 123
Figure 4.24: Streamflow growth curves 125

ACRONYMS

AD	Anderson Darling
APR	Areal Precipitation Ratio
AMS	Annual Maximum Series
COI	Cone of Influence
CWT	Continuous Wavelet Transform
DEM	Digital Elevation Model
ENSO	El Nino Southern Oscillation
FAO	Food for Agriculture Organization
FT	Fourier Transform
FFT	Fast Fourier Transform
GIS	Geographical Information System
IDW	Inverse Distance Weighting
IOD	Indian Ocean Dipole
JJA	June-July-August
KMD	Kenya Meteorological Department
KSM	Kisumu
LFTC	Londiani Forest Training College
LVBC	Lake Victoria Basin Commission
MAM	March-April-May
M-K	Mann-Kendall
OND	October-November-December
PoT	Peak -Over -Thresholds
PWM	Probability Weighted Moment
QBO	Quasi Biennial Oscillation

Q-Q	Quantile- Quantile
RFA	Regional Frequency Analysis
SST	Sea Surface Temperature
SNHT	Standard Normal Homogeneity Test
SR	Spearman’s (Rho)
WMO	World Meteorological Society
WRMA	Water Resources Management Authority
WT	Wavelet Transform
XWT	Cross Wavelet Transform
WTC	Wavelet Transform Coherence

CHAPTER ONE

BACKGROUND OF THE STUDY

1.1 Introduction

This chapter presents an introduction to the current study and emphasizes the need to investigate the rainfall and streamflow characteristics within the Nyando River basin. The chapter introduces trend, periodicity, and frequency analysis of rainfall and streamflow.

Nyando River system is one of the main river systems within the Kenyan side of the Lake Victoria drainage basin and drains into the Lake's Winam Gulf. The Nyando River basin suffers from frequent floods, especially in the lower Kano plains. The upper part of the catchment, which encompasses Nandi Hills and Mau West Escarpment, receives heavy rainfall during long and short rainy seasons in March-May and October-December, respectively. The upper and middle parts of the Nyando basin have experienced high deforestation rates and intense agricultural practices which have resulted in severe soil erosion and sediment deposition and have modified the catchment morphology and surface cover (Owuor *et al*., 2012). Therefore, it is imperative to explore the changes exhibited by hydro-climatic parameters in order to understand the basin's present and future hydrological characteristics for better planning, management, and utilization of the water resources and other ecosystem services.

Sustainable water resources management depends on reliable hydrological data and forecasts. The basis of water resources management is to collect and analyse hydrological data so that informed decisions can be made and future strategies would be based on assessing the available facts. Generally, hydro-climatic data aid in planning and designs of projects such as water supply, irrigation and hydropower systems. It is

usually assumed in the design of such works that the statistical characteristics of the time series exhibit stationarity, implying the characteristics do not change with time (Grinsted *et al*., 2004). Noting that there are presumable climate changes due to increase in greenhouse gases in the atmosphere, such an assumption can no longer be reliable and presents water resources management challenges. For example, whereas floods are considered an outcome of stationary hydro- meteorological processes, trends (possibly due to anthropogenic influences) and long-term climate variability have been reported by Jain and Lall (2000).

Parametric and non-parametric (distribution- free) tests are commonly used to detect trends in hydro meteorological time series data. There are advantages of non-parametric tests since their assumptions are weaker and fewer than those associated with parametric tests (Kundzewicz and Robson, 2004). However, flexibility in parametric tests allows for testing a wider range of hypotheses. Mann-Kendall and Spearman's Rho tests are the most common non-parametric tests for analysing time series trends. According to Khisa, *et al*. (2013), the rank-based Mann-Kendal (M-K) has been widely applied in trend detection.

Periodicities in hydrologic time series are induced by astronomical cycles. According to Khisha *et al*. (2013), periodicities are mainly attributed to large scale atmospheric circulation. These periodicities are associated with high or low rainfall, which translates into floods or droughts, respectively. Their impact harms water resources systems.

1.2 Problem Statement

The high flood frequency in the Nyando River basin is a concern in the wake of climate variability and possible climate change. Specifically, there is need for proper techniques to estimate flood and drought frequencies for effective water resources management in

the Nyando River basin. Nyando River basin has experienced adverse weather conditions characterized by devastating floods due to erratic rainfall patterns and prolonged droughts, leading to property destruction and human suffering.

According to Owuor *et al. (*2012), most parts of the basin have undergone large-scale deforestation and poor agricultural practices, resulting in increased floods and severe soil erosion. Generally, catchment degradation has changed the hydrological behaviour of the Nyando basin and has reduced land and water potential by causing a water flow of inferior quality, quantity, and timing.

Studies on rainfall and streamflow variability are therefore required to mitigate such disasters according to Nyakundi and Rael (2016), noting that the rainfall and streamflow characteristics within Nyando River basin are not fully understood. Additionally, there is a lack of reliable and adequate data for design of hydrological structures for water resource management, although a significant task remains for hydro-meteorologist to develop objective techniques for forecasting seasonal and annual rainfall magnitudes and their frequency of occurrence. Previous studies have been done on trend and periodicity in East Africa, Kenya and specifically Nyando River basin (e.g. Nyakundi *et al*., 2010; Ogallo, 1984) but most of these studies have focused on rainfall component only and missed out on streamflow. This study was carried out to better understand the rainfall and streamflow characteristics in the Nyando basin for proper management of the water resources and mitigation of adverse environmental impacts within the Nyando River basin.

1.3 Justification of the Study

The current study provides information on hydro-climate parameters behaviour in terms of trend, periodicity and frequency. Knowledge on these parameters is essential in water resource system planning and management like flood management, droughts, siltation,

early warning systems, and the basin livelihoods in food security, socio-cultural and economic activities. The results of trend analysis of the hydro-climatic variables, for example, can be incorporated into prediction models of future scenarios applied to many different fields, such as in agriculture (e.g., growing seasons, irrigation schemes, crop productions), food security, water supplies, and extreme weather forecast (Nalley *et al.* (2012). Further, trend, periodicity, and frequency analysis of hydro-climatic variables can also bring out significant issues in the adaptation and mitigation efforts associated with climate change. According to Nalley *et al*. (2012), policies created to address climate change impacts for a specific region should be done based on that particular region's knowledge rather than global climate change information.

Besides, there is a need for an optimum rainfall and flood frequency analysis models to design water management infrastructure in the basin. For other regions, similar studies have been done on rainfall and flood frequency analysis, including the studies done by Lim (2007), Noto and La Loggia (2009), Hosking and Wallis (1997), Dhorde and Zarenistanak (2013) and Eregno (2014).

1.4 Study Objectives

The primary objective of this research was to analyse hydrometeorological time series and to determine their optimum probability distributions in Nyando River basin.

Specific Objectives

The specific objectives of the study were to:

1. Determine trends in rainfall and streamflow time series.
2. Investigate and determine periodicity in the rainfall and streamflow time series.
3. Determine the optimum probability distribution for rainfall and streamflow.

1.5 Study Area

1.5.1 Location

The Nyando River basin is located in Western Kenya and is defined by the area drained by the Nyando River and its tributaries. The basin, which covers about 3,580 km^2, is situated within Lake Victoria South Drainage Basin. The location of interest is found within latitudes 0^o 7′ N and 0^o 25′ S and longitudes 34^o 34′ E and 35^o 34′ E (Figure 1.1).

1.5.2 Hydrology

Nyando River originates from the Mau Forest Complex located on the Kenyan Rift Valley's western shoulder. It passes through Kano Plains and discharges its waters into Winam Gulf of Lake Victoria. Peak discharges are experienced mainly in April and early May. In the last 50 years of the 20th Century, the annual release has averaged 22.22 m^3/s varying from a mean monthly discharge of 6.26 to 29.07 m^3/s (Khisa *et al*., 2013). The arrival of seasonal floods from the upper catchment through the main tributaries of Ainamotua and Nyando causes a stage rise of up to 8 m at Ogilo Bridge in the northern part of Kano plains. At this point, the river channel can contain water levels of up to 10 m high, and therefore the seasonal flood wave only inundates the flanking plains downstream.

1.5.3 Climate

Nyando River Basin experiences long rains from March to May and short rains from September to November with annual rainfall from 1000 mm to 1600 mm (Owuor *et al*., 2012). Temperature ranges from 13 to 31°C with two peaks in March and October (Khisa *et al*., 2013).

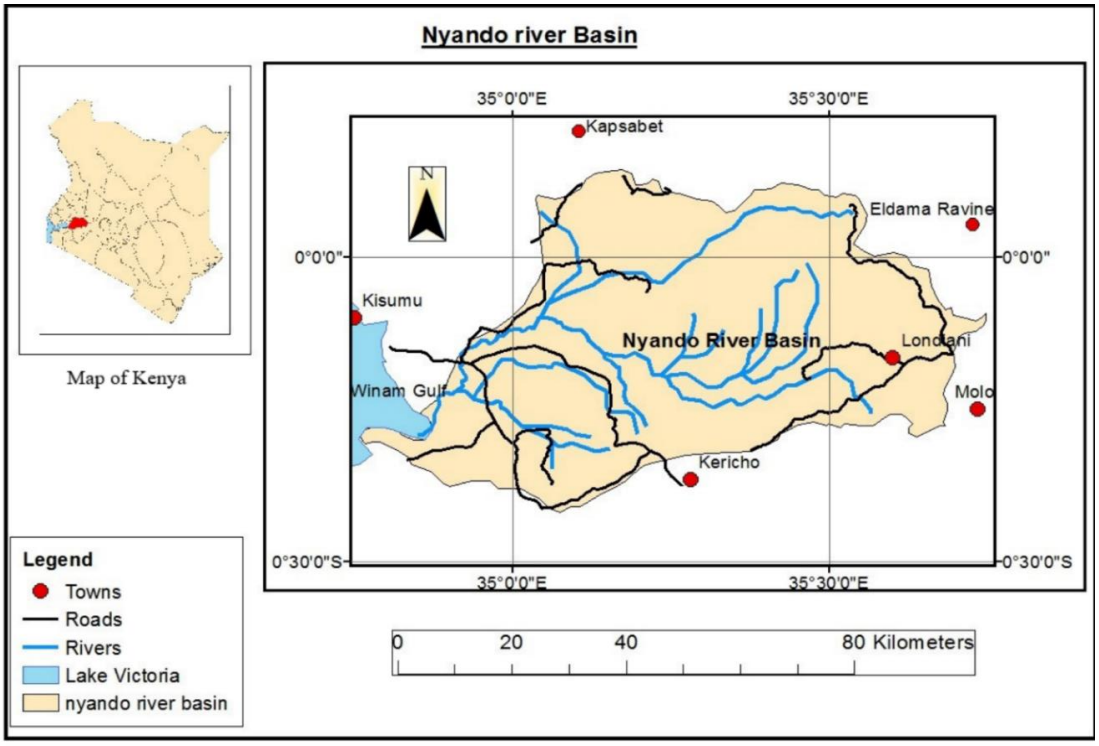

Figure 1.1: Location map of Nyando Basin in Kenya

1.5.4 Geology and soils

Geologically, the Nyando River basin consists of extrusive igneous (volcanic) rocks, mainly phonoliths and metamorphic rocks and varies from recent quaternary sediments to old rocks of Archean age (Opere and Okello, 2011). According to Kosgei (2018), due to impeded soil drainage on account of the prevalence of vertical clays, water logging occurs extensively in the plains during and immediately after the rains. Eutric Vertisols with a sodic phase are dominant soil types on the flat to very gently undulating slopes of 0-1%. The soils are generally imperfectly drained to poorly drained, deep to very deep, dark greyish brown to black, firm to very firm, cracking, clay and sodic deeper subsoil.

The main geological feature in the study area is the Kavirondo Rift. The faulting has allowed the accumulation of Pleistocene sediments and possibly tuffs of a vast thickness. These sediments and tuffs are now covered by alluvial material. The significant factors that have influenced sedimentation are the supply of different types

of residues by rivers depositing gravel and sands during periods of high discharge, clay and silt during periods of low release, and the development of the Kavirondo Rift Valley, which control the hydraulic gradient of the rivers and the deposition environment (land or lake). However, some West Kano area sections are dominated by porous sedimentary sandy loams (Kosgei, 2018).

1.5.5 Land Use

The dominant land use activities in the Nyando catchment include farming and settlement. The main crop is sugar cane, which doubles as the main cash crop for the inhabitants and is dominant in the catchment's northern parts. Rice and cotton are other crops in the catchment and are prevalent in the southern regions. Maize, beans, and sorghum are the main subsistence crops in the area (Nyakundi *et al*., 2010). According to Kosgei (2018), rice and sugarcane irrigation within the wetlands and tea farming in the highlands have ultimately introduced complex hydrological pathways, primarily due to canalization.

1.5.6 Landforms

Nyando basin's landforms vary from low plains near Lake Victoria's shores to plateaus and mountains to the east, with elevations ranging from 1134 m to over 3000 m above mean sea level.

CHAPTER TWO

LITERATURE REVIEW

2.1 Introduction

Various investigators have tried several techniques to detect trends and periodicity and analyse flood frequencies for different river basins. This chapter outlines a literature review on the relevant issues, including rainfall seasonality, data quality analysis and checks (e.g., tests for homogeneity, normality, independence and stationarity), trend and periodicity detection, and methods of frequency analysis.

2.2 Rainfall Seasons in Kenya

Previous rainfall studies by Gitau *et al*. (2013) have shown that East African rainfall is bimodal and sometimes tri-modal, with the significant rainfall seasons experienced in March-May (MAM) and October-November-December (OND). According to Owiti and Zhu (2012), rainfall seasonality over East Africa is influenced by geographical variations. Some parts like Northern Uganda, which receive rainfall throughout the year have three peaks in May, August, and October.

For the highland parts of Kenya that straddle the equator, there are two seasons: MAM and OND. Nearer to the equator, two rainfall and two dry seasons are observed within the year (bimodal regime) according to Owiti and Zhu (2012).

According to Beltrando's (1990) account in Indeje *et al*. (2000), rainfall in Western Kenya, has been grouped into three seasons of March - May, June - September and October - December. In the current study therefore, seasonal time series have been aligned to the seasons of MAM, JJA and OND for the cases study application and analysis.

2.3 Trend Analysis

Time series fluctuations can be gradual (trend), abrupt (step change) or may be complex which may alter the statistical parameters of time series data (Kundzewicz and Robson, 2004). The methods for detecting trends in time series hydrologic data are categorized into parametric and non-parametric. In parametric methods, the population is close to normal while non-parametric approaches do not rely on the distribution and has fewer and weaker assumptions according to Kundzewicz and Robson (2004).

According to Giakoumakis and Baloutsos (1997), increasing or decreasing trends are attributed to climate variability or land-use changes. Statistical and graphical analysis techniques are used in trend detection (Nyakundi *et al*., 2016; Ogallo, 1979). However, the examination of trend by graphical methods has several disadvantages such as dependence on individual judgment, loss of data by smoothening techniques and alteration of amplitude (Maragatham, 2012).

Miao *et al*. (2012) analyzed seasonal precipitation to detect trends and periodicities for Beijing. The analysis involved a comprehensive precipitation trend and periodicity analysis at seasonal scale. The trend component was analyzed using M-K test and least squares methods while periodicity aspect was analyzed by wavelet technique. The results revealed significant increasing trends starting from the year 1980. Further, the results showed strong periodicities in the ranges such as from 30 to 170 years, 80 to 90 years, 75 to 95 years and 55 to 65 years. According to Ahmad *et al*. (2015), M-K is the most common non-parametric tests when working with time series trends.

Tihumins *et al*. (2010) carried out a study on long-term trends and fluctuations on Baltic Region River runoff using wavelet analysis. The Multivariate M-K approach was used for analyzing monotonic trend in the time series while periodicity was tested first by

spectral analysis and further tests done by wavelet transforms. Further, Hafliga and Lim (2012) analyzed peak annual flows for flooding trend changes in the upper Mid-West of North America. M-K was first applied to determine the presence of an overall trend in the entire time series. Two additional tests namely, the moving average and the ratio of means method were used to test when the trend changes might have occurred. Next, the flow data was analyzed using wavelet analysis to study the flooding periodicity. The wavelet technique focused on different flooding patterns that can reoccur at various cyclic lengths (periodic components).

Khisa *et al*. (2013) studied the spatio-temporal changes and analyzed factors that contributed to Nyando wetland evolution. Rainfall and streamflow data of 60 years record were statistically analyzed. Trend was tested using the Spearman's rank test, while change point was detected by Pettit test and the standard normal homogeneity test (SNHT). Further, split record tests for variance and mean were performed by (F-test) and (t-test), respectively. The missing data was more than 50% and was filled using linear regression and interpolation methods. The Nyando rainfall and streamflow data were found to be homogeneous, the change point results indicated that the Nyando rainfall declined in 1979, while the discharge recorded significant upward change in 1961.

Adamowski *et al.* (2013) examined precipitation trends in the Swat River basin in Pakistan using non-parametric M-K and Spearman's Rho (SR) statistical tests. Annual and seasonal precipitation time series were computed from the monthly precipitation values. Both the standard normal homogeneity test (SNHT) and Buishand's range (BS) test were used to test for homogeneity of time series. The results of the study showed both increasing and decreasing trends.

2.4 Periodicity Detection

Periodicity has been defined as the quality, state or fact of being regularly recurrent or having periods (Franco-Viloria *et al*. (2012). A system that displays irregular periodicity is referred to as quasi-periodic. An example of quasi-periodicity in climatology is the El Niño Southern Oscillation (ENSO). Periodic and quasi-periodic changes are observed frequently in natural phenomena. Detection and understanding of periodicities often lead to better understanding of the relevant phenomenon.

The periodicity of river discharge changes have been previously explained with the haile cycles (11 and 22 years) and Gleissberg Solar activity cycles, Solar-Lunar tidal periods as well as other periodically occurring phenomena (Tihumins *et al*., 2010). According to Tihumins *et al*. (2010), streamflow periodicities have been detected in Central Europe, attributed mainly to atmospheric circulations of large scale magnitudes.

In the current study, both Fourier and Wavelet transform techniques were used to analyse for periodicity in rainfall and streamflow.

2.4.1 Fourier Transform in Spectral Analysis

Ogallo (1984) investigated temporal fluctuations of seasonal rainfall patterns in East Africa using harmonic analysis on yearly basis. In this particular analysis, Fourier Transform was used to decompose the time series into a sum of sinusoidal terms. When a time series is subjected to harmonic (wave) analysis, the magnitudes of the amplitudes determine the major harmonics of the time series while the phase angle may be used to describe the time of the maximum or minimum for any harmonic considered. The distribution of the first harmonic is unimodal; the second harmonic has bimodal distribution while the third harmonic will have tri-modal distribution, etc.

Tihumins *et al*. (2010**)** analysed long-term fluctuations of the Baltic Region River runoff using spectral analysis and periodograms. A periodogram relates individual frequencies to the time series regression. Periodograms were calculated using spectral analysis and the results showed periodicities in the range of 27-33 years.

Roshani *et al*. (2012) studied rainfall and streamflow periodicities in the Ghaleroudkhan basin, Iran using M-K and spectral techniques. The study considered data records for the period 1966-2002 from stations within the Ghaleroudkhan basin. M-K was used in the detection of trend while spectral analysis was used in the investigation of cycles. The trend test results showed occurrence of trend and abrupt changes in the rainfall and streamflow time series. The spectral results indicated existence of non-sinus cycles and that the seasonal cycles were more pronounced than the monthly.

2.4.2 Wavelet-based Periodicity Detection

Wavelet transforms were developed for easy study of time series data that may contain non-stationary power with multi-frequency scales (Franco-Viloria *et al*., 2012). Wavelets decompose raw time series data into wave-like structures time series resembling fluctuations at various frequencies.

Nalley *et al.* (2012) analysed trends in temperature, precipitation and streamflow data over Southern Ontario and Quebec using the discrete wavelet transform (DWT). The objective of the study was to detect and analyse trends in mean surface air temperature, total precipitation and mean streamflow obtained from several stations in Ontario and Quebec, Canada. In order to accomplish the objective, the study co-utilized the DWT and M-K techniques. The time series used were decomposed via the DWT in order to separate their high frequency components prior to testing their statistical significance

with the M-K trend test. The trend was assumed to be contained in the low frequency component of the data.

The trends in temperature, precipitation and streamflow were assessed on different time scales: monthly, seasonal and annual. Temperature trends for the different seasons (i.e. winter, spring and autumn) were also assessed. The study recognized the advantage of WT technique as highlighted by its ability to extract time-frequency information contained in the analysed time series which were manifested in the form of periodicities ranging from annual to decadal events. The overall results led to a conclusion that WT provides very detailed information on the analysed time series by extracting its different periodicities.

Santos *et al*. (2003) applied wavelet transform technique in analysing rainfall time series data (1900-2000), selected from several stations globally. Monthly rainfall data from Lisbon, Madrid and Barcelona in the Iberian Peninsula, Matsuyawa in Japan, and Angicos in north-eastern Brazil were used. The wavelet Power Spectra indicated periodic and quasi-periodic cycles of 1.5-2 years for all the regions studied.

According to Grinsted *et al*. (2004), WT has been classified into continuous (CWT) and discrete (DWT). The DWT has the capability of reducing data redundancy and is useful in trend detection. CWT is effective in decomposing data into several frequencies and is useful in periodicity studies. Grinsted *et al*. (2004) examined relationships between winter Atlantic Oscillations (AO) and Baltic Sea ice extent by performing cross-wavelet and wavelet coherence analysis. The phase relationships between the series were explored in the light of the expected links. Maximum annual ice level in the Baltic Sea (BMI) (1720-2000) and winter AO index (1851-1997) were used in the wavelet analysis. The Morlet wavelet was used due to its structure which resembles that of a

rainfall/streamflow time series data (Torrence and Compo, 1998). To ignore edge effects due to incomplete localization of the CWT, a cone of influence was included during the analysis.

The results of both the AO and the BMI series showed significant 5-year period in 1940 and 2-7 year period between1860 to1900. In order to obtain clear results, a cross-wavelet transform analysis (XWT) was carried out between AO and BMI and the common features between the two series stood out to be significant at the 5% level. Further, wavelet coherence analysis was done to establish coherence of the CWT in the frequency space.

2.5 Flood Frequency Analysis using L-moments

Lim (2007) suggests that regional approach in analysing flood frequency is better than the at- site method, noting that the information in the regional analysis may extend to all the sites in a homogeneous region.

Noto and La Loggia (2009) performed a regional flood frequency analysis to identify homogeneous regions in Sicily, Italy. In the study, data records of more than 50 stations were analysed for homogeneity. The study area was delineated using L-moment method into clusters using cluster techniques. The results identified Generalized Extreme Value distribution as the best fitted distribution for the entire Sicily. Vogel and Wilson (1996) performed flood frequency analysis of streamflow in the United States. L-moment ratio diagrams were used to select the optimum distributions for floods. The study considered 1,570 streamflow gauging stations spread all over the entire United States. Daily mean streamflow data were used to compute annual maximum, mean and low flows. According to Vogel and Wilson (1996), L-moment coefficient of variation (L-cv), L-moment coefficient of skewness (L-skew), and L-moment coefficient of kurtosis (L-

kurtosis) and their population counterparts can easily be compared by looking at the L-moment ratio diagrams. Additionally, L-moments are superior to ordinary product moments as L-moment ratios have no bias for any probability distributions, compared to ordinary product moments. The study revealed that Log-Normal (LN3), log-Pearson Type III (LP3) and Generalized Extreme Value (GEV) distributions were the optimum probability distributions for floods.

2.6 Conclusion

According to the literature review, many studies have been carried out on trend and periodicity analyses in rainfall and streamflow parameters. However, most of the studies have looked at either trend, periodicity or frequency analysis separately. This was seen as a gap which the current study has addressed by conducting the three studies together since the frequency and periodic nature of a hydrological time series are related to its trend. A number of studies from the literature review have also indicated wide-spread use of the M-K method in linear trend analysis. The M-K test, being a non-parametric test is distribution free and the assumptions underlying its use are fewer and weaker than those associated with parametric tests. However, whereas most of the reviewed studies have used the M-K method with additional other conventional techniques, the current study used M-K and Wavelet transform analysis, since Wavelet technique has a good balance in the time-frequency localization (e.g. Grinstead *et al*., 2004).

Additionally, whereas most studies from the current literature review revealed increasing use of Wavelet approach in analysing hydrological series, few of the studies have considered use of cross-wavelets and wavelet coherences. In the current study, inter-series wavelets and wavelet coherences were carried out to uncover the correlations between the rainfall and streamflow time series. Further, whereas most

authors have published on trend, periodicity and frequency analysis separately, the current study looked at all the aspects for in-depth and combined understanding of the three phenomena. Further, several studies (e.g. Noto and La Loggia, 2009; Lim, 2007; Vogel and Wilson, 1996) noted the following features of L-moment approach which make it superior in selecting best fit distributions: (i) Several distribution fits can be compared against many data samples using L-moment ratio diagrams, (ii) L-moment ratios are approximately unbiased for all probability distributions, (iii) L-moments are insensitive to peak and low hydrometeorological values, hence allows parameter estimation to be more robust.

CHAPTER THREE

MATERIALS AND METHODS

3.1 Introduction

This chapter presents the data types and methods used in the current study. The source of data and the selected stations are described together with brief explanations of how the raw data were processed.

3.2 Data

Data discussed in this sub- section relate to rainfall and streamflow. Additional data are of Digital Elevation Models used in delineation of the watershed. Tests for homogeneity, normality and independence of data, trend and periodicity analysis techniques, and finally approach for Regional Frequency analysis are also presented.

Daily and monthly data for 10 rainfall and 8 streamflow gauging stations (Fig. 1.1) within the Nyando River basin were used. Rainfall data from 8 stations with average lengths of 41 years were obtained from Water Resources Authority. Additional rainfall data of lengths 36 and 100 years, respectively were sourced from Kenya Meteorological Department and Finlay Kenya Limited. Streamflow data with average length of 48 years were also obtained from Water Resources Authority. A summary of the stations with data lengths are presented in Tables 3.1 and 3.2. The Tables indicate the names of rainfall gauging stations selected within Nyando River basin with their codes, geographical coordinates, record lengths and the percentage of missing data. The lattitudes and longitudes are rounded off to four (4) decimal points so as to be convertible to degrees and minutes.

Table 3.1: Details of the rainfall gauging stations

Station code	Station name	Latitude (degrees)	Longitude (degrees)	Data Periods	Data length (yrs)	% Missing
9034086	Ahero Irrigation	-0.1333	34.9333	1962-2001	39	3.8
8935095	Nandi Tea	0.1000	35.1833	1957-1988	31	1.9
9035188	Tinga Monastery	-0.0833	35.4500	1958 - 1991	33	1.2
9035003	Kericho Water	-0.3833	35.2833	1926-1986	60	0.5
9035258	Kipkelion	-0.2000	35.4667	1957 - 1991	34	0.8
9035226	Londiani	-0.1500	35.5828	1926-1986	60	1.1
9035244	Timbilil	-0.3500	35.3500	1963-2000	37	2.4
9035341	Finlay	-0.3500	35.2900	1905-2005	100	0.6

Table 3.2: Details of the streamflow gauging stations

Station Code	Station Name	Latitude (degrees)	Longitude (degrees)	Data length	Data length (yrs)	% Missing data
1GC06	Nyando, Kericho	-0.2000	35.4667	1969- 2014	45	9.0
1GD07	Nyando, Kisumu	-0.1639	35.1639	1967- 2013	46	1.8
1GB05	Ainamotua	-0.0264	35.175	1962- 1994	32	1.5
1GB06	Mbogo	-0.0578	35.14333	1950-2014	64	3.8
1GB11	Ainopiswa	-0.0250	35.1764	1950-1987	37	3.5
1GC05	Masaita	-0.1944	35.5347	1959- 2014	55	4.0
1GD04	Nyando	-0.1014	35.0444	1963- 2011	48	1.0
1GC04	Tugenon	-0.2528	35.4139	1951- 2012	61	1.2

The daily rainfall and streamflow data were first converted into monthly time series data by taking the daily averages and the monthly totals calculated, taking into account the number of days in each month. The seasonal (MAM, JJA and OND) were computed and used in the analysis of trend and periodicity. Annual maximum series (AMS) were also derived and used in the frequency analysis. The Digital Elevation Model DEM for Nyando River basin was sourced from Regional Centre of Mapping and Resource Development for use in watershed delineation.

3.3 Methodology

Figure 3.1 presents a summary of the methods applied in the study.

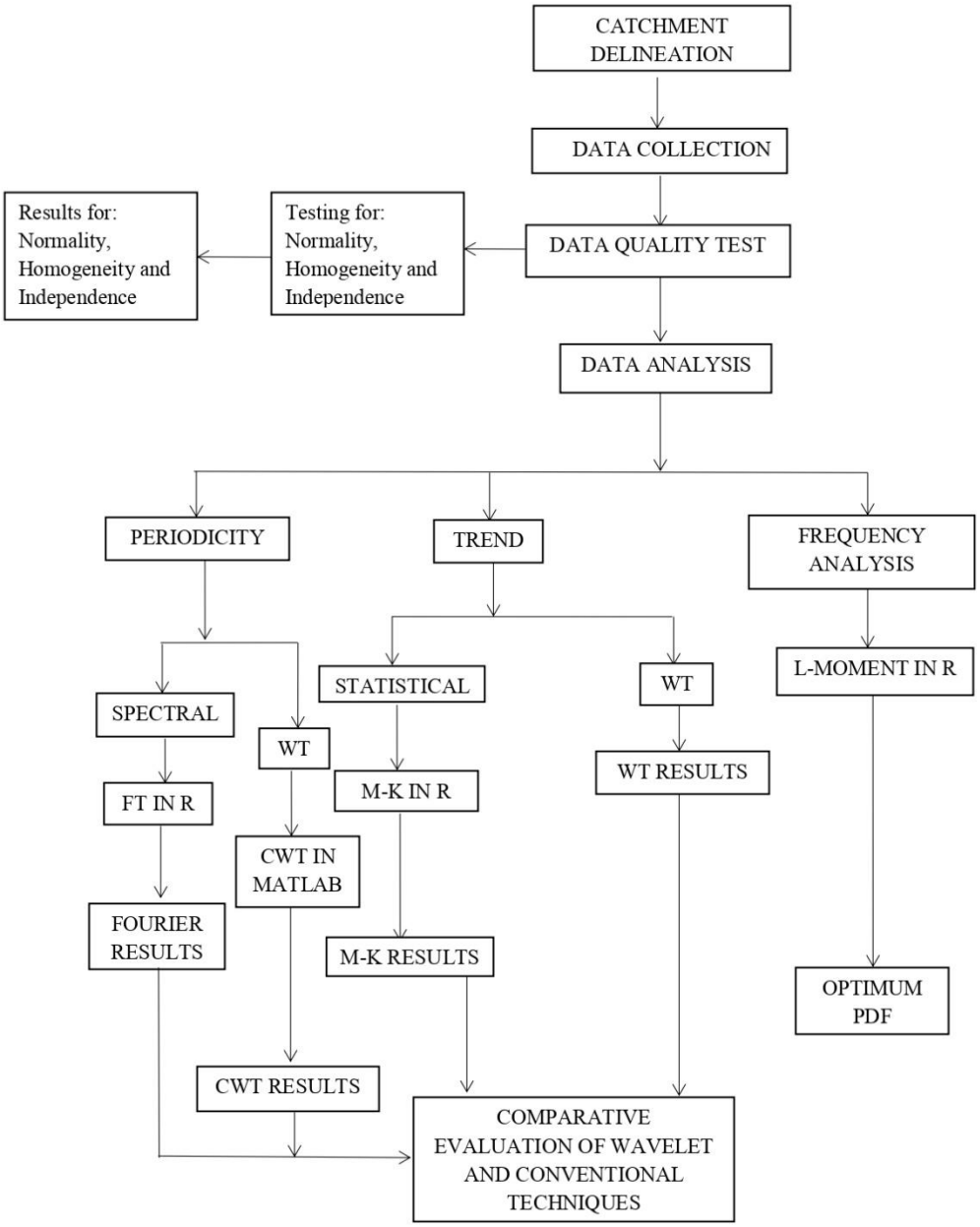

Figure 3.1: Summarized Flow Chart on Methodology.

3.3.1 Watershed delineation

In the current study, the stream network approach was adopted. The clipped DEM was then smoothed using the fill tool in order to remove any sinks or towers due to incorrect elevation data. The following sequence describe steps followed in watershed delineation:

(1) Location of the streams were determined. In this process, the flow direction tool was used to find flow through the DEM. Appendix 2A shows the extracted DEM for Nyando River basin and the flow direction.

(2) Flow accumulation of water in each pixel was determined using the flow accumulation tool. Water that aggregates in certain areas creates a stream and it is from the flow accumulation dataset that the stream network was created. Flow accumulation is shown in Appendix 2C.

(3) Stream network was created using the flow accumulation dataset by determining a threshold value for what is considered a stream. In the current study, a threshold of 500 pixels was chosen, that is one pixel of 30m x 30m has at least other 500 pixels flowing into it in order to be called a stream. The contributing area was therefore 900 m^2 for one pixel giving a total area of 900 x 500 (450,000 m^2) or 45 Hectares.

(4) Stream datasets were divided into small segments based on flow direction using the stream link tool.

(5) A grid of stream links was created using stream links function. Subsequently, the stream links were converted into vector to allow for vector representation.

(6) The order was determined using the Strahler technique by assigning each stream segment a value 1-6. Order 1 streams represent initial headwaters, order 2 represents where two order 1 streams meet and where two order two streams

meet, the segment was assigned a 3. Appendix 2D illustrates the strahler network for Nyando river basin.

(7) A shape file was created using the coordinates of the gauging stations and subsequently, the boundaries of the river system were determined (Figure 1.1).

3.3.2 Data Quality Analysis

Data quality has been examined in this study for data characteristics, percentage gaps, homogeneity, normality and independence.

a) Percentage missing data

The data was considered suitable for use since the total missing value was less than 10% in all the stations. According to World Meteorological Organization guidelines (WMO, 2018), the data should be considered only when data values are available for at least 80% of the records for the entire period of data. The missing values computed for the selected rainfall and streamflow stations in the current study were less than 5% and 10% respectively, as already illustrated in Table 3.1 and Table 3.2. Further tests were done to check for homogeneity, normality and independence of data.

b) Homogeneity testing of data

Homogeneity testing of data aims to identify and eliminate (or reduce) non-climate factors such as changes in instruments, observation practices, station relocations and station environments. Inhomogeneity is a change-point caused by non-climate factors (Dhorde and Zarenistanak (2013). An incorrect application of homogenization procedures to climate data could subsequently lead to unreliable climate analysis and therefore a good strategy is to compare detected break-points by several techniques. According to Toreti et al. (2011), the comparison gives robust results by avoiding overestimation and correction of false homogeneities. Homogeneity of data in the current study was tested using three techniques. The standard normal homogeneity

(SNHT) test, Buishand range (BR) test, and the Pettit test were selected. Under the null hypothesis, the seasonal values Y_i of the testing variables Y are independent and identically distributed and the series are considered as homogeneous. Meanwhile, under alternative hypothesis, the SNHT, BR and the Pettit tests assume the series consisted of break in the mean and are therefore considered as inhomogeneous. The details of the methods are explained in the subsequent sub-sections.

i. Pettitt test

Pettit (1979) developed a non-parametric test for analysing jumps in hydro-climatic time series data (Dhorde and Zarenistanak, 2013). The test detects breaks in the middle of the series (Dhorde and Zarenistanak, 2013).

The statistic used for the Pettit test was computed through the following steps:

In the first step, U_k statistic was computed using the formula:

$U_k = 2\sum_{i=0}^{n} m_i$- k (n+1) Equation (3.1)

Where U_k is the test statistic representing the results of the test, m_i is the rank of the i-th observation when the values x_1, x_2,….,x_n are arranged in ascending order, n is the number of observations and k is the year when the change occurs.

In the second step, statistical change point (SCP) was defined as:

$K = \max_{1 \le k \le n} |U_k|$ Equation (3.2)

Where SCP, denoted by k represents the year when the change has occurred. The change point occurs when k assumes maximum value K.

ii. Standard Normal Homogeneity test (SNHT)

This test was formulated by Alexanderson (1986), which described a statistic T(k) to compare the mean of the first k years of the record with that of the last n-k years.

$T(k) = kz_1^2 + (n-k)kz_2^2$ k=1… n Equation (3.3)

Where:

$\bar{z_1} = 1/k \sum_{i=k+1}^{n} (Y_i - \bar{Y})/S,$ and

$\bar{z_2} = \frac{1}{n-k} \sum_{i=k+1}^{n} (Y_i - \bar{Y})/S$ Equation (3.4)

Where Y_i is the testing variable, $\bar{Y}$ is the mean and S is the standard deviation. If a break is located at the year k, then T(k) reaches a maximum near the year k=K. To reject the null hypothesis, the test statistic:

$T_0 = \max_{1 \le k \le n} T(k)$ Equation (3.5)

is greater than the critical value, which depends on the sample size. The critical value was then compared with the critical value given by Pettit (1979) given as 6.95. In this study, SNHT was the second technique used to compute the critical values for time series for the selected stations.

iii. Buishand Range test

Buishand (1982) analysed data for homogeneity using adjusted partial sums which are defined as:

$S_o^* = 0$ and $S_k^* = \sum_{i=0}^{k} \langle Y_i - \bar{Y} \rangle$ K =1… n Equation (3.6)

When a series is homogeneous the value of S_k^* fluctuates around zero, because no systematic deviations of the Y_i values with respect to their mean will appear. If a break is present in year k, then S_k^* reaches a maximum (negative shift) or minimum (positive shift) near year k = K. The significance of the shift can be tested with the rescaled adjusted range R, which is the difference between the maximum and the minimum of S_k^* values by the sample standard deviation. Buishand gives critical values for $R/\sqrt{n}$. The critical values were then compared with the critical value given by Pettit (1979) as 1.43. BR test was a mong the three techniques used in the current study to compute the critical values for the rainfall and streamflow series.

a) Normality testing of data

Normality testing was done in this study using Anderson-Darling (A-D) test, in order to understand whether the data assumes normal distribution.

H_0: The data follow the distribution

The (A-D) test was defined as:

H_a: The data do not follow the distribution

The (A-D) test is defined as in Equation 3.8:

$$S = \sum_i^N \frac{2i-1}{N} [LnF(Y_i) + Ln(1 - F(Y_{N+1-i}))]. \quad \text{Equation (3.7)}$$

Where F is the cumulative distribution function of the specified distribution while the $Y_i's$ are the ordered data. The critical values for the Anderson-Darling test are dependent on the specific distribution that is being tested. Tabulated values and formulae have been published (Stephens, 1976) for a few specific distributions (Normal, lognormal, exponential, Weibull, logistic, and extreme value type I). The test is a one sided test and the hypothesis that the distribution is a specific form is rejected if the test statistic is greater than the critical value.

b) Wald-Wolfowitz test for independence and stationarity

The runs test, also called Wald-Wolfowitz test, is a non-parametric test that checks a randomness hypothesis for a two-valued data sequence. More precisely, it can be used to test the hypothesis that the elements of the sequence are mutually independent.

A “run” of a sequence is a maximal non-empty segment of the sequence consisting of adjacent equal elements. For example, the sequence "++++−−−+++−−++++++−−−−" consists of six runs, three of which consist of +'s and the others of −'s. If +s and −s alternate randomly, the number of runs in a sequence of length N for which it is given that there are N_+ occurrences of + and $N_–$ occurrences of - (so $N = N_+ + N_–$) is a random

variable whose conditional distribution-given the observation of N_+ and N_- – is approximately normal with:

- mean: $\mu = \frac{2N_+ + N_-}{N} + 1$
- variance: $\sigma^2 = \frac{2N_+ + N_- \ (2N_+ + N_- - N}{N^2(N-1)} = \frac{(\mu-1)(\mu-1)}{N-1}$

These parameters do not depend on the "fairness" of the process generating the elements of the sequence in the sense that +'s and -'s must have equal probabilities, but only on the assumption that the elements are independent and identically distributed. If there are too many runs more or less than expected, the hypothesis of statistical independence of the elements were rejected.

The following hypothesis was tested for dependence and independence of the time series data:

H_0 = Dependent, and

H1≠ Independent

Where H_0 was the null hypothesis and H_1 was the alternative hypothesis. For lower *p*-values, i.e. less or equal to the significant level, H_0 was not rejected but for higher p-values i.e. greater than or equal to the significance level, H_0 was rejected, meaning the time series for the rainfall stations showed independence.

3.3.3 Trend analysis

Trend Analysis was carried out in this study to detect trend and periodicity in the Nyando River basin rainfall and streamflow. Mann-Kendall and Wavelet Transform techniques were used to analyse trend. Mann-Kendall was used to test the statistical significance of the trends at 95% confidence limit whereas the wavelet tool was used to decompose the series into higher and lower frequency components.

(i) Trend analysis using Mann-Kendall method

Mann-Kendall test, a non- parametric technique is popularly applied in testing for trend in hydrological time series (Chingombe *et al*., 2005). The test was applied both to the long term data (ranging from 31-100 years for rainfall and 32-61 years for streamflow) and thirty-year grouped data to detect statistically significant trends. In the current study the test was:

Null hypothesis (H_0): there was no trend in streamflow/rainfall over time, and Alternative hypothesis (H_1): there was a trend (increasing or decreasing) over time.

The formulae for computing M-K statistic S, V(S) and standard test statistic Z are:

$$S = \sum_{i=1}^{n-1} \sum_{j=i+1}^{n} sign(x_i - x_j) \qquad \text{Equation (3.8)}$$

$$sign(x_i - x_j) = \begin{cases} +1 & if\ (x_i - x_j) > 0 \\ 0 & if\ (x_i - x_j) = 0 \\ -1 & if\ (x_i - x_j) < 0 \end{cases} \qquad \text{Equation (3.9)}$$

$$V(S) = \frac{1}{18}\left[n(n-1)(2n+5) - \sum_{p=1}^{q} t_p(t_p - 1)(2t_{p-1})\right] \qquad \text{Equation (3.10)}$$

$$Z = \begin{cases} \frac{S-1}{\sqrt{VAR(S)}} & if\ S > 0 \\ 0 & if\ S = 0 \\ \frac{S+1}{\sqrt{VAR(S)}} & if\ S < 0 \end{cases} \qquad \text{Equation (3.11)}$$

In these formulae, x_i and x_j are the time series observations in chronological order, n is the length of the time series, t_p is the number of times for p^{th} value and z is the number of tied values. Positive z values indicate an upward or increasing trend in the hydrologic time series; negative z values indicate a downward or decreasing trend. In the implementation, if $|Z| > Z_{1-\frac{\alpha}{2}}$, (H_0) is rejected and a statistically significant trend existed in the hydrologic time series. The critical value of $Z_{1-\frac{\alpha}{2}}$ for a *p*-value of 0.05 from a standard normal table is 1.96.

In the current study, M-K was first applied using complete and secondly by repeating the test using data grouped into sets of maximum 30 years in length depending on the period of data at each of the selected stations. This two stage analysis was for purposes of analysing the effect of splitting the data into shorter lengths.

Table 3.3: Rainfall time series grouped data

Station name	Sub-series I	Sub-series II	Sub-series III	Sub-series Iv
Ahero	1962-1989	1990-201	-	-
Nandi Tea	1957 - 1988	-	-	-
Tinga/M	1958 - 1987	1988 - 1991	-	-
Kipkelion	1957 - 1986	1987 - 1991	-	-
Kericho water	1926 - 1955	1956 - 1986	-	-
Timbilil	1963- 1989	1990 - 2000	-	-
Finlay	1905 - 1934	1935 - 1964	1965 - 1994	1995 - 2005
Chemelil	1966 - 1995	1996 - 2006	-	-
K/Met	1974 - 2004	2005 - 2010	-	-

Table 3.4: Streamflow time series grouped data

Station name	Sub-series I	Sub-series II
Nyando	1962-1992	1993- 2011
Ainamotua	1962 - 1987	-
Ainopsiwa	1950- 1987	-
Masaita	1959 - 1989	1990 - 2014
Mbogo	1950- 1980	1981 - 2014
N/Kisumu	1967 - 1997	1998 - 2013
N/Kericho	1969 - 1999	2000 - 2014
Tugenon	1951 - 1981	1982 - 2012

(ii) Trend analysis using Wavelet technique

Wavelet Transform (WT) breaks data series into logically ordered wave-like oscillations (wavelets) analogous to data vis-à-vis time within a range of frequencies. Time series can be depicted with regards to a wavelet expansion that uses the coefficients of the wavelet functions. Different wavelets can be constructed from a function Ψ (t) known as a "mother wavelet "which is restricted in a finite/bound interval. That is, WT expresses/breaks a given signal into frequency bounds, and then analyses them in time.

Wavelet Transform is classified into continuous Wavelet Transform (CWT) and Discrete Wavelet Transform (DWT). The CWT of a signal f (t) is expressed as:

$$W_{a,b} = \frac{1}{\sqrt{a}} \int_{-\infty}^{\infty} f(t)\, \Psi^* \left(\frac{t-b}{a}\right) dt \qquad \text{Equation (3.12)}$$

Where * denotes the complex conjugate. CWT looks for correlations/mutual relationships between the signal and wavelet function. This measurement is done at distinct scales of *a* and locally around the time of *b*. The result is a ripple/wavelet coefficient $W_{a,b}$ outline sketch. However, enumerating the wavelet/ripple coefficients at every likely scale (resolution level) demands a huge amount of data and calculation time. Section 3.3.3 (ii) elaborates more about CWT. In the current study, DWT was used in the analysis of trend whereas CWT was used in periodicity analysis.

Discrete Wavelet Transform analyses a given time series with distinct resolutions for a distinct range of frequencies. This is carried out by decaying the data into coarse approximations and detailed coefficients. For this, the scaling and wavelet/ripple functions were utilized. Choosing the scales *a* and positions *b* based on the powers of two (binary scales and positions), DWT for a discontinuous time series f_i becomes:

$$W_{m,n} = Z^{-m/2} \sum_{i=0}^{N-1} f_i\, \Psi^*(2^{-m_{i-n}}) \qquad \text{Equation (3.13)}$$

Where i is the integer time steps (i= 0, 1, 2, ….., N-1 and N= 2^M), m and n are integers that control respectively, the scale and time; $W_{m,n}$ is wavelet coefficient for the scale factor a= 2^m, the time factor b= 2^mn. The original signal can be built back/re-created using the inverse discrete wavelet transform as:

$$f_i = A_{M,j} + \sum_{m=1}^{M} D_{m,j} \qquad \text{Equation (3.14)}$$

Where $A_{M,j}$ approximation sub-signal at level M and $D_{m,j}$ are details of sub-signals at levels M= 1. 2,,…, N. The approximation coefficients $D_{m,j}$ represent the low scale high frequency component of the signal.

3.3.4 Periodicity analysis of rainfall and streamflow

Attempts were made in the current study to detect periodic components of the seasonal time series using both spectral and wavelet techniques. In the history of spectral analysis technique, various approaches have been developed for the computation of spectral estimates from the observed data. A good account of these methods has been provided by Ogallo (1984). Newer statistical method, namely wavelets are also presented here and this was applied to rainfall and streamflow data to investigate existence of periodicity. As already stated, wavelet analysis is a useful tool for analysing non-stationary time series to capture local behaviour at different frequencies (Torrence and Compo, 1998).

(i) Spectral analysis for periodicity detection

Spectral analysis using Fourier Transform involved detecting the presence and the period of a signal, and estimating the harmonic content (i.e. the magnitude of frequency and its multiples). A good procedure for this detection involves use of the periodic nature of the expected signal. One example is grouping and averaging the data with respect to periods and then examining the appearance of the resulting average curves, although this examination is often subjective. An objective procedure related to folding is least-squares fitting of sine waves of various periods to the data (Scargle, 1982). Another approach is periodogram analysis (Scargle 1982).

Periodogram analysis technique was used in the current study. Periodogram, a basic tool for spectral analysis is the discrete Fourier transform (DFT) which is defined for an arbitrary sampled data, $\{X(t_i), i = 1, 2, \ldots . N_o\}$, as:

$$FT_x = \sum_{j=1}^{N_o}(t_j)\ exp\ (-i\omega t) \qquad \text{Equation (3.15)}$$

The periodogram is then defined as:

$$P_x = \frac{1}{N_o}|FT_x(\omega)|^2 = \frac{1}{N}\left|\sum_{j=1}^{N_o} Xt_i \exp(-i\omega tj)\right|^2 \quad \text{Equation (3.16)}$$

$$= \frac{1}{N_o}\left[\left(\sum X_j Cos\omega t_j\right)^2 + \left(\sum X_j\, Sin\omega t_j\right)^2\right] \quad \text{Equation (3.17)}$$

This function is referred to as the classical periodogram and it can be evaluated for any value of the frequency. The reason for using the periodogram was that if X contains a sinusoidal component of frequency ω_0, then at and near $\omega = \omega_0$, the factors X (t) and exp(-iωt) are in phase and make a large contribution to the sums in Equation (3.17). At other values of ω the terms in the sums are randomly positive and negative and the resulting cancellation yields a small sum. Hence the presence of a sinusoid is indicated by a large value of P near one value of ω, i.e. as a distinct narrow peak in the spectrum. If the observation times are evenly spaced (as in this study), at interval Δt, it is customary to take $\Delta t = 1$, $t = j$, and $X_j = X(T_j)$, so that

$$P_x(\omega) = \frac{1}{N_o}\left[\sum_{j=1}^{N_0} X_j \exp(-ij\omega\right]^2 \quad \text{Equation (3.18)}$$

While this expression can also be evaluated at any frequency, it was traditionally evaluated at a special set of $N = {}^{N_o}/_{2}$ evenly spaced frequencies.

(ii) Wavelet Analysis for periodicity detection

A wavelet Ψ (t) is a complex-valued square integrable function generated by functions of the form:

$$\Psi_{(u,\ s)}(t) = \frac{\Psi\left(\frac{t-u}{s}\right)}{\sqrt{s}} \quad \text{Equation (3.19)}$$

with scale *s* and location *u* at time t. Given the admissibility condition, any time series can be re-constructed back from its wavelet transform. A wavelet has zero mean and is standardly normalized so that $\int_{-\infty}^{\infty} \Psi(\mathrm{t})dt = 0$, and $\int_{-\infty}^{\infty} |\Psi|^2(\mathrm{t})dt = 1$. A continuous

wavelet transform W_x (u, s) is obtained via the projection of a wavelet Ψ (.) on the examined series x (t) so that $W_{xy}(u, s = \int_{-\infty}^{\infty} x(t) \frac{\Psi^*\left(\frac{t-u}{s}\right)}{\sqrt{s}} dt$ Equation (3.20)

Where Ψ^* is a complex conjugate of Ψ (.). The original series is re-constructed from the continuous wavelet transform for given frequencies so that there is no information loss. From a wide range of complex valued wavelets that allow for a multivariate analysis, Morlet wavelet provides a good balance between time and frequency localization (Grinsted *et al*., 2004). The Morlet wavelet was used in this study.

The wavelet transform is most easily understood when compared with the more commonly used Fourier transform. The Fourier transform breaks up a signal into sine waves and expresses a signal in terms of the frequency (x) and power (y) of its constituent sine waves, without reference to when the frequencies occur. Localization in time is achieved with the Fourier transform by transforming the data within a specified window of time and shifting this window along the time series according to Lafreniere and Sharp (2003). However, in this case the window length has to remain fixed regardless of the frequency. The wavelet transform addresses this problem by breaking up a signal into scaled versions of a wavelet function, where the scale of the wavelet (window) varies with frequency. Thus, the wavelet is narrow in time at high frequencies and the scale of the wavelet increases with decreasing frequency. The wavelet transform therefore, expresses a time series in three-dimensional space: time (x), scale/frequency (y) and power (z). In the current study, the continuous wavelet transform was used to analyze for periodicity. The mother wavelet designed to oscillate like a wave, is required to span an area that sums to zero and dies out rapidly to zero as t tends to infinity to satisfy the admissibility condition, i.e.

$\int \Psi(t)dt = 0 \qquad (t \longrightarrow \infty)$ Equation (3.21)

The Morlet wavelet (with the non-dimensional frequency w_0 = 6), was used since its nature is similar to that of a hydrologic time series as given in Equation 3.21 (Torrence and Compo, 1998). Examples of other wavelet functions include the Paul, Mexican hat and derivative of Gaussian (DOG), their details given in Torrence and Compo (1998).

$$\Psi(t) = \pi^{-1/4} e^{\omega_0 it} e^{-t^2/2} \qquad \text{Equation (3.22)}$$

Where $\Psi(t)$ is the wavelet value at non-dimensional time (t) and w_0 is the non-dimensional frequency in order to satisfy the admissibility condition, which means the function must have zero mean and must be localized in both time and frequency space to be admissible as a wavelet (Torrence and Compo, 1998).

The continuous wavelet transform W_n (u, s) of a discrete sequence of observations x_n is defined as the convolution of x_n with a scaled and translated wavelet $\psi(\eta)$ that depends on a non-dimensional time parameter η

$$W_n(u,s) = \sum_{n'=0}^{N-1} \psi\, x_n * \left[\frac{(n'-n)\delta t}{s}\right] \qquad Equation\ (3.23)$$

Where n is the localized time index, n' is the final point in the time series, s is the wavelet scale, δt is the time step (sampling period), N is the number of points in the time series and the asterisk indicates the complex conjugate. Since complex wavelets lead to complex continuous wavelet transform, the wavelet power spectrum, defined as,$|W_n(u,s)|^2$ is a convenient description of the fluctuation of the variance at different frequencies (Torrence and Compo, 1998). Also note that the non-dimensional parameter η does not appear in the scaled wavelet.

Further, when normalized by σ^{-2} (where σ^2 is the variance) it gives a measure of the power relative to white noise (white noise refers to where the constant power and frequency) since the expectation value for a white noise process is σ^{-2} at all n and s. Normalization is carried out in order to ensure that the wavelet transforms at each scale s are directly comparable to each other and to the transforms of other time series. The wavelet function at each scale s is therefore normalized to have unit energy. To determine significance levels for wavelet spectrum, an appropriate background spectrum was chosen.

For many geophysical phenomena, an appropriate background spectrum is either white noise (with a flat Fourier spectrum) or red noise (increasing power with decreasing frequency) (Torrence and Compo, 1998). It has been shown on average that the local wavelet power spectrum is identical to the Fourier power spectrum given by:

$$P_k = \frac{1 - \alpha^2}{1 + \alpha^2 - 2\alpha \cos\left(\frac{2\pi k}{N}\right)} \qquad Equation\ (3.24)$$

Where $k = 0.....N/2$ is the frequency index, N is the number of points in the time series. By choosing an appropriate lag-1 autocorrelation, Equation (3.24) can be used to model a red-noise spectrum. If $\alpha = 0$ in Equation (3.24) then it models a white noise spectrum. In the current study, the Morlet wavelet was used to study rainfall and streamflow in the Nyando River basin.

If x_n is a normally distributed random variable, then both the real and imaginary parts of $\hat{x}_k$ are normally distributed (Torrence and Compo, 1998). Hence $|\hat{x}_k|^2$ is Chi-square distributed with two degrees of freedom, denoted by χ^2_2 where the subscript 2 denotes 2 degrees of freedom (Watts *et al*., 1968). In order to determine the 95% confidence level, the background spectrum (Equation 3.20) is multiplied by the 95th percentile value of

χ_2^2 (Gilman *et al.*, 1963). The confidence interval at each scale is then used to construct confidence contours.

(i) Cross Wavelet Transform (CWT)

Wavelet analysis was performed to study temporal correlations between two selected time series x and y. The selected series were of rainfall/rainfall, rainfall/streamflow, zone I/Zone I, Zone II/Zone II and Zone I/zone II. The cross wavelet analysis generated cross wavelet transform (CWT) as:

$$W_{xy}(u,s) = W_x(u,s)W_y^*(u,s) \qquad \text{Equation (3.25)}$$

Where $W_x(u,s)$and $W_y(u,s)$ are continuous wavelet transforms of series x(t) and y(t), respectively.

As the cross wavelet transform is in general complex, the cross wavelet power $|W_{xy}(u,s|$ is usually used as a measure of the co-movement between the two series. The cross-wavelet power uncovers regions in the time frequency space where the series have common high power, and it can be thus understood as a covariance localized in time-frequency space. However, as for the standard covariance, the explanation power of $W_{xy}(u,s)$ is limited because it is not bound.

(iii) Wavelet Transform Coherence (WTC)

To resolve the challenge of limited power, coherence analysis was performed

$$R_{xy}^2 = \frac{|S(S^{-1}W_{xy}(u,s)|^2}{S\left(S^{-1}|W_{xy}(u,s|^2\right)S\left(S^{-1}|W_y(u,s|^2\right)} \qquad \text{Equation (3.26)}$$

Where S is a smoothing operator (Grinsted *et al*., 2004). The squared wavelet coherence ranges between 0 and 1. And it can be interpreted as a squared correlation localized in time and frequency. Due to the above mentioned complexity of the used wavelets in turn, the use of the squared coherence rather than coherence itself, information about

the direction of the relationship is lost. For this purpose, a phase difference is introduced as:

$$\varphi_{xy\,(u,s)} = Tan^{-1}\left\{\frac{\Im\left(S\left[\frac{W_x(u,s)}{s}\right]\right)}{\Re\left(S\left|\frac{W_{xy}(u,s)}{s}\right|\right)}\right\} \qquad \text{Equation (3.27)}$$

Where $\Im$ and $\Re$ represent an imaginary and a real part operator, respectively.

Graphically, the phase difference is represented by an arrow. If the arrow points to the right (left), the series are positively (negatively) correlated, i.e., they are in the in-phase or the anti-phase respectively, and if the arrow points to the northeast, the series are positively correlated and the second series leads the first. The interpretation of phase relationship is particularly dependent on specific expectations about the relationships because leading relationships in the anti-phase can easily be a lagging relationship in the anti-phase (Grinsted, 2004). The statistical significance level of the wavelet coherence is estimated using Monte Carlo methods. A large ensemble of surrogate data set pairs with the same AR1 coefficients as the input data sets is generated. For each pair, the wavelet coherence is calculated and then the significance level for each scale is estimated using only values outside the COI.

In this study cross wavelet transform (CWT) and wavelet transform coherence (WTC) were performed to establish linkages between some selected rainfall and streamflow time series. The CWT and WTC were performed between rainfall and streamflow of MAM, JJA and OND seasonal time series in order to examine the relationships between the rainfalls and their corresponding streamflow. Further tests were also done for March rainfall against April streamflow, June rainfall against July streamflow and October rainfall against November streamflow for all the years considered.

3.3.5 Regional frequency analysis

Regional frequency analysis has been performed in the current study using L-Moment in determining the best probability distribution for floods in Nyando River basin. Annual maximum peak rainfall and streamflow data from 10 rainfall and 8 streamflow stations, were analysed. The rainfall data had a range of 31-105 years and streamflow had a data range of 30-46 years in length.

a) L- Moments

L-moments method, proposed by Hosking and Wallis (1997; 1993) is based on probability weighted moments (PWM). The most important feature of L-moments method is that it is not so sensitive to the maximum and minimum values compared to ordinary moments. In this study, L-moments method was used to estimate the parameters of considered statistical models. Probability Weighted Moments defined by Dhorde and Zarenistanak (2014) are the precursors of L-moments. For a given sample $x_1, x_2, x_{3,\leq}\ldots x_n$ arranged in ascending order, let $x_{1,n} \leq x_{2,n} \leq \ldots \leq x_n$ denote the order statistics of this series. According to the definition of L-moments, the first four order L-moments according to Xiong and Guo (2004) are:

$$l_1 = b_0 \quad \text{Equation (3.28)}$$

$$l_2 = 2b_1 - b_0 \quad \text{Equation (3.29)}$$

$$l_3 = 6b_2 - 6b_1 + b_0 \quad \text{Equation (3.30)}$$

$$l_4 = 20b_3 - 30b_2 + 12b_1 - b_1 \quad \text{Equation (3.31)}$$

Where,

$$b_0 = \frac{1}{n}\sum_{j=2}^{n} x_{j,n}\,, b_1 = \frac{1}{n}\sum_{j=2}^{n} \frac{j-1}{n-1} x_{j,n}\,, b_2 = \frac{1}{n}\sum_{j=3}^{n} \frac{(j-1)(j-2)}{(n-1)(n-2)} x_{j,n} \quad \text{Equation (3.32)}$$

$$b_3 = \frac{1}{n}\sum_{j-4}^{n} \frac{(j-1)(j-2)(j-3)}{(n-1)(n-2)(n-3)} x_{j,n} \quad \text{Equation (3.33)}$$

The first L-moment (l_1) is the measure of mean which measures the central tendency, second L-moment (l_2) is the standard deviation, a measure of dispersion. Third and fourth L-moments are $l_3$and l_4 respectively. L-moment ratios such as L-CV, L-Skewness and L-Kurtosis are defined as follows:

L-Coefficient of Variation (L-CV), (t) =$\frac{l_1}{l_2}$, L-Coefficient of Skewness (L-Skewness), (t_3) =$\frac{l_3}{l_2}$, L-Coefficient of Kurtosis (L-Kurtosis), (t_4) =$\frac{l_4}{l_2}$, L-Skewness (t_3) is a measure of degree of symmetry of a sample. The symmetric distributions have t_3 = 0 and its value lies between -1 and +1. L-Kurtosis (t_4) is a measure of peakedness or the flatness of the frequency distributions near its centre.

After the calculation of the L-moments for each gauging site, Regional L-moments were computed by taking the weighted average of the L-moments of the group of gauging sites.

Where, n(i) is the record length of ith site, N is the total number of sites:

Regional $l_1 = \sum_i^N n_{(i)} l_1^{(i)} / \sum_{i=1}^N n_{(i)}$ Equation (3.34)

Regional $l_2 = \sum_i^N n_i l_2^{(i)} / \sum_{i=1}^N n_i$ Equation (3.35)

Regional $l_3 = \sum_i^N n_i\, l_3^{(i)} / \sum_{i=1}^N n_i$ Equation (3.36)

Regional $l_4 = \sum_i^N n_i\, l_4^{(i)} / \sum_{i=1}^N n_i$ Equation (3.37)

b) Procedure for regional frequency analysis

Regional frequency analysis in this study involved four stages according to the methodology summarized in Hosking and Wallis (1997) as; performing discordancy measure (Di) tests to check and eliminate discordant sites; performing heterogeneity measure (H) tests to delineate homogeneous zones; performing goodness-of-fit (Z) measure tests to select frequency distribution, and estimating the Parameter of the regional frequency distribution.

(i) Discordancy (D_i) Measure

The aim of the regional frequency analysis was to select the best fit frequency. Therefore the first step involved checking that the data were suited for the analysis. Discordancy measure was done to screen out any data from the sites whose sample L-moments could have been markedly different from the other sites. Hosking & Wallis (1997) defined the discordancy measure (D_i) considering the presence of N sites in the group. The discordancy measure for site 'i' was defined as:

$$D_i = \frac{1}{3}\lceil (u_i - \bar{u})^T (u_i - \bar{u}) S^{-1} \rceil \quad \text{Equation (3.38)}$$

Where $\boldsymbol{u_i} = \left[\boldsymbol{L_{cv}^{(i)}} \boldsymbol{L_{skew}^{(i)}} \boldsymbol{L_{kur}^{(i)}}\right]^{\boldsymbol{T}}$ is a vector containing the three sample LMRs values for site i, $\boldsymbol{\bar{u}}$ is the vector containing the un-weighted average LMRs and T denotes transposition of a vector or matrix

$$\bar{u} = N^{-1} \sum_{i=1}^{N} u_i \quad \text{Equation (3.39)}$$

And S is the sample covariance matrix (matrix of sums of squares and cross products) expressed by:

$$S = (N-1)^{-1} \sum_{i=1}^{N} (u_i - \bar{u})\,(u_i - \bar{u})^T \quad \text{Equation (3.40)}$$

Generally, a site is discordant from the group as a whole if D_i is greater than a critical value that usually depends on the number of stations in the group (Hosking & Wallis, 1997). The same authors tentatively suggest $D_i \geq 3$ as a criterion for declaring a site to be discordant.

(ii) Heterogeneity (H) Measure

The second step was carried out to detect presence of heterogeneity in the data. Hosking & Wallis (1997) proposed a heterogeneity measure (H) for the identification of a homogeneous region using L-moment statistics. A heterogeneity statistic, H, is a measure of the departure of V from similar statistics obtained from the simulation of a

large number of realizations for a region with N sites. The weighted standard deviation of an L-moment ratio in a homogeneous region was calculated by the formula:

$$H = \frac{V-\mu_v}{\delta_v} \qquad \text{Equation (3.41)}$$

Where μ_v and δ_v are the mean and the standard deviation respectively, of the values of V obtained from simulations, while V is calculated from the regional data and is based on a corresponding V-statistic defined as follows:

$$V = \left[\sum_{i=1}^{N} N_i \left(t^{(i)} - t^2\right)^2 \Big/ \sum_{i=1}^{N} n_i\right]^{1/2} \qquad \text{Equation (3.42)}$$

Where N is the number of sites, n_i is the record length at site i, $t^{(i)}$ is the sample L-cv. For this study and in order to obtain reliable values of μ_v and δ_v, five hundred simulations were carried out using four parameter Kappa distributions for computing the measure of homogeneity (Hosking and Wallis, 1997).

The quantile function of the distribution was given by:

$$Q(F) = \zeta + \alpha\left\{1 - \left[\frac{(1-F^h)}{h}\right]^k\right\}/k \qquad \text{Equation (3.43)}$$

Where F is the probability and Q(F) is the flood quantiles. ζ, α, k and h are parameters of the distribution. It includes as special cases the generalized logistic (h= -1), Generalized extreme–value (h→0) and generalized Pareto (h= +1) distributions. Its L-moments were chosen to match the group average L-cv, L-skewness and L-kurtosis of the observed data using an algorithm from Hosking (1990). The H criteria established by Hosking & Wallis (1993) indicate that the region is acceptably homogeneous if $H < 1$, possibly heterogeneous if $1 \leq H < 2$ and definitely heterogeneous if $H \geq 2$.

(iii) Goodness-of-Fit Test

In the third step, the goodness-of-fit was computed. Given a set of sites that constitute a homogeneous region, the aim was to test whether a given distribution adequately fits the

data closely for regional frequency analysis. A related aim was to choose from a number of candidate distributions, the ones that approximate the best fit to the data. The L-moments of the sites in a homogeneous region are well summarized by the regional average; the scatter of the individual sites' L-moments about the regional averages no more than sampling variability. The distributions being tested have location and scale parameters which were chosen to match the regional average mean and L-cv. The goodness-of-fit was therefore judged by how well the L-skewness and L-kurtosis of the fitted distribution matched the regional average L-skewness and L-kurtosis of the observed data.

The GEV distribution fitted by the method of L-moments has L-skewness equal to the regional average difference between the L-kurtosis τ_4^{GEV} of the fitted GEV distribution and the regional average Lkurtosis $\bar{\tau}_4$. In order to assess the significance of this difference, it was compared with the sampling variability of $\bar{\tau}_4$. By Letting δ_4 denote the standard deviation of $\bar{\tau}_4$ which were obtained by repeated simulation of a homogeneous region with a GEV frequency distribution and sites having record lengths the same as those of observed data, then

$$Z^{GEV} = (\bar{\tau}_4 - \tau_4^{GEV})/\delta_4 \qquad \text{Equation (3.44)}$$

is a goodness-of-fit measure: Small values of Z^{GEV} are consistent with the GEV being the true underlying frequency distribution for the region.

It was assumed that δ_4 is the same for all of the three- parameter candidate distributions; this is reasonable because all of the fitted distributions have the same L-skewness and are therefore likely to resemble each other to a large extent. Given this assumption, it was also assumed that the best fitting kappa distribution has a δ_4 value close to those of the candidate distributions as δ_4 was obtained by repeated simulations of the Kappa

distribution. Those simulations were the same ones used in the calculation of the heterogeneity measure described above.

According to Hosking and Wallis (1997) the goodness of fit- test for each of various distributions is defined in terms of L-moments and is termed the Z- statistic:

$$Z^{DIST} = \left(\tau_4^{DIST} - \bar{\tau}_4 + \beta_4\right) \Big/ \delta_4 \qquad \text{Equation (3.45)}$$

Where τ_4^{DIST} is L-kurtosis of the fitted distribution, $\bar{\tau}_4$ is the weighted regional average L-kurtosis, β_4 is bias of the $\bar{\tau}_4$, and δ_4 is the standard deviation of the $\bar{\tau}_4$ obtained from simulation. The bias (β_4) and standard deviation (δ_4) of the $\bar{\tau}_4$ respectively, defined as:

$$\beta_4 = \frac{1}{N_{sim}} \sum_{m=1}^{Nsim} (\bar{\tau}_4{}^m - \bar{\tau}_4) \qquad \text{Equation (3.46)}$$

$$\beta_4 = \left[\frac{1}{N_{sim}} \left\{\sum_{i=1}^{N_{sim}} (\bar{\tau}_4{}^m - \bar{\tau}_4) - N_{sim}\beta_4\right\}^{1/2}\right] \qquad \text{Equation (3.47)}$$

Where $\bar{\tau}_4{}^m$ the regional average L-kurtosis and is to be calculated for the mth simulated region. N_{sim} is the number of simulated regional data sets generated using a kappa distribution.

The L-moment ratio diagrams were derived and used in this study to compare the L-skewness against L-kurtosis relations of different distributions and data samples. The aim was to give a visual indication of which distribution may be expected to give a good fit to a data points (at-site values) by plotting them on a graph of L-skewness verses L-kurtosis. The distributions considered include: Generalized Logistics (GLO), Generalized extreme value (GEV), Generalized Pareto (GPA), Generalized Normal (GNO) and Pearson Type III (PE3).

3.4 Summary of Methodology

The summary steps involved in the current study are summarized in the following sequence:

1. The boundary for the Nyando River basin was delineated using the Hydrology Tool in ArcGIS 16.0.

The appropriate rainfall and streamflow gauging stations which fell within the boundaries were selected. In this selection, some rainfall stations e.g. Kericho Met, Kericho Water Office and Finlay rainfall stations fell slightly outside the boundary but their areas of influence overlapped inside the delineated boundaries. The stated stations drain through the Sondu Miriu River basin. Data from the selected stations were sourced from the Water Resources Authority (WRA**)**, Kenya Meteorological Department (KMD) and Finlay Kenya Limited.

2. Preliminary tests were done to check for data gaps, homogeneity, normality and independence of streamflow data prior to Trend, Periodicity and Frequency analysis.
3. Trend was tested in this study using M-K and Discrete Wavelet techniques while Periodicity was tested using Spectral and Continuous Wavelet Techniques in Matlab.
4. L-Moment method in R-Studio was applied in the Regional Frequency Analysis.

CHAPTER FOUR

RESULTS AND DISCUSSIONS

4.1 Introduction

This chapter presents the analysis and discussions on the study findings. The presentations include results for homogeneity, normality, independence, trend, periodicity and frequency analysis.

4.2 Rainfall and streamflow data quality analysis

Data quality analysis was carried out by examining the missing data gaps and data characteristics. Additional tests were done for homogeneity, normality and independence of the data series.

4.2.1 Percentage missing data

Table 3.1 and Table 3.2 contain the percentage data gaps for the rainfall and streamflow series, respectively. The percentage gaps were less than 10% and data was therefore considered suitable according to WMO (2018).

4.2.2 Rainfall and streamflow data characteristics

Descriptive statistics were computed in this study for rainfall and streamflow time series and are presented in subsequent sub sections.

(i) Rainfall data characteristics

A summary of the descriptive statistics for rainfall data series used in this study are indicated in Table 4.1. The highest mean annual rainfall of 2,193 mm/year was observed at Timbilil station, with Londiani Forest station recording the lowest rainfall value of 1,086 mm/year. In general, the highland stations (e.g. Kericho Met, Kericho water and Finlay) received more rainfall than stations in the plateau (Kipkelion and Londiani) and the lowland stations (e.g. Ahero and Chemelil). Table 4.1 shows the station names and

their codes, annual mean, standard deviation, maximum and minimum rainfalls for Nyando River basin.

Table 4.1: Nyando Annual Rainfall characteristics

S/N	S/Code	S/ Name	Mean (mm/year)	Std. dev (mm/year)	Max (mm/year)	Min (mm/year)
1	9034086	Ahero	1,253	331	3029	883
2	8935013	Nandi Tea	1,491	233	1879	952
3	9035188	Tinga M.	1,359	248	1763	927
4	9035003	Kericho W	1,860	291	2498	1256
5	9035258	Kipkelion	1,333	247	1750	906
6	9035226	Londiani	1,086	265	1520	164
7	9035341	Finlay	1,976	329	2693	1167
8	9035244	Timbilil	2,193	747	5753	698
9	9034087	Chemelil S	1,486	208	1835	1106
10	9035279	Kericho Met	2,022	276	2719	1747

From Table 4.1, it is seen that the standard deviations vary from 208 mm/year at Chemelil to 746.8 mm/year at Timbilil. The results showed that the spread from the mean was fairly large implying high rainfall variability.

(ii) Streamflow data characteristics

Table 4.2 indicates a summary of the descriptive statistics for stream flow data series used in this study. Nyando station recorded the highest mean annual stream flow of 3,467 m^3/s whereas the lowest mean streamflow of 112 m^3/s was observed at Tugenon river gauging station. Table 4.2 presents streamflow characteristics for Nyando River basin. Table 4.2 shows the station names and their codes, annual mean, standard deviation, maximum and minimum streamflow for Nyando River basin.

Table 4.2: Nyando Annual Streamflow characteristics

S/No	Station Code	S/ Name	Mean (m^3/s)	Std. dev (m^3/s)	Max (m^3/s)	Min (m^3/s)
1	1GC06	Nyando Kericho	616.19	294.77	1248.26	55.36
2	1GD07	Nyando Kisumu	2392.47	163.42	7351.33	783.52
3	1GB05	Ainamotua	1362.52	961.39	3855.76	57.54
4	1GB06	Mbogo	311.14	327.61	1217.53	29.92
5	1GB11	Ainopsiwa	624.69	633.53	3342.14	45.11
6	1GC05	Masaita	957.66	938.87	1538.16	116.43
7	1GD04	Nyando	3466.90	237.60	11893.21	632.78
8	1GC04	Tugenon	112.41	63.25	282.82	22.04

Based on Table 4.2, the standard deviation varied from the lowest of 63.2 m^3/s at Tugenon station to the highest of 961.39 m^3/s at Ainamotua River gauging station.

4.2.3 Results of homogeneity tests

In order to properly ascertain the homogenic conditions of the data prior to application, three-way approach was used in the current study. As presented in Chapter Three, SNHT, BR and Pettitt tests were all used to compute the *p*-values. In each of the tests, the null hypothesis was rejected for *p*-value less than the significant level of 0.05. The result was considered heterogeneous if the series failed in all the three tests. Results of rainfall homogeneity tests are contained in Appendix 3A. Figure 4.1 shows the variation of the test statistical *p*-values for rainfall.

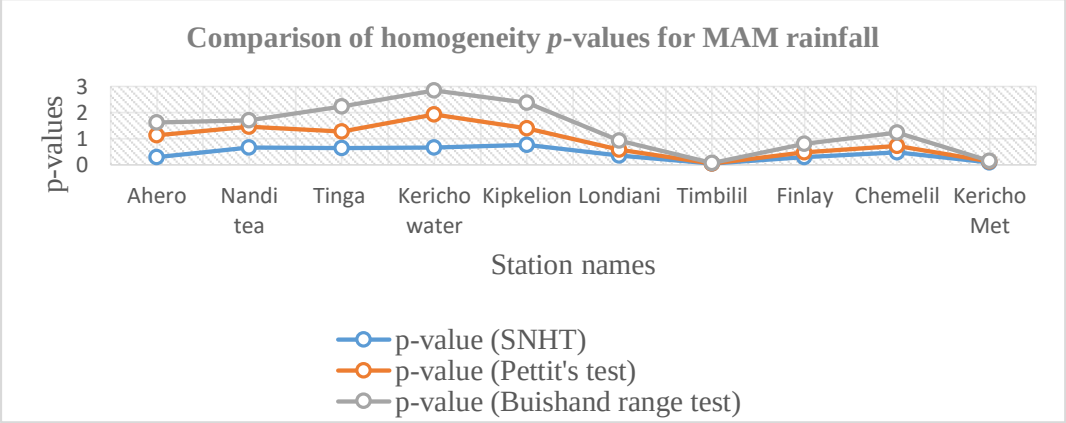

Figure 4.1: (a) Homogeneity plots for MAM rainfall.

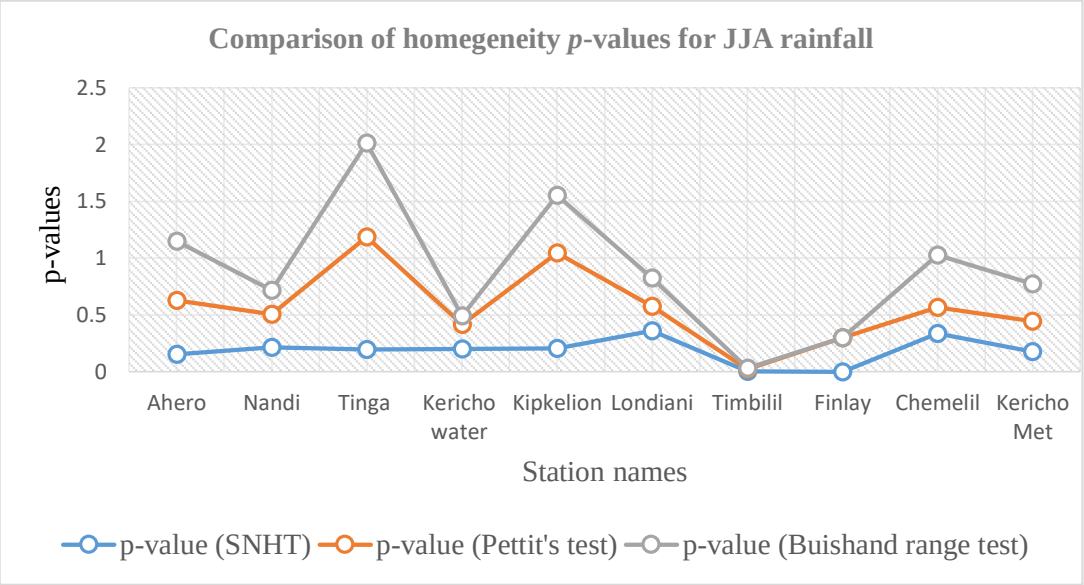

Figure 4.1: (b) Homogeneity plots for JJA rainfall.

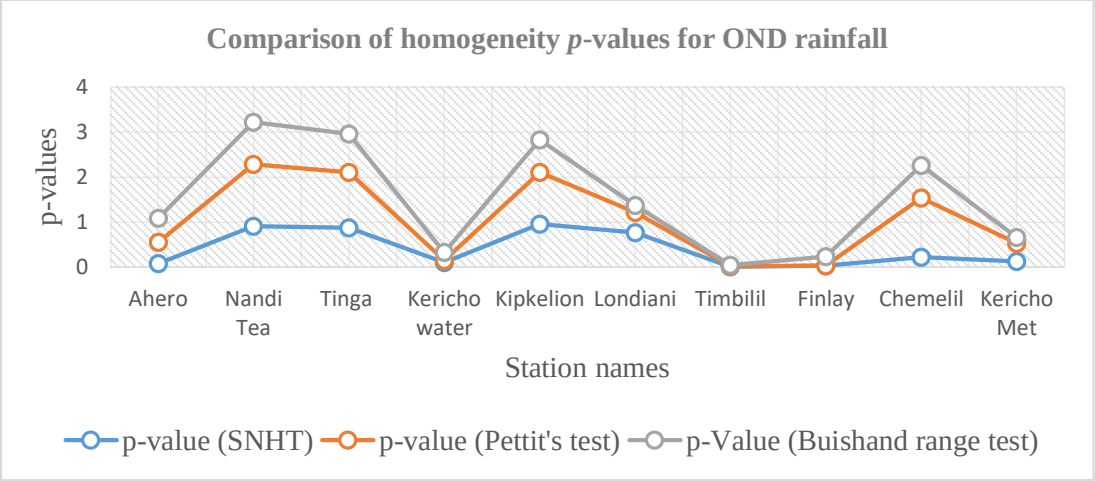

Figure 4.1: (c) Homogeneity plots for OND rainfall.

Figure 4.1(a, b & c) shows the variation of the homogeneity *p*-values for rainfall, obtained using SNHT, Pettit's and Buishand Range tests. For the MAM series indicated in Figure 4.1 (a), Pettit test shows highest *p*-value for Kericho water but indicates lower *p*-values in all the other stations. Buishand range test generally shows highest *p*-values and compares well with SNHT values in most of the rainfall stations. For JJA and OND results shown in Figure 4.1 (b) and (c), Pettit test indicate highest *p*-values followed by Buishand range test, SNHT maintains the lowest *p*-values. From the results, Pettit and BR tests revealed more homogeneity than SNHT.

According to Toreti *et al*. (2011), SHNT detects breaks more easily at the beginning and at the end of a climate series whereas BR and Pettit tests are more sensitive to breaks located in the middle of the series. It was therefore concluded from the results that the Nyando rainfall series had more breaks in the middle than at the beginning and the ends. The results of homogeneity test as contained in Appendix 3A revealed that only Timbilil station was heterogeneous in all the seasons but was still used in the frequency analysis since the analysis was based on annual maximum series. Kericho Met was heterogeneous only in MAM series. Although JJA series at Finlay station was heterogeneous by SNHT and BR, the series were still considered homogeneous, having been accepted by Pettit's test. Similarly, the other data series were all homogeneous since the null hypothesis for at least one of the three (SNHT, BR and Pettit's) tests were not rejected at 5% level of significance.

From the results, it was concluded that the rainfall data for the Nyando River basin were homogeneous and could therefore successfully be used in hydrometeorological analysis. According to Ogallo (1979), heterogeneity may arise as a result of changes in the site, height or exposure of rain gauges which may make the rainfall values before and after these changes not comparable. Ogallo (1979) observed that some of the very old stations may have been affected by one or more of such changes. The results for change point analysis are summarized in Table 4.3 with full results contained in Appendix 4 (A & B). From Table 4.3, the change points are contained as period of years within which the observed changes were recorded and the time series of MAM, JJA and OND seasons.

In MAM time series: three stations recorded change points from 1961-1971, two stations recorded change points from 1961-1964, six stations recorded change points from 1979-1982 and three stations recorded change points from 1996-1998. In JJA: one station

recorded a change point from 1961-1971, five stations recorded change points from 1961-1964, one station recorded a change point from 1979-1982, and four stations recorded change points from 1996-1998. In OND, no station recorded change point from 1961-1971, three stations each recorded change points from 1961-1964, 1979-1982 and 1996-1998. Table 4.3 shows time series abrupt change points during different periods.

Table 4.3: Rainfall change point results

Years	MAM	JJA	OND
1961 - 1971	Nandi Tea, Londiani, Chemelil	Londiani	
1961 - 1964	Tinga Monastery, Kipkelion, Chemelil, Nandi tea, Londiani	Nandi Tea, Tinga, Monastery, Londiani, Kipkelion, Finlay	Tinga Monastery, Kipkelion, Finlay
1979 - 1982	Ahero, Tinga, Kericho Water, Kipkelion, Kericho Water	Tinga	Kericho Water, Kipkelion, Kericho Met
1996 - 1998	Ahero, Timbilil, Kericho Met, Chemelil, Nandi tea	Kericho Met, Chemelil, Kericho Water, Kipkelion	Chemelil, Kericho Water, Finlay, Kericho Met

The abrupt changes observed from 1961-1964 and 1996-1998 were attributed mainly to Indian Ocean Dipole (IOD) and the El Niño peaks respectively, which were witnessed during the particular periods. According to Tarhule and Woo (1998), non-homogeneities in climate series may be introduced by an abrupt change or (jump) superimposed on by a gradual trend or by a jump. Total annual or seasonal rainfall at a location is influenced by several variables including the frequency of rainfall events, the duration of rainy period and the intensity of rainfall of individual events. The non-homogeneities in the rainfall events therefore reflected changes in these contributory variables. Similarly, Figure 4.2 shows the variation of the *p*-values of the statistical tests in streamflow.

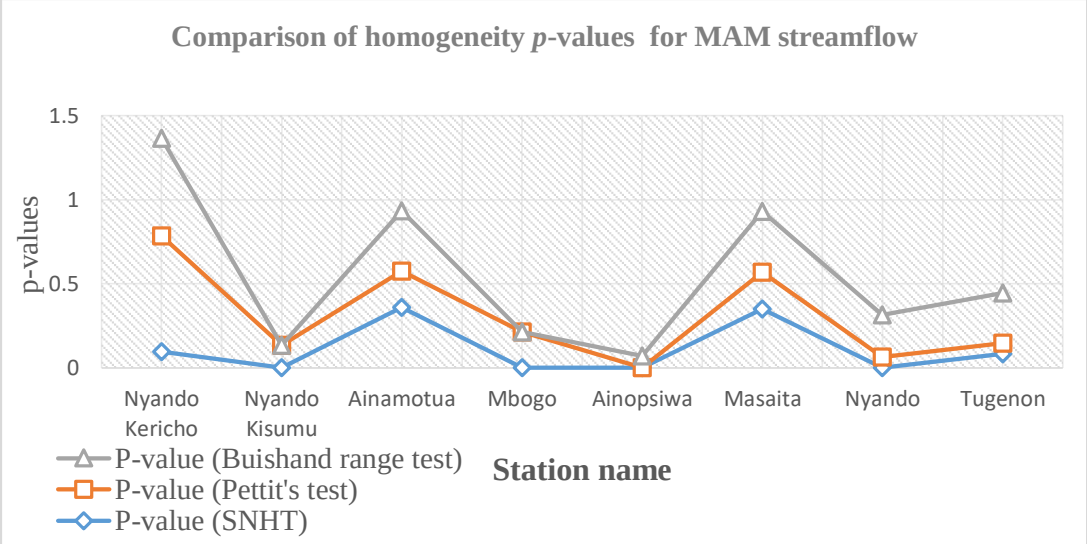

Figure 4.2: (a) Homogeneity plots for MAM streamflow.

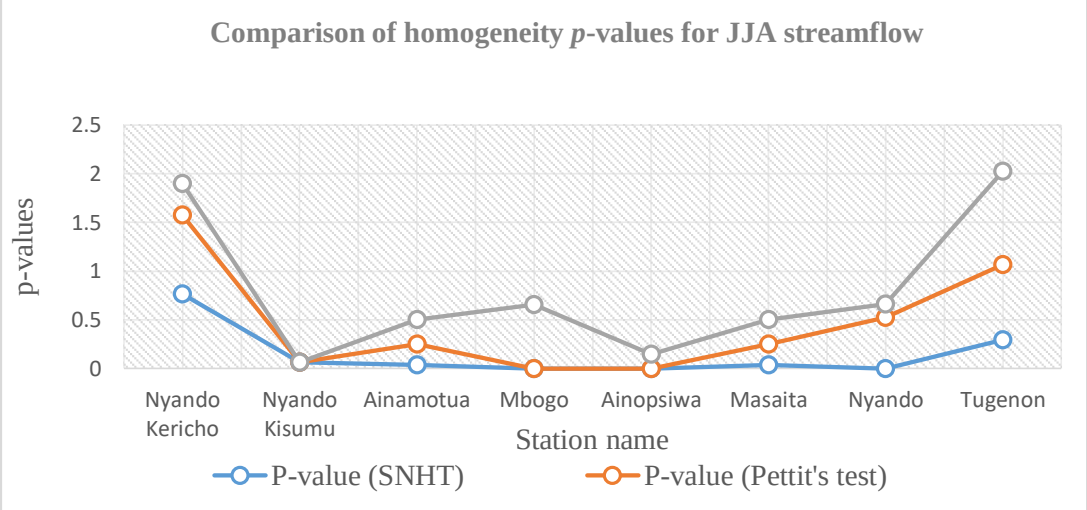

Figure 4.2: (b) Homogeneity plots for JJA streamflow.

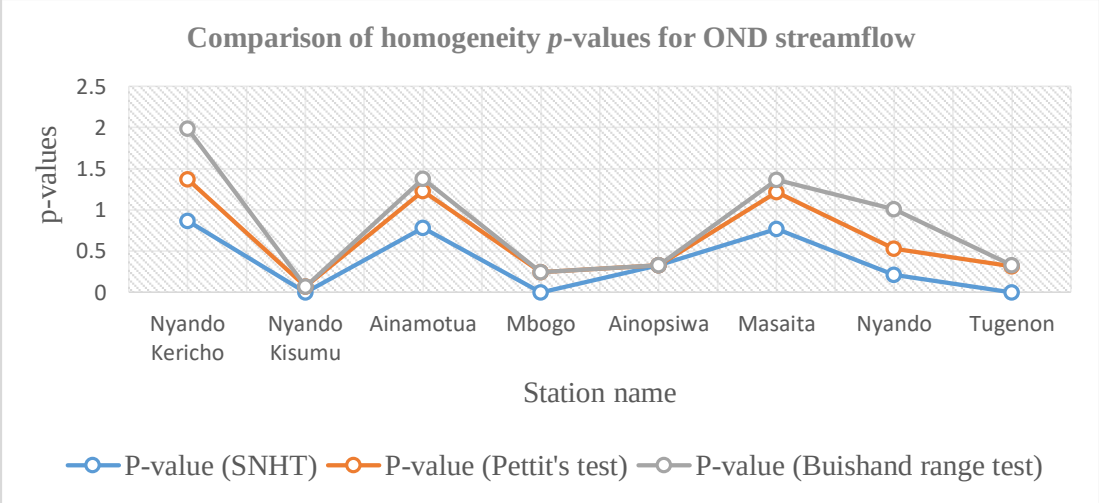

Figure 4.2 (c): Homogeneity plots for OND streamflow.

Figure 4.2 shows the variation of the homogeneity *p*-values for streamflow obtained using SNHT, Pettit's and Buishand Range tests. For the MAM and OND streamflow series indicated in Figure 4.2 (a) and (b), respectively, highest *p*-values in most streamflow stations were shown by Buishand range test followed closely by Pettit's test. For OND results shown in Figure 4.2 (c), SNHT results showed high *p*-values followed by Pettit's test. Generally, from the results, BR and Pettit's test revealed more homogeneity in MAM and JJA. SNHT showed more homogeneity only in OND.

The results for change point analysis are summarized in Table 4.4. From the results, the change points are contained as period of years within which the observed changes were recorded and the time series of MAM, JJA and OND seasons. In MAM streamflow series: two stations each recorded change points from 1961-1965, from 1983-1986, from 1991-1993 and from 1995-1998. In JJA: one station each recorded change points from 1983-1986 and 1991-1993, two stations recorded change points from 1995-1998. In OND: one station recorded a change point from 1983-1986, two stations each recorded change points from 1991-1993 and from 1995-1998.

Table 4.4: Streamflow change point results

Year	MAM	JJA	OND
1983 - 1986	Nyando-Kericho, Nyando- Kisumu	Ainopsiwa	Masaita
1991- 1993	Nyando-Kericho, Nyando-Kisumu	Ainopsiwa	Nyando-Kericho, Nyando-Kisumu, Mbogo, Ainopsiwa
1995 - 1998	Ainopsiwa, Masaita	Masaita, Tugenon	Nyando- Kisumu, Ainamotua

Appendix 3B shows the homogeneity test results for streamflow. Results of homogeneity indicate that none of the streamflow series failed in all the three tests. The

series were all homogeneous since the null hypothesis for at least one of the three (SNHT, BR and Pettit's) tests, were not rejected at 5% level of significance. Notably, the three tests (SNHT, Pettit & BR) performed competitively.

In rainfall analysis, SNHT and BR revealed heterogeneity in four and five series, respectively while Pettit revealed heterogeneities in six series spread across all the seasons almost equally. In streamflow analysis, SNHT and Pettit revealed nine and six heterogeneous series, respectively spread across all the seasons like in the rainfall series. Similar to the rainfall results, it was concluded that the streamflow data for Nyando River basin were homogeneous and were therefore suitable for use in the analysis.

Hydrological processes are always under the influence of climate change and human activity. Some particular climate phenomena such as El Niño, as well as all kinds of large scale water resource development projects, may alter hydrological process suddenly and lead to abrupt change in the hydrological time series. The impact of the IOD and El Niño episodes of 1964 and 1998 respectively, may have manifested in the abrupt changes in the rainfall and streamflow as seen from the homogeneity test results.

4.2.4 Results of normality tests

The results of the normality test using Anderson-Darling in R-software were interpreted by comparing the observed *p*-values with 0.05- the null hypothesis - then normality was either rejected or accepted. In the normality test carried out in this study, the null hypothesis was rejected if the *p*-value was less than the 5% level of significance. A significance level of 0.05 indicates that the risk of concluding the data do not follow a normal distribution-when actually the data do follow a normal distribution is 5%. Figure 4.3 shows the variance of the statistical *p*-values of the tests for rainfall.

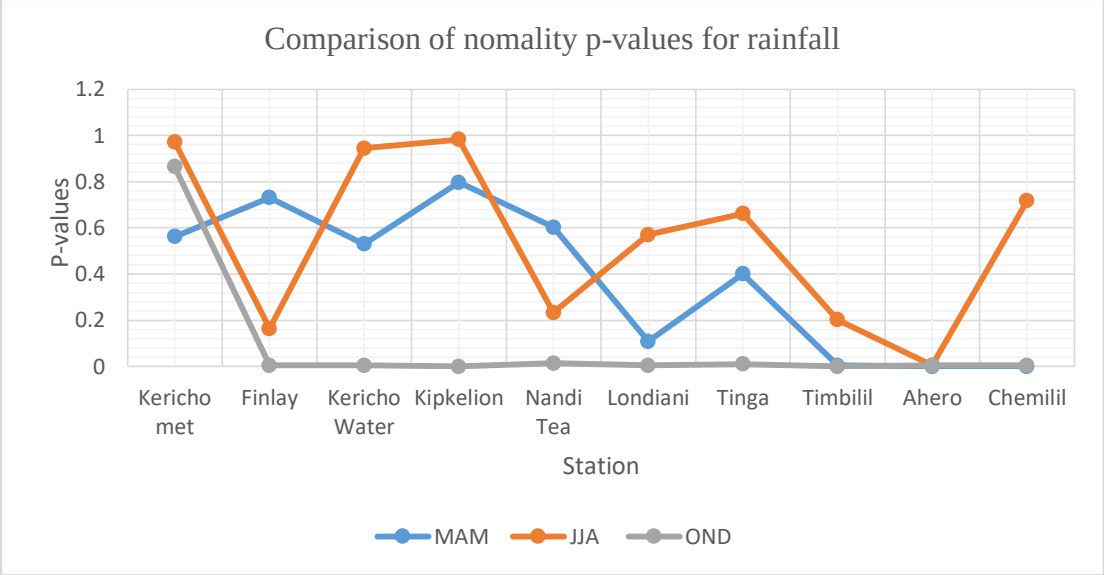

Figure 4.3: Normality plot for statistical *p*-values in rainfall.

Figure 4.3 shows the variation of the normality *p*-values for rainfall, obtained using Anderson Darling tests. Figure 4.3 shows that *p*-values in OND and JJA were higher than in MAM for most of the rainfall stations. Generally, the normality results as seen in Appendix 5A indicated that 70% of Nyando rainfall data was normally distributed and only 30% was non-normal. Further, the results indicated that the long rains of MAM were mostly normally distributed while the short rains of OND were mostly non-normal. Figure 4.4 presents the normality curves for MAM, JJA & OND at Finlay. Finlay station contained the longest data length of 100 years.

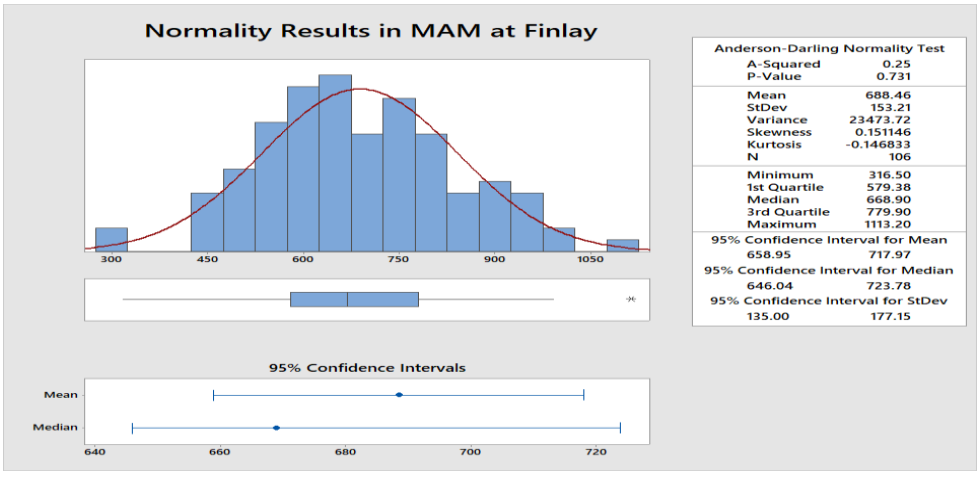

Figure 4.4: (a) Normality plot for MAM rainfall at Finlay.

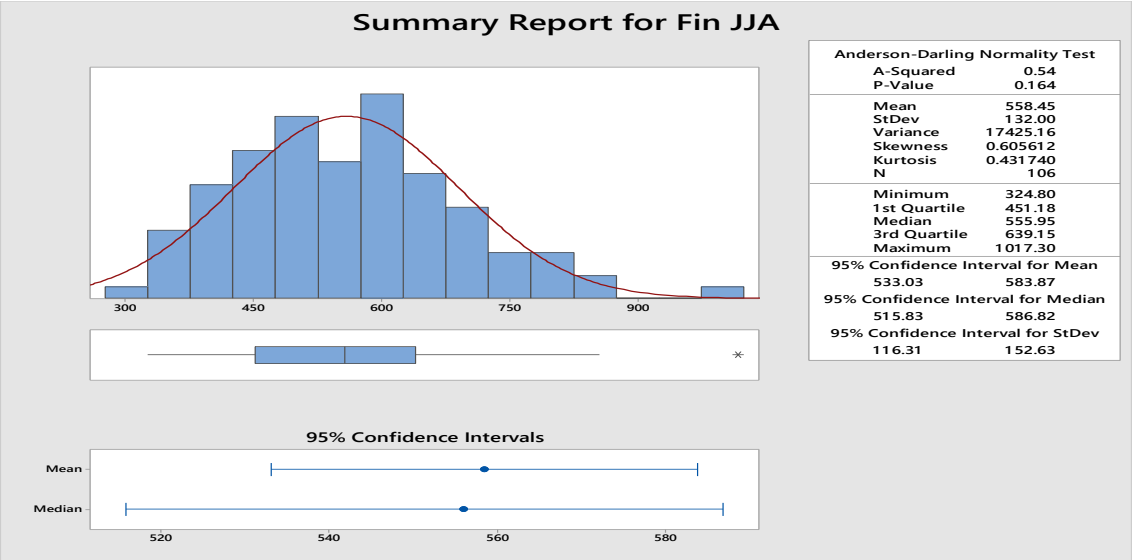

Figure 4.4: (b) Normality plot for JJA rainfall at Finlay.

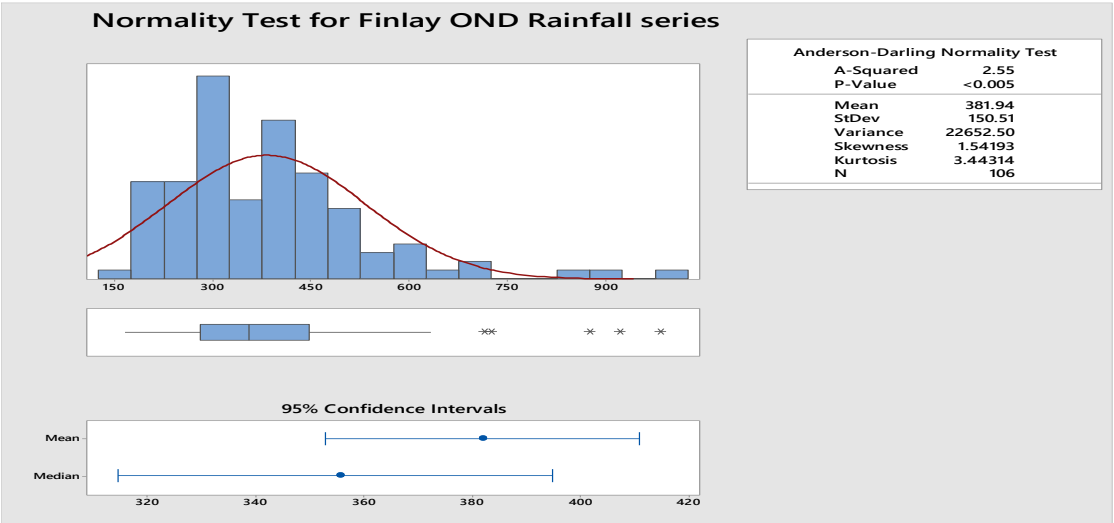

Figure 4.4: (c) Normality plot for OND rainfall at Finlay.

Figure 4.4 shows the normality curves for rainfall at Finlay station, obtained using Anderson Darling tests. The 95% confidence interval is shown for mean and median. Figure 4.4(a) presents normality result for Finlay MAM series. The *p*-value for MAM as shown in Fig 4.3 is 0.731 which is greater than 0.05- the critical value. It was therefore concluded that MAM series were normally distributed. The *p*-value for JJA series at Finlay is seen in Figure 4.4(b) as 0.164, also indicating that JJA at Finlay station

was normally distributed. Figure 4.4(c) indicates that OND series at Finlay station was not normally distributed as the *p*-value is indicated as less than 0.005. This means the *p*-value is statistically insignificant.

The normality of Nyando rainfall data observed at 70% strengthens the assumption that the data lengths considered in the current study met the sample size thresholds. According to studies done by Kirithikadata (2014), small sample size results in non-normal distribution and vice versa. This is as a result of inadequate estimation of the dispersion of the data and the frequency distribution does not result in a normal curve for the case of a small sized sample data. Non-normality observed in the OND rainfall was attributed mainly to non-stationarity of the rainfall time series. Figure 4.5 shows the variance of the statistical *p*-values of the normality tests for the streamflow.

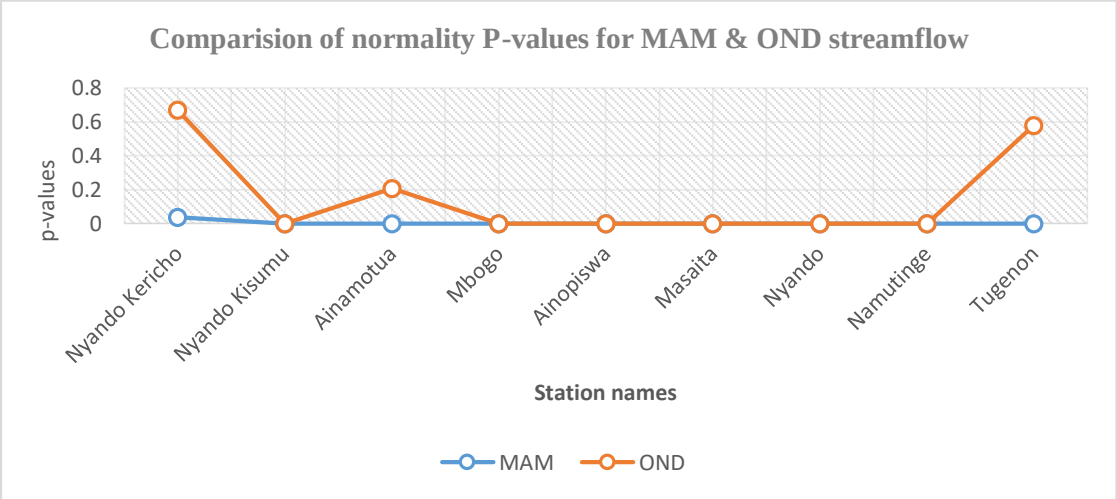

Figure 4.5: (a) Normality plot for MAM & OND statistical *p*-values in streamflow.

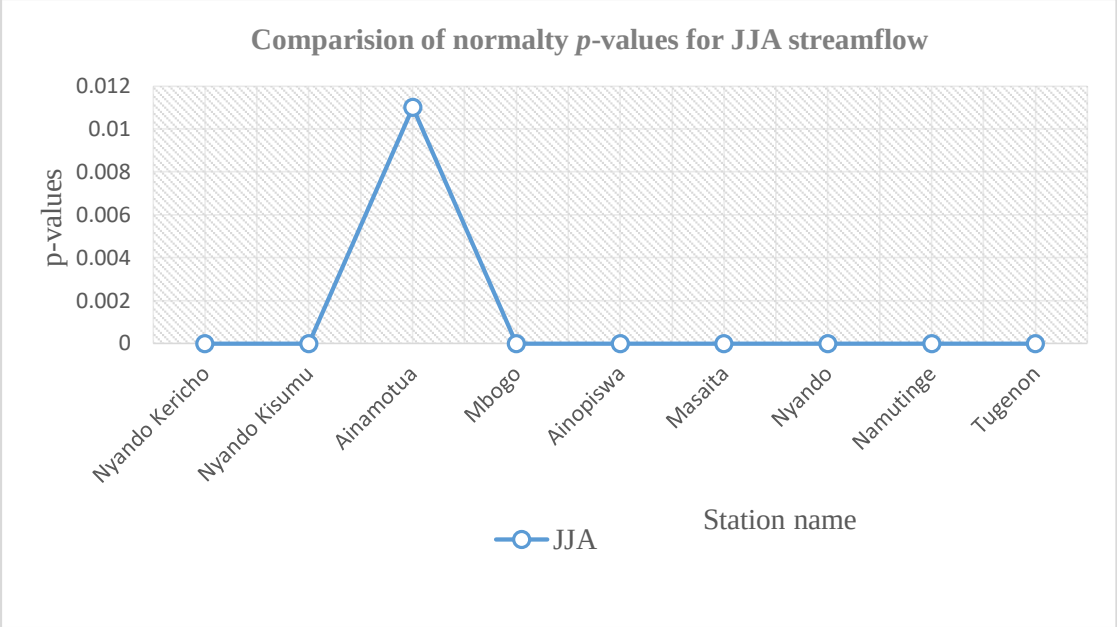

Figure 4.5: (b) Normality plot for JJA statistical *p*-values in streamflow.

Figure 4.5 shows the variation of the normality *p*-values for rainfall, obtained using Anderson Darling tests. Figure 4.5 shows that *p*-value is highest in JJA and very low in MAM and OND as observed in the plotted *p*-values. Appendix 5 (B) contains the streamflow normality test results. As can be seen, the *p*-values are mostly less than the level of significance, hence most of the data are non-normally distributed. Generally, from the results presented in Appendix 3B, 15% of streamflow time series data was normal while 85% was non-normal. Figure 4.6 presents the normality curves for MAM, JJA & OND at Nyando 1GD04. Nyando 1GD04 station is located midstream where the flow is neither turbulent nor flooded.

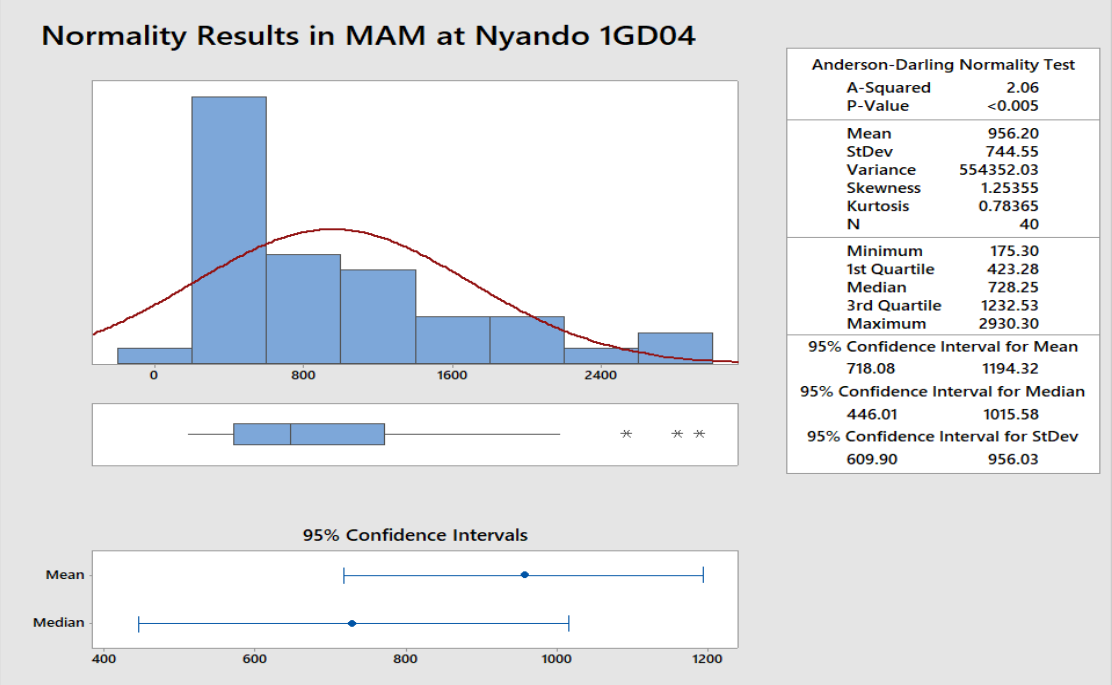

Figure 4.6: (a) Normality plot for MAM streamflow at Nyando station.

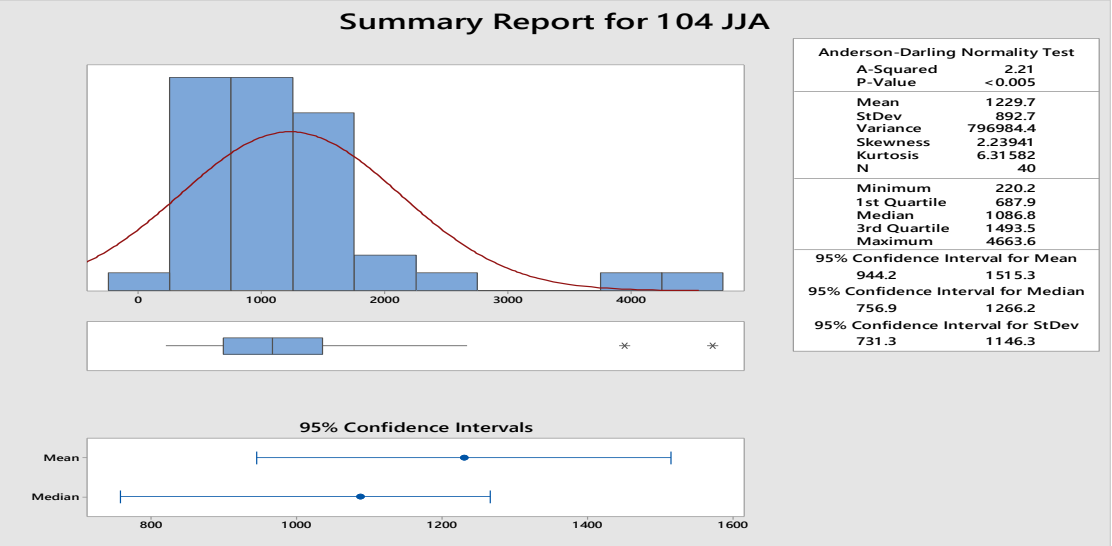

Figure 4.6: (b) Normality plot for JJA streamflow at Nyando station.

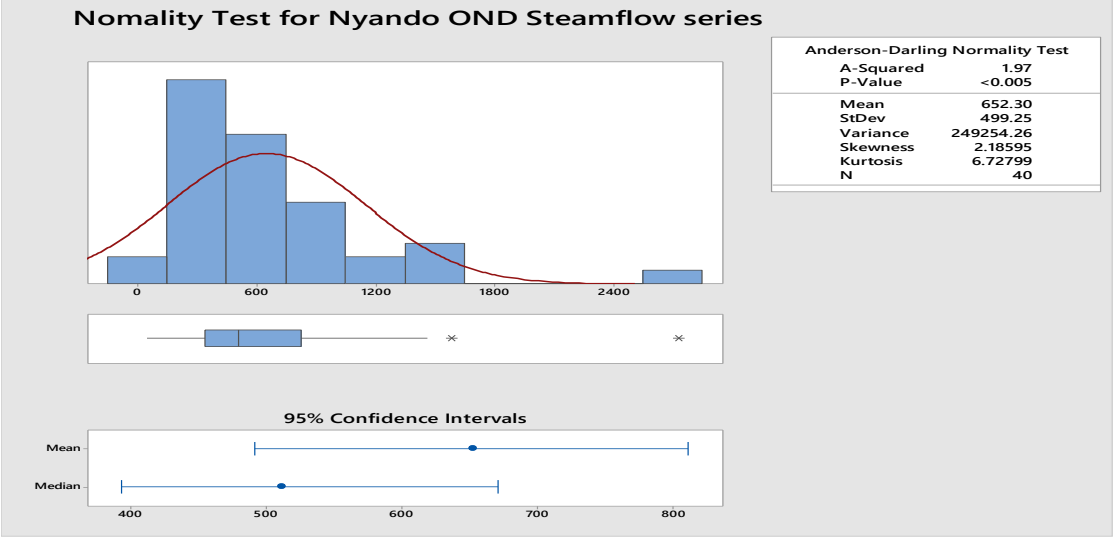

Figure 4.6: (c) Normality plot for OND streamflow at Nyando station.

Figure 4.6 shows the normality curves for streamflow at Nyando station, obtained using Anderson Darling tests. In Figure 4.6, the x and y-axes contain streamflow in m^3/s and % streamflow data, respectively. The 95% confidence interval is shown for the mean and the median. Figure 4.6 (a) presents normality result for MAM series at Nyando 1GD04. The *p*-value for MAM was reported as less than 0.05 meaning the value is statistically insignificant. It was therefore concluded that MAM series was not normally distributed. Similar results are shown in Figures 4.6 (b) and (c) also indicating that JJA and OND series at Nyando 1GD04 were non-normally distributed.

The results indicated that normality in all the time series for all the seasons was very low. Normality in the long rains of MAM streamflow was higher than the JJA and the short rains of OND streamflow series. As explained already for the OND rainfall, none-normality in the streamflow data was attributed to non-stationarity of the Nyando streamflow data which may likely be as a result of climate change and/or to anthropogenic activities within the basin.

4.2.5 Results of independence tests

Tests were carried out in the current study to detect the tendency of the successive values of the streamflow series to remember their antecedent values and to be influenced by them. Independence test was restricted to streamflow only, noting that rainfall is usually random and does not exhibit serial correlation. For the *p*-values greater than the significant level of 0.05, the null hypothesis was rejected meaning the data showed independence and the opposite was true for dependence. Figure 4.7 shows plots of the statistical *p*-values for streamflow.

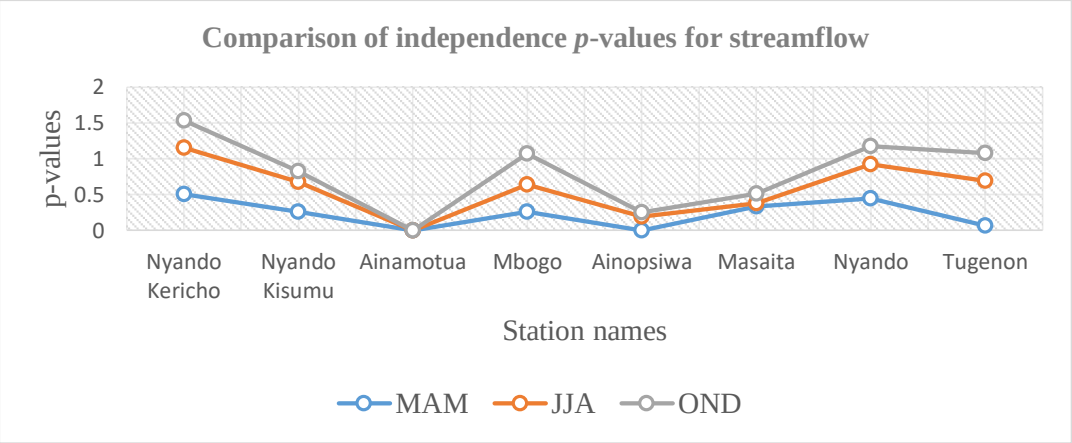

Figure 4.7: Independence plots for streamflow.

Figure 4.7 shows the variation of the independence *p*-values for streamflow obtained using Wald-Wolfowitz method. Similar to the rainfall independence results, Figure 4.7 indicates that streamflow independence was mostly in OND series, moderate in JJA but least in MAM. Table 4.5 contains streamflow independence test results. The *p*-values of most of the series were greater than the significant level of 0.05; hence H_o was rejected, meaning streamflow data differed significantly and did not show marked dependence. From the results shown in Table 4.5, it was estimated that the dependence in the data series constituted about 17% with the remaining independent series accounting for about 83%. This is consistent with findings by Olang and Furst (2011) which revealed that

bigger floods in the Nyando basin tended to attenuate quickly downstream within very short times to peak discharges.

Table 4.5: Results of streamflow independence tests

Station code	Station name	MAM	JJA	OND
1GC06	Nyando Kericho	0.5032^{I}	0.6523^{I}	0.3748^{I}
1GD07	Nyando Kisumu	0.2607^{I}	0.4137^{I}	0.1546^{I}
1GB05	Ainamotua	0.000019^{D}	2.505E-07^{D}	4.9E-08^{D}
1GB06	Mbogo	0.2607^{I}	0.378^{I}	0.432^{I}
1GB11	Ainopiswa	6.4E-06^{D}	0.194^{I}	0.0567^{I}
1GC05	Masaita	0.3377^{I}	0.03798^{I}	0.1347^{I}
1GC04	Tugenon	0.06606^{I}	0.6237^{I}	0.3906^{I}

Notes: ^{I} indicates independence, ^{D} indicates dependence

The reason being that most of the catchments are located in a region largely dominated by poorly drained soils with low infiltration characteristics. The soil types within Ainamotua Sub- catchments are more permeable and have higher infiltration capacities as evident from a number of existing springs. The observed high dependence for Ainamotua streamflow may be attributed to the complex hydrological pathways introduced by sugarcane farming according to studies by Kosgei (2018). Generally, it can be concluded that the Nyando streamflow data was independent and was therefore suitable for this study.

4.2.6 Summarized results of the data quality analysis

Based on the data quality checks carried out in the current study, it can be acknowledged that Nyando River basin mostly exhibited homogeneous and independent streamflow data. Further, the rainfall series were mainly normally distributed as required and were therefore suitable for trend analysis using the conventional techniques. However, streamflow series in the sampled stations were not normally distributed, implying that the Nyando basin streamflow data was mostly non-normal.

In the current study therefore, the decision to use Mann-Kendal, a non- parametric test for trend analysis was based on the non-normal results mainly of OND rainfall and the streamflow data. According to Machiwal and Jhia (2006), non-parametric tests are commonly applied to assess the statistical significance in trend detection when applying non-normally distributed data.

4.3 Results of trend analysis

This section presents results for Mann-Kendall and Wavelet based trend analysis methods. Trend revealed gradual change over time in the probability distribution from which the series values arose.

4.3.1 Results of Mann-Kendall trend analysis

To perform the M-K test, Kendal's S statistic was computed from the series values (Y), time (T) data pairs using Trend Toolkit obtained freely from the internet. The Kendal's statistic was computed for the series of MAM, JJA and OND for all the years. The null hypothesis of no change was rejected when S (and therefore Kendall's Z of Y verses T) was significantly different from zero and was therefore concluded that there was a trend in Y over time.

(i) Results of rainfall trend analysis using Mann- Kendall method

The results for the rainfall trend analysis using M-K are presented in Appendix 6A. The results for MAM series indicated increasing trends for Finlay and Chemelil stations but showed decreasing trends for Londiani and Kericho Met stations. JJA series indicated significant increasing trend for Finlay but showed decreasing trends for Chemelil and Kericho Met stations. OND indicated significant increasing trend only for Finlay and Kericho Water stations but did not indicate significant trends in other stations. Generally, MAM series exhibited increasing trends for two stations and decreasing

trends also for two stations, JJA indicated significant increasing trend only for one rainfall station but decreasing trends for two stations. OND indicated significant increasing trends for two stations but showed no decreasing trend.

Further, results were obtained by repeating the analysis using the series which were split into sub-series of maximum thirty years each. Finlay and Kericho water data sets were long enough and were split into four sub-series. The other stations had shorter series lengths and had data only in either two or three sub-series. Different results were observed after partitioning the complete sets into sub-series. In MAM for example, no significant trends were observed in sub-series I & II whereas subseries III and IV revealed decreasing and increasing trends, respectively for Kericho Met station. JJA series indicated significant decreasing trends for stations of Chemelil sub-series IV, Finlay sub-series III and Kericho water sub-series II whereas OND showed significant increasing trends for stations of Ahero sub-series III and Londiani subseries II. The other sub-series did not show any significant trends after splitting the complete series.

Table 4.6 presents summarized results for the MAM sub-series and contains the observed *z*-statistic values. The start date of 1905 for Finlay station was adopted as the base year in splitting the sub-series. The sub-series I, II, III & IV indicate the first, second, third and fourth data sets, respectively, noting that some rainfall series had start dates later than the base year and further, some contained shorter data lengths which left some sub-series blank. The entire sub-series trend results can be seen in Appendix 6A.

Table 4.6: Z-statistics for MAM sub-series rainfall trend analysis

Station code	S/name	Sub-series	Sub-series II	Sub-series III	Sub-series IV
9034386	Ahero Irrigation	-0.488^{ns}	0.476^{ns}		
8935095	Nandi Tea	0.894^{ns}	-	-	-
9035188	Tinga	1.252^{ns}	0.631^{ns}	-	-
9035003	K/Water	-1.09^{ns}	-0.292^{ns}	-	-
9035258	Kipkelion	-0.537^{ns}	-0.716^{ns}	-	-
9035244	Timbilil	-0.716^{ns}	0^{ns}	-	-
9035341	Finlay	0.068^{ns}	0.285^{ns}	0.089^{ns}	1.525^{ns}
9034087	Chemelil	-1.09^{ns}	1.632^{ns}	-	-
9035279	Kericho Met	-2.059^{-T}	1.769^{+T}	-	-

Notes: $^{-T}$ indicates significant values for negative (decreasing) trend, $^{+T}$ indicates significant values for positive (increasing) trend at 5% significant level.

From Table 4.6, only Kericho Met station indicated significant decreasing and increasing trends in sub-series III and sub-series four, respectively. The other sub-series did not show any significant trends.

Table 4.7 presents summary of the test results for complete rainfall series and contains the observed *z*- statistic values.

Table 4.7: Z-Statistics for MAM sub-series rainfall trend analysis

Station code	Station name	MAM	JJA	OND
9034086	Ahero Irrigation	-0.067^{ns}	-1.224^{ns}	0.876^{ns}
8935095	Nandi Tea	-0.049^{ns}	1.314^{ns}	$-0{,}308^{ns}$
9035188	Tinga	1.156^{ns}	0.445^{ns}	-0.385^{ns}
9035003	Kericho Water	-0.392^{ns}	-0.741^{ns}	-0.685^{+T}
9035258	Kipkelion	1.079^{ns}	0.341^{ns}	-0.426^{ns}
9035341	Finlay	1.791^{+T}	3.565^{T}	2.454^{+T}
9034087	Chemelil	1.831^{+T}	-1.943^{-T}	-0.011^{ns}
9035279	Kericho Met	0.068^{-T}	-1.258^{-T}	0.476^{ns}

Notes: $^{-T}$ indicates significant values for negative (decreasing) trend, $^{+T}$ indicates significant values for positive (increasing) trend at 5% significant level and ns indicates no significant trends.

Table 4.7 shows trend test results using complete rainfall data series. MAM series indicated significant decreasing trends at Londiani and Kericho Met and rainfall stations but indicated increasing trends at Finlay and Chemelil stations. JJA series indicated significant increasing trend only at Finlay but indicated decreasing trends at Chemelil and at Kericho Met stations. OND series indicated significant increasing trends both at Finlay and at Kericho water stations and did not show significant trends at any other station. The results of Kericho Met and Kericho Water Office showed some difference. The difference may be attributed to the observed change of location for Kericho Water Office, causing a possible shift in the data values.

By comparing the results of spilt time series (Tables 4.6) and the results of the complete time series (Table 4.7), it can be seen that the trends observed in the complete series tended to diminish when the series were split. Figure 4.8 presents trend results in complete rainfall at Finlay station.

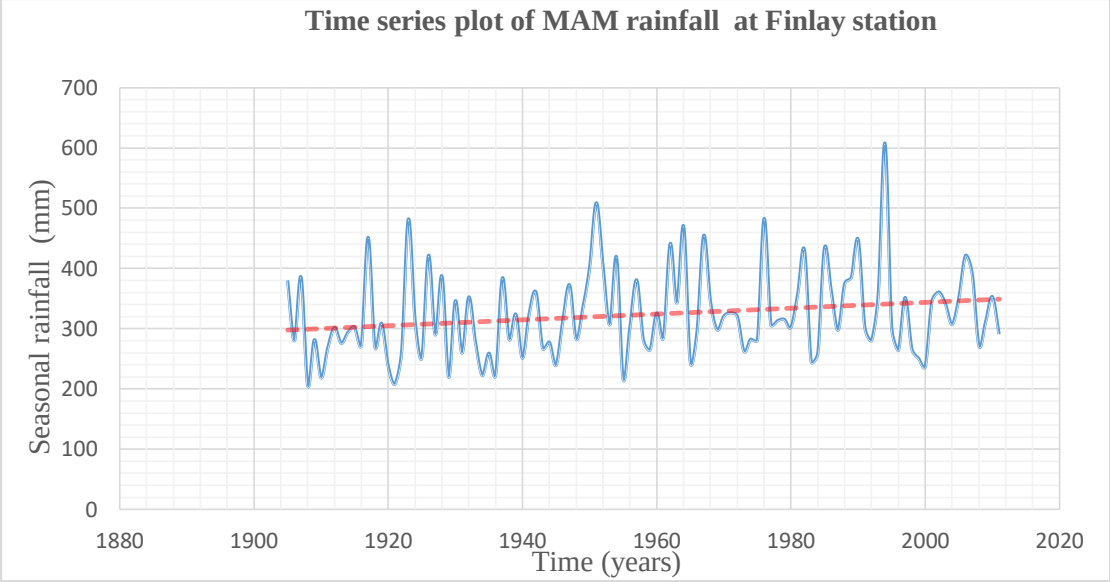

Figure 4.8: (a) Mean MAM rainfall variability at Finlay station.

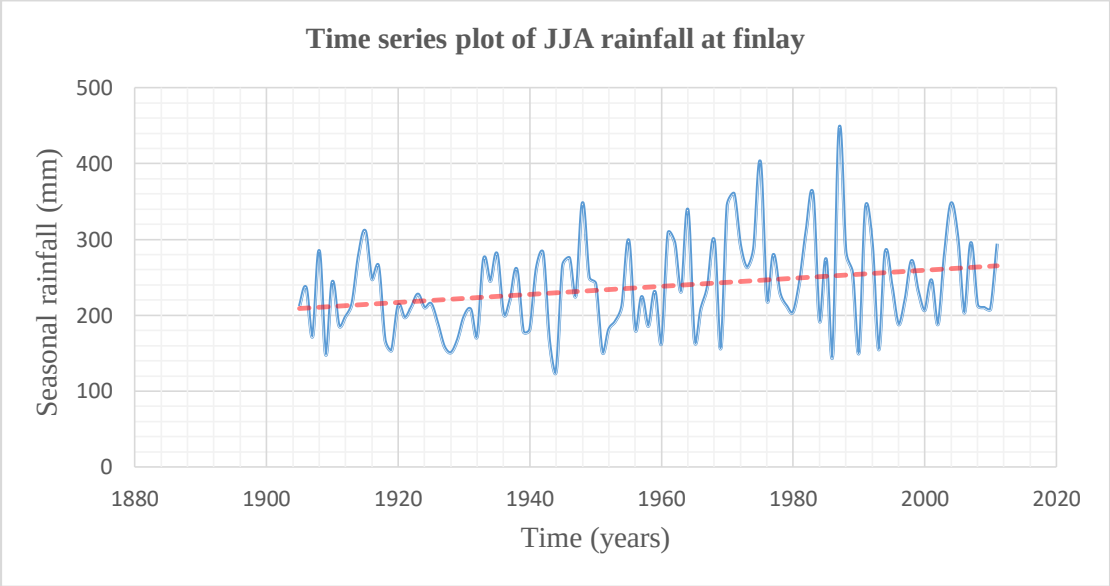

Figure 4.8: (b) Mean JJA rainfall variability at Finlay station.

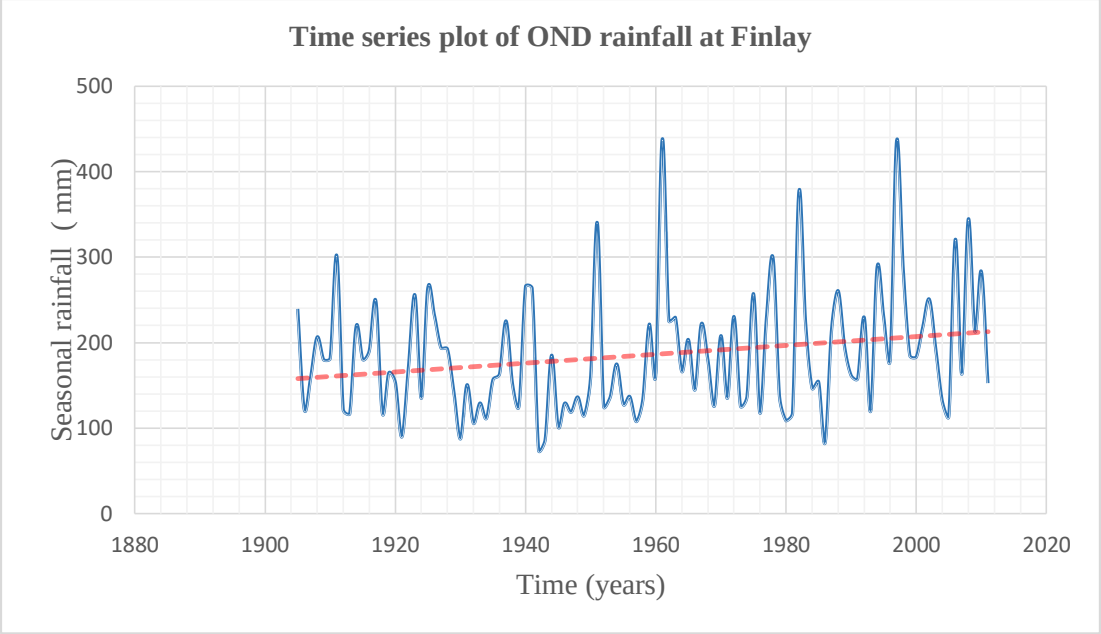

Figure 4.8: (c) Mean OND rainfall variability at Finlay station.

The Figures 4.8(a, b & c) indicate mean rainfall variability in MAM, JJA & OND at Finlay rainfall station. Time series plots of MAM and OND at Finlay station showed general increasing trends in the variability of rainfall and the statistical significance was confirmed by the M-K statistical test. However, JJA showed a decreasing trend.

From the Mann-Kendall trend test results, the study could not conclude the existence of trend or none of it in the rainfall component, as neighbouring stations showed either increasing or decreasing trends. Studies by Paul and Birthal (2016) and Pandey *et* al. (2007) indicate that trends significantly depend upon the period and locations of gauge stations. It is also possible for trends to arise from some local factors such as change of rain gauge stations or due to local influences such as topography.

(ii) Results of streamflow trend analysis using M-K method

The results for the streamflow trend analysis using M-K are presented in Appendix 6B for the MAM, JJA and OND series. MAM series indicated significant increasing trends for Nyando Kericho, Ainamotua, Mbogo and Ainopsiwa stations and also showed decreasing trends for Nyando and Masaita stations. JJA series indicated increasing

significant trends for Ainamotua, Ainopsiwa and Mbogo stations and also showed decreasing trends for Masaita and Nyando stations. OND series indicated significant increasing trends only for Nyando Kericho, Ainamotua, Ainopsiwa and Mbogo stations.

Similarly, further results were obtained by repeating the analysis when the series were split into two sub-series**.** MAM series indicated significant increasing trends in sub-series I for both Ainamotua and Mbogo stations, Ainopsiwa sub-series II and a significant decreasing trend in sub-series I of Nyando station. JJA series indicated significant increasing trends in sub-series I of both Ainamotua and Mbogo and in sub-series II of Ainamotua, Ainopsiwa and Nyando stations. Significant decreasing trends were not observed in JJA sub-series. For OND series, significant increasing trends were indicated in the subseries I of both Ainamotua and Mbogo, sub-series II of Ainamotua.

Table 4.8 presents summarized results for MAM series and shows the observed *z*-statistic values. The sub-series I & II, indicate the first and second data sets respectively, noting that the streamflow series fitted into only two sub-series. Whereas Appendix 7B contains the streamflow sub-series trend results, Table 4.8 shows streamflow sub-series results for MAM. Sub-series I of MAM showed significant increasing trends for Ainamotua and Mbogo stations and a significant decreasing trend for Nyando station. Sub-series II showed a significant increasing trend for Ainopsiwa and no significant decreasing trend was shown in sub-series II.

Table 4.8: Z-statistics for MAM streamflow sub-series trend analysis

Station code	Station name	Sub-series I	Sub-series II
1GC06	Nyando Kericho	0.693^{ns}	1.508^{ns}
1GD07	Nyando Kisumu	0.28^{ns}	0.754^{ns}
1GB05	Ainamotua	2.583^{+T}	0.929^{ns}
1GB06	Mbogo	3.892^{+T}	1.073^{ns}
1GC05	Masaita	0.628^{ns}	0.807^{ns}
1GD04	Nyando	$- 1.851^{-T}$	0.109^{ns}
1GC04	Tugenon	0.169^{ns}	-0.606^{ns}

Notes: $^{-T}$ indicates significant values for negative (decreasing) trend, $^{+T}$ indicates significant values for positive (increasing) trend at 5% significant level.

Table 4.9 presents summary of the M-K trend test results for streamflow series.

The sub-series defined by the split data showed some differences with the complete series like in the rainfall case. From the results, fewer sub-series showed either significant increasing or decreasing trends compared to the full series. The difference however, was more elaborate in rainfall than in streamflow. In some instances, complete series results showed significant decreasing trends but the trend either disappeared or changed to increasing trend in the split series.

Table 4.9: Z-statistics for streamflow complete series trend analysis

Station Code	Station name	MAM	JJA	OND
1GC06	Nyando Kericho	2.494^{+T}	1.064^{ns}	3.742^{+T}
1GD07	Nyando Kisumu	-0.884^{ns}	-0.306^{ns}	-0.816^{ns}
1GB06	Mbogo	5.258^{+T}	4.888^{+T}	5.166^{+T}
1GB11	Ainopiswa	4.663^{+T}	$5.56+^{T}$	4.99^{+T}
1GC05	Masaita	-3.008^{-T}	-2.824^{-T}	-1.577^{ns}
1GD04	Nyando	-2.855^{-T}	-2.07^{-T}	-1.643^{ns}
1GC04	Tugenon	-0.606^{ns}	0.384^{ns}	0.524^{ns}

Notes: $^{-T}$ indicates significant values for negative (decreasing) trend, $^{+T}$ indicates significant values for positive (increasing) trend at 5% significant level.

Figure 4.9 presents trend results in MAM, JJA and OND series at Ainamotua streamflow station.

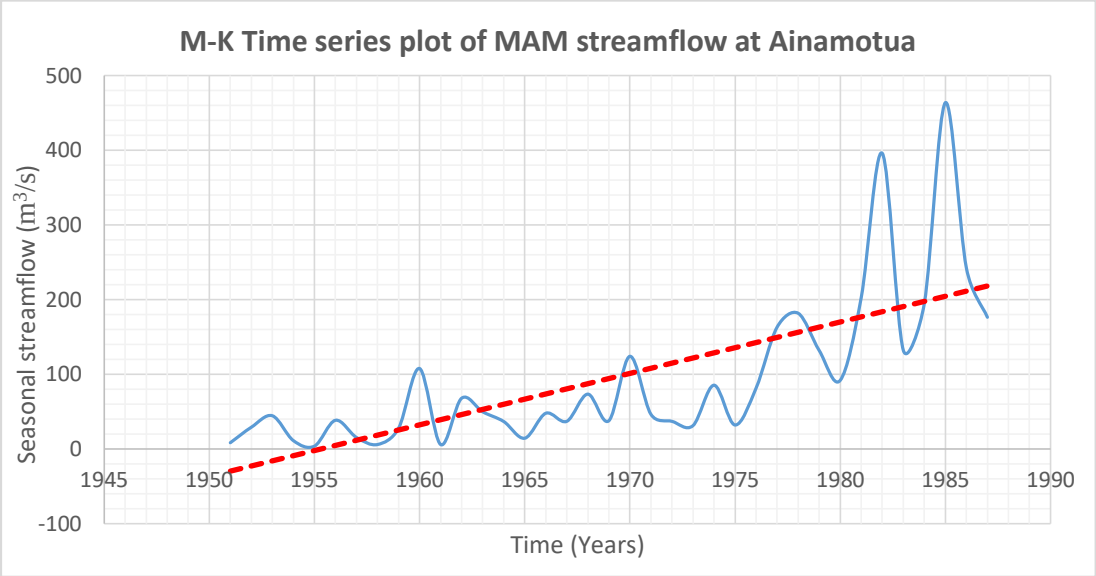

Figure 4.9 (a): MAM Mean streamflow variability for Ainamotua.

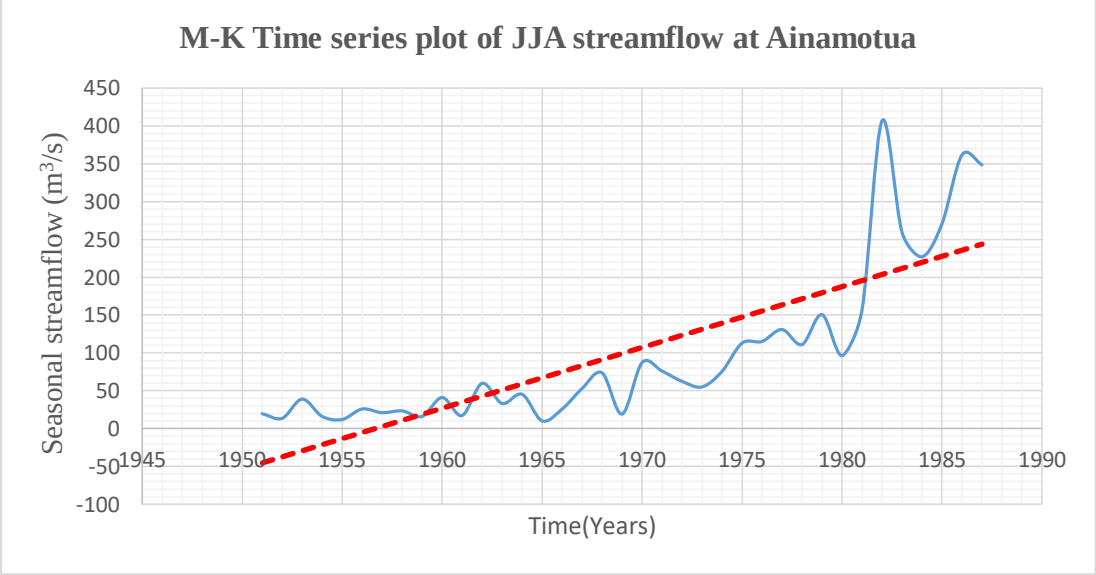

Figure 4.9: (b) JJA Mean streamflow variability for Ainamotua.

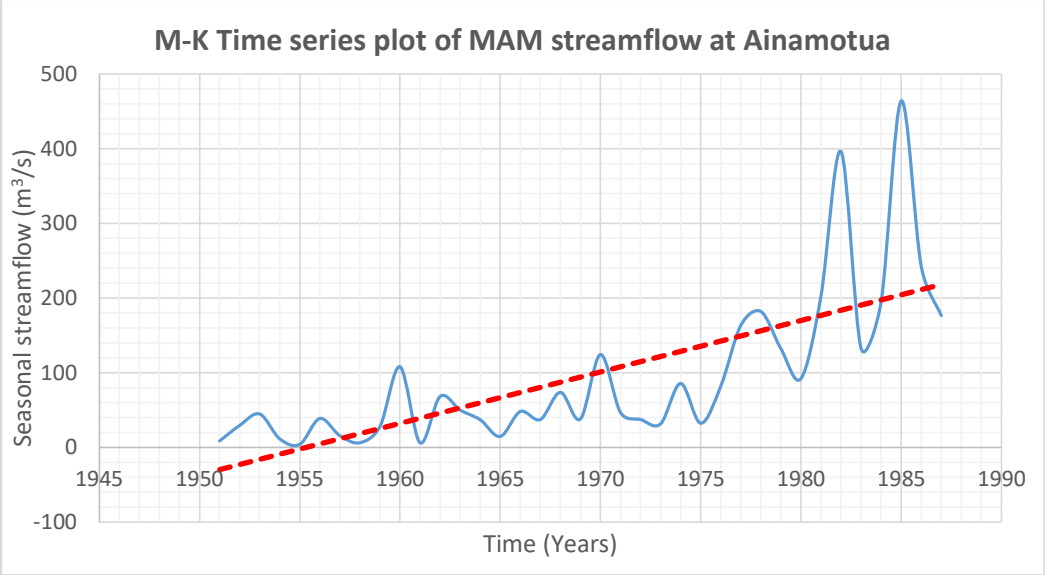

Figure 4.9: (c) OND Mean streamflow variability for Ainamotua.

The Figures 4.9(a, b & c) indicate mean streamflow variability in MAM, JJA & OND for Ainamotua station. The x-axis represents the time in years and the y-axis represents the observed streamflow.

All the plots at Ainamotua showed general significant increasing trends and the statistical significance was confirmed by the M-K method. It was generally observed from the M-K results in Table 4.9 that the streamflow in Nyando River basin has undergone increasing trend although stations including Masaita indicated significant decreasing trends. The results showed more definite trends in streamflow as compared to rainfall.

The decrease in trends at some streamflow stations may be attributed to some human activities within some sub-basins such as unregulated water abstraction and deforestation for agricultural practices. More elaborate trends in streamflow than in the rainfall component may possibly be attributed to some uncontrolled human activities.

4.3.2 Results of trend analysis using Wavelet transform

Wavelet transform (WT) was used to decompose time series into low frequency (trend) and high frequency (noise). The results indicated the hydrological time series plots decomposed by wavelets into low frequency components. The results are presented for rainfall and streamflow.

(i) Results of rainfall trend analysis using wavelet transform

In MAM: Ahero station showed significant decreasing trend from 1965 to 1970 and an increasing trend from 1990 to 1998; Nandi Tea showed a decreasing trend from 1960 to 1985; Timbilil, Tinga-Monastery and Kericho water stations showed erratic rainfall patterns without any definite trends; Kipkelion station showed increasing trend from 1960 to 1965 and another increasing trend from 1975 to beyond 1990; Londiani station showed decreasing trend from 1930 to 1980; Finlay station showed increasing trend from 1970 to 1978 and another increase from 1985 to 1998; Kericho Met station showed increasing trend from 1980 to 1988, decreasing trend to 2000; Chemelil station showed an increasing trend from 1968-1977 then decreased to 1984. The pattern became oscillatory with abrupt changes in 1985, 1987 and 1998.

In JJA: Ahero showed decreasing trend from 1962 to 1975 and an increasing trend to 1998; Nandi Tea showed decreasing trend from 1960 to 1975; Tinga station showed increasing trend from 1950 to 1962 and an increasing trend from 1965 to 1976; Kericho Water and Kipkelion stations showed erratic patterns with no definite trends; Londiani station showed increasing trend from 1930 to 1945, increasing trend from 1950 to 1970; Finlay showed increasing trend from 1920 to 1979, increasing trend from 1995 to 1998; Chemelil showed increasing trend from 1960 to 1975 and a decreasing trend to 2002; Kericho Met station showed a decreasing trend from 1980 to 2010.

In OND: Ahero irrigation showed decreasing trend from 1962 to 1970 and increases to 1998; Nandi tea showed increasing trend from 1950 to 1960; Tinga showed increasing trend from 1955 to 1962, another increasing trend to 1970 and finally decreased to 1990; Kericho Water station showed increasing trend from 1930 to 1964 and another increasing trend 1998. Kipkelion showed increasing trend from 1945 to 1964 and another increasing trend from 1965 to 1976; Londiani showed increasing trend from 1930 to 1963, a decreasing trend to 1976 and finally an increase to 1980; Finlay station showed decreasing trend from 1905 to 1930 and an increasing trend from 1950 to 2010; Chemelil showed decreasing trend from 1960 to 1975 and an increasing trend to 1998; Kericho Met station showed erratic rainfall pattern in OND.

Figure 4.10 shows wavelet based mean rainfall variability for MAM, JJA & OND series at Finlay station. Appendix 8A contains all the wavelet-based trend results and Table 4.10 indicates a summary of the wavelet-based trend test results. Percentage increases and decreases have been computed as indicated by the figures enclosed in brackets. The percentage increases and decreases refer the percentages of falling and rising limbs, respectively. In computing the net trends, the negatives (decreasing trends) and the positives (increasing trends) are summed up and the net trends are estimated.

From Table 4.10, overall increasing trend in rainfall can be seen in the series of Ahero (MAM & OND), Nandi Tea (JJA), Tinga Monastery (MAM), Kericho Water Office (JJA & OND), Kipkelion (MAM), Londiani (OND), Finlay (MAM & JJA), Chemelil (MAM), Timbilil (MAM, JJA & OND), Kericho Met (MAM & OND). Similarly, overall decreasing trends can be observed in the series of Ahero (JJA), Nandi Tea (MAM & OND), Kipkelion (JJA & OND), Tinga Monastery (JJA & OND), Londiani (MAM

& JJA), Kericho Water Office (MAM), Finlay (OND) and Chemelil (JJA & OND) and Kericho Met (JJA).

Table 4.10: Summary of rainfall wavelet trend test results

Station/Trend	MAM		JJA		OND	
	Increased	**Decreased**	**Increased**	**Decreased**	**Increased**	**Decreased**
Ahero (39 years)	1960-1980 **(+53.85%)**	1985-2000 **(-41.03%)**	1985-2000 **(+41.03%)**	1960-1980 **(-3.85%)**	1975-2000 **(+66.67)**	1960-1975 **(-41.03%)**
Nandi Tea (31 years)	-	1957-1988 **(-100%)**	1957-1972 **(+51.61%)**	1976-1988 **(-41.93%)**	1957-1970 **(+45.16)**	1973-1988 **(-51.61%)**
Tinga M (33 years)	1958-1975 **(+54.55%)**	1983-1991 **(-27.27%)**	1958-1970 **(+39.39%)**	1977-1991 **(-45.46%)**	-	1975-1991 **(-51.52%)**
Kericho Water (60 years)	1926-1950 **(+41.67%)**	1970-2009 **(-66.67%)**	1926-2009 **(+48.33%)**	-	1926-2009 **(+48.33)**	-
Kipkelion (34 years)	1957-1975 **(+55.88%)**	1977-1991 **(-44.12%)**	1957-1970 **(+41.18%)**	1975-1991 **(-50.00%)**	1957-1970 **(+41.18)**	1980-1991 **(-64.71%)**
Finlay(100 years)	1906-1980 **(+75%)**	-	1906-2010 **(+100%)**	-	1906-1940 **(+35.00)**	1950-2010 **(-61%)**
Chemelil (40 years)	1966-2000 **(+87.50%)**		-	1985-2006 **(-52.50%)**	1990-2006 **(+42.50)**	1966-1985 **(-50%)**
Timbilil (37 years)	1975-2000 **(+70.27%)**	1960-1970 **(-29.72%)**	1960-1980 **(+56.75%)**	1990-2000 **(-29.72%)**	1980-2000 **(+56.75)**	1960-1975 **(43.24%)**
Kericho Met (36 years)	1974-2000 **(+75%)**	2003-2010 **(-22.22%)**	-	1974-2010 **(-100%)**	1974-2010 **(+100%)**	-
Londiani (60 years)	1926-1950 **(+41.67%)**	1958-1986 **(-48.33%)**	1926-1950 **(+41.67%)**	1956-1986 **(-48.33%)**	1926-1950 **(+41.67)**	1968-1986 **(-31.68%)**

In summary therefore, it was estimated from the results that the increased trend accounted for 53.3 % whereas the decreased trend accounted for 46.7%. It was therefore concluded that some trend has occurred according to the Wavelet technique. From the results, MAM revealed 7 major percentage increases of 53%, 54%, 55%, 75%, 87%, 70% and 75% compared to 3 decreases of 100%, 66% and 48%. JJA revealed 4 major percentage increases of 51%, 48%, 100% and 56% compared to 6 decreases of 53%, 45%, 50%, 48%, 52% and 100%. OND revealed 5 major percentage increases of 66%, 48%, 41%, 56% and 100% compared to 5 major percentage decreases of 51%, 51%, 64%, 61% and 50%. It can therefore be concluded that MAM rainfall has undergone

increase, JJA has decreased and OND rainfall has remained stationery during the study period. Figure 4.10 presents wavelet-based trend results at Finlay station.

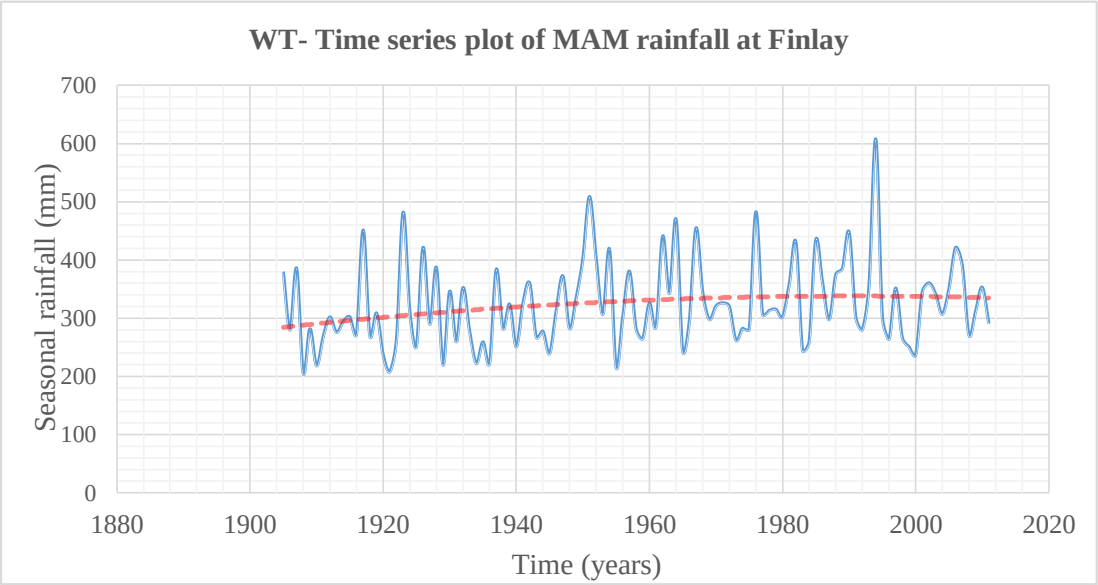

Figure 4.10: (a) Wavelet--based mean rainfall variability in MAM at Finlay

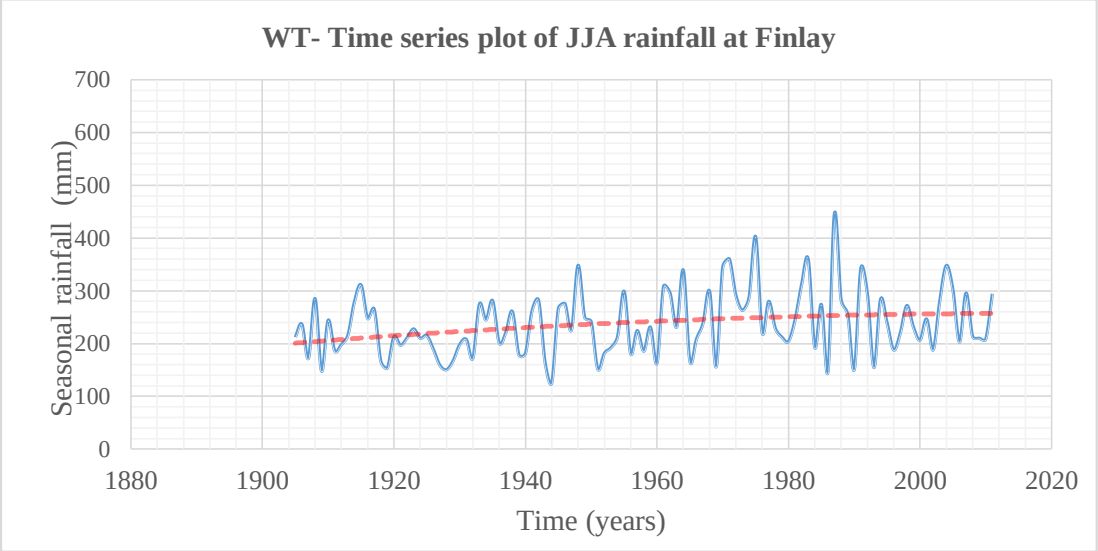

Figure 4.10(b): Wavelet-based mean rainfall variability in JJA at Finlay.

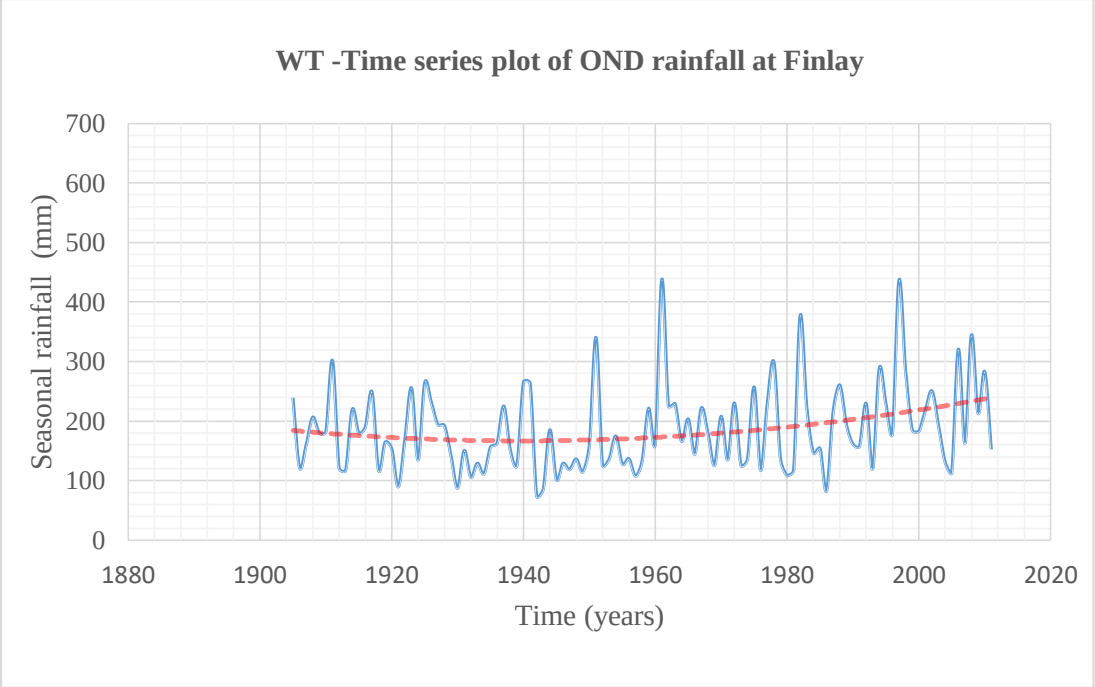

Figure 4.10(c): Wavelet- based mean rainfall variability in OND at Finlay.

The Figures 4.10(a, b & c) indicates mean rainfall variability in MAM, JJA & OND for Finlay station. The results as seen from Figures 4.10 (a), (b) & (c) indicate increasing rainfall trends in MAM, JJA and OND which were confirmed statistically significant using M-K technique.

The results observed from wavelet analysis showed some difference with those of M-K. Mann-Kendall technique showed some minimal trends and declared most of the trends insignificant, wavelet results revealed the trends more clearly by showing the increasing and decreasing aspects. From the wavelet results, it was possible to compute the overall trends. The results showed that some increase in rainfall had occurred in the Nyando River basin possibly as a result of climate change and variability.

(ii) Results of streamflow trend analysis using Wavelet transform

In MAM: Ainamotua station showed decreasing trend from 1960 to 1975 and an increasing trend from 1975 to 1998; Masaita showed a decreasing trend from 1976 to 1996 and a jump in 2002; Mbogo streamflow station showed increasing trend from 1955

to 1985; Nyando Kericho showed increasing trend from 1995 to 2010 with abrupt changes in 1998 and 1978; Nyando station showed decreasing trend from 1963 to 1995 with jumps in 1963, 1980 and 1990; Nyando Kisumu station indicated a jump in 1978 with erratic streamflow pattern. Tugenon also indicated jumps in 1970, 1980 and 1990. In JJA: Ainamotua showed increasing trend from 1960 to 2000; Masaita showed decreasing trend from 1976 to 1987, increasing trend from 1996 to 2006 then decreasing trend to 2010; Ainopsiwa showed increasing trend from 1965 to 1978, increasing trend again from 1981 to 2000; Mbogo stations showed increasing trend from 1955 to 1995; Nyando Kericho indicated erratic flow pattern with jumps in 1978 and 1990; Nyando showed decreasing trend from 1962 to 1986; Nyando Kisumu showed increasing trend from 1965 to 1975 and a decreasing trend to 1985; Tugenon showed an increasing trend from 1965 to 1978 and an increase from 1985 to 1998.

In OND: Ainamotua station showed increasing trend from 1968 to 1990 and increasing trend from 2000 to 2010; Ainopsiwa showed increasing trend from 1970 to 2010; Masaita showed erratic flow pattern and indicated jumps in 1976 and 1981; Mbogo showed increasing trend from 1955 to 1985; Nyando Kericho showed increasing trend from 1985 to 2010 with jumps in 1978 and 1998; Nyando Kisumu showed erratic streamflow pattern with a jump in 1978; Nyando and Tugenon stations indicated jumps in 1963 and erratic patterns with no definite trends. Appendix 8(B) contains all the wavelet trend results for streamflow, and Table 4.11 indicates a summary of wavelet based trend test results for Nyando streamflow. Percentage increases and decreases have been computed as indicated by the figures enclosed in brackets. In computing the net trends, the negatives (decreasing trends) and the positives (increasing trends) are summed up and the net trends are estimated.

From the results shown in Table 4.11, overall increase in streamflow can be observed in the series of Nyando-Kericho (MAM, JJA & OND), Ainamotua (MAM, JJA & OND), Ainopsiwa (MAM, JJA & OND), Mbogo (MAM, JJA & OND) and Tugenon (JJA). Similarly, overall decreases can be observed in the streamflow series of Nyando-Kisumu (MAM, JJA & OND), Masaita (MAM, JJA & OND) Nyando (MAM, JJA & OND) and Tugenon (MAM & OND). In summary therefore, it was estimated from the results that the increased streamflow trend accounted for 54.2 % whereas the decreased trend accounted for 45.8%. It was therefore concluded that some streamflow trend has occurred according to the wavelet technique, also consistent with the M-K streamflow results.

Table 4.11: Summary of streamflow wavelet trend test results

Station/Trend	MAM		JJA		OND	
	Increased	**Decreased**	**Increased**	**Decreased**	**Increased**	**Decreased**
Nyando-Kericho (46 years)	1967-2010 **(+95.65)**	-	1967-1995 **(+63.04)**	1995-2013 **(-39.13%)**	1980-2013 **(+73.91)**	-
Nyando-Kisumu (30 years)	-	1967-1993 **(-90.00%)**	1967-1975 **(+30.00)**	1980-1993 **(-46.67%)**	1967-1975 **(+30.00)**	1978-1993 **(-53.33%)**
Ainamotua (58 years)	1951-2009 **(+100%)**	-	1951-2009 **(+100%)**	-	1951-2009 **(+100%)**	-
Ainopsiwa (48 years)	1975-2008 **(+70.83)**	1960-1970 **(-22.91%)**	1960-2008 **(+100%)**	-	1975-2008 **(+72.91)**	1960-1970 **(-22.91%)**
Mbogo (36 years)	1962-1987 **(+72.22)**	1951-1960 **(-27.78%)**	1962-1987 **(+72.22)**	1951-1960 **(-27.78%)**	1962-1987 **(+72.22)**	1951-1960 **(-27.78%)**
Masaita (46 years)	2000-2010 **(+23.91)**	1964-1995 **(-69.56%)**	2000-2010 **(+23.91)**	1964-1995 **(-69.56%)**	-	1951-2009 **(-100%)**
Nyando (39 years)	1985-1995 (+**28.21)**	1956-1980 **(-64.10%)**	1985-1995 **(+28.21)**	1956-1980 **(-64.10%)**	-	1956-1995 **(-100%)**
Tugenon (39 years)	-	1960-1999 **(-100%)**	1960-1999 **(+100%)**	-	1990-1999 **(+25.64)**	1960-1985 **(-66.67%)**

From the results, MAM revealed major percentage increases of 95%, 100%, 70% and 72% compared to the decreases of 90%, 69%, 64% and 100%. JJA revealed major percentage increases of 63%, 100%, 100%, 72% and 100% compared to the decreases of 46%, 69% and 64%. OND revealed 4 major percentage increases of 73%, 100%, 72% and 73% compared to 4 major percentage decreases of 53%, 100%, 100% and 66%. It

can therefore be concluded that MAM, JJA and OND streamflow increased during the study period. Figures 4.11 present wavelet-based trend results at Ainamotua streamflow station.

The wavelet -based results as indicated from Figure 4.11(a, b & c) show increasing trends for MAM, JJA & OND at Ainamotua station and the results were shown to be statistically significant by the M-K technique. M-K results indicate the statistical significance at 5% significance level and additionally displays the mean seasonal variability at the rainfall stations.

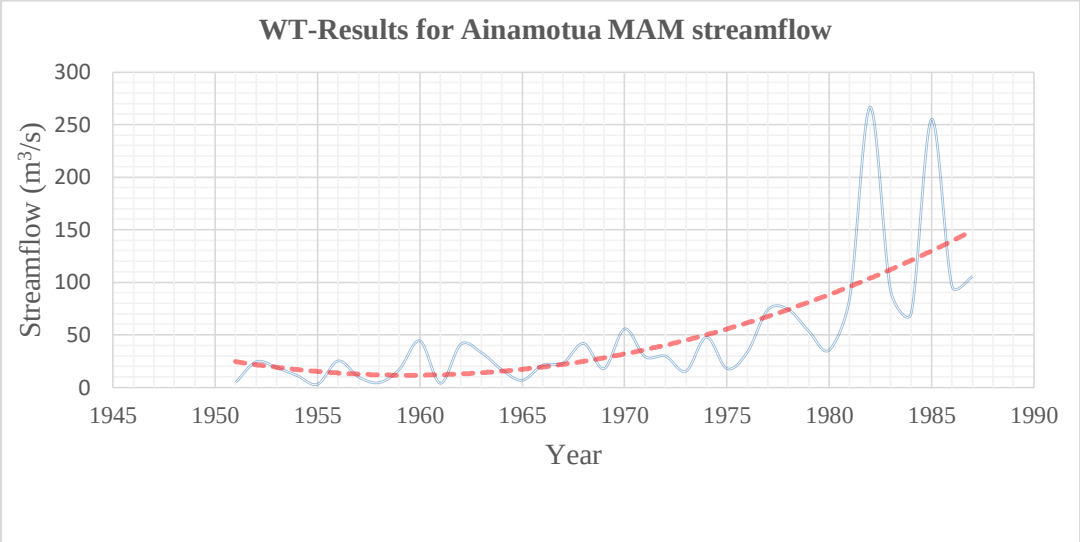

Figure 4.11: (a) Wavelet-based mean streamflow variability in MAM at Ainamotua.

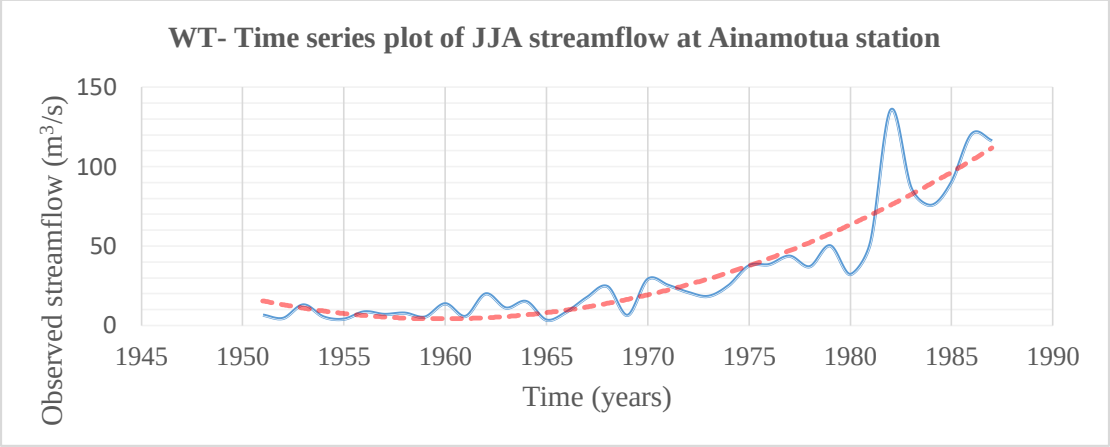

Figure 4.11: (b) Wavelet-based mean stream flow variability in JJA at Ainamotua.

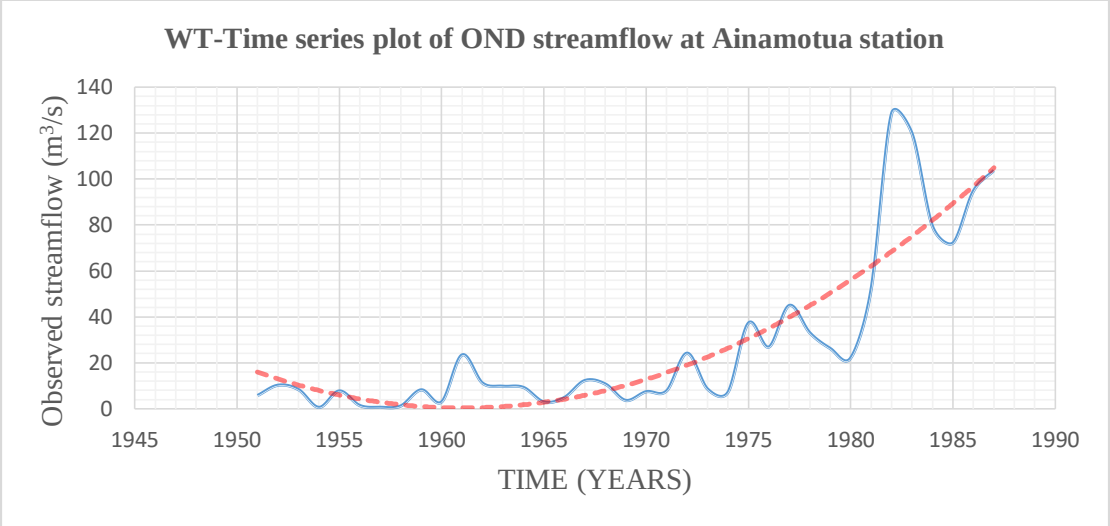

Figure 4.11: (c) Wavelet-based mean streamflow variability in OND at Ainamotua.

The fall from the year 1950s to 1960 was attributed to drought events experienced during the decade. The rising limb from 1961 was attributed to the occurrence of the El Niño Southern Oscillation (Indeje *et al.*, 2000).

In comparing the two techniques, the M-K approach only estimated the statistical significance at 95% whereas an improvement by wavelet disclosed the temporal-frequency information. Wavelet method showed trend lines which were further analysed and computed for more definite results. Use of wavelet revealed generally the decreasing

(negative) and increasing (positive) trends and other important features such as some turning points and amplitude of fluctuations over time.

The results showed generally that some positive or increasing trend occurred in the streamflow in the Nyando basin. The streamflow trend was higher than in the rainfall component. The increasing trends were attributed to possible climate change and variability, and also to anthropogenic activities in the Nyando River basin such as uncontrolled deforestation for agricultural purposes.

The El Niño cycles of between 2-7 years were indicated in the results of both the rainfall and streamflow components as presented in Section 4.4.2. These cycles are associated with flood events and have been manifested in the Nyando River basin from time to time. Ogwang *et al*. (2014) argue that spatial differences in stream flow trend can occur as a result of spatial differences in the changes in rainfall and temperature and spatial differences in the catchment characteristics that translate meteorological inputs into hydrological response. They explain that the distribution of flows of water in a season depends on a number of factors e.g., soil conditions and land cover among other conditions. The results for Masaita, Nyando Tugenon and Nyando Kisumu can easily be explained by the human activities such as unregulated water abstractions within the sub-catchments. According to studies by Olang and Furst (2011), some sub-catchments have exhibited declining trends due to increase in water demands especially for irrigated agriculture.

Kizza *et al.* (2009) has shown that on longer time scale, Lake Victoria basin experienced a predominantly positive trend over the 20th Century with 1960s representing a significant upward jump in the basin rainfall. According to Roshani *et al*. (2012), there is a clear connection between the trends and large scale climate changes. Rainfall in the

entire East Africa is known for its inter-annual variability which has contributed to devastating droughts and floods. El Niño Southern Oscillation (ENSO) has shown multiple effects in rainfall. Warming of the ocean temperature leads to an increase in rainfall and change in direction of the Inter tropical convergence zone (ITCZ). Indian Ocean Dipole (OD) on the other hand represents the surface temperature variability in the tropical Indian Ocean and this change significantly affects the climate of East Africa. In general, rainfall variability in East Africa, particularly the inter-annual variability is modulated by large scale climate forcings and changes in sea surface temperatures which affects the rainfall amounts by changing wind patterns and moisture fluxes (Black *et al*., 2003).

El Niño refers to conditions when the sea's surface in an area along the equator in the Central and Eastern Pacific Ocean gets warmer than usual. The average water temperature in that area is typically just 1-3°C warmer than normal, but it has the effect of adding huge amounts of heat and moisture to the atmosphere, ultimately affecting patterns of air pressure and rainfall across the Pacific and beyond.

The climatological counterpart to El Niño is La Niña. La Niña refers to periods when sea-surface temperatures in the equatorial Central and Eastern Pacific are cooler than normal. The lower surface temperatures suppress transfer of heat and moisture to the atmosphere, again affecting air pressure and rainfall patterns across a large region. According to Black *et al*. (2003), El Niño exerts some influence on equatorial and Coastal East African rainfall, with warm events being associated with high rainfall and cold events with low rainfall. This sea surface temperature (SST) pattern is conducive for enhancing rainfall over the Country. Even in the absence of El Niño conditions, this pattern over the Indian Ocean results in heavy rainfall during the short rains season as was the case in the 1961-1962, 1997-1999 and 2006-2007 rainfall events.

4.4 Results of periodicity analysis

This section presents periodicity results showing the oscillations of the time series examined using both spectral and wavelet techniques.

4.4.1 Results of periodicity analysis using spectral technique

The spectral analysis results were obtained by extracting frequency information from the rainfall and streamflow time series. Periodograms were calculated and plotted against the frequency components of the series.

(i) Results of rainfall periodicity analysis using spectral technique

Significant rainfall periodicities are indicated as: (i) for MAM series; Ahero irrigation station showed 5-year period; Nandi Tea showed 3.3-year; Tinga Monastery and Kipkelion stations showed 4-year period; Kericho Water showed 4.8-year and 10-year period; Londiani station showed 5.2-year period; Finlay station showed 2.2, 4.8 & 11-year periods; Kericho Met station showed 8.3-year period; (ii) for JJA series: Ahero irrigation showed 2.5 & 8.3-year periods; Londiani station showed 8.3-year period; Finlay station showed 2.2, 4 & 6.7-year periods and (iii) for OND series: Nandi tea showed 5.6-year period; Kericho Water showed 2.5, 3, 5 & 14-year period; Kipkelion station showed 6.3-year period; Finlay station showed 2.5, 3.3, 5 &11-year periods; Chemelil station showed 2.5 & 5.2-year periods; and Kericho Met station showed a 6-year period. Figures 4.12 shows the major rainfall periods detected at Finlay, Ahero and Nandi Tea. Appendix 9(A) contains all the rainfall spectral results.

In the Figure 4.12 (a), (b) & (c), the X-axis shows the frequencies and the Y-axis shows the spectral densities. The spectral density gives information on the relative power at a certain frequency. Values of the spectra represent the magnitude of the variance in the series at a given spectral scale. Additionally, the Period T is defined as the sampling

frequency, calculated as 1/f and the actual peaks indicate the periodic oscillations. The significant peaks fall above the significant line shown in the figures by a small horizontal mark. The insignificant peaks have no marks.

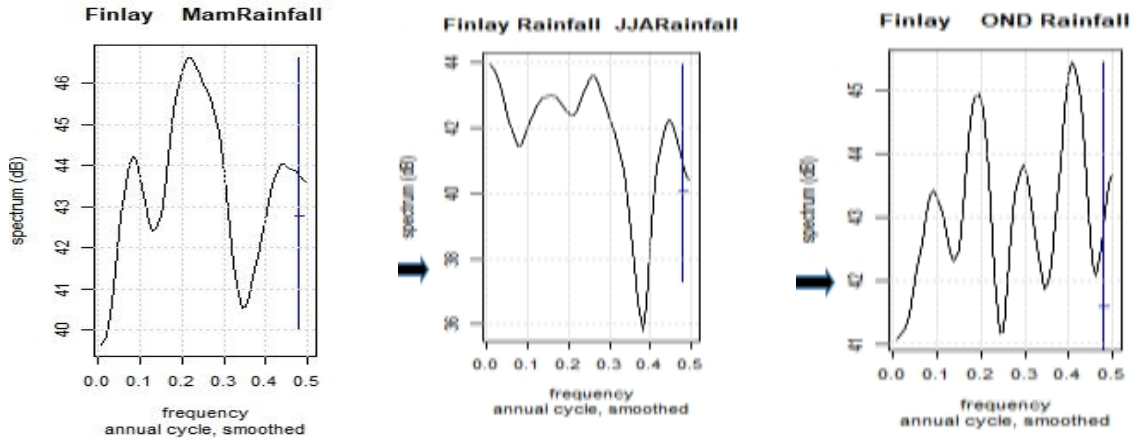

Figure 4.12 (a): Rainfall periods at Ahero station

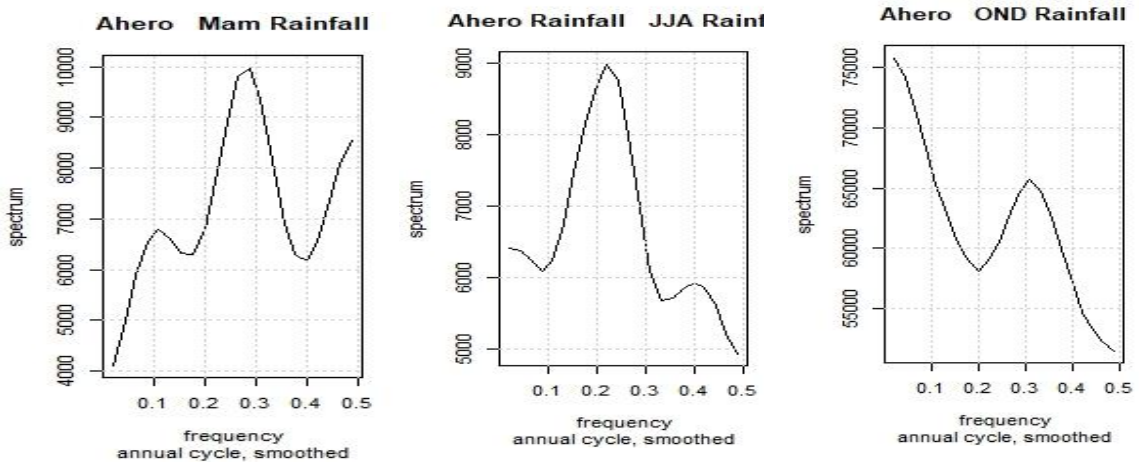

Figure 4.12 (b): Rainfall periods at Ahero station

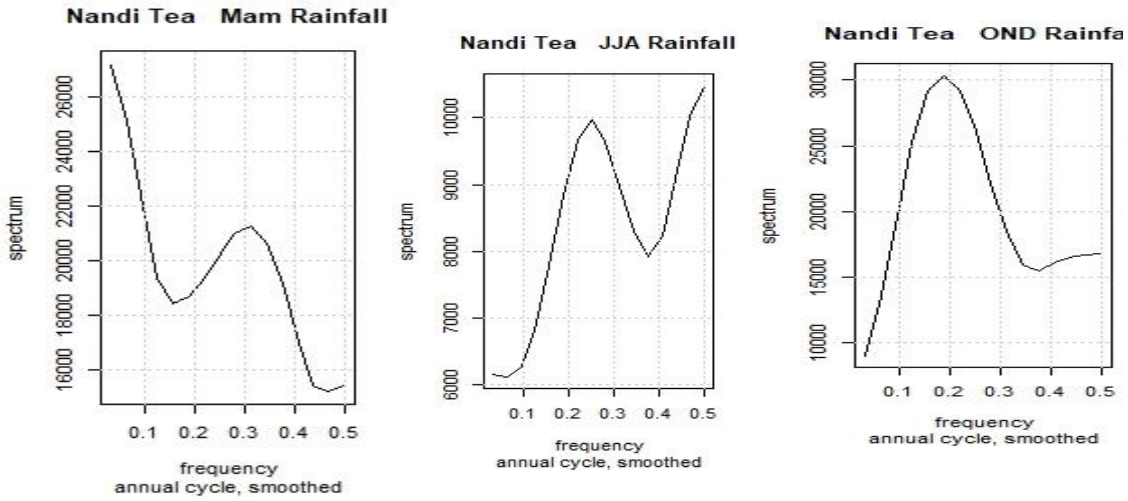

Figure 4.12 (c): Rainfall periods at Nandi Tea station

The arrows show the smoothening process of the peaks using either the spectral density or the frequency as indicated in the vertical scales. It is observed from Figure 4.12 that most of the variance of the time series have been described by high frequencies (short periods).

As already stated above, the periods are the reciprocals of the frequencies indicated in the x-axes of the spectral plots. The crests/peaks of the curves indicate the exact frequencies for computing the periods. Figure 4.12(a) shows the periodicities in MAM, JJA and OND at Finlay station. MAM series indicate three periods (peaks) of 2.2 year, 4.5, & 10 years; JJA indicate periods of 2.2, 4.2 and 6.6 and OND has four periods of 2.4, 3.5, 5.5 & 12.5. Figure 4.12(b) shows periodicities of 10, 3.2 & 3.2 at Ahero Irrigation station in MAM, JJA and OND series respectively but the peaks are not significant. Figure 4.12 (c) shows periodicities of 3.2, 4 & 5.5 at Nandi Tea in MAM, JJA and OND, respectively although the peaks are not significant. A summary of rainfall spectral analysis results for Nyando rainfall are presented in Table 4.12.

Table 4.10: Summary results of rainfall spectral analysis

Station Code	Station Name	Periodicity in Years		
		MAM	JJA	OND
9034086	Ahero Irrigation	5 & 10^{ns}	2.5 & 8.3 4.0^{ns}	3.3^{ns}
8935095	Nandi Tea	3.3	4.0^{ns}	5.6
9035188	Tinga	4	5.2^{ns}	-
9035003	Kericho Water	4.8 & 10	(2.2 & 4.8 4.0)^{ns}	2.5, 3, 5 &14
9035258	Kipkelion	4	7.6^{ns}	6.3
9035226	Londiani	5.2	8.3	12.5^{ns}
9035341	Finlay	2.2, 4.8, & 11	2.2, 4 & 6.7	2.5, 3.3, 5.2, & 11
9034087	Chemelil	2.73^{ns}	4.3	2.5, 5.2
9035279	Kericho Met	8.3	(7.8, 4.0)^{ns}	6.0

Notes: ^{ns} indicates values are non- significant for periodicity at the 95% significance level

(ii) Results of streamflow periodicity analysis using spectral technique

Significant streamflow periodic oscillations are indicated as: (i) for MAM series; Nyando Kericho station indicated 3&10 year periods; Nyando Kisumu indicated a 6.6-year period; Mbogo and Nyando stations indicated a 3.3-year period each; and Tugenon indicated a 4.0-year period; (ii) for JJA series: Nyando Kericho indicated a 6.6-year period; Ainamotua station indicated a 6.3-year; Mbogo and Masaita stations indicated 4-year period; Ainopsiwa station indicated 2.6 & 5-year periods; and Tugenon station indicated a 4-year period, and (iii) for OND series: Ainamotua indicated 3 & 7-year periods; Ainopsiwa indicated 2.5, 3, 5 & 14-year periods; Kipkelion station indicated a 6.3-year period; Finlay station indicated 2.5, 3.3, 5 & 11-year periods; Chemelil station indicated a 5- year period; and Masaita station a 5.9- year period.

A summary of streamflow spectral analysis results are presented in Table 4.13. Some of the periodicities were not significant at the 5% significance level. These included the peaks of MAM series at Ainamotua, Ainopsiwa and Masaita, peaks of JJA series at

Nyando Kisumu, and the peaks of OND series at Nyando streamflow stations. Figure 4.13 presents periodicities for streamflow series at Mbogo, Nyando Kericho and Masaita stations. The other spectral results are contained in Appendix 8B.

The same definitions and descriptions for Figure 4.12 apply to Figure 4.13. Figure 4.13 indicates that most of the variance of the time series are described by high frequencies (short periods) similar to the periods in the rainfall seasons. Figure 4.13 (a) indicates a 3.3-year period for MAM and a 4-year period for JJA streamflow series at Mbogo station. OND series at Mbogo shows a weak 4.3-year period. Figure 4.13 (b) indicates a 3.7 & 10-year period for MAM series, a 6.7-year period for JJA and a 5.5-year period for OND at Nyando Kericho station.

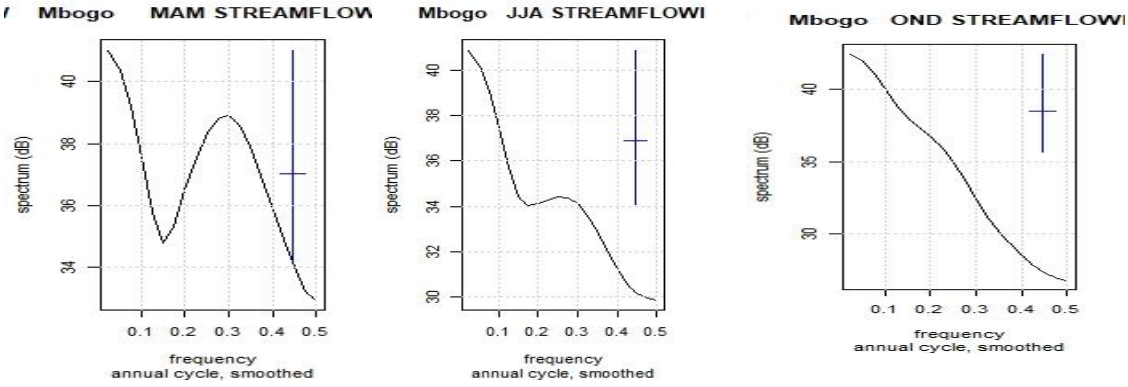

Figure 4.13: (a) Streamflow periods at Mbogo station.

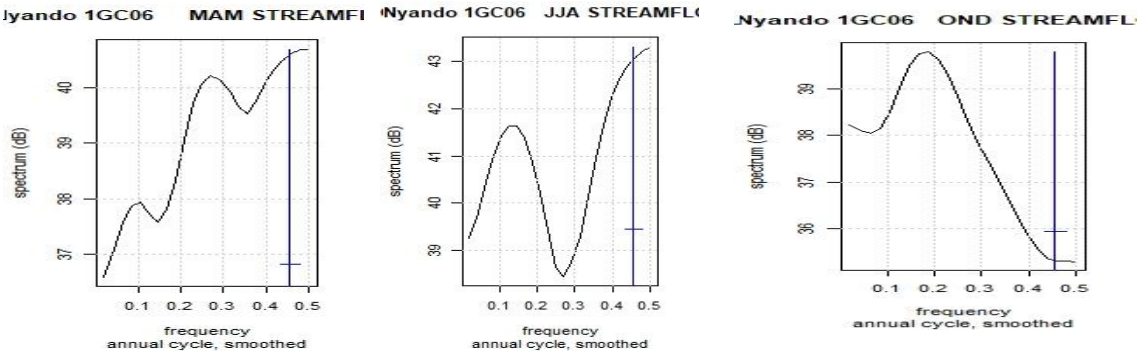

Figure 4.13: (b) Streamflow periods at Nyando Kericho station.

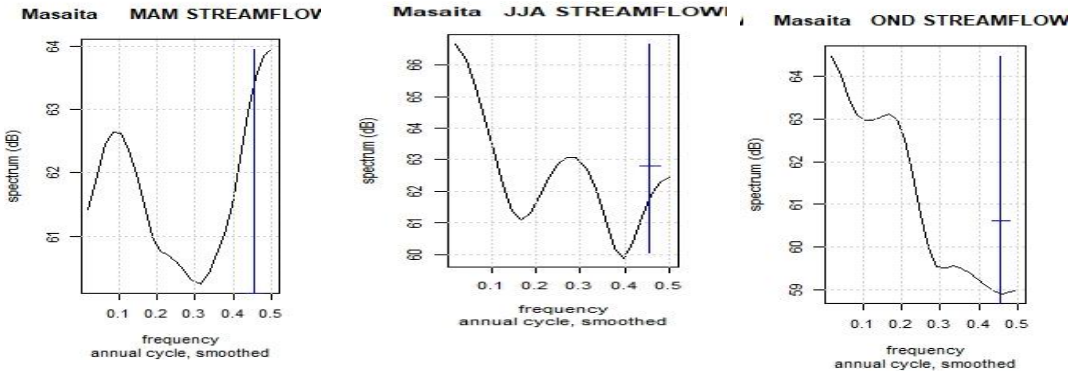

Figure 4.13: (c) Streamflow periods at Masaita station.

Figure 4.13(c) indicates a no significant period for MAM but shows a 3.7-year and 6.3-year periods for JJA and OND series, respectively at Masaita. Table 4.13 presents a summary of streamflow spectral results for Nyando basin. Table 4.13 shows significant periods of 3.0, 3.3, 4.0 & 6.6 years. The other periods marked ns are not significant at the 95% confidence interval. Spectral technique showed only the peaks but was not able to indicate the time of the peaks.

Table 4.11: Results of spectral analysis for streamflow

Station Code	Station Name	Periodicity in Years		
		MAM	JJA	OND
1GC06	Nyando Kericho	10 & 3	6.6	-
1GD07	Nyando Kisumu	6.6	(2.8, 4.0)^{ns}	-
1GB05	Ainamotua	(6.7 & 0.3)^{ns}	6.3	3 & 7
1GB06	Mbogo	3.3	20	20 & 4 ^{ns}
1GB11	Ainopiswa	(5.6 & 2.3)^{ns}	5 & 2.6	5
1GC05	Masaita	10^{ns}	4	5.9
1GD04	Nyando	3.3	6.6	(2.9, 6.7, 4.0)^{ns}
1GC04	Tugenon	4	3.5	-

Notes: ^{ns} indicates values are non- significant for periodicity at the 95% significance level.

Due to this limitation, Continuous Wavelet Transform (CWT) was therefore used to additionally reveal localized intermittent periodicities due to ability of the wavelet to expand time series into time- frequency space.

4.4.2 Results of periodicity analysis using wavelet transform

Wavelet analysis has followed the method of Torrence and Compo (1998). The software used was sourced from URL: http://paos.colorado.edu/research/wavelets. Although the methods were reviewed in the present study, readers are referred to Torrence and Compo (1998) for details. The results presented indicate the wavelet power spectra of the time series. The significance of the wavelet power spectrum were evaluated by comparing the spectra with a background (or noise) spectrum. The background spectrum depends on the nature of the data. In geophysical process, the background spectrum is either a white noise (constant variance across all scales, or frequencies) or a red noise (increasing variance with increasing scale or decreasing frequency).

(i) Results of rainfall periodicity analysis using wavelet transform

From the wavelet analysis, significant rainfall periodic oscillations for MAM series were: Ahero irrigation indicated 5-7 year period between 1940-1950 and 10-12 year between 1945-1965; Nandi Tea indicated 4-year period detected between 1963-1970; Tinga Monastery station indicated 3-4-year period observed between 1963-1970 and 4-7-year period between 1975-1980; Kericho Water showed a period of 5-6 years between 1940-1960 and 10-12-year period between 1940-190; Kipkelion station showed period of 3-5 years between 1950-1965; Londiani station showed 6-6-year period between 1940-1950; Finlay station showed 6-7-year period between 1975-1980 and 3.5- year period between 1995-2000; Chemelil station showed 2.5-year period from 1985-1990 and 3.5- year period from 1980-1990; Kericho Met station showed 3.5-year period between 2002-200.

For JJA series: Nandi tea station showed a period of 3.5 years observed from 1963-1970; Kericho Water showed a period of 4-year period detected in 1940, 6-8 years period detected between 1945-1955 and 3-4 years period in 1970; Londiani station showed 8-year period between 1945-1955 and 7-year period between 1965-1975; Finlay station showed a 4-year period between 1965-1970 and 1980-1975; Chemelil station showed period of 3.5-year between 1990-1995; Kericho Met showed 2.5-year peak between 2003-2005. For OND series: Nandi tea showed 5-year period between 1973-1980; Tinga Monastery showed 5-7 years period from 1975-1982; Kericho Water showed 10-12 year period between 1952-1965; Kipkelion station showed 6-year period between 1975-1983; Londiani showed 6- year period between 1982-1985; Finlay station showed 4-year period in 1940, and 3-year period in 1950; Chemelil showed 5-7 year period between 1975-1985 and 2-3 year period between 1995-2000; and Kericho Met station showed 3-4 year period between 2003-2005. Some of the resulting wavelet power

spectra showing periodicities for Finlay rainfall station are presented in Figure 4.14 whereas the entire results are contained in Appendix 10(A).

Figures 4.14 shows the power which is the square of the absolute value (absolute value)^2 of the wavelet transform for the total seasonal rainfall at Finlay station. The (absolute value)^2 gives information on the relative power at a certain scale and at a certain time. The values of the wavelet spectrum represent the magnitude of the variance in the series at a given wavelet scale and location in time. The figure shows the actual oscillations of the individual wavelets, rather than just their magnitudes. In the wavelet power spectra, the thick contour designates the 5% significance level against red noise and the Cone of Influence (COI) where edge effects might distort the picture is shown as a lighter shade.

The CWT normally has edge artefacts because the wavelet is not completely localized in time. It is therefore useful to introduce the cone of influence in which edge effects cannot be ignored. The COI is taken as the area in which the wavelet power caused by a discontinuity at the edge has dropped to e^{-2} of the value at the edge.

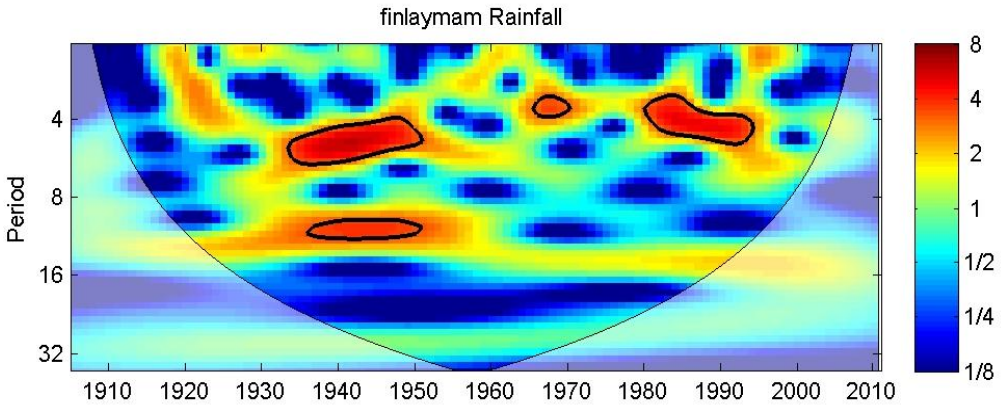

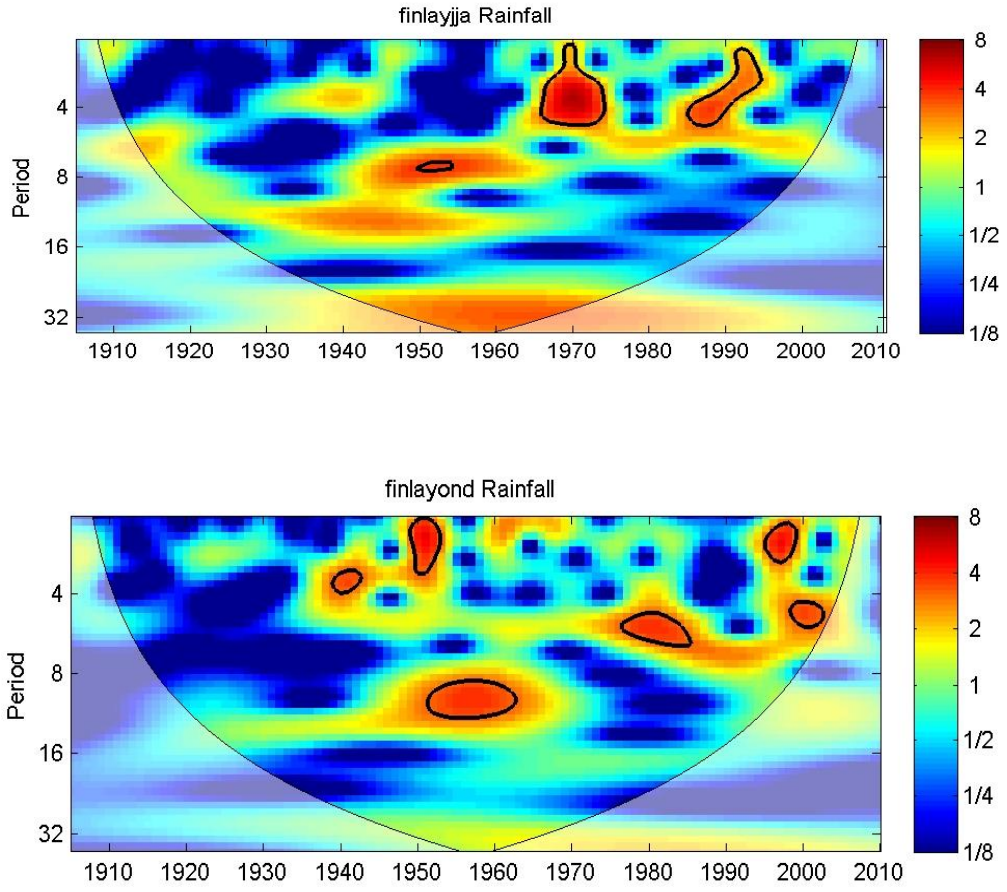

Figure 4.14: (a) Wavelet power spectra for rainfall at Finlay.

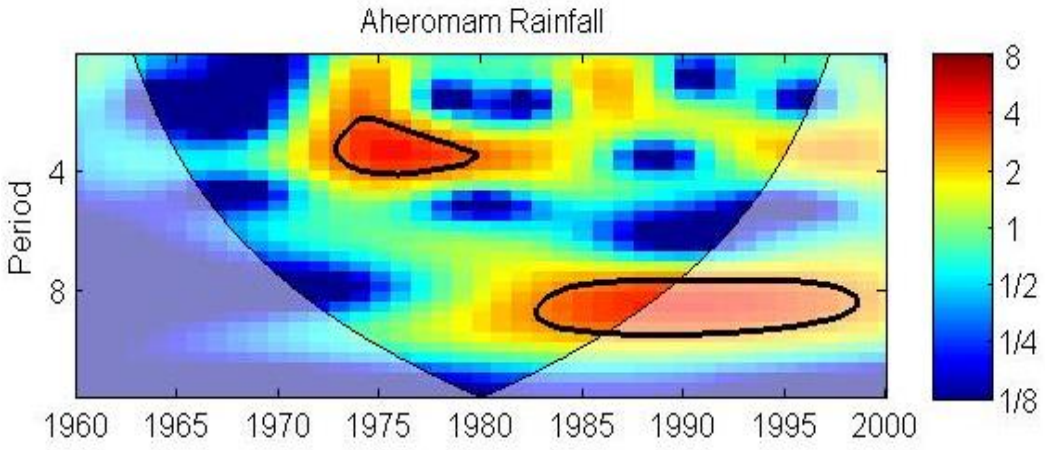

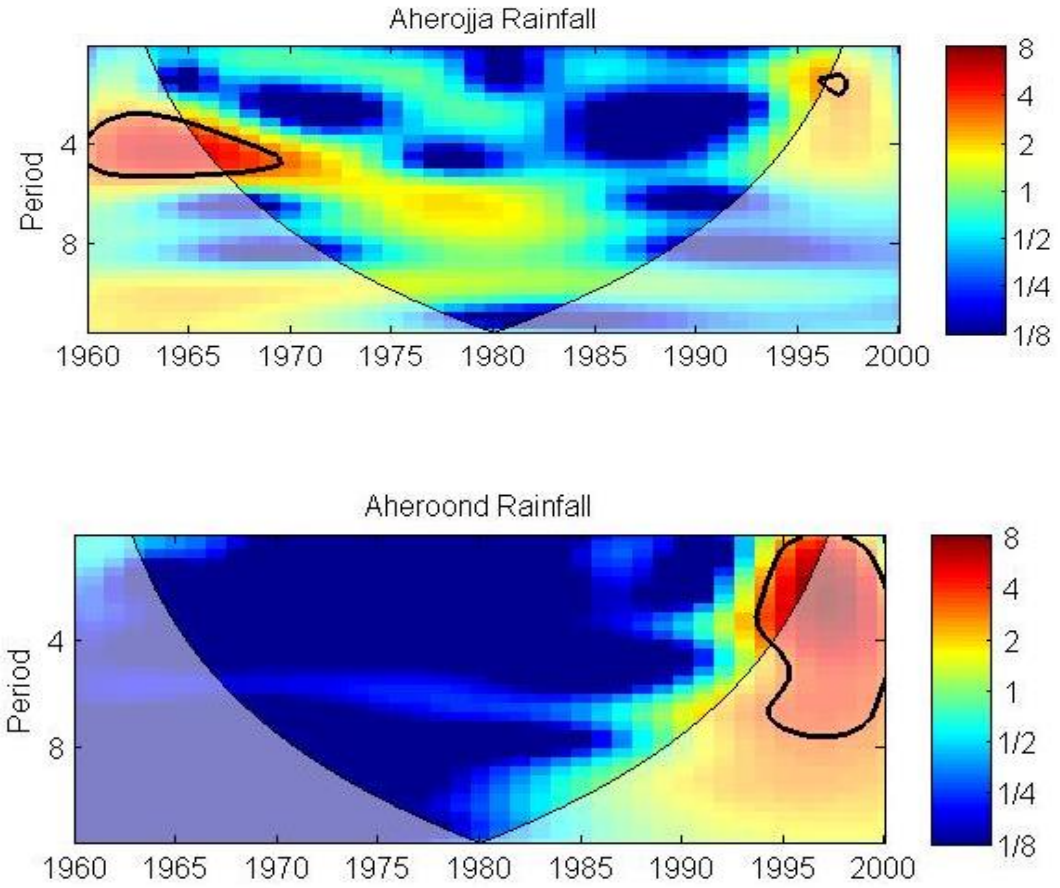

Figure 4.14: (b) Wavelet power spectra for rainfall at Ahero.

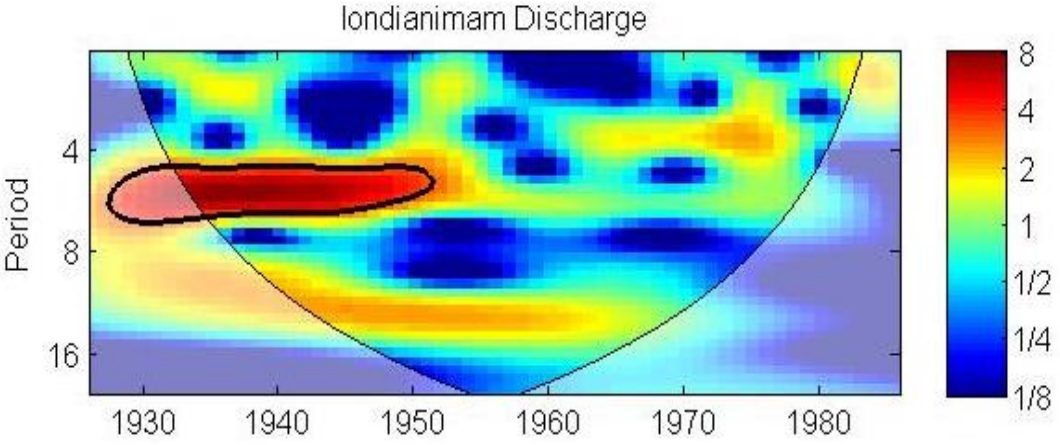

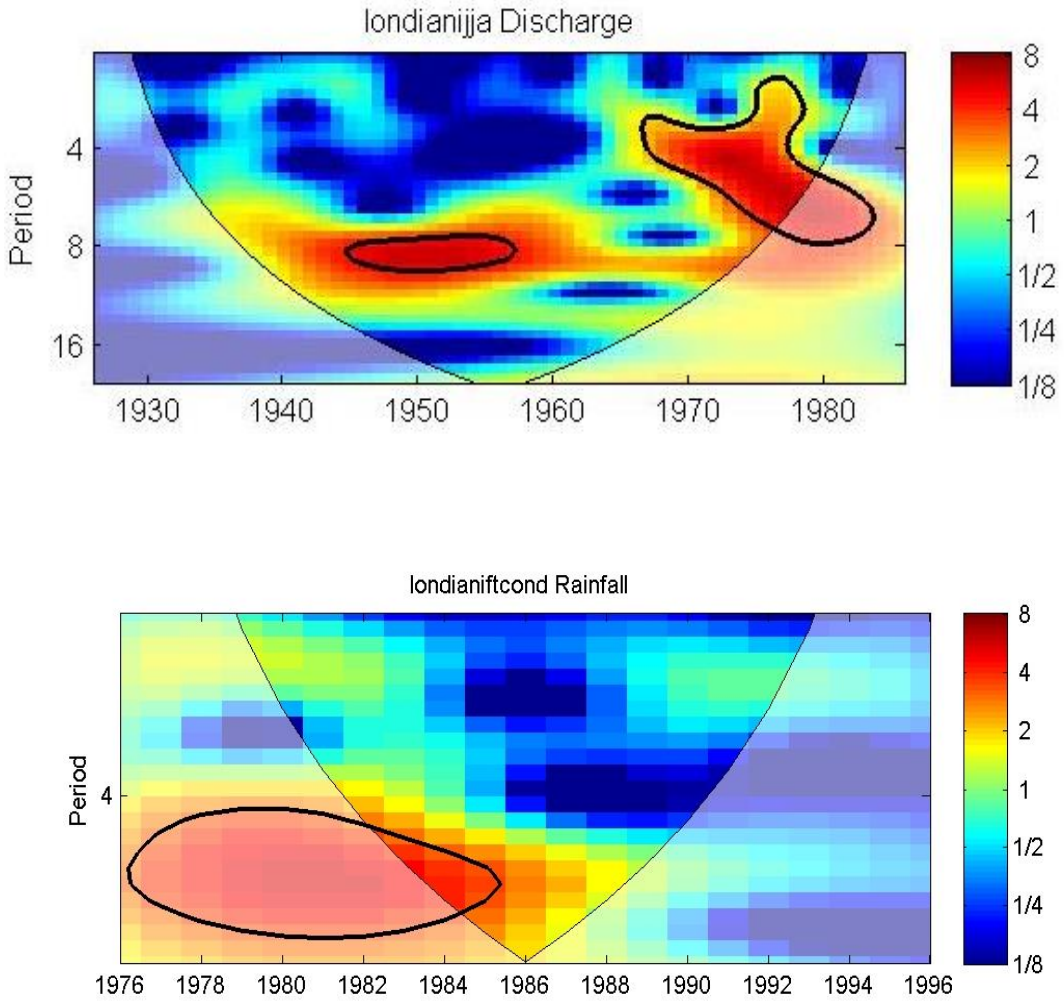

Figure 4.14: (c) Wavelet power spectra for rainfall at Londiani.

Figure 4.14 **(c)** shows the relationship of power and the frequency or the time domain. The intensity of the colormap represents the variance of the time series that is associated with particular frequencies (y-axis) through time (x-axis). The X and Y-axes represent the time units of the sampling interval and the sampling interval, respectively. The scale bar on the right side of the wavelet spectrum indicates the frequency bands. The weakest to the strongest correlations in time-frequency space are represented by the colors from blue to red respectively.

Figure 4.14 (a) shows wavelet power spectra for rainfall at Finlay station. The MAM series at this station manifests four significant periodic oscillations (periods) of 4-6 years and 9-12 years occurring from 1935 to 1955, 2-3 year periods in 1970 and 2-4 years occurring from 1975-1992. Although the MAM series reflects some features of the April spectra, the latter indicates three oscillations, all falling before 1965. The JJA series indicate 2-7 year periods from 1965-1975. Similarly, OND rainfall is shown to have 3-year periods in 1950, 4-year period in 1940, and a 9-year period from 1950-1960).

Figure 4.14 (b) shows wavelet power spectra for rainfall at Ahero rainfall station. The MAM series manifest a 5-7 year period from 1940-1950) and a 10-12 year period from 1945-1965). At this station, JJA and OND series manifest weak signals and do not show any oscillations. In Figure 4.14(c) for Londiani rainfall station, MAM series show a 6-7 year period from 1940-1950, JJA series show a 7-8 year period from 1945-1955. OND shows a 6-year period from 1982-1955). Table 4.14 presents a summary of wavelet-based periodicity results indicating major oscillations.

Table 4.14 contains names of rainfall stations and station codes, periodic oscillations denoted by P and the years of occurrence. In general the peaks are centred on 2-4 years, 3.5 years, 5-6 years, 6-7, years, 7-8 years and 10-12 years. The 2-4 year periods indicate existence of the Quasi-biennial Oscillations (QBO). The 2-7 year periods are associated with El Niño Southern Oscillation (ENSO), and the 10-12 year shows the existence of Decadal Oscillations (DO).

Table 4.14: Results of rainfall periodicity analysis using wavelet transform

Station code	Station Name	MAM		JJA		OND	
		P (Yrs)	Year	P (Yrs)	Year	P (Yrs)	Year
9034386	Ahero	5 - 7 10 - 12	1940-1950 1945-1965	-	-	-	
8935095	Nandi Tea	4	1963-1970	3.5	1963-1970	5	1973-1980
9035188	Tinga	2 - 4	1963-1970 1975-1980	-	-	5 - 7	1975-1982
9035003	Kericho Water	5 - 6 10-12	1935-1950 1940-1960	4 6 - 8 3 - 4	1940 1945-1955 1970	10-12	1952-1965
9035258	Kipkelion	3 - 5	1950-1965	-	-	6	1975-1983
9035226	Londiani	6 - 7	1940-1950	7 - 8 7	1945-1955 1965-1975	6	1982- 1985
9035341	Finlay	4 -6 9-12 2 - 3 2 - 4	1935-1950 1935-1950 1970 1975-1992	2-7	1965-1975 1985-1994	4 3	1940 1950-1960

The study by Anyah and Semazzi (2004) indicates that major climate factors that regulate the Lake Victoria basin include ENSO, the QBO, the Inter-Tropical Convergence Zone and the Monsoon winds. According to Kizza *et al*. (2009) as already stated, the inter-annual variability in received rainfall corresponds to ENSO changes.

(ii) Results of streamflow periodicity analysis using wavelet transform

Sample streamflow periodicity results are presented in Figure 4.15 with full results in Appendix 10B. Significant streamflow periodicities were indicated for MAM series as: Nyando Kericho station indicated 2-3 year period between 1987-1992 and 1988-1993; Nyando Kisumu and Ainamotua showed 2-3 year period between 1975-1980; and Tugenon showed 2-3 year period between 1965-1993; For JJA series: Nyando Kericho showed 5-7 year period between 1985-1993; Nyando Kisumu 2-3 year period from 1975-1980; and Tugenon station showed 2-3 year period between 1966-1970 and from

1987-1992. For OND series: Nyando Kericho station showed period of 6-years from 1980-1993; Nyando Kisumu showed period of 3 years from 1973-1977 and 6-years period from 1976-1980; Ainamotua showed period of 6 years in 1960 and from 1976-1980; Mbogo station showed 3-year period in 1960 and from 1983-1990 and 7-year period from 1980-1987; and Masaita station showed 2-year period in 1975 and 6-year period from 1976-1986.

Figures 4.15 shows the results for MAM at Nyando (GD104), JJA at Nyando Kisumu (GD107) and for OND, also at Kisumu (GD107), respectively. The entire wavelet spectra showing periodicities may be seen in Appendix 10B. Nyando Kisumu station is located far downstream towards the Lake Victoria and is assumed to accumulate the stream discharges from all the tributaries upstream. Optimal flow at this station is normally observed during JJA and OND. The MAM streamflow at this station normally overflows and bursts the river banks and hence the streamflow is not fully captured by the gauge. The MAM series at Nyando-1GD04, located upstream and where the streamflow is relatively calm is also presented.

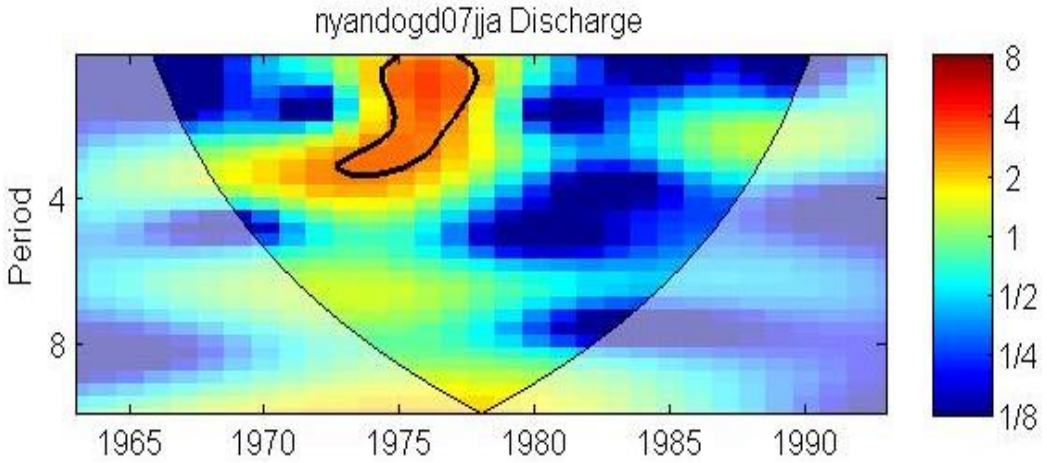

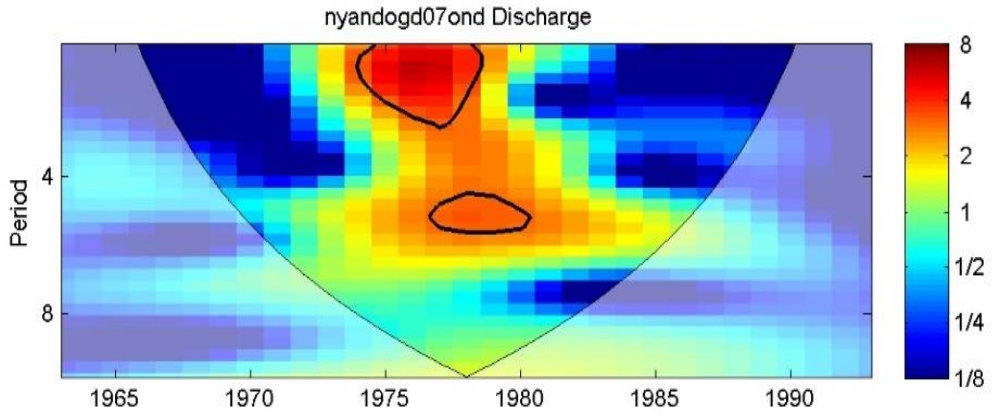

Figure 4.15: (a) Wavelet power spectra for streamflow at Nyando 1GD07.

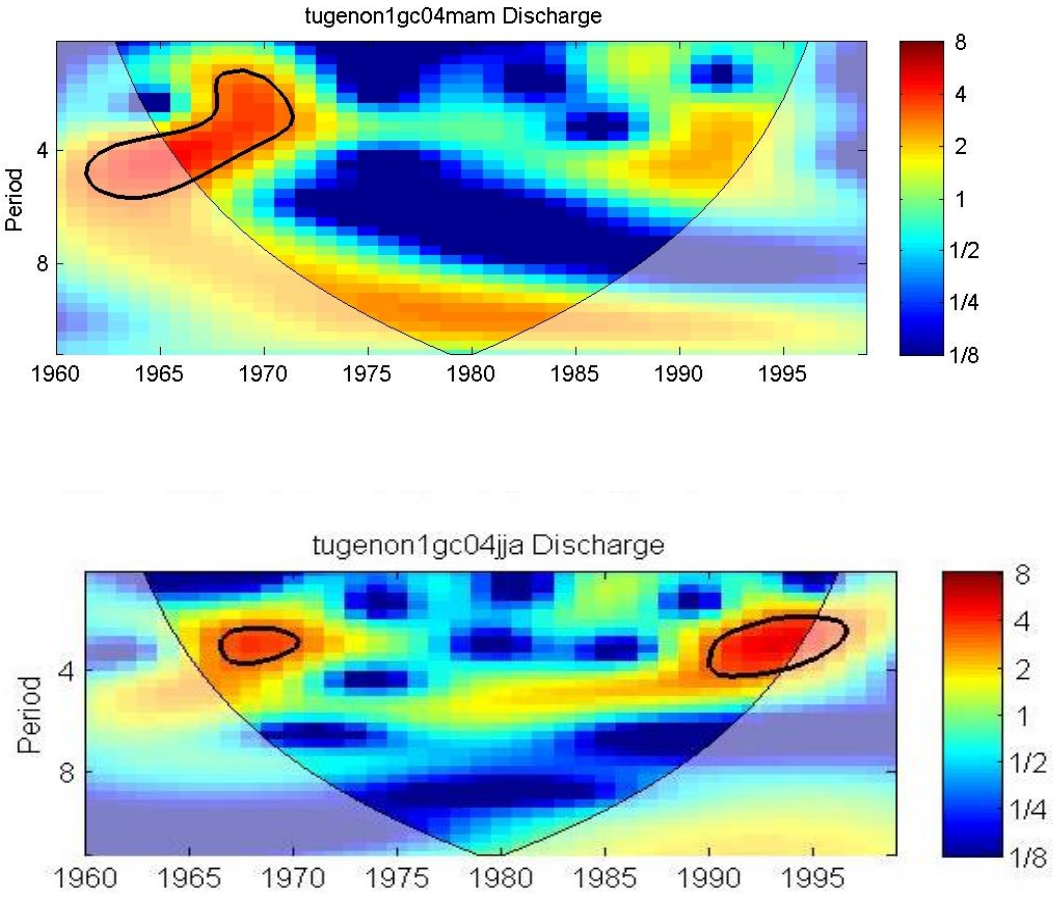

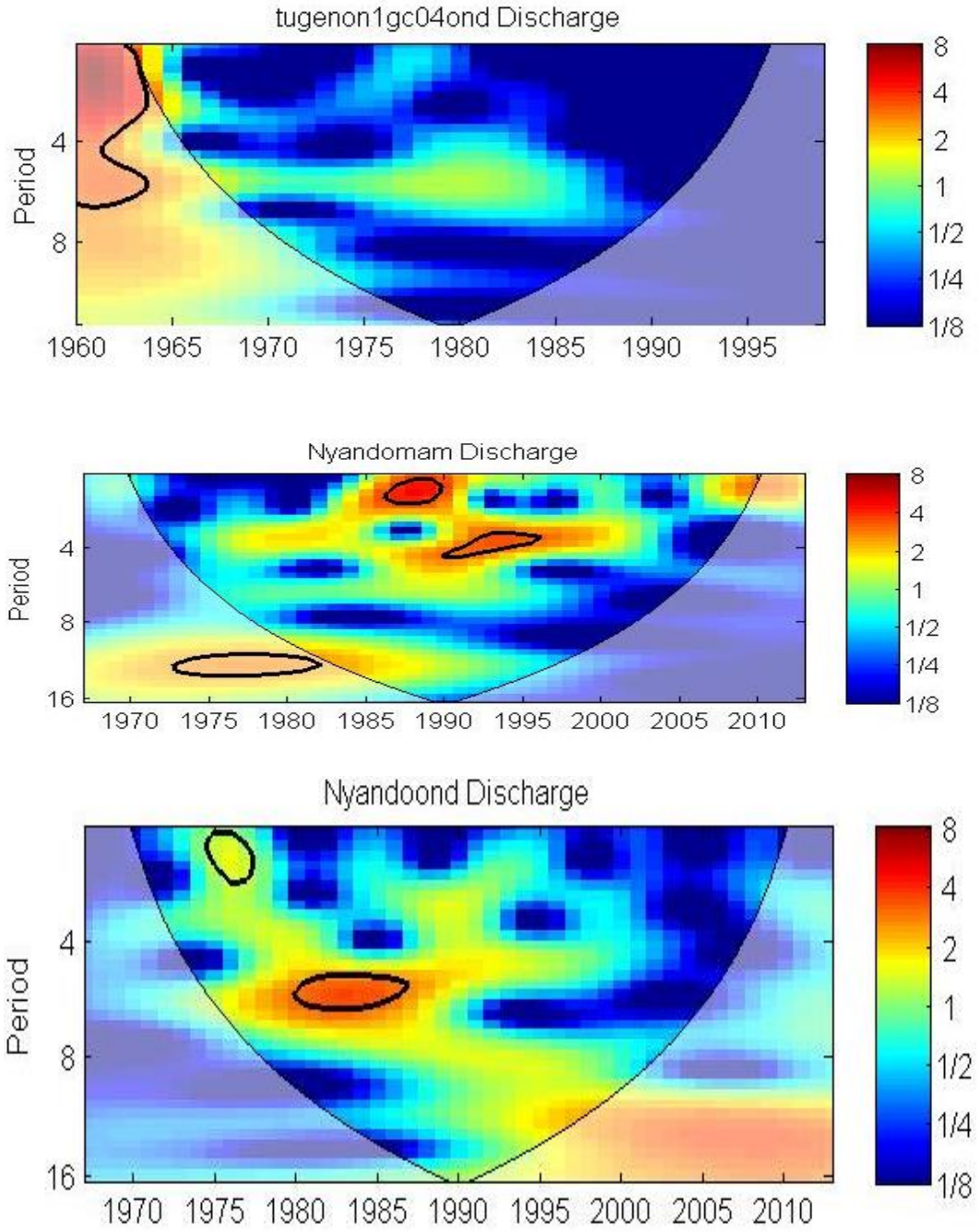

Figure 4.15: (b) Wavelet power spectra for streamflow at Tugenon

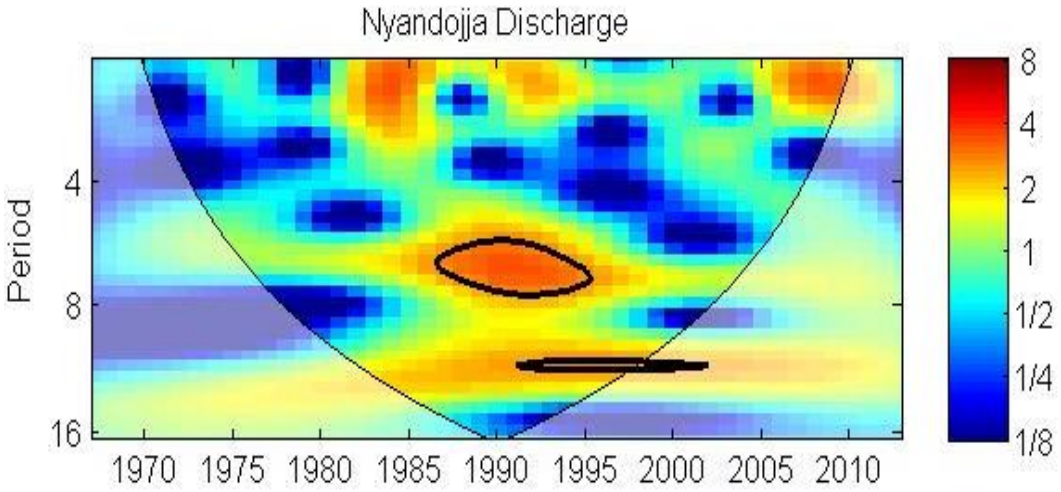

Figure 4.15: (c) Wavelet power spectra for streamflow at Nyando.

The descriptions in Figure 4.14 also apply for Figure 4.15. Figure 4.15(a) shows wavelet power spectra for MAM, JJA and OND series at Nyando 1GD07 station. MAM and JJA indicate a 2-3 year period each. OND series indicate a 3.5-year period from 1973-1977 and a 6-year period from 1976-1980). Figure 4.15(b) shows wavelet power spectra for streamflow series at Tugenon station streamflow series. MAM show a 2-3 year period from 1965-1990), JJA shows 2-3 year periods from 166-1970 and also from 1987-1992. OND series at Tugenon station does not manifest any significant period. In Figure 4.15 (c), Only MAM series manifest a 2-3 year period from 1985-1990 and a 4-6 year period from 1990-1998 at Nyando streamflow station. JJA and OND do not show any significant signal.

A summary of streamflow spectral analysis results are presented in Table 4.15. The streamflow series at Mbogo and Ainopsiwa do not show any periodic cycles and are therefore not shown in the results. The Table indicates names of the streamflow stations, station codes, periodic cycles, year of occurrences and the signal strengths for the streamflow series.

Table 4.12: Results of Streamflow periodicity analysis using wavelet transform

Station code	S/Name	MAM		JJA		OND	
		P (Yrs)	Year	P (Yrs)	Year	P (Yrs)	Year
1GC06	Nyando	2 - 3	1987-1995	2 - 7	1985-1995	6	1980 -1996
	Kericho	2 - 3					
1GD07	Nyando	2 - 3	1975-1980	2 - 3	1975-1980	3.5	1973 - 1977
	Kisumu					6	1976 - 1980
1GD04	Nyando	2 - 3	1985-1990	-	-	-	-
		4 - 6	1990- 1998				
1GB05	Ainamotua	2 - 3	1975-1980	-	-	3.5	1960
						3.5	1983-1990
						7	1980-1987
1GC05	Masaita	-	-	-	-	2	1975
						6	1976-1986
1GC04	Tugenon	2 - 3	1965-1990	2 - 3	1966-1970	-	-
				2 - 3	1987-1992		

As already stated, the peaks centred around 2-7 years are associated with El Niño events according to historical records. An El Niño cycle has a peak of 2-7 years and is the cause of frequent floods in the Nyando River basin. El Niño and La Niña episodes tend to recur after every two to seven years. Whereas one may associate the 2-4 year period with the quasi-biennial oscillation (QBO) found primarily in the circulation of the tropical stratosphere, the physical interpretation of the 3.5-year peak is not immediately obvious. According to Berlenge's (1957) account in Rodhe and Virji (1976), a 3.5-year period is mentioned in indo-pacific weather as an "outstanding phenomenon". This would support the idea that the 3.5-year periodicity also has a physical origin rather than being due to random fluctuations.

According to Roshani *et al.* (2012), runoff changes in relation to rainfall is normal but its rate and intensity are different by considering the conditions of season, physiography, climate and plant coverage. The episodic rainfall events of 1996-1998 that exceeded

flooding problems in the entire Lake Victoria basin have been reported by Khisha *et al.*, (2013) in which episodic flood and drought events have been linked to the El Niño-Southern-Oscillation (ENSO), Indian Ocean Dipole (IOD) and many other large scale climate systems in the East African region.

As the results of this study have suggested, the relative frequency and magnitude of floods in the basin may be explained both by climate change and human activities within the Nyando River basin. Human activities are mainly the unregulated cutting of trees for settlement and agricultural purposes. There are evidences that changes in land use have influenced the hydrological regime of various river basins (Khisa *et al.,* 2013). It is however more challenging to quantify the impact of land-use change on the rainfall run-off relations for large basins where the interactions between land-use, climatic characteristics and underlying hydrological processes are often more complex and dynamic (Khisa *et al*., 2013). According to Lafreniere and Sharp (2003), inter-catchment differences in run-off regimes may reflect differences in the run-off sources in the flow- routing within the catchments.

(iii) Results of cross wavelet analysis of two time series

In this study, co-variance of two sets of time series were examined in order to reveal existence of any relationships between the time series. The cross-wavelet is an extension of wavelet approach to the simultaneous analysis of two time series. The purpose of cross wavelet was to uncover the correlation between two series at different frequencies. The clusters established for streamflow in Figure 4.19 of section 4.5.3 was modified to form zones I, II, & III which were used in the cross wavelet analysis.

In the creation of zones, clusters three and four were merged to come up with zone I (Ainamotua Masaita, Nyando Kericho and Tugenon). Zone I stations are located

geographically within the highland areas of the basin. Zone II include Ainopsiwa and Mbogo stations which are located within the middle plateau. Nyando 1GD04 and Nyando Kisumu-1GD07 are located within the lower stretch of Nyando River towards Lake Victoria in zone III. Similarly, for rainfall stations, Zone I contain Londiani, Tinga Monastery, Kipkelion and Kericho Met stations. Zone II contains Kericho Met and Kericho Water, and zone III contains Ahero irrigation and Chemelil rainfall stations.

(a) Results of rainfall and streamflow cross wavelets

Some of the cross wavelets between rainfall and streamflow time series showed strong links therefore implying that rainfall most likely affected the streamflow as was revealed in this study.

Appendix 9C contains cross wavelet results. The results revealed strong correlations between: November rainfall and OND streamflow of zone I indicating that the November rainfall influenced the OND streamflow; March rainfall and April streamflow indicating that rainfall in March influenced the April streamflow; July rainfall and July streamflow zone I indicating some influence of July rainfall on the July streamflow in zone I; July rainfall and JJA streamflow zone I, showing the July rainfall influences JJA streamflow; April rainfall and April streamflow in zone I, implying there is influence by April rainfall on April streamflow. The cross wavelet between June rainfall and July streamflow zone I however showed no link, implying June rainfall did not influence July streamflow in zone I. Similarly, October rainfall had no link with the OND streamflow implying the October rainfall hardly influenced the short rains of OND. Figure 4.16 indicates examples of the relationships between the Nyando rainfall and streamflow. Entire cross wavelet results are shown in Appendix 9C.

In the Figure 4.16, cross wavelet is represented by colored contour: The x–axis represents time and the y-axis represents the period. The matching of colors and correlation levels are represented by the scale on the right side of the graph. The weakest to strongest correlations in time-frequency space are represented by colors from blue to yellow respectively. Statistically significant correlations are highlighted by a thick black curve around the significant regions; significance is based on Monte Carlo simulations against the null hypothesis of the red noise, i.e. an autoregressive process of order one. The cone of influence separating the regions with reliable and less reliable estimates is represented by bright and pale colors, respectively.

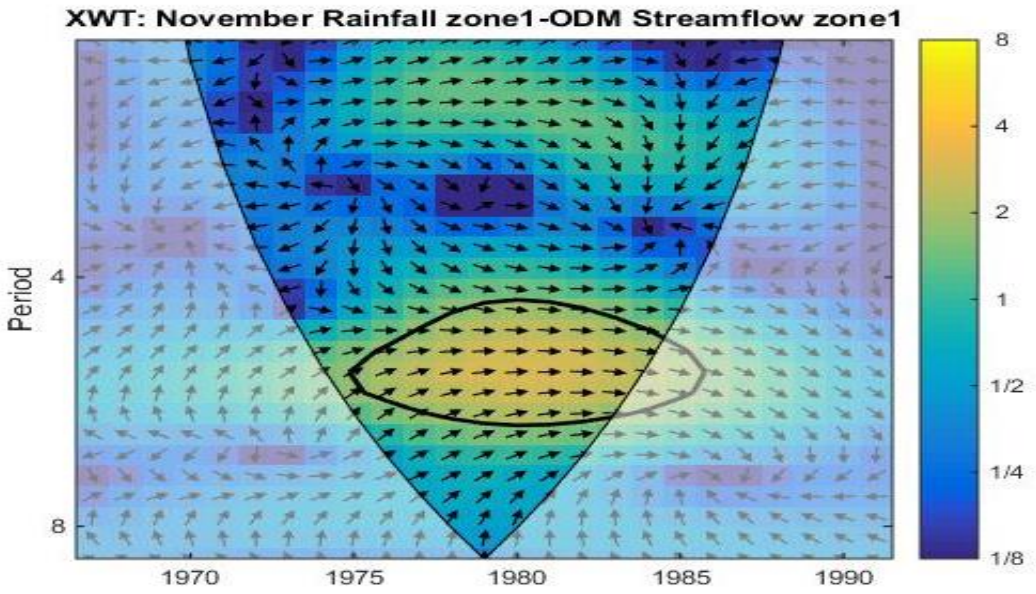

Figure 4.16 (a): Cross wavelets in November rainfall –OND streamflow.

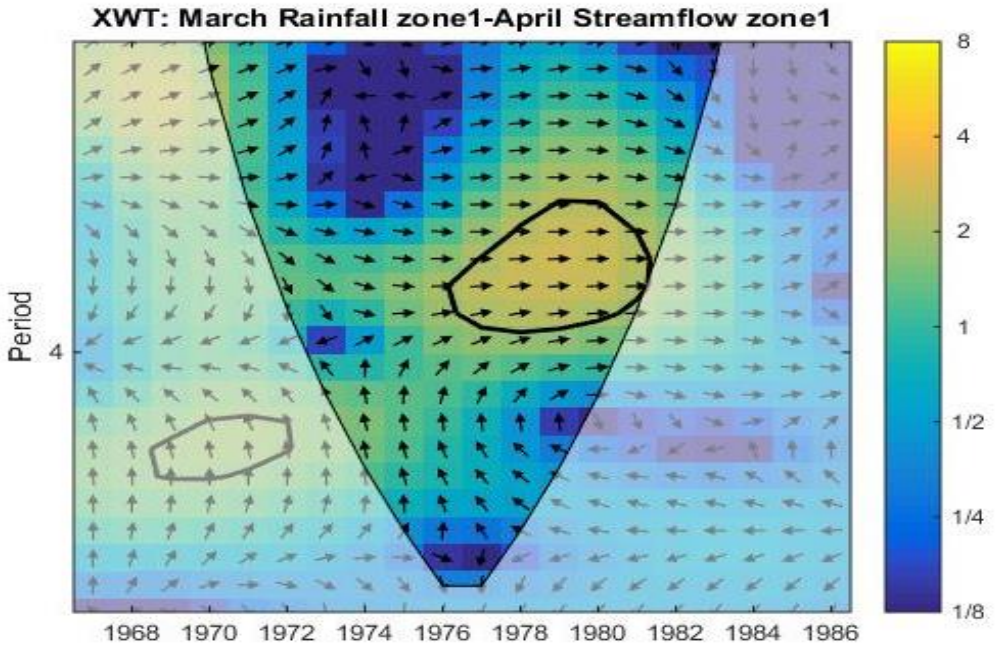

Figure 4.16 (b): Cross wavelets in March rainfall –April streamflow.

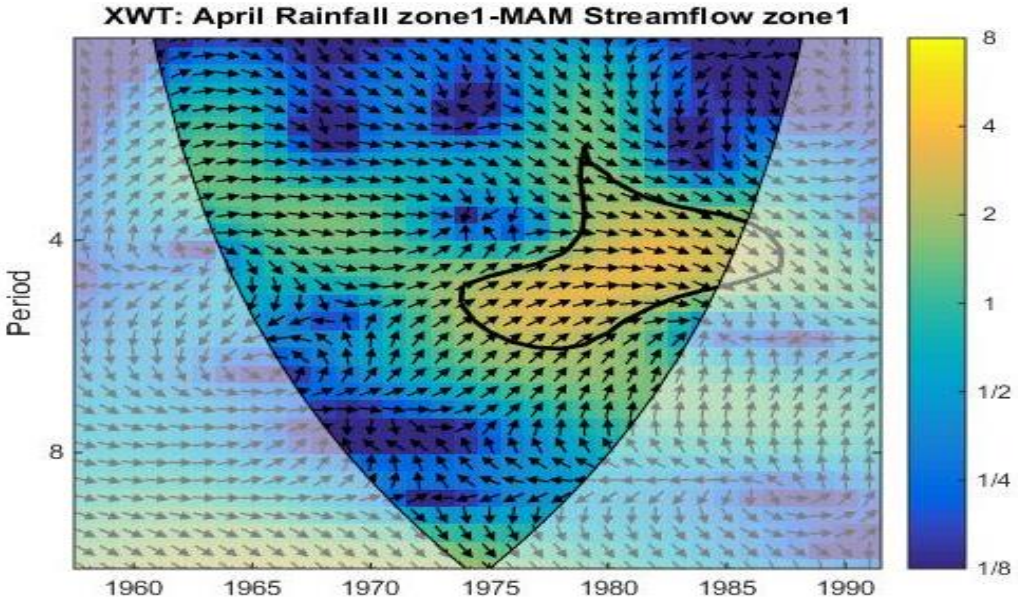

Figure 4.16 (c): Cross wavelets in April rainfall –MAM streamflow Zone 1

Phase (lag-lead) relationships are shown by the arrows-a positive correlation is represented by an arrow pointing to the right, a negative correlation by one to the left, leadership of the first variable is shown by a downward pointing arrow and if it lags, the relationship is represented by an upward pointing arrow.

(b) Results of streamflow and streamflow cross wavelets

Similarly, inter-streamflow cross wavelets uncovered some strong correlations which imply that particular streamflow most likely affected some other streamflow. The results showed that OND streamflow for zones II & III were strongly linked, implying that the zone II streamflow influenced the downstream zone III; OND and November streamflow in zone I showed strong link, implying that the November streamflow influenced the OND streamflow; MAM streamflow of zone I and MAM streamflow of zone III were strongly correlated but the link was weak, showing that MAM streamflow zone I influenced MAM streamflow of zone III only to a small extent. Figure 4.17 indicates example of the cross wavelet between zones 2 & 3 of OND streamflow whereas the other results are shown in Appendix 9(C) as already stated.

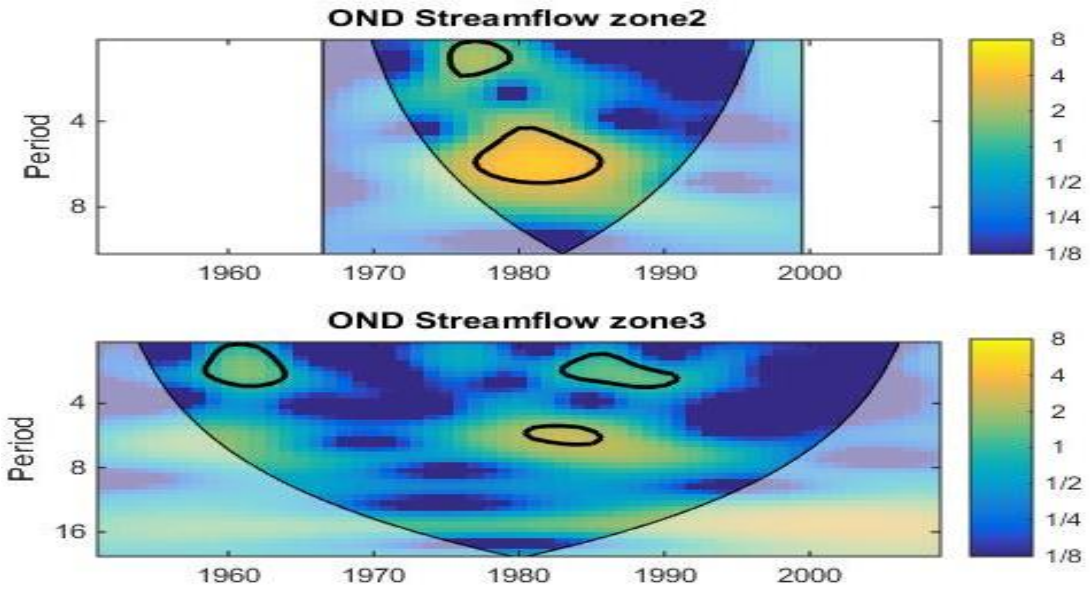

Figure 4.17: (a) Wavelet power for zones I & III of OND streamflow.

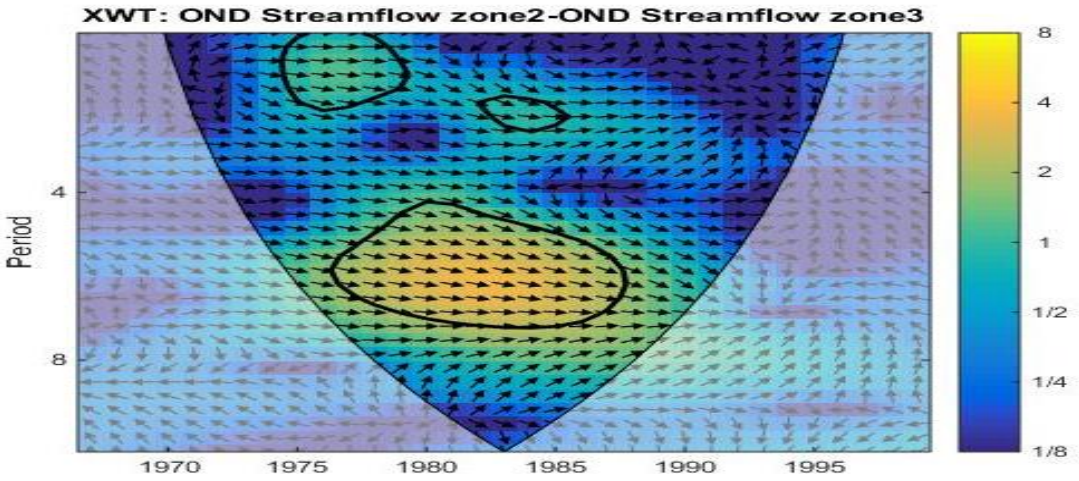

Figure 4.17: (b) Cross wavelet power between zones I & II of OND streamflow.

Figure 4.17(a) shows separate wavelet power spectra for OND streamflow for zones II & III before the two series were crossed. There are clearly common features in the wavelet power of the two time series. OND streamflow of zone II shows significant peaks in the 2–3-year period from 1976-1980- and 5-7-year period from 1978 to1985 while the OND streamflow for zone III shows periods in the 2-3 year peak from 1960 to1964 and from (1982 to 1993 and a 5-7 year period from 1980 to1985.

Figure 4.16 (b) shows cross wavelet power between OND streamflow for zones I & II. The vectors indicate the phase difference between OND streamflow for zones I & II (a horizontal arrow pointing from left to right signify in-phase between the two streamflow series). The thick black line is the 5% significance level using the red noise model, and the thick black line indicates the cone of influence. The two time series are linked to form a 5-7 year peak from 1976-1987. The peak stands out as more prominent and being significant at the 5% significance level. The two time series are in-phase with each other with no evident leader (as the arrows point towards the right side of the spectra). It was therefore speculated that the OND streamflow in the two zones influenced each other.

(iv) Results of wavelet coherence analysis

Wavelet transform coherence analysis was done in order to reveal how coherent the generated cross-wavelets were. From the wavelet coherence analysis, positive correlations were revealed between: (a) April rainfall and MAM streamflow for zones I, (b) March rainfall and April streamflow, (c) November rainfall and OND streamflow zone I, (d) OND streamflow zone I and OND streamflow zone II, (f) OND streamflow zone II and OND streamflow zone III, (g) MAM streamflow zone I and MAM streamflow in zone III.

Additionally, positive correlations were also observed where October rainfall was seen leading November streamflow in zone I, July rainfall was seen leading July and JJA streamflow in zone I. There were however no coherences between June rainfall and July streamflow in zone 1 and between OND streamflow zone I and OND streamflow zone II.

Figure 4.17 indicates an example of the wavelet coherence between zones I & II of OND streamflow while the other results are shown in the appendix 9(D).

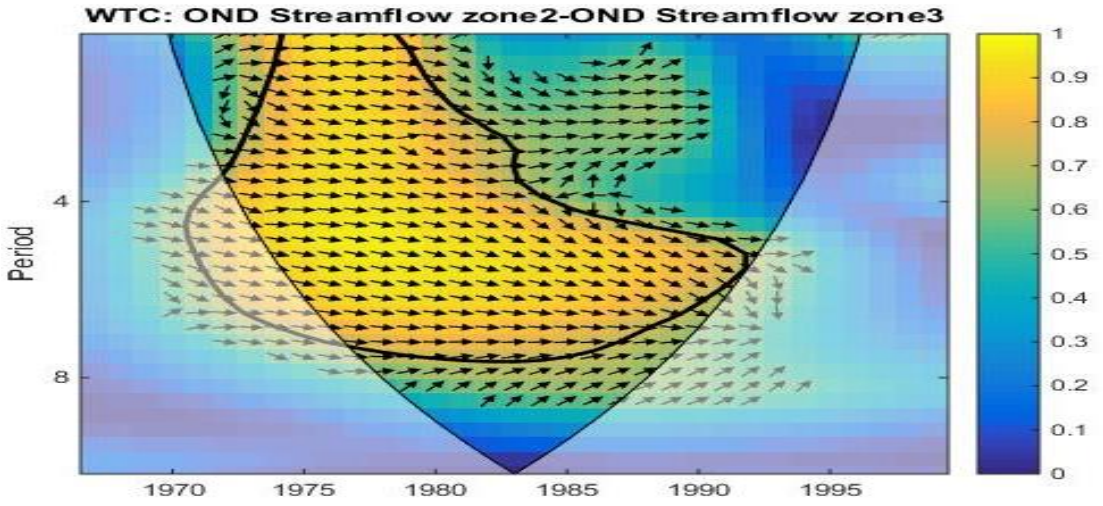

Figure 4.18: WTC for OND streamflow zones II & III.

Figure 4.18 shows correlations between OND streamflow for zones II & III. The Vectors indicate the phase difference between the OND streamflow in zones II & III (a horizontal arrow pointing from left to right imply the OND streamflow for zones I & II are in-phase). The thick black line is the 5% significance level using the red noise model, and the thin black line indicates the cone of influence. Compared with the cross wavelet transform (CWT) in Figure 4.17, it is observed that a large section stands out as being significant and all these areas show in-phase relationship between the OND series of zones II & III.

Further, the significant region in Figure 4.18 is so extensive that it is very unlikely that this is simply by chance. In addition, the sub-catchments clustered into zones are also correlated, noting that in terms of streamflow, the zones are in series since water flows downstream from zone I to zone III.

The November rainfall was seen to contribute to the OND streamflow time series. Similarly, the July rainfall contributed significantly in JJA streamflow and April rainfall in the same way contributed much in the MAM streamflow time series. Similar results obtained by Roshani *et al*. (2012) revealed that streamflow was dependent upon rainfall directly and any small change in rainfall will led to identical change in streamflow although the rate and intensity were different by considering the complexities of the seasons, climate and plant covering of the basin. The mean monthly rainfall for Nyando River basin according to Khisa *et al*. (2013) has the highest values in April, August and November. The hydrograph of the river peaks after one month time-lag after the onset of the long rains but peaks during the same month in the subsequent rains periods. The long rains are usually preceded by the long dry spells, hence allowing the catchment to absorb the first rains before the river peaks.

4.5 Comparative Evaluation of Wavelet and Conventional Methods

In this study, wavelet technique was used in addition to conventional methods to study trend and periodicity of rainfall and streamflow. The conventional techniques though complimentary to the wavelet approach have limitations in detecting the trend and periodic components of the time series.

Trend was analysed using two approaches, namely Mann-Kendall and Wavelets. In the Mann-Kendall analysis, the trends are displayed graphically indicating the increases and decreases in the hydrometeorological time series over the years. Further, Mann-Kendall technique computes the statistical significance at 95% confidence limit although this leaves out the changes taking place outside the 95% confidence limit. In the wavelet technique, the time series are decomposed into high and low frequency components. Low frequency components of time series are associated with trends and reveal monotonic (small step changes) trends in the time series. Whereas both the methods graphically display the changes, Mann-Kendall graphs are more of straight lines while Wavelet graphs indicate gradual curves. Examples are seen in Figure 4.9 showing the red dotted straight line for M-K and Figure 4.11 showing the red dotted curved line for wavelet. Wavelet method however, does not confine the changes to any level of significance but graphically gives a visual indication of the changes. This explains why the wavelet trend results were more pronounced than the Mann-Kendall results.

Additionally, the analysis for periodic components was done using Fourier and Wavelet transforms. The Fourier technique was done using periodogram analysis and revealed the periods but the technique is not able to indicate the time of occurrence. The significance of the period is indicated by a small horizontal mark which appears below a significant peak as seen for example in Figure 4.13 (c) of streamflow periods at

Masaita station. Wavelet method is an improvement over the traditional Fourier, noting that in the wavelet case, years of occurrence are clearly indicated for each periodic/spectral component of the time series. Further, the significance of the period is indicated by the colour of the spectra. An example is seen in Figure 4.14 (a) for rainfall wavelet power spectra at Finlay station. The values of the wavelet spectrum represent the magnitude of the variance in the series at a given wavelet scale and location in time. Actual oscillations of individual wavelets are also seen in addition to their magnitudes. The 5% level of significance against red noise is designated by a thick contour.

4.6 Results of frequency analysis

This section presents results for the regional frequency analysis carried out using the method of Hosking and Wallis (1997). The results included are for the discordancy and heterogeneity measures, L-moments diagrams and the regional growth curves for the probability distributions.

4.6.1 Discordancy measure (Di)

A statistic Di was computed according to equation 3.37 appearing in sub-section 3.6.1 (i) to check for discordant values in the time series. Table 4.16 and Table 4.17 show discordancy measure (Di) results for rainfall and streamflow, respectively for the Nyando River basin. L-cv denotes L-coefficient of variation, L-Skew denotes L-coefficient of skewness and L-Kur denotes L-coefficient of kurtosis. Appendix 10 (A & B) indicates the annual maximum rainfall and streamflow used in deriving the L-moment ratios in this study.

Table 4.13: L-Moments and Discordancy values for rainfall stations

Station code	Station Name	No. of years	Mean (mm)	L_Cv	L_Skew	L_kurt	Di
9034386	Ahero Irrigation	41	236.2811	0.1533	0.3546	0.4111	2.3613
8935095	Nandi Tea	29	265.8221	0.155	0.2466	0.1423	2.3624
9035188	Tinga Monastery	32	249.5613	0.1223	0.0554	0.0332	0.4233
9035003	Kericho Water	48	327.8152	0.1225	0.1232	0.0427	0.2828
9035258	Kipkelion	32	248.7623	0.1241	0.0722	0.0201	0.3121
9035226	Londiani	27	212.2942	0.1633	0.2517	0.1422	2.1413
9035341	Finlay	51	357.8444	0.1146	0.1111	0.1313	0.7724
9035003	Kericho Water	48	327.8145	0.1261	0.1226	0.0407	0.2881
9034087	Chemelil	41	269.833	0.1235	0.0711	0.0411	0.2903
9035279	Kericho Met	37	333.9912	0.1215	0.1155	0.0728	0.0723

Table 4.14: L-moments and Discordancy values for streamflow stations

Station Code	Station Name	No. of Years	Mean (m^3/s)	L-CV	L-Skew	L-Kur	Di
1GC06	Nyando Kericho	47	2.2927	0.1819	0.0478	0.1817	2.0102
1GD07	Nyando Kisumu	31	11.0590	0.4878	0.4263	0.2132	0.4123
1GB05	Ainamotua	59	4.7340	0.3148	0.0454	0.0229	1.9642
1GB06	Mbogo	37	0.9826	0.5167	0.4763	0.2663	0.6312
1GB11	Ainopsiwa	49	2.2563	0.4714	0.4442	0.3075	0.7631
1GC05	Masaita	47	31.0415	0.2896	0.1360	0.0388	1.3944
1GD04	Nyando	40	12.0911	0.3650	0.3171	0.1843	0.8113
1GC04	Tugenon	40	0.5885	0.3903	0.2775	0.1810	0.0533

It is observed that none of the discordant values from all the rainfall and streamflow stations is higher than 3, thus data of all gauging sites are suitable for frequency analysis.

4.6.2 Results of heterogeneity measure (H)

A statistic H, based on the weighted variance of the L-coefficient of variation (L-cv) was computed according to Equations 3.40 and 3.41 in sub-section 3.6.1, part (i) Heterogeneity measure, to estimate the degree of heterogeneity in the considered

stations and to establish whether the stations can be treated as one homogeneous region. The H statistic compares the inter-station variations in sample L-moments for the group of stations with what would be expected of a homogeneous region. Alternative heterogeneity measure, H_1 is considered based on L-cv and L-skewness and H_2 is a measure based on L-skewness and L-kurtosis.

The H criteria established by Hosking & Wallis (1993) indicate that a region is acceptably homogeneous if $H < 1$, possibly heterogeneous if $1 \leq H < 2$ and definitely heterogeneous if $H \geq 2$. According to Hosking and Wallis (1993), H_1 and H_2 lack power to discriminate between homogeneous and heterogeneous regions (Hosking & Wallis 1993). They rarely yield H values larger than 2 even for grossly heterogeneous regions. The heterogeneity measure computed for 10 rainfall stations by carrying out of Monte Carlo simulations after estimating parameters of Kappa distribution were: H= 1, H_1=1.77 and H_2= 2.96. The H test statistics indicated that the region was heterogeneous since the value of H is equal to 1, thus it was not possible to consider the region as acceptably homogeneous in rainfall. The values of heterogeneity measures for streamflow stations of 8 sites were; H=7.72, H_1=6.96, H_2=5.13. The result for H is greater than 1 therefore the region was declared definitely heterogeneous in streamflow according to Hosking and Wallis (1993) criteria. Nyando River basin was therefore clustered into homogeneous sub-regions for frequency analysis. Three (3) rainfall clusters and four (4) streamflow clusters were therefore established as shown in Figure 4.19 and Figure 4.20, respectively.

4.6.3 Results of cluster analysis

Hierarchical cluster trees (dendrograms) were generated using Ward's method (Ward, 1963) in order to summarize the information about the possible clusters. The scale

indicated on the y-axis shows the height of the dendrogram which controls the number of clusters obtained. The homogeneous clusters are indicated using colored borders enclosing the rainfall and streamflow stations. Figure 4.19 shows the entire region demarcated into three different rainfall homogeneous clusters I, II and III shown using red, green, deep blue and pale blue rectangles. In this cluster analysis, the sub-clusters shown in red and green colours were merged to form cluster I after confirming the goodness of fit using the heterogeneity measure. The developed clusters are summarized in Table 4.15.

Table 4.15: Summary of clusters for Rainfall stations

Cluster I	Cluster II	Cluster III
9034086-Ahero Irrigation	9035279-Nandi Tea	9035258-Kipkelion
9035244- Timbilil	9035341-Tinga Monastery	9035226-Londiani
	9035003-Kericho Water	9035341-Finlay
	9035279-Kericho Met	9034087-Chemelil

From Table 4.18 Cluster I contains two rainfall stations, Clusters II & III have four rainfall stations each.

Figure 4.19 shows four different homogeneous streamflow Clusters of I, II, III and IV shown using red, green and blue rectangles respectively.

Table 4.16: Summary of cluster for streamflow within Nyando

Cluster I	Cluster II	Cluster III	Cluster IV
1GB11-Ainopsiwa	1GD04- Nyando	1GB05-Ainamotua	1GC05-Masaita
1GB06- Mbogo	1GD07-Nyando Kisumu		1GC06-Nyando Kericho

From Table 4.19, Clusters I and II contain two streamflow stations each, Cluster III has only one streamflow station and Cluster IV contains three stations. The clusters were

chosen to represent the homogeneous rainfall and streamflow regions in the Nyando River basin and the goodness and or adequacy of these choices were confirmed further using the heterogeneity measure H.

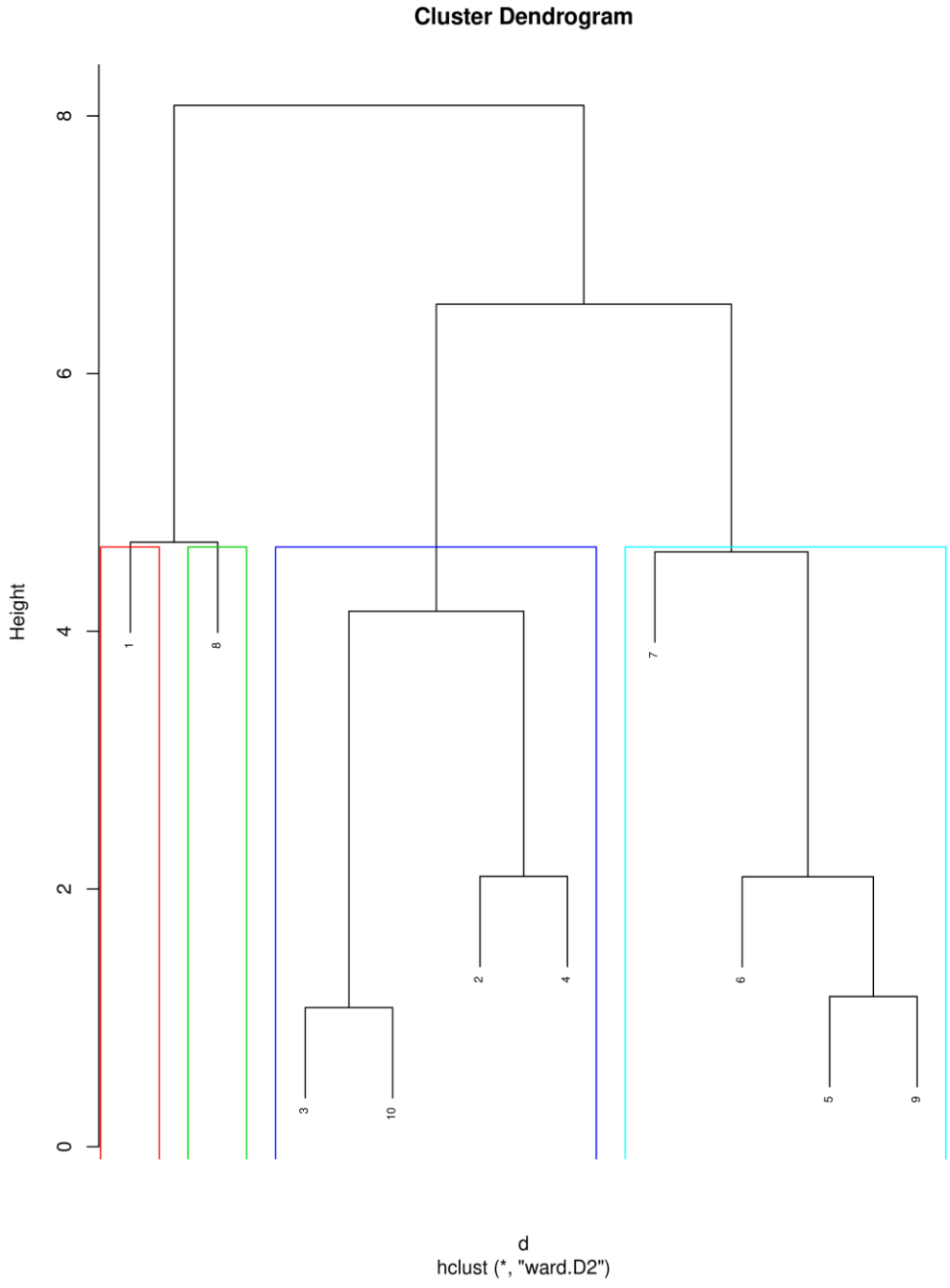

Figure 4.19: Cluster dendrogram developed for Nyando Rainfall.

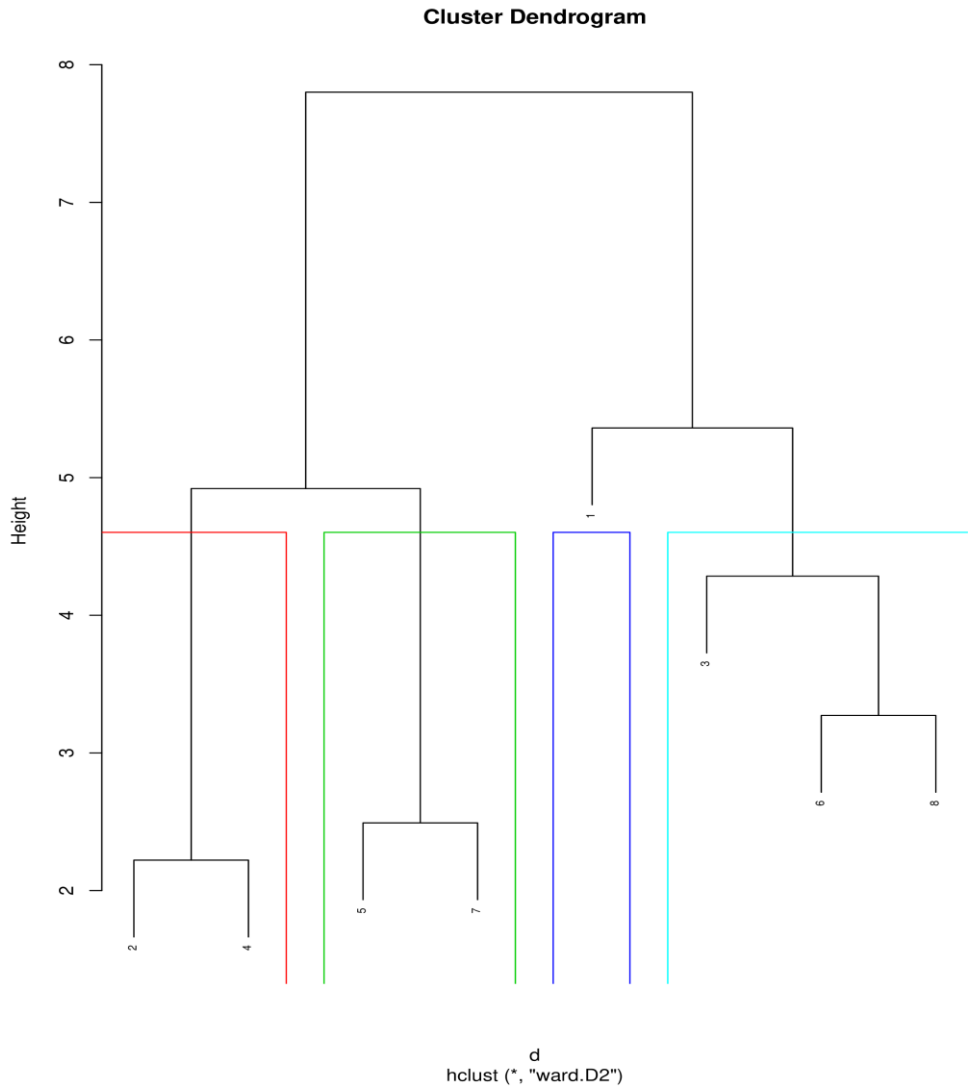

Figure 4.20: Cluster dendrogram developed for Nyando streamflow.

4.6.4 Results of distribution selection

In addition to the goodness of fit tests, the relationships between population L-skewness and L- kurtosis for a range of distributions were analysed by obtaining L-moment ratio diagrams. The regional average L-skewness and L-kurtosis values for each site were computed and plotted combining with theoretical distribution curves (L-moment diagrams) as shown if Figure 4.21 and Figure 4.22.

(i) Results of rainfall distribution selection

Figures 4.21 presents the L-moment diagrams for the rainfall in Nyando River basin. The theoretical distributions, GLO, GEV, GPA, GNO and PE3 represent Generalized Logistic, Generalized Extreme Value, Generalized Pareto, Generalized Normal and Pearson Type III Distributions, respectively.

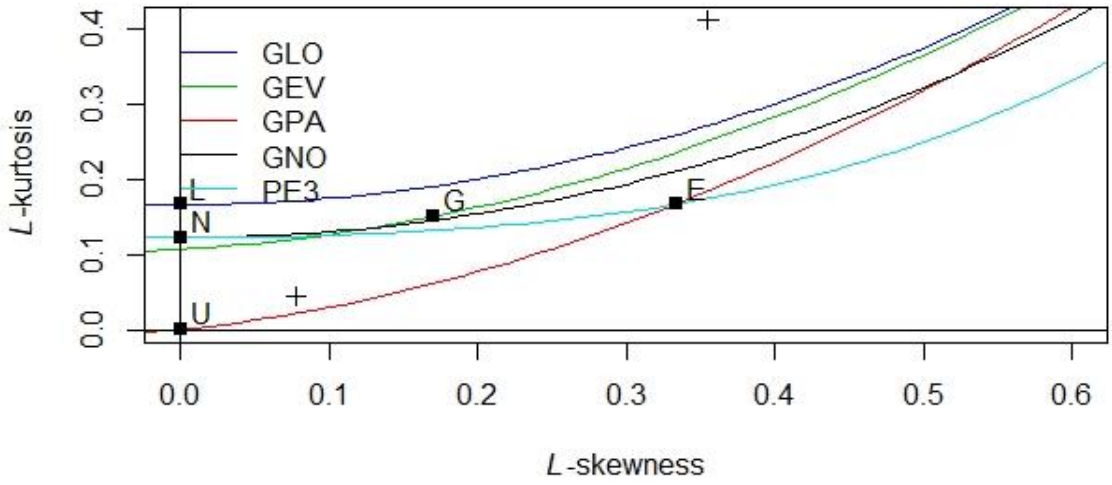

Figure 4.21: (a) Regional average L-moments for Cluster I rainfall.

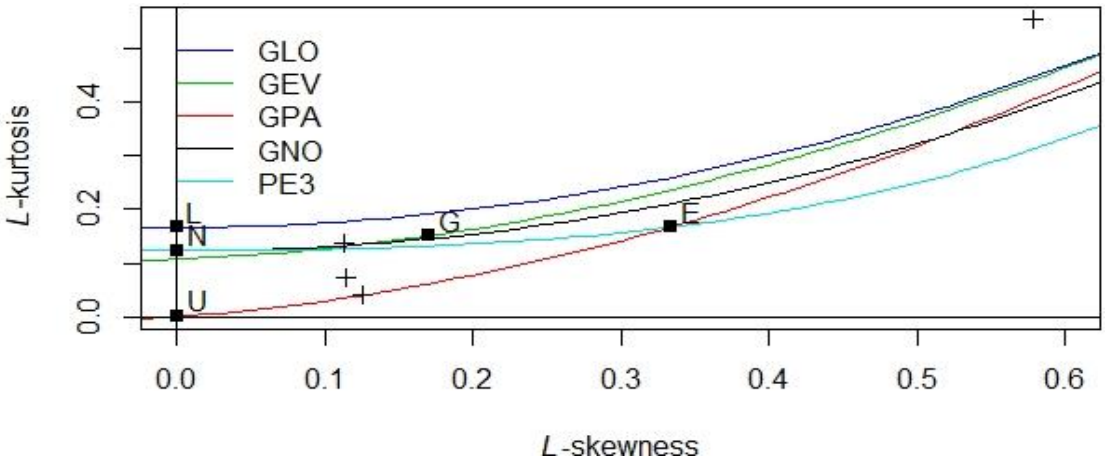

Figure 4.21: (b) Regional average L-moments for Cluster II rainfall.

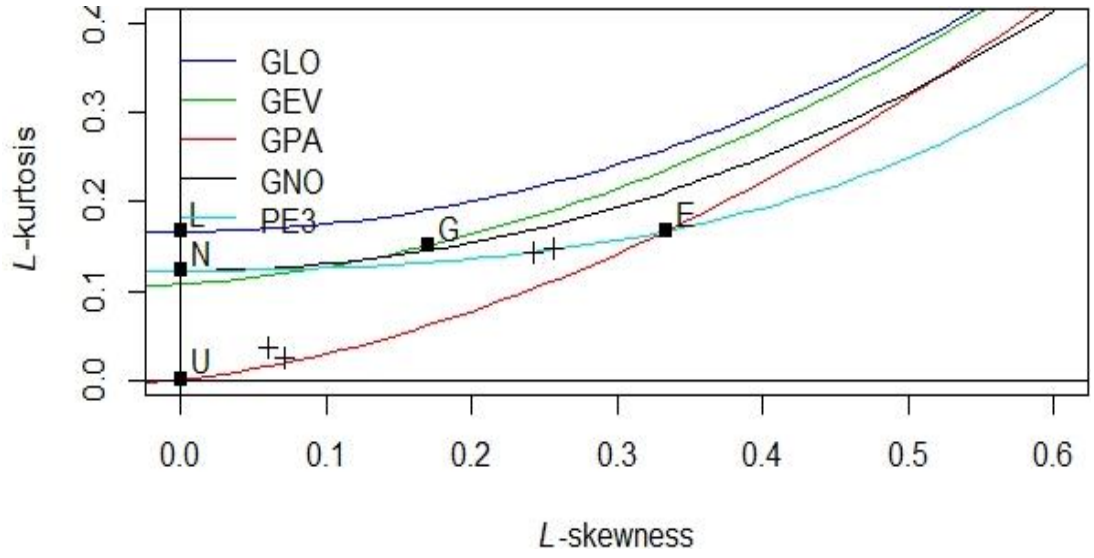

Figure 4.21: (c) Regional average L-moments for Cluster III rainfall

Figure 4.21 (a, b & c) presents the plots of L-kurtosis against L-skewness for the rainfall. The areas enclosed by the curves show the L-skewness and L-kurtosis values attained by the Kappa distribution. Special cases are shown for the Logistic (L), Gumbel (G), Exponential (E), Normal (N) and Uniform (U). The data points generated by the Kappa distribution are indicated by plus (+) sign and appear scattered.

Since L-Moment ratio estimators L-skewness and L-kurtosis are approximately unbiased, regardless of the underlying probability distribution, it is expected that approximately half the points lie above the theoretical curve and approximately half lie below the curve.

Figure 4.21(a) shows the L-moment diagram for rainfall in Cluster I. On careful examination of the curves, the data points are seen to be distributed above and below the GLO, GEV, GNO and PE3 and hence the distributions give acceptable regional fits. However, the data points are scattered outside of the GPA curve, hence GPA is not an acceptable fit. Further, the data points are seen to be equidistant from the PE3 curve therefore making PE3 the best distribution fit followed by GNO, GEV and GLO.

The results observed in Figure 4.21(b) for the L-moment ratio diagram for Cluster II indicate that PE3, GNO and GEV were all acceptable distributions since the points are distributed one above and one below each curve and all the curves pass through the third data point. Therefore GPA and GLO were least acceptable. Similarly, in Figure 4.20(c), only PE3 and GPA distributions are seen to give the acceptable distribution fits for Cluster III since GLO, GEV and GNO distribution curves are all outside the data points. The acceptable rainfall distributions for the Nyando River basin were therefore GEV, GNO PE3 and GLO for Cluster I; PE3, GNO & GEV for Cluster II; PE3 & GPA distributions were acceptable for Cluster III.

In this study, PE3, GEV, GNO, GPA and GLO probability distributions which were accepted in at least one of the clusters and were therefore considered as candidate distributions. The adequacy of all the candidate distributions for each cluster was confirmed further by computing their goodness-of-fit measures (z-statistics) according to Hosking and Wallis (1997). From the results, it is seen that PE3 appeared for all the three clusters, GEV and GNO appeared for both clusters I & II. GLO appeared for Cluster I only and GPA appeared for cluster III only, as candidate distributions having passed the acceptability criteria.

(ii) Results of streamflow distribution selection

Figure 4.22 presents L-moment diagrams for the streamflow in Nyando River basin. The theoretical distributions, GLO, GEV, GPA, GNO and PE3 represent Generalized Logistic, Generalized Extreme Value, Generalized Pareto, Generalized Normal and Pearson Type III Distributions, respectively.

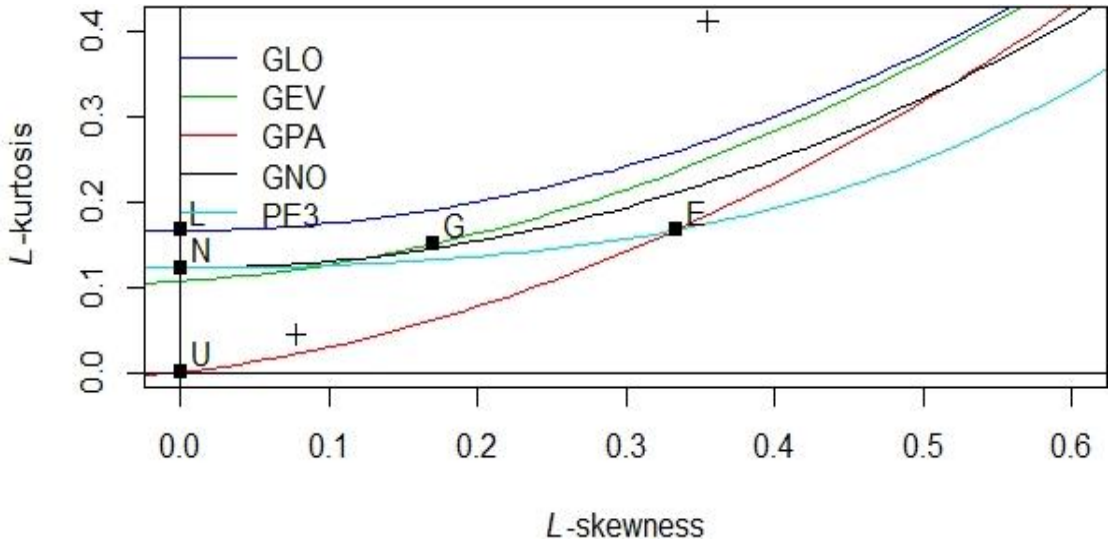

Figure 4.22: (a) Regional average L-moments for cluster I streamflow

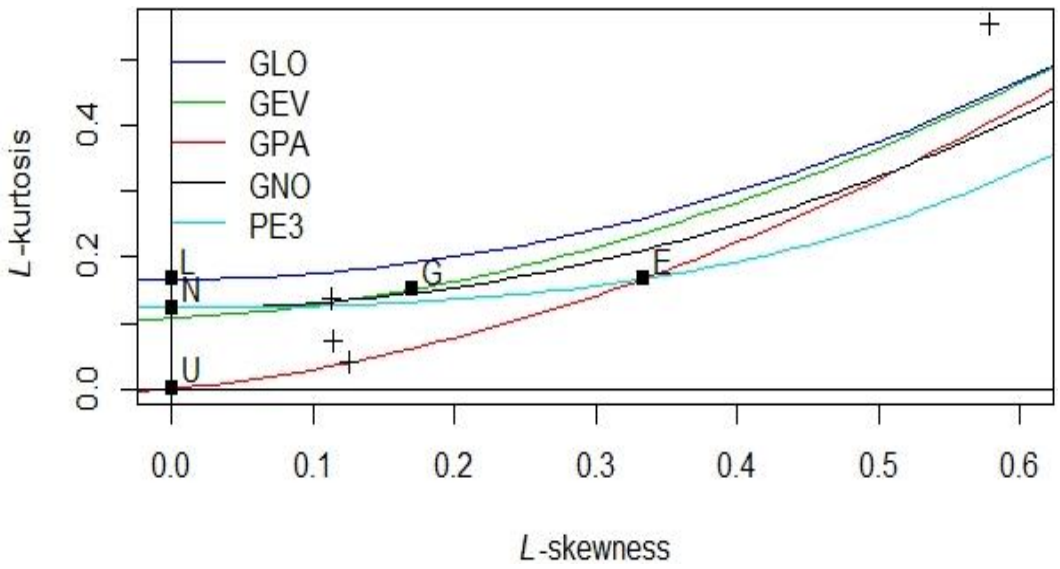

Figure 4.22: (b) Regional average L-moments for cluster II streamflow

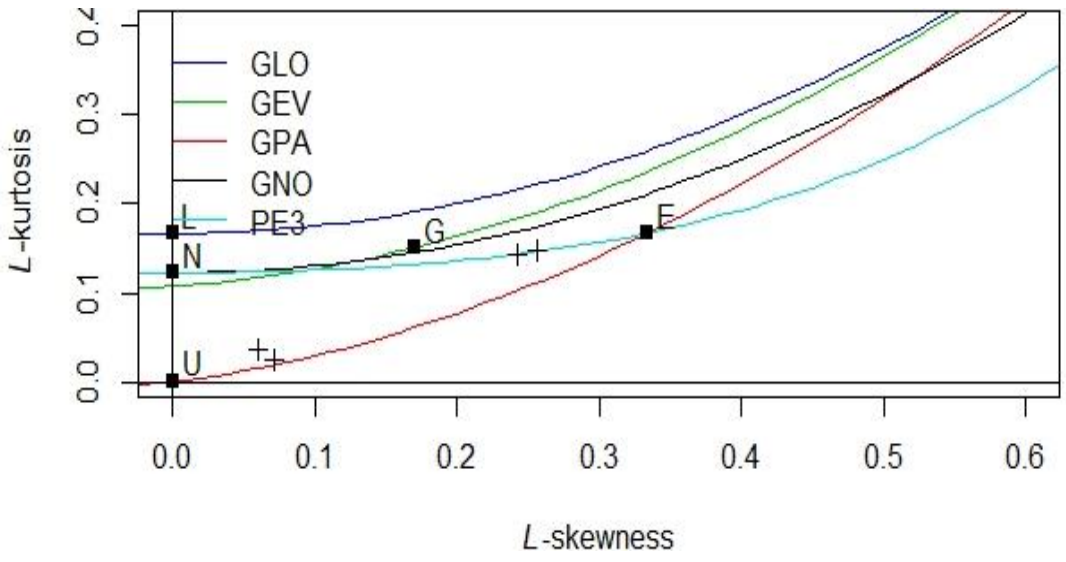

Figure 4.22: (c) Regional average L-moments for cluster III streamflow

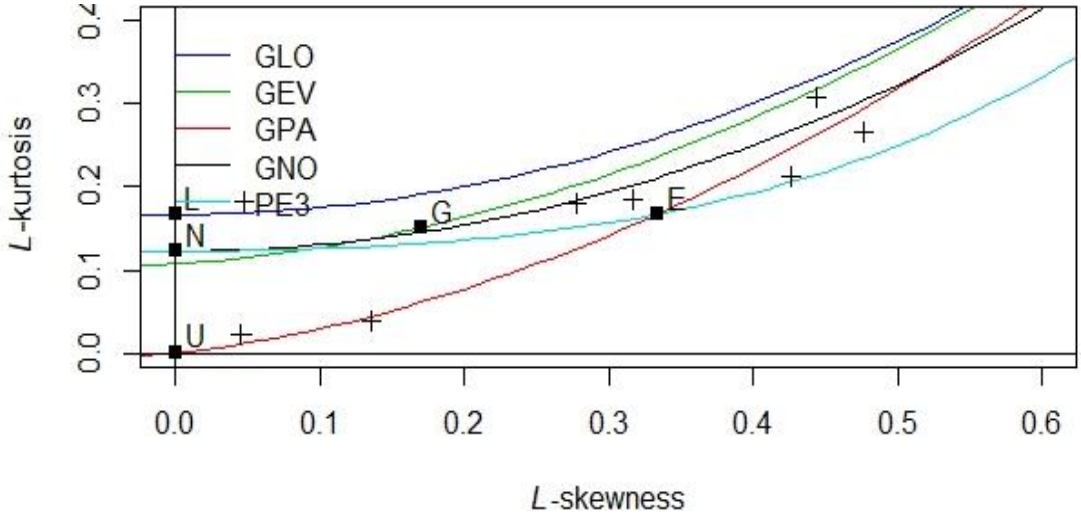

Figure 4.22: (d) Regional average L-moments for cluster IV streamflow

The Figure 4.22 (a, b, c & d) indicates the plots of L-kurtosis against L-skewness for the Nyando streamflow. As already described for Figure 4.21, the areas enclosed by the curves show the L-skewness and L-kurtosis values attained by the Kappa distribution. Special cases are shown for the Logistic (L), Gumbel (G), Exponential (E), Normal (N) and Uniform (U). The data points generated by the Kappa distribution are indicated by plus (+) sign and appear scattered

By careful examination of data points, some best fit curves are identified. It is seen in Figures 4.22(a) that for GLO, GEV, GNO and PE3 distribution curves, one point appears above and one point appears below and these distributions have therefore been considered acceptable fits for cluster I. However, GPA distribution curve, denoted by the red colour passes outside the data points and is therefore a non-acceptable fit for cluster I.

For Figure 4.22(b) it is seen that GEV, GNO and PE3 are bound by one point above the curves and two below. Further, these curves pass through another point. They were therefore considered to give acceptable fits to the regional average L-moments for cluster II. Whereas GLO follows closely, GP was considered non-acceptable since most points appear above the distribution curve and only few appear below the curve. In Figures 4.22(c) it was seen using the same criteria that PE3 and GPA were acceptable candidate distributions whereas GNO, GLO and GEV have all data points lying below the curves and the distributions were therefore not accepted for cluster III. For Figure 4.21, the points were concentrated around GPA, GNO and PE3 which were postulated to give the best fits to the regional average L-moments.

In the current study, PE3, GEV, GNO, GLO and GPA probability distributions were accepted in at least one of the clusters and were therefore considered as candidate distributions. The adequacy of all the candidate distributions for each cluster were confirmed further by computing their goodness-of-fit measures (z-statistics). From the results, it can be seen that PE3 appears for all the four clusters, GEV appears for both clusters I & II. GNO appears for clusters I & II. GLO appears for clusters I & II and GPA appears for clusters III & IV as candidate distributions having passed the acceptability tests.

4.6.5 Results of Goodness-of-fit tests

In order to further confirm the adequacy of the candidate distributions, the goodness-of-fit measure (z-statistic) was computed for each of the distributions using Equation 3.44. The distribution fit is declared adequate if Z^{DIST} is sufficiently close to zero with a reasonable criterion being $|Z^{DIST}| \leq 1.64$ according to Hosking & Wallis (1997). The results are shown in Tables 4.20 and 4.21.

(i) Results of rainfall Goodness-of-fit tests

Table 4.20 presents the goodness-of-fit test results in rainfall. The theoretical distributions, GLO, GEV, GPA, GNO and PE3 represent Generalized Logistic, Generalized Extreme Value, Generalized Pareto, Generalized Normal and Pearson Type III Distributions, respectively.

Table 4.17: Goodness -of- fit measure for rainfall distributions

Clusters	Theoretical distributions				
	GLO	**GEV**	**GNO**	**PE3**	**GPA**
Cluster 1	2.29	0.87	0.92	0.68	2.44
Cluster 2	2.02	0.79	1.01	0.71	2.52
Cluster 3	2.72	3.55	2.61	0.65	1.23

Table 4.20 indicates the theoretical probability distributions and the goodness-of -fit test results. It was observed from Table 4.20 that PE3 was the optimum probability distribution for clusters I, II, & III noting that GEV distribution follows very closely only in clusters I & II and GPA is second best fit to PE3 in cluster III.

(ii) Results of streamflow Goodness-of-fit tests

Annual maximum streamflow series were also tested against GLO, GEV, GNO, PE3, and GPA candidate distributions and the results are shown in Table 4.21. The theoretical distributions, GLO, GEV, GPA, GNO and PE3 represent Generalized Logistic,

Generalized Extreme Value, Generalized Pareto, Generalized Normal and Pearson Type III Distributions respectively.

Table 4.18: Goodness -of- fit measure for different streamflow

Clusters	Theoretical distributions				
	GLO	GEV	GNO	PE3	GPA
Cluster 1	1.29	0.58	0.62	0.54	2.14
Cluster 2	3.02	0.62	0.64	0.61	1.12
Cluster 3	1.52	3.55	1.61	0.72	0.87
Cluster 4	2.81	2.13	2.12	0.69	0.79

Table 4.21 indicates the theoretical probability distribution and the goodness-of-fit test results. From the results of the goodness of fit test (Table 4.21), clusters I, II, II & IV revealed PE3 as the optimum probability distributions for the Nyando River basin. It was also observed that GEV and GNO distributions followed closely in clusters I & II while GPA distribution followed closely in clusters III & IV. It was therefore concluded from the analysis that the best fit distribution for both rainfall and streamflow data for Nyando River basin was Pearson Type III (PE3).

4.6.6 Regional growth curves

The regional growth curves for rainfall and streamflow were therefore derived from the quantile functions of PE3 Probability Distribution. Due to the small size of the data, the growth curves were developed for return periods of 2, 5, 10, 20, 50 and 100 years. Appendix 11 (A & B) presents regional rainfall growth curves for Nyando river basin.

(i) Regional growth curves for rainfall

Figure 4.22 shows the Nyando rainfall growth curves for the clusters I, II and II which are presented separately with further details in Appendix 11A.

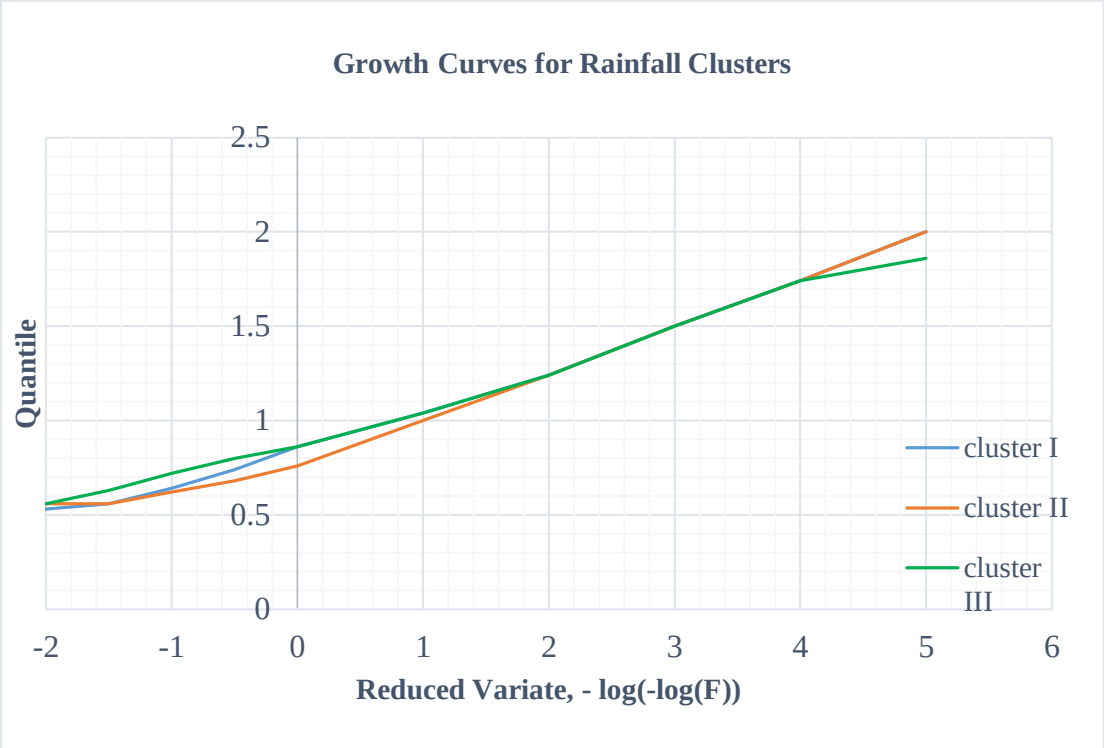

Figure 4.23: Rainfall growth curves

It is observed that the regional growth curves for regions I and III are fairly similar as both the curves reveal merged sections. Cluster II stands out as different from clusters I and III as the line isolates from the beginning and at the end. This may suggest that on statistical grounds, there may be little justification for treating all the clusters as distinct and that clusters I and III may as well be merged to form a larger cluster. The extreme rainfall quantiles for the region and for a given return period were obtained by multiplying the average maximum rainfall of the series by the corresponding quantile function extracted from the regional growth curve presented in Appendix 11A. The average maximum rainfall was computed for the separate and the merged clusters. Table 4.22 summarizes the extreme rainfall events for the return periods in clusters I & III (merged) and cluster II. T denotes Return Period in years, Q_F denotes quantile function, R_T denotes extreme rainfall for the return period and R_{AM-} denotes average maximum rainfall.

Table 4.19: Extreme rainfall events in clusters I and III

T (years)	2	5	10	20	50	100
Q_F	0.80	1.10	1.30	1.40	1.60	1.90
R_{AM} (mm)	301.30	301.30	301.30	301.30	301.30	301.30
R_T (mm)	241.04	331.43	391.69	421.82	482.08	572.47

Table 4.20: Extreme rainfall events in clusters II

T (years)	2	5	10	20	50	100
Q_F	0.90	1.20	1.50	1.70	1.80	1.90
R_{AM} (mm)	294.30	294.30	294.30	294.30	294.30	294.30
R_T (mm)	264.87	353.0	441.45	500.31	529.74	559.17

Table 4.22 indicates the lowest and highest rainfall peaks of 241 mm and 572.47 mm at 2 years and 100 years return periods respectively, for sub-basins described by clusters I & III of the Nyando River Basin. Similarly, Table 4.23 indicates lowest and highest rainfall peaks of 264.87 mm and 559.17 mm at 2 years and 100 years return periods respectively for the sub-catchment described by cluster II. It is observed from Tables 4.22 and Tables 4.23 that rainfall peaks in the various sub-catchments had more or less similar return levels.

(ii) Regional growth curves for streamflow.

Figure 4.24 shows the Nyando rainfall growth curves for the clusters I, II, III and IV which are presented separately with further details in Appendix 11B.

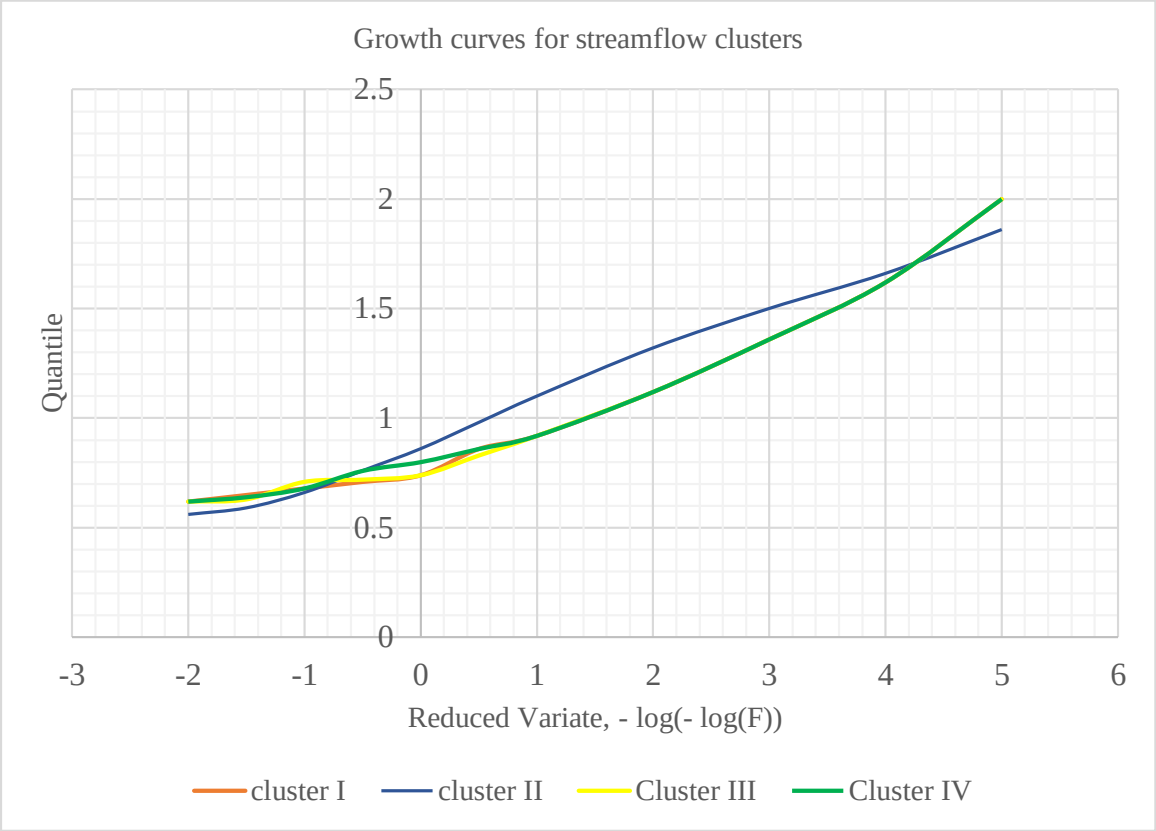

Figure 4.24: Streamflow growth curves

The extreme streamflow quantiles for the region and for a given return period were obtained by multiplying the average maximum streamflow of the time series of each cluster by the corresponding quantile function extracted from the regional growth curves presented in Appendix 11B. Tables 4.24 and 4.25 summarize the extreme streamflow events for the return periods for the clusters I, III & IV (merged) and cluster II. T denotes Return Period, Q_F denotes quantile function, Q_T denotes extreme streamflow for the return period and Q_{AM-} denotes average maximum streamflow.

Table 4.21: Extreme streamflow events in cluster I

T (years)	2	5	10	20	50	100
Q_F	0.800	1.200	1.400	1.500	1.600	1.800
Q_{AM} (m^3/s)	1.620	1.620	1.620	1.620	1.620	1.620
Q_T (m^3/s)	1.296	1.944	2.268	2.430	2.754	3.078

Table 4.22: Extreme streamflow events II

T (years)	2	5	10	20	50	100
Q_F	0.900	1.100	1.400	1.500	1.600	1.800
Q_{AM} (m^3/s)	11.580	11.580	11.580	11.580	11.580	11.580
Q_T (m^3/s)	10.42	12.733	15.054	16.212	18.296	20.880

Table 4.23: Extreme streamflow events III

T (years)	2	5	10	20	50	100
Q_F	0.800	1.200	1.400	1.500	1.600	1.800
Q_{AM} (m^3/s)	4.730	4.730	4.730	4.730	4.730	4.730
Q_T (m^3/s)	3.784	5.678	6.622	7.095	7.568	8.568

Table 4.24: Extreme streamflow events in cluster IV

T (years)	2	5	10	20	50	100
Q_F	0.9	1.1	1.3	1.6	1.7	1.8
Q_{AM} (m^3/s)	11.31	11.31	11.31	11.31	11.31	11.31
Q_T (m^3/s)	10.179	12.441	14.703	18.096	19.227	21.358

Table 4.24 indicates the lowest and highest flood levels of 1.296 m^3/s and 3.078 m^3/s at 2 years and 100 years return periods, respectively for cluster I which is composed of Ainopsiwa and Mbogo sub-catchments. Observations in Table 4.25 indicate flood levels of 10.422m^3/s and 20.88 m^3/s at 2 years and 100 years return periods, respectively for

clusters II which form Nyando and Nyando-Kisumu sub-catchment of the Nyando basin. Table 4.26 indicates flood levels of 3.784 m^3/s and 8.568 m^3/s at 2 years and 100 years return periods respectively for cluster III which was formed by Ainamotua sub catchment. Similarly, Table 4.27 of cluster IV formed by Nyando-Kericho, Masaita and Tugenon sub-catchments, the flood levels observed were 10.179 m^3/s and 21.358 m^3/s at 2 years and 100 years respectively.

The results indicated that Masaita, Nyando-Kericho and Tugenon which form the upper sub-catchments of the Nyando Basin contributed the highest streamflow of about $22m^3/s$ for the Nyando river basin. With additional streamflow from Ainamotua, Ainopsiwa, Mbogo and other sub-catchments contributing approximately $12m^3/s$, the minimum flood levels downstream at Nyando and Nyando-Kisumu sub-catchments was expected to be approximately $34m^3/s$ whereas only about $21m^3/s$ was recorded. It therefore implies that during peak rainfall, part of the streamflow from the upper sub-catchments flow through the flood plains and were not recorded at the gauging stations installed inside the rivers. This explains why the Nyando River inundates the flood plain perennially. Figure 1.1 indicates the sub-catchments of Nyando River basin and the delineation of clusters can be observed in Table 4.19. The results further confirmed the adequacy of using the PE3 as universally the optimum Probability distribution function for the Nyando River basin.

CHAPTER FIVE

CONCLUSIONS AND RECOMMENDATIONS

5.1 Conclusions

This study examined trend and periodicities, and analysed frequencies in the Nyando Rainfall and streamflow. Various techniques were applied: trend was studied using Mann-Kendall and wavelet approaches, periodicity was studied using spectral and wavelet techniques and, frequency was analysed by L-moment method.

Rainfall and streamflow trends in MAM, JJA and OND were revealed by the M-K and wavelet transform techniques. Mann-Kendall trends in rainfall mostly disappeared after splitting the series into smaller data sets.

Whereas there were minimal apparent rainfall trends according to the M-K approach, the wavelet technique revealed more definite trends for rainfall and streamflow. The M-K technique estimated the statistical significance at 95% confidence limit whereas an improvement by wavelet disclosed the temporal-frequency information and showed trend lines which were further analysed for more definite results. Rainfall trends were more pronounced in the results of wavelet than in M-K. Use of wavelet revealed generally the decreasing (negative) and increasing (positive) trends and other important features such as some turning points and amplitude of fluctuations over time. It was therefore concluded from the Mann-Kendall and wavelet results that trend has occurred in the Nyando rainfall and streamflow in the last thirty years. Further, wavelet technique is more effective in trend detection than the conventional Mann-Kendall approach.

Fourier and wavelet transforms confirmed that Nyando River basin rainfall and streamflow regimes exhibited periodic changes. Basic periodicities were revealed at 2-7 years, 2.7-3.3 years, 3.5-4 years, 5.6-6.5 years, 7-8 years and some weaker

periodicities at 10-12 years. Wavelet transformation further confirmed the periodicity of the Nyando River basin streamflow and rainfall changes by revealing the peaks and the localization of the peaks in time. Spectral technique only showed the peaks but failed to locate the time of the peaks. It is becoming increasingly important to understand the nature of variability of rainfall and streamflow so as to be able to optimally utilize the rainfall and streamflow for agricultural purposes and other water supply needs. The efficiency of wavelet method showed that this approach can be applied in studies of climatological and meteorological parameters. The study therefore concluded that the wavelet method reveals more successfully periodic and quasi-periodic changes in hydrometeorological time series than Fourier based spectral technique.

Treating the Nyando basin initially as a single region, the Heterogeneity statistics (H) for rainfall and streamflow were evaluated. The H-statistics for rainfall and streamflow were determined as 1 and 7.72, respectively. Using Ward's method, cluster analysis was performed for rainfall and streamflow parameters. Nyando River basin was therefore delineated into 3 rainfall and 4 streamflow homogeneous clusters since in each case, the H-statistic was greater than 1.

For each homogeneous region, L-moments method was used to select the best fitted distributions for annual maximum rainfall and streamflow series. The return periods were subsequently computed for 2, 5, 20, 50 and 100 years. It is concluded from the study that the best rainfall distribution fit is PE3 for Nyando River basin followed by GEV and GPA. The best streamflow distribution fit is also PE3 for all the streamflow followed by GEV and GNO. Additionally, the study concluded that L-moments method can be considered simpler as L-moment statistics can be obtained by linear expressions to shorten the process of analysis.

5.2 Recommendations

This study recommends that the M-K and wavelet transform should be applied together to better analyse trend in hydrological time series. Further, wavelet transform should be applied together with spectral analysis technique to better detect hydro-meteorological periodic oscillations.

It is recommended that similar studies should be carried out in other River basins in Kenya to ensure design of hydraulic structures are based on proper probability distributions. The study further recommended that the regional flood frequency results generated can be applied to ungauged catchments in the Nyando River basin within or in proximity of identified homogeneous regions. Moreover, the methodology used can be adopted for other regions of Kenya provided that sufficient flood records are available.

REFERENCES

Adamowski, J., Adamowski, K., & Prokoph, A. (2013). A spectral analysis based Methodology to detect climatological influences on daily urban water demand. *Mathematical Geosciences*, *45*(1), 49-68.

Ahmad, I., Tang, D., Wang, T., Wang, M., & Wagan, B. (2015). Precipitation trends over time using Mann-Kendall and spearman's rho tests in swat river basin, Pakistan. *Advances in Meteorology*, *2015*.

Alexandersson, H. (1986). A homogeneity test applied to precipitation data. *Journal of climatology*, *6*(6), 661-675.

Black, E., Slingo, J., & Sperber, K. R. (2003). An observational study of the relationship between excessively strong short rains in coastal East Africa and Indian Ocean SST. *Monthly Weather Review*, *131*(1), 74-94.

Buishand, T. A. (1982). Some methods for testing the homogeneity of rainfall records. *Journal of hydrology*, *58*(1-2), 11-27.

Chingombe, W., Gutierrez, J. E., Pedzisai, E., & Siziba, E. (2005). A study of hydrological trends and variability of Upper Mazowe Catchment-Zimbabwe. *Journal of Sustainable Development in Africa*, *7*(1), 1520-550.

Dhorde, A. G., & Zarenistanak, M. (2013). Three-way approach to test data homogeneity: an analysis of temperature and precipitation series over south western Islamic Republic of Iran. *J. Indian Geophys. Union*, *17*(3), 233-242.

Eregno, F. E. (2014). Regional Flood Frequency Analysis Using L-Moment in the Tributaries of Upper Blue Nile River, South Western Ethiopia.

Franco Villoria, M., Scott, M., Hoey, T., & Fischbacher Smith, D. (2012). Temporal investigation of flow variability in Scottish rivers using wavelet analysis.

Gitau, W., Ogallo, L., Camberlin, P., & Okoola, R. (2013). Spatial coherence and potential predictability assessment of intraseasonal statistics of wet and dry spells over Equatorial Eastern Africa. International Journal of Climatology, 33(12), 2690-2705.

Giakoumakis, S. G., & Baloutsos, G. (1997). Investigation of trend in hydrological time series of the Evinos River basin. *Hydrological sciences journal*, *42*(1), 81-88.

Gilman, D. L., Fuglister, F. J., & Mitchell Jr, J. M. (1963). On the power spectrum of "red noise". *Journal of the Atmospheric Sciences*, *20*(2), 182-184**p.**

Grinsted, A., Moore, J. C., & Jevrejeva, S. (2004). Application of the cross wavelet transform and wavelet coherence to geophysical time series. *Nonlinear processes in geophysics*, *11*(5/6), 561-566.

Hafliger, K., & Lim, Y. H. (2012). *Techniques of Assessing Changes in River Flooding Patterns in the Upper Midwest*. North Dakota Water Resources Research Institute, North Dakota State University.

Hosking, J. R. M., & Wallis, J. R. (1993). Some statistics useful in regional frequency analysis. *Water resources research*, *29*(2), 271-281.

Hosking, J. R. M., & Wallis, J. R. (1997). Regional frequency analysis of floods in central Appalachia.

Hosking, J. R. (1990). L-moments: Analysis and estimation of distributions using linear combinations of order statistics. *Journal of the Royal Statistical Society: Series B (Methodological)*, *52*(1), 105-124.

Indeje, M., Semazzi, F. H., & Ogallo, L. J. (2000). ENSO signals in East African rainfall seasons. *International Journal of Climatology: A Journal of the Royal Meteorological Society*, *20*(1), 19-46.

Jain, S., & Lall, U. (2000). Magnitude and timing of annual maximum floods: Trends and large-scale climatic associations for the Blacksmith Fork River, Utah. *Water Resources Research*, *36*(12), 3641-3651.

Kizza, M., Rodhe, A., Xu, C. Y., Ntale, H. K., & Halldin, S. (2009). Temporal rainfall variability in the Lake Victoria Basin in East Africa during the twentieth century. *Theoretical and applied climatology*, *98*(1), 119-135.

Khisa, P. S., Uhlenbrook, S., van Dam, A. A., Wenninger, J., van Griensven, A., & Abira, M. (2013). Ecohydrological characterization of the Nyando wetland, Lake Victoria, Kenya: a state of system (SoS) analysis. *African Journal of Environmental Science and Technology*, *7*(6), 417-434.

Kosgei, J. R. (2018). Wetland Characterization and Implications on Agriculture in L. Victoria Basin. In *Water Resources Management* (pp. 251-268). Springer, Singapore.

Kirithikadatta, J. (2014) Normal Distribution. J Conserv. Dent 2014; 17:97--7

Kundzewicz, Z. W., & Robson, A. J. (2004). Change detection in hydrological records—a review of the methodology/revue méthodologique de la détection de changements dans les chroniques hydrologiques. *Hydrological sciences journal*, *49*(1), 7-19.

Lafreniere, M., & Sharp, M. (2003). Wavelet analysis of inter-annual variability in the runoff regimes of glacial and nival stream catchments, Bow Lake, Alberta. *Hydrological Processes*, *17*(6), 1093-1118.

Lim, Y. H. (2007). Regional flood frequency analysis of the Red River basin using L-moments approach. In *World Environmental and Water Resources Congress 2007: Restoring Our Natural Habitat* (pp. 1-10).

Machiwal, D., & Jha, M. K. (2006). Time series analysis of hydrologic data for water resources planning and management: a review. *Journal of Hydrology and Hydromechanics*, *54*(3), 237-257.

Maragatham, R. S. (2012). Trend analysis of rainfall data—a comparative study of existing methods. *International Journal of Physics and Mathematical Sciences*, *2*(1), 13-18.

Miao, L. I., Jun, X., & Dejuan, M. (2012). Long-term trend analysis of seasonal precipitation for Beijing, China. Journal of Resources and Ecology, 3(1), 64-72.

Nalley, D., Adamowski, J., & Khalil, B. (2012). Using discrete wavelet transforms to analyze trends in streamflow and precipitation in Quebec and Ontario (1954–2008). Journal of hydrology, 475, 204-228.

Nyakundi, R. M. I. (2016). *Groundwater Level Variability in Ruiru Location, Kiambu County, Kenya* (Doctoral dissertation, COETEC, JKUAT).

Nyakundi, H., Mwanzo, I., & Yitambe, A. (2010). Community perceptions and response to flood risks in Nyando District, Western Kenya. *Jàmbá: Journal of Disaster Risk Studies*, *3*(1), 346-366.

Noto, L. V., & La Loggia, G. (2009). Use of L-moments approach for regional flood frequency v analysis in Sicily, Italy. *Water resources management*, *23*(11), 2207-2229.

Ogallo, L. (1979). Rainfall variability in Africa.

Ogallo, L. J. (1984). Temporal fluctuations of seasonal rainfall patterns in East Africa.

Ogwang, B. A., Chen, H., Li, X., & Gao, C. (2014). The influence of topography on East African October to December climate: sensitivity experiments with RegCM4. *Advances in Meteorology*, *2014*.

Olang, L. O., & Fürst, J. (2011). Effects of land cover change on flood peak discharges and runoff volumes: model estimates for the Nyando River Basin, Kenya. *Hydrological Processes*, *25*(1), 80-89.

Opere, A. O., & Okello, B. N. (2011). Hydrologic analysis for river Nyando using SWAT. *Hydrology and Earth System Sciences Discussions*, *8*(1), 1765-1797.

Owiti, Z., & Zhu, W. (2012). Spatial distribution of rainfall seasonality over East Africa. *Journal of Geography and Regional Planning*, *5*(15), 409-421.

Owuor, J. B., Raburu, P. O., & Kwena, F. (2012). Community based approach to the management of Nyando wetland, Lake Victoria Basin, Kenya.

Pandey, B. K., Tiwari, H., & Khare, D. (2017). Trend analysis using discrete wavelet transform (DWT) for long-term precipitation (1851–2006) over India. *Hydrological sciences journal*, *62*(13), 2187-2208.

Paul, R. K., & Birthal, P. S. (2016). Investigating rainfall trend over India using the wavelet technique. *Journal of Water and Climate Change*, *7*(2), 353-364.

Pettit, A. N. (1979). A non-parametric approach to the change-point problem. *Applied statistics*, *28*(2), 126-135.

Rodhe, H., & Virji, H. (1976). Trends and periodicities in East African rainfall data. *Monthly Weather Review*, *104*(3), 307-315.

Roshani, M., Ramazanipour, M., Sotoudeh, F., & Aveily, J. G. (2012). The analysis of trend and cycle between rainfall and discharge in Ghaleroudkhan basin. *World Applied Sciences Journal*, *16*(2), 244-249.

Santos, C. A., Galvão, C. D. O., Suzuki, K., & Trigo, R. M. (2001). Matsuyama city rainfall data analysis using wavelet transform. *Proceedings of hydraulic engineering*, *45*, 211-216.

Scargle, J. D. (1982). Studies in astronomical time series analysis. II-Statistical aspects of spectral analysis of unevenly spaced data. *The Astrophysical Journal*, *263*, 835-853.

Stephens, M. A. (1976). Asymptotic results for goodness-of-fit statistics with unknown parameters. *The Annals of Statistics*, 357-369.

Tarhule, A., & Woo, M. K. (1998). Changes in rainfall characteristics in northern Nigeria. *International Journal of Climatology: A Journal of the Royal Meteorological Society*, *18*(11), 1261-1271.

Timuhins, A., Rodinovs, V., & Klavins, M. (2010, September). Wavelet analysis of the Baltic region river runoff longh-term trends and fluctuations. In *Proceedings of the Latvian Academy of Sciences* (Vol. 64, No. 5-6, p. 229). De Gruyter Poland.

Torrence, C., & Compo, G. P. (1998). A practical guide to wavelet analysis. *Bulletin of the American Meteorological society*, *79*(1), 61-78.

Toreti, A., Kuglitsch, F. G., Xoplaki, E., Della-Marta, P. M., Aguilar, E., Prohom, M.& Luterbacher, J. (2011). A note on the use of the standard normal homogeneity test to detect inhomogeneities in climatic time series. *International Journal of Climatology*, *31*(4), 630-632.

Ward Jr, J. H. (1963). Hierarchical grouping to optimize an objective function. *Journal of the American statistical association*, *58*(301), 236-244.

Watts, D. G., & Jenkins, G. (1968). Spectral analysis and its applications. *San Francisco*.Wearing, J. H. (2010). Spectral Analysis in R. McMaster University. Department of Mathematics and Statistics.

(WMO) World Meteorological Organization. (2018). *Guide to climatological*

practices (WMO-No. 100). Geneva, Switzerland: World Meteorological Organization.

Vogel, R. M., & Wilson, I. (1996). Probability distribution of annual maximum, mean, and minimum streamflow in the United States. *Journal of hydrologic Engineering*, *1*(2), 69-76.

Xiong, L., & Guo, S. (2004). Trend test and change-point detection for the annual discharge series of the Yangtze River at the Yichang hydrological station.*Hydrological sciences journal*, *49*(1), 99-112.

APPENDICES

Appendix 1: Simplified Flow Chart for Catchment Delineation

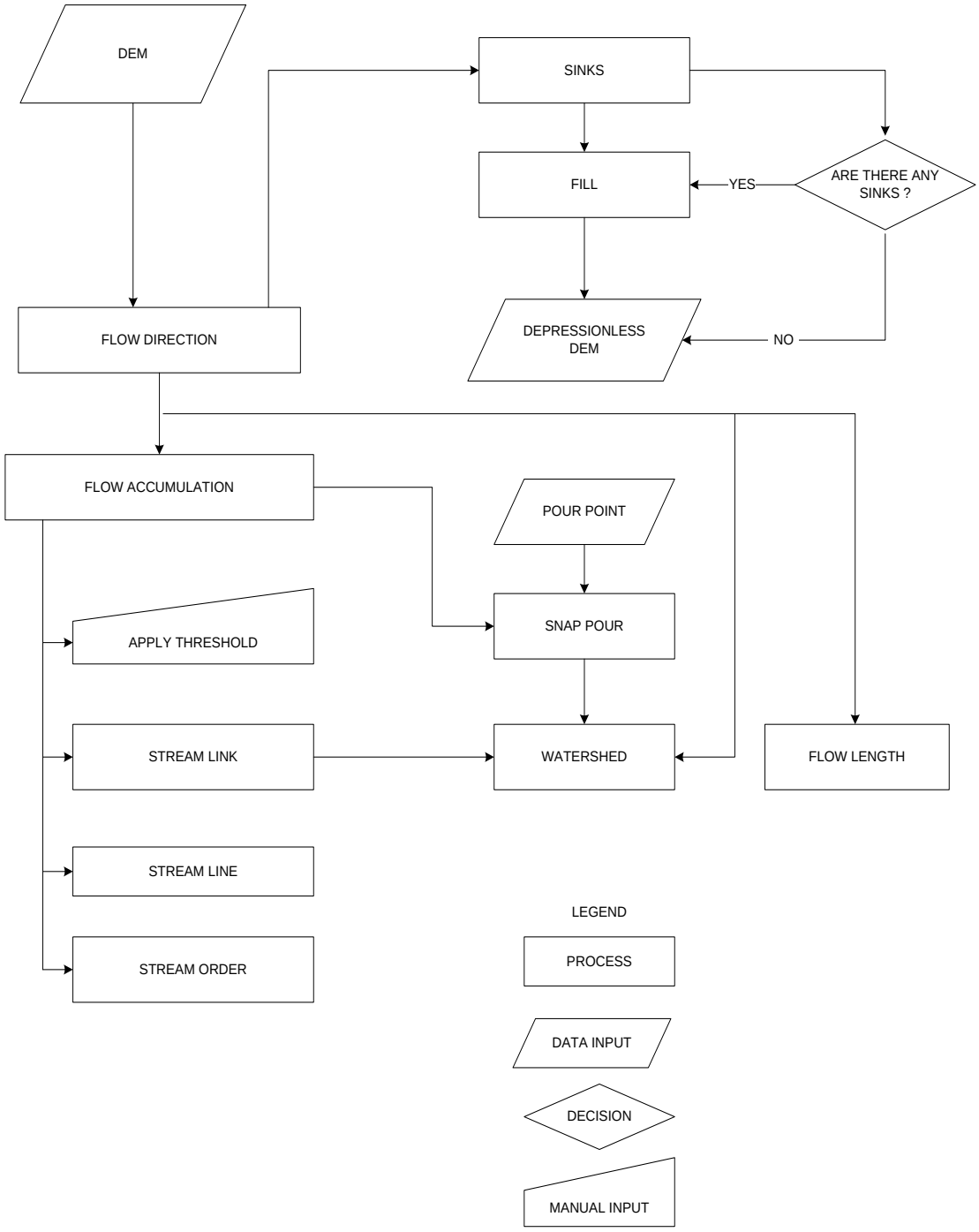

Appendix 2: Catchment Delineation

Appendix 2A: Digital Elevation Model for Nyando River basin area.

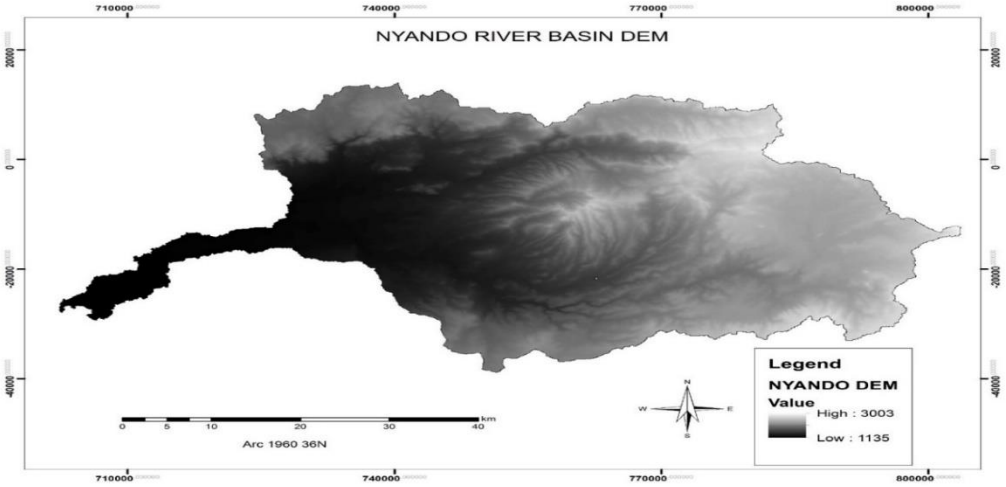

Appendix 2B: Flow direction map for Nyando River basin.

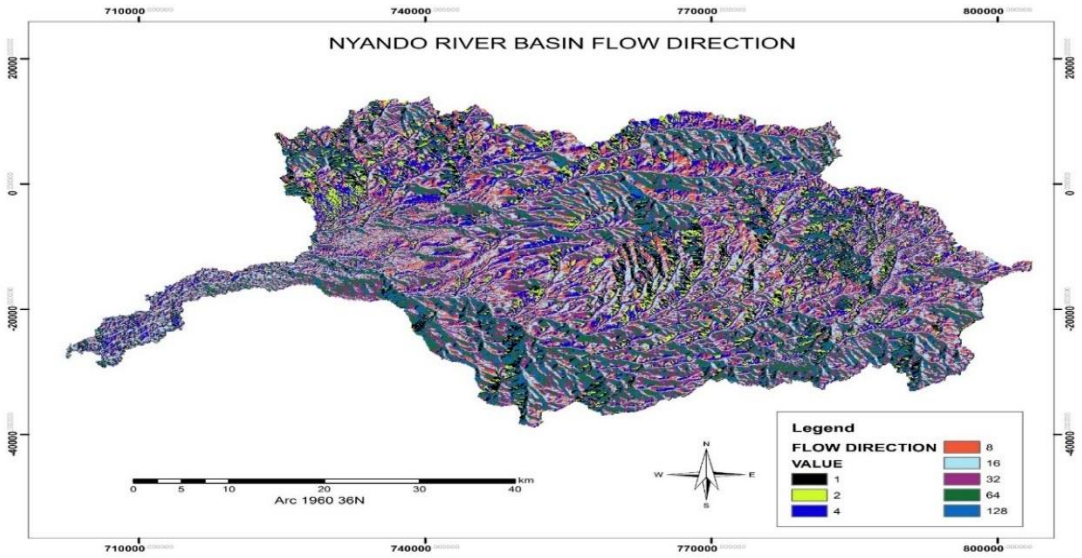

Appendix 2C: Flow accumulation map for Nyando River basin.

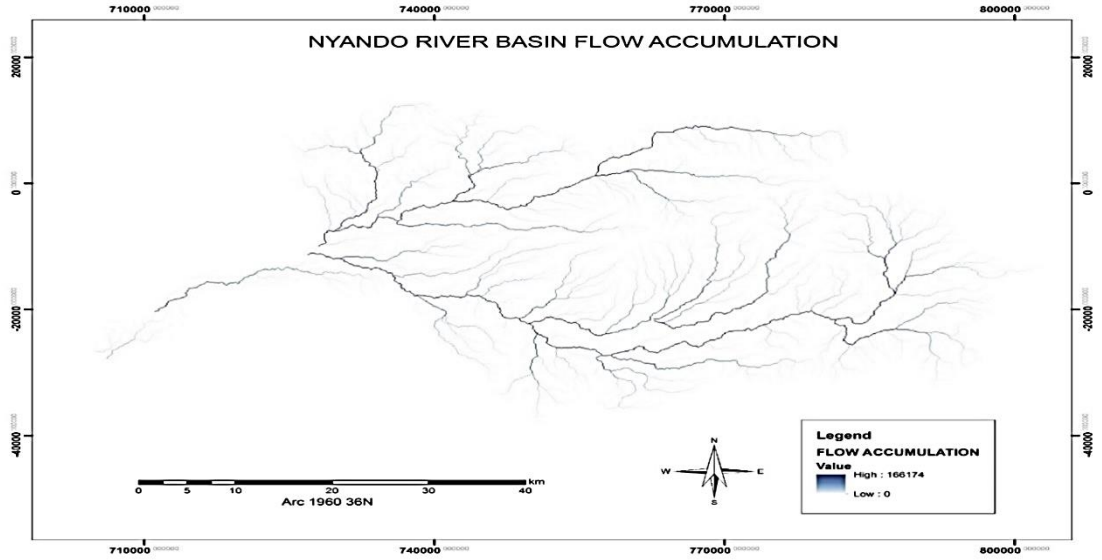

Appendix 2D: Strahler stream network for Nyando River basin.

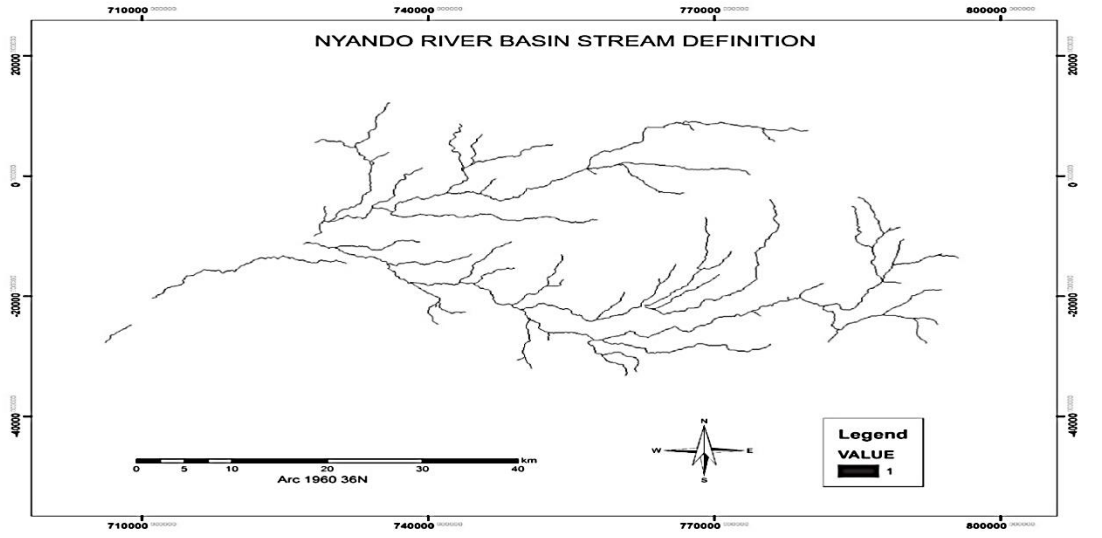

Appendix 3A-Rainfall Homogeneity Test Results for Rainfall

Table 3A (i): Comparison of homogeneity results of MAM rainfall series.

S/Code	S/Name	SNHT		Pettit's test		Buishand range test		Classification
		P-value	Break point	P-value	Break point	P-value	Break point	
903486	Ahero I. S	0.3007	1981	0.8405	1987	0.4793	1996	Class 1
8935095	Nandi Tea	0.663	1969	0.7967	1969	0.2437	1969	Class 1
9035188	Tinga	0.6395	1963	0.6343	1964	0.9502	1980	Class 1
9035003	K. water	0.6611	1933	1.262	1933	0.9284	1979	Class 1
9035258	Kipkelion	0.7611	1963	0.6323	1980	0.9791	1932	Class 1
9035226	Londiani	0.3537	1969	0.2178	1969	0.3617	1984	Class 1
9035244	Timbilil K	0.0481	1998	0.0062	1977	0.0232	1997	Class 3
9035341	Finlay	0.3025	1954	0.1758	1946	0.3312	1946	Class 1
9034087	Chemelil	0.4768	1970	0.2397	1985	0.5169	1985	Class 1
903527	K. Met	0.09	1979	0.0339	1991	0.0339	1997	Class 2

Table 3A (ii): Comparison of homogeneity results of JJA rainfall series.

S/Code	S/Name	SNHT		Pettit's test		Buishand range test		Classification
		P-value	Break point	P-value	Break point	P-value	Break point	
903486	Ahero I. S	0.01535	1965	0.4757	1969	0.5185	1969	Class 1
8935095	Nandi Tea	0.214	1960	0.2931	1972	0.2098	1971	Class 1
9035188	Tinga	0.1974	1961	0.9872	1961	0.829	1961	Class 1
9035003	K. water	0.2036	1998	0.2118	1998	0.0777	1951	Class 1
9035258	Kipkelion	0.2076	1961	0.8373	1998	0.5066	1961	Class 1
9035226	Londiani	0.03585	1977	0.2178	1969	0.2486	1976	Class 1
9035244	Timbilil K	0.00513	2002	0.02	1970	0.006	2002	Class 3
9035341	Finlay	4e-04	1961	0.3006	1961	4e-04	1961	Class 2
9034087	Chemelil	0.3383	2004	0.2271	1998	0.4617	1984	Class 1
903527	K. Met	0.1764	1997	0.2681	1986	0.3315	1997	Class 1

Table 3A (iii): Comparison of homogeneity results of OND rainfall series.

S/Code	S/Name	SNHT		Pettit's test		Buishand range test		Classification
		P-value	Break point	P-value	Break point	P-Value	Break point	
903486	Ahero I. S	0.0782	1998	0.4757	1998	0.533	1998	Class 1
8935095	Nandi Tea	0.908	1985	1.374	1985	0.9453	1973	Class 1
9035188	Tinga	0.8781	1964	1.235	1979	0.8464	1964	Class 1
9035003	K. water	0.1052	1982	0.0450	1982	0.1835	1982	Class 1
9035258	Kipkelion	0.9601	1961	1.146	1979	0.7279	1979	Class 1
9035226	Londiani	0.7741	1985	0.4471	1974	0.1541	1951	Class 1
9035244	Timbilil K	0.0065	2000	0.0125	1976	0.0312	1969	Class 3
9035341	Finlay	0.0329	1961	0.0043	1960	0.1995	1969	Class 2
9034087	Chemelil	0.2266	2004	1.311	1973	0.7208	1998	Class 1
903527	K. Met	0.1311	1981	0.4014	1988	0.1311	1981	Class 1

Appendix 3B- Homogeneity Test Results for Streamflow.

Table 3B (i): Comparison of results of MAM streamflow series.

S/Code	S/Name	SNHT		Pettit's test		Buishand r/test		Class
		P-value	Break point	P-value	Break point	P-value	B/point	
1GC06	N. Kericho	0.0978	1970	0.6871	1989	0.582	1985	Class 1
1GD07	N. Kisumu	2e-16	1993	0.135	1992	1e-04	1993	Class 2
1GB05	Ainamotua	0.3587	1989	0.2178	1989	0.357	1989	Class 1
1GB06	Mbogo	2e-16	1977	0.215	1978	5e-05	1978	Class 2
1GB11	Ainopsiwa	2e-16	1997	1e-05	1978	0.072	1978	Class 2
1GC05	Masaita	0.351	1998	0.218	1998	0.362	1998	Class 1
1GD04	Nyando	2e-04	1965	0.064	1979	0.025	1972	Class 2
1GC04	Tugenon	0.083	1961	0.065	1961	0.297	1961	Class 1

Table 3B (ii): Comparison of results of JJA streamflow series.

S/Code	S/ Name	SNHT		Pettit's test		Buishand r/ test		Class
		P-value	Break point	P-value	Break point	P-value	Break point	
1GC06	N. Kericho	0.767	1984	0.8114	1985	0.3231	1984	Class 1
1GD07	N. Kisumu	0.062	1991	4e-06	1986	1e-04	1993	Class 2
1GB05	Ainamotua	0.0338	1986	0.2178	1986	0.2486	1985	Class 1
1GB06	Mbogo	2e-16	1981	4e-06	1975	0.653	1994	Class 2
1GB11	Ainopsiwa	2e-16	1990	1e-05	1976	0.1454	1984	Class 2
1GC05	Masaita	0.034	1998	0.218	1983	0.248	1997	Class 1
1GD04	Nyando	2e-16	1975	0.524	1974	0.139	1975	Class 1
1GC04	Tugenon	0.295	1995	0.769	1974	0.960	1973	Class 1

Table 3B (iii): Comparison of results of OND streamflow series.

S/Code	S/Name	SNHT		Pettit's test		Buishand r/test		Class
		P-value	Break point	P-value	Break point	P-value	Break point	
1GC06	N. Kericho	0.864	1997	0.5048	1989	0.619	1975	Class 1
1GD07	N. Kisumu	2e-16	1998	0.0713	1991	2e-16	1998	Class 2
1GB05	Ainamotua	0.782	1987	0.447	1998	0.150	1987	Class 1
1GB06	Mbogo	2e-16	1981	0.245	1974	5e-05	1994	Class 2
1GB11	Ainopsiwa	0.326	1989	2e-05	1978	2e-16	1991	Class 2
1GC05	Masaita	0.770	1985	0.447	1977	0.149	1984	Class 1
1GD04	Nyando	0.212	1972	0.316	1991	0.479	1972	Class 1
1GC04	Tugenon	0.001	1994	0.3163	1979	0.011	1981	Class 2

Appendix 4: Change point Test Results

Appendix 4A: Change point test results for rainfall

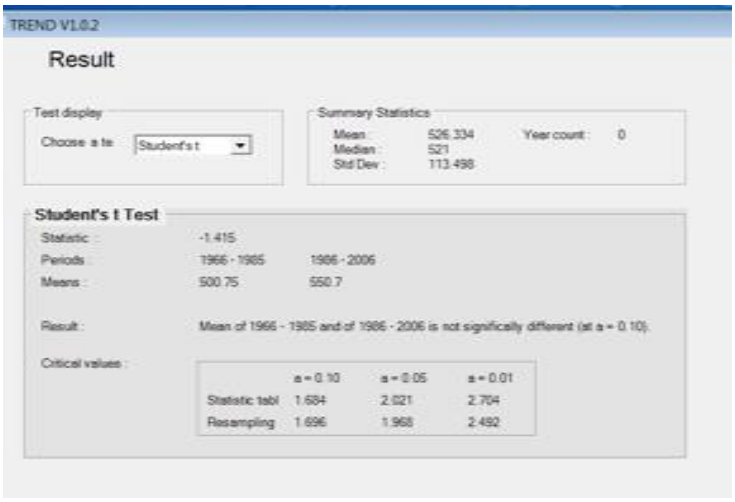

Chemelil MAM

Chemelil JJA

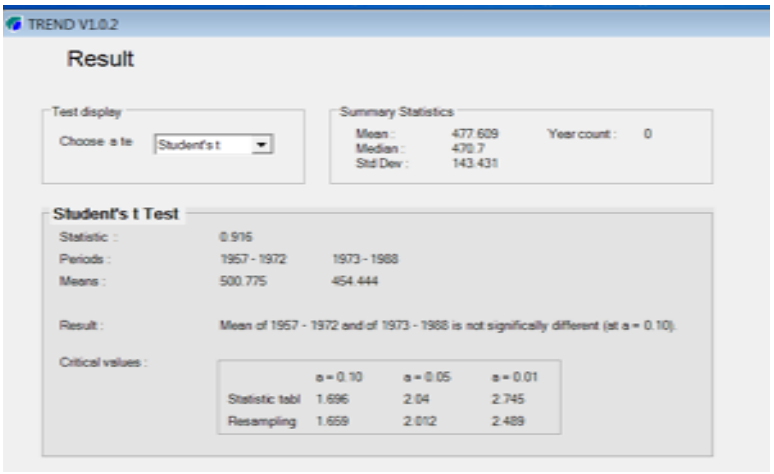

Nandi Tea MAM

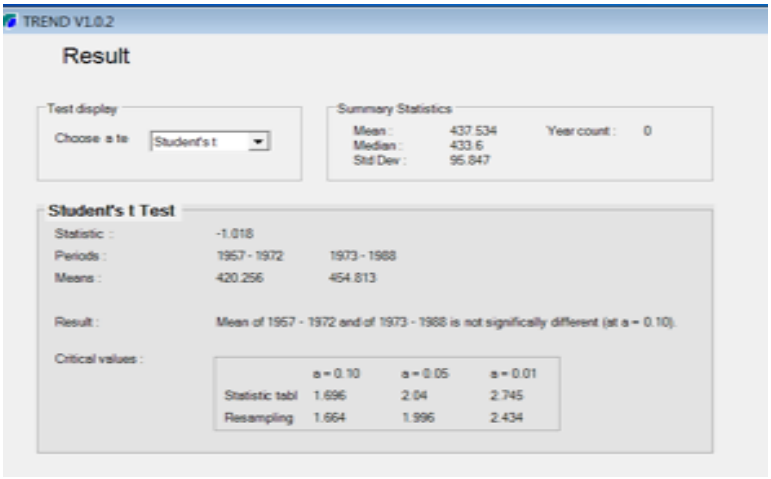

Nandi Tea JJA

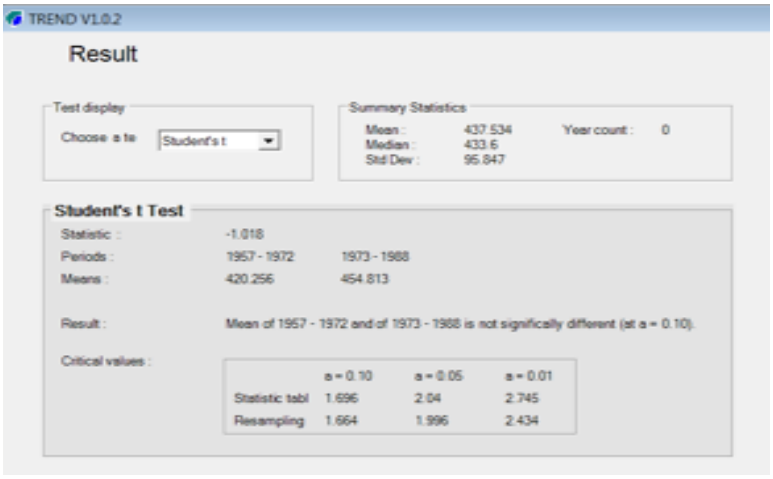

Kipkelion MAM

Tinga MAM

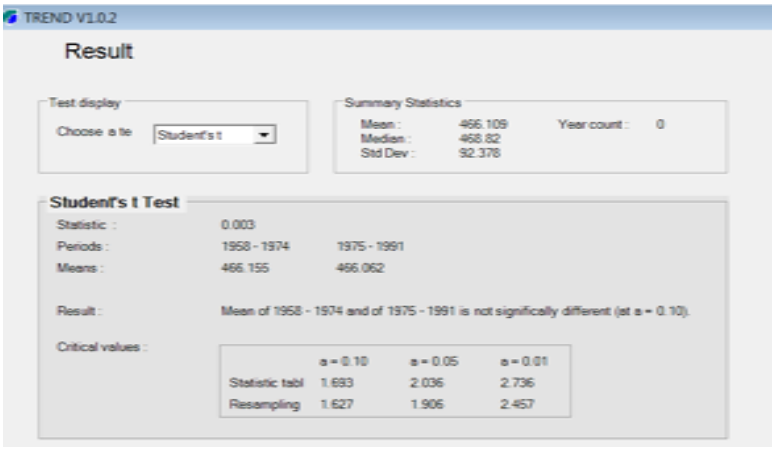

Tinga JJA

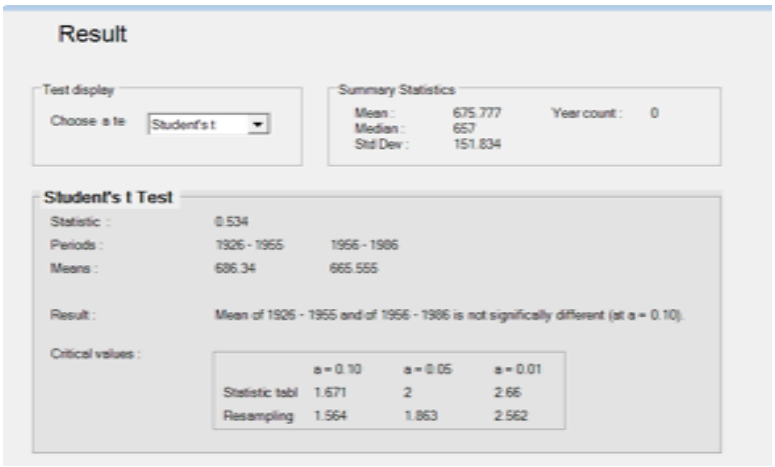

Kericho Water MAM

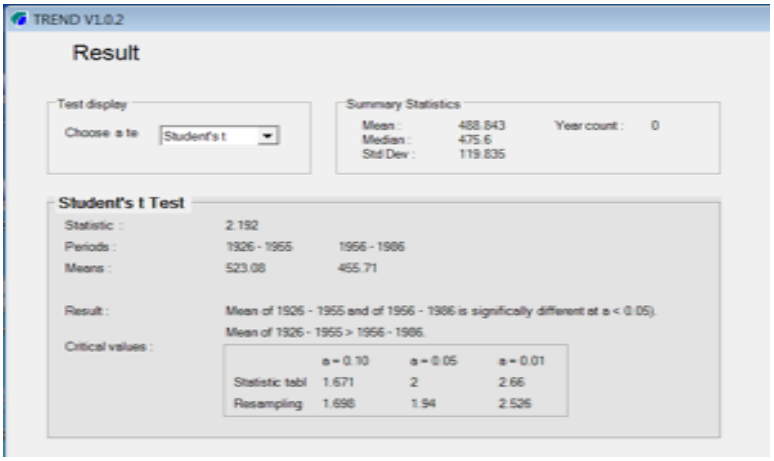

Kericho Water JJA

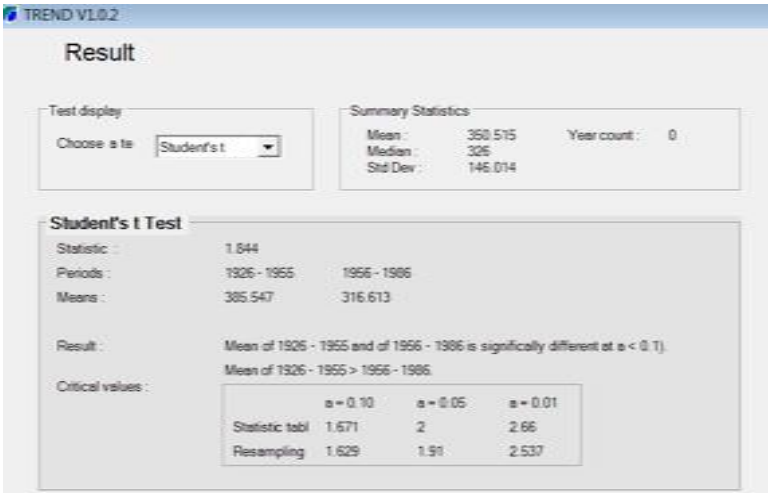

Londiani MAM

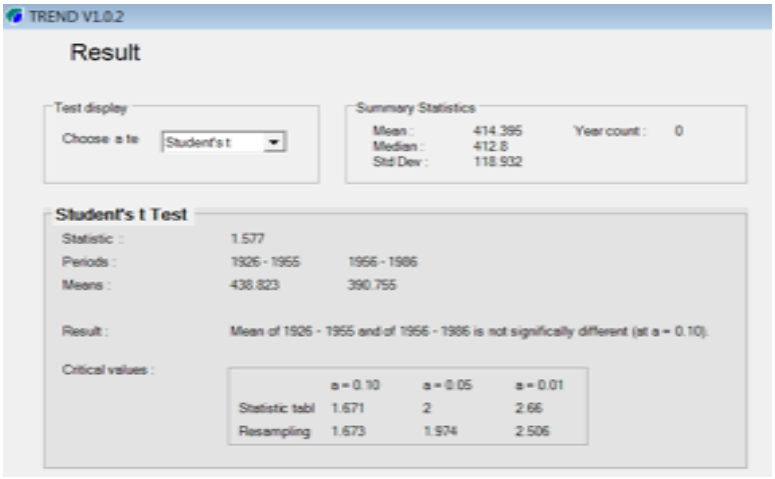

Londiani JJA

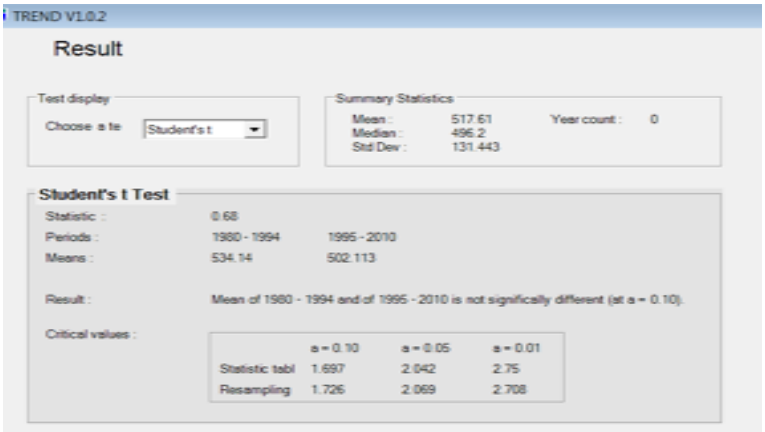

Kericho Met MAM

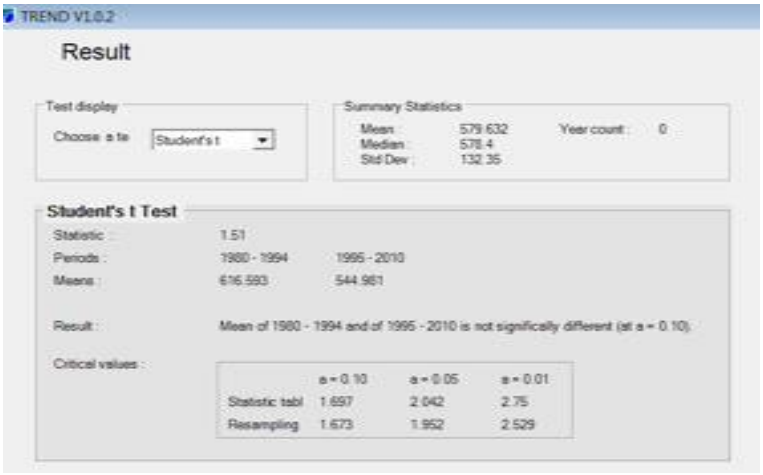

Kericho Met JJA

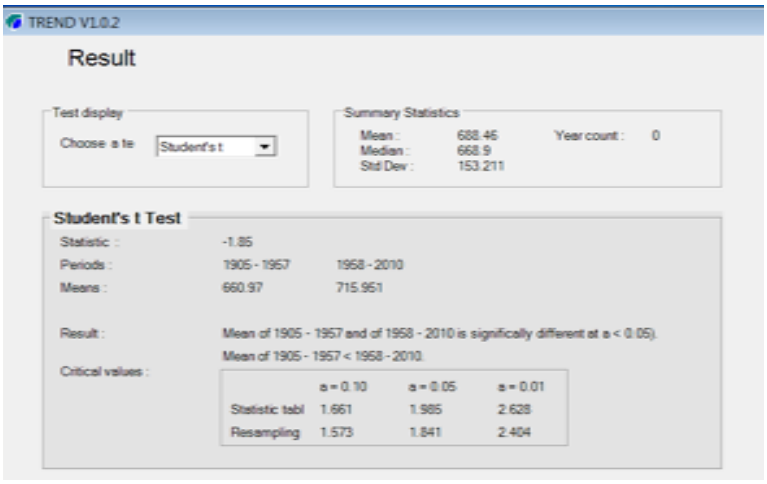

Finlay MAM

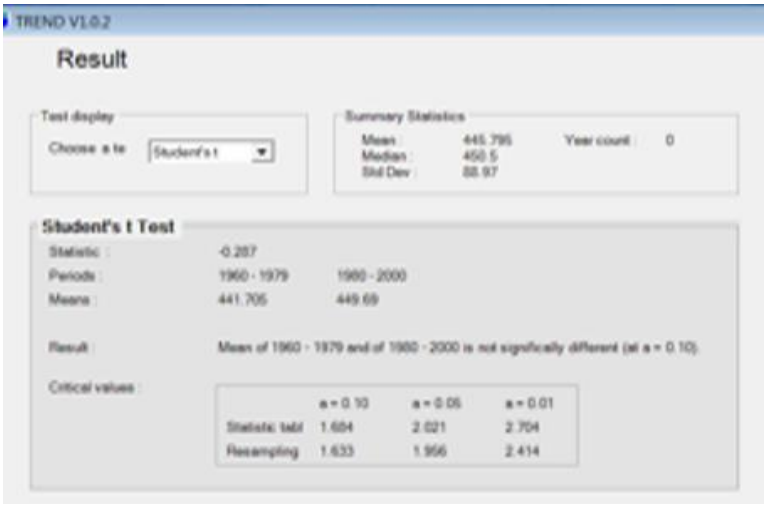

Finlay JJA

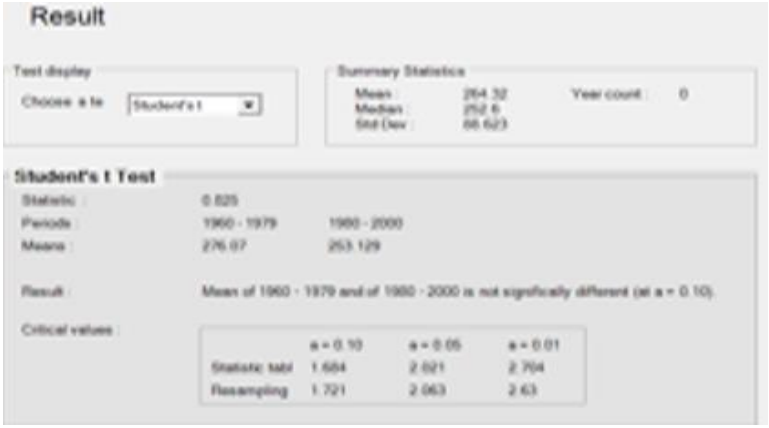

Ahero MAM

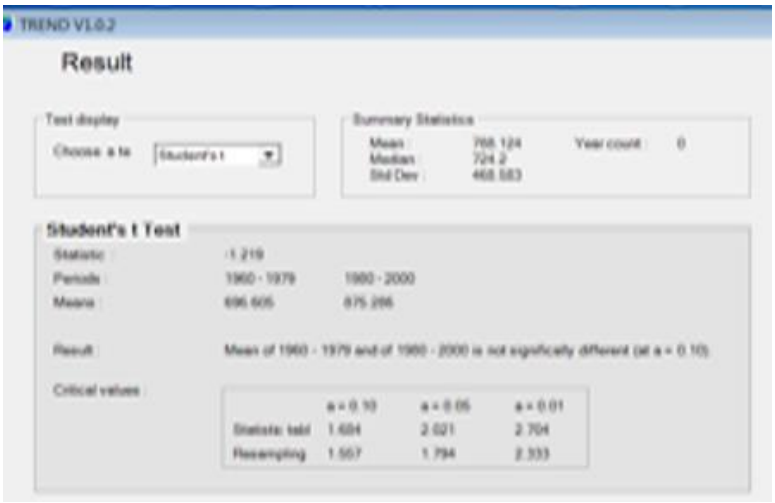

Ahero JJA

Appendix 4B: Change point test results for streamflow.

Ainamotua MAM

Ainamotua JJA

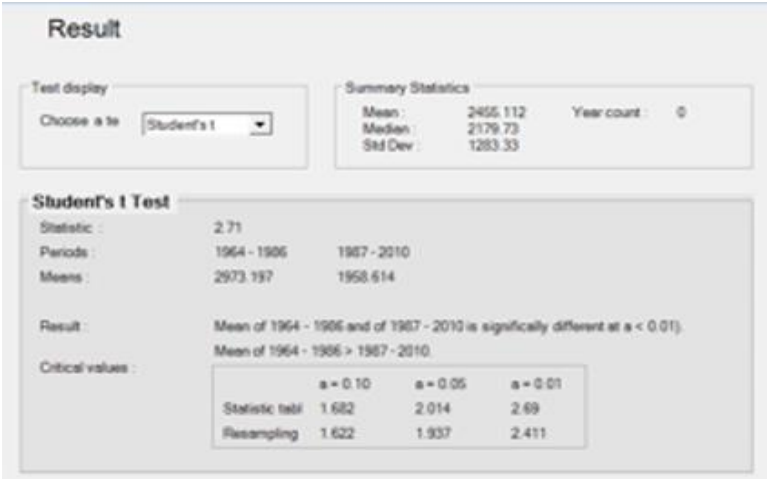

Ainopsiwa MAM

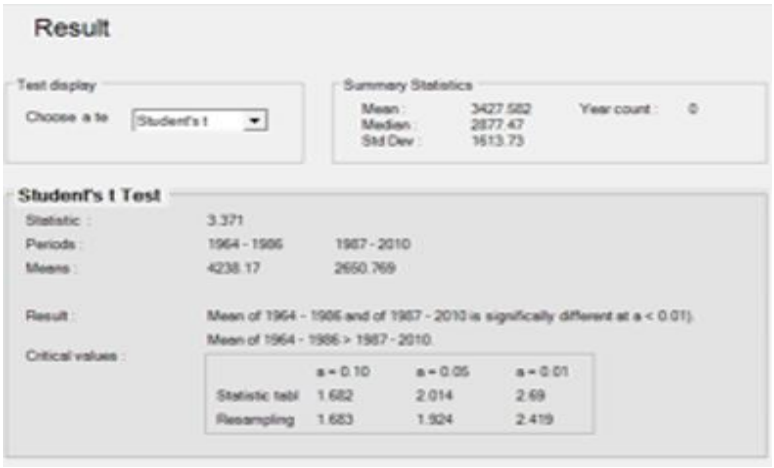

Ainopsiwa JJA

Masaita MAM

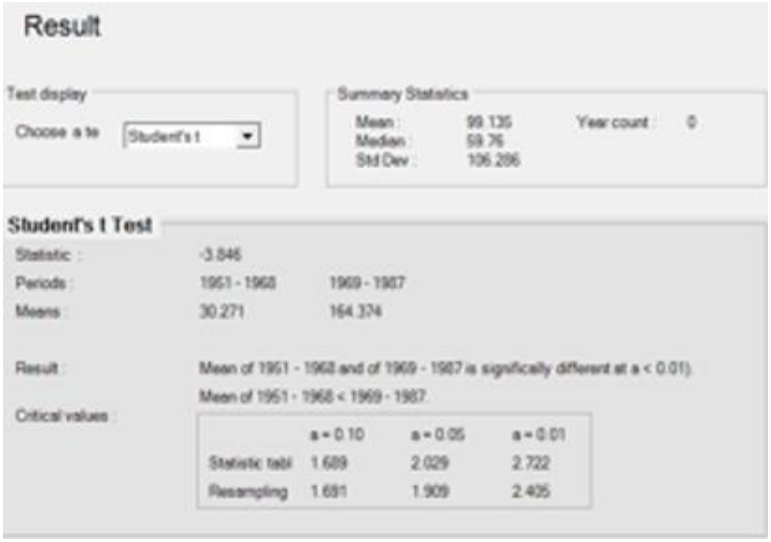

Masaita JJA

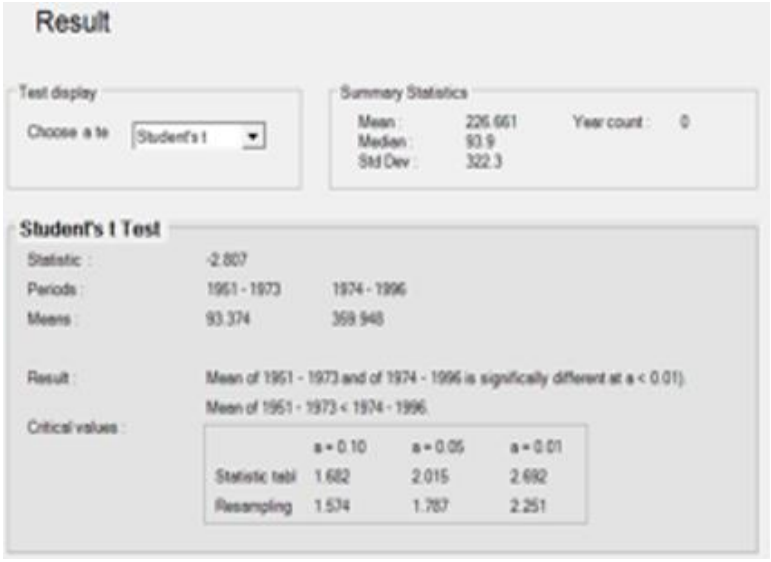

Mbogo MAM

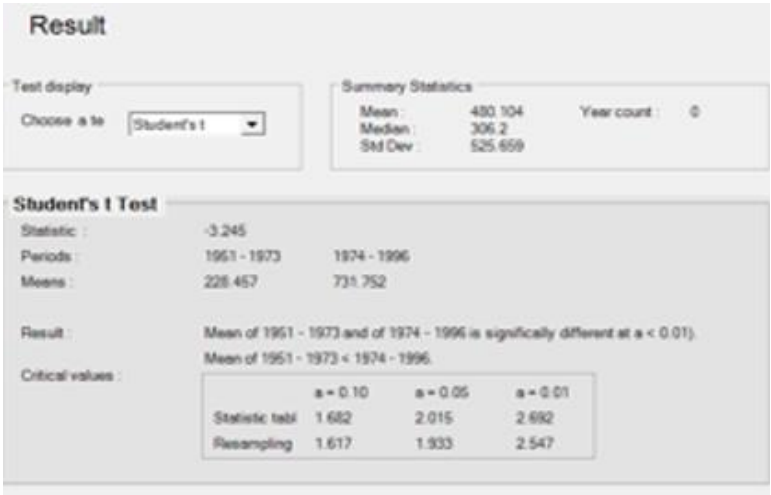

Mbogo JJA

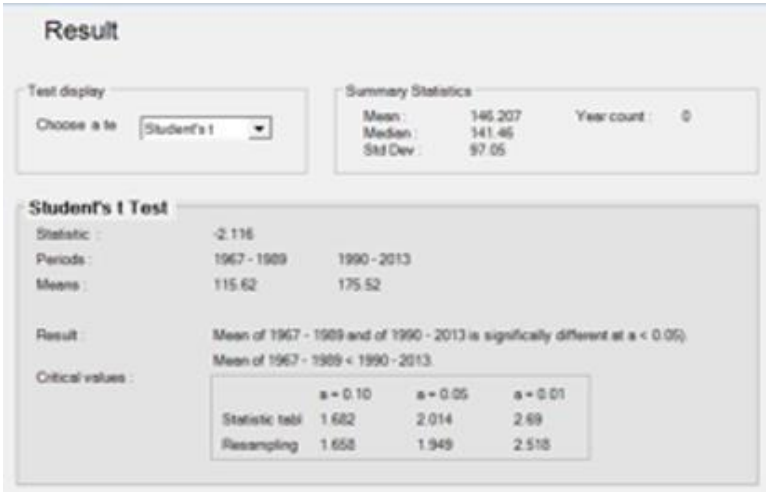

Namuting MAM

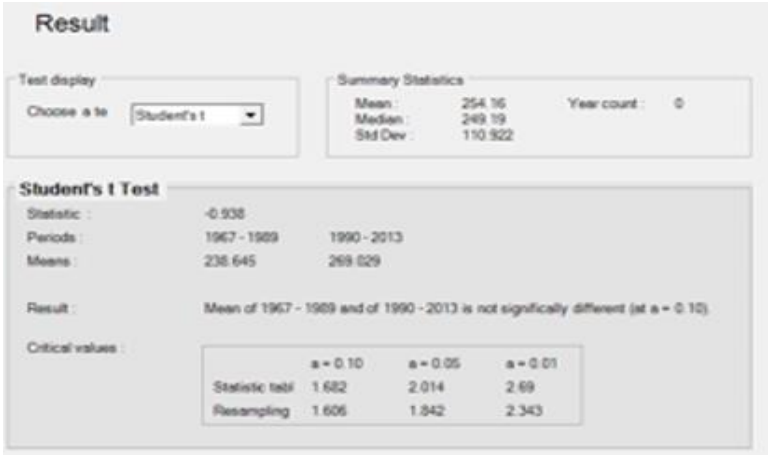

Namuting JJA

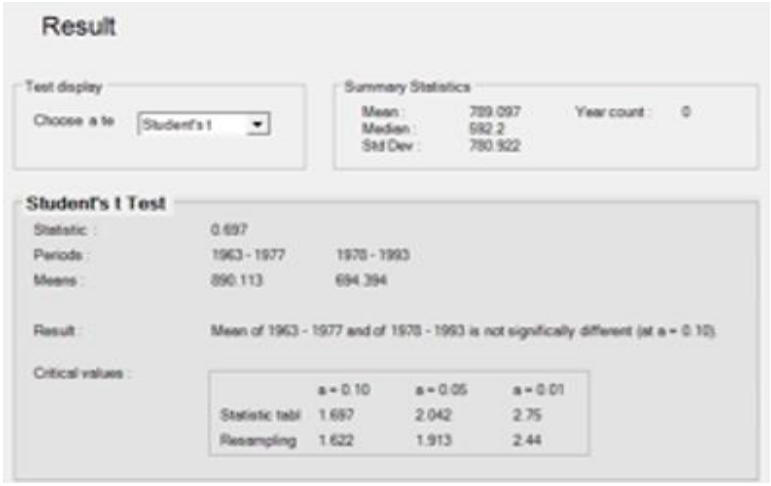

Nyando 1GC06 MAM

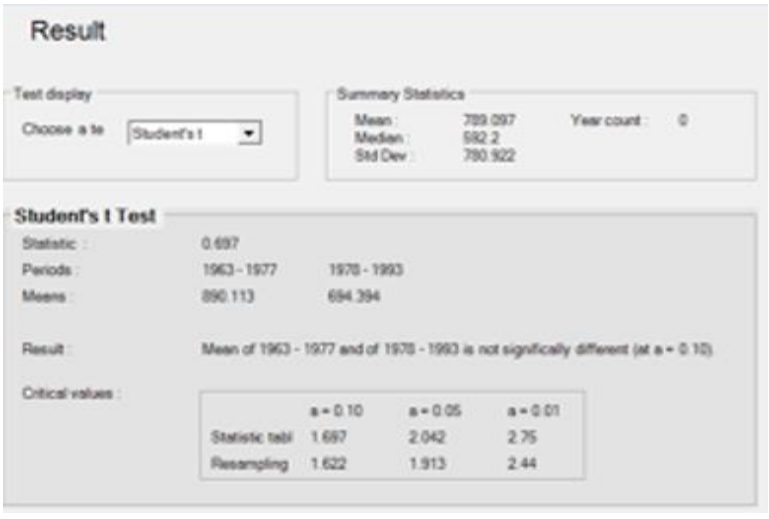

Nyando 1GC06 JJA

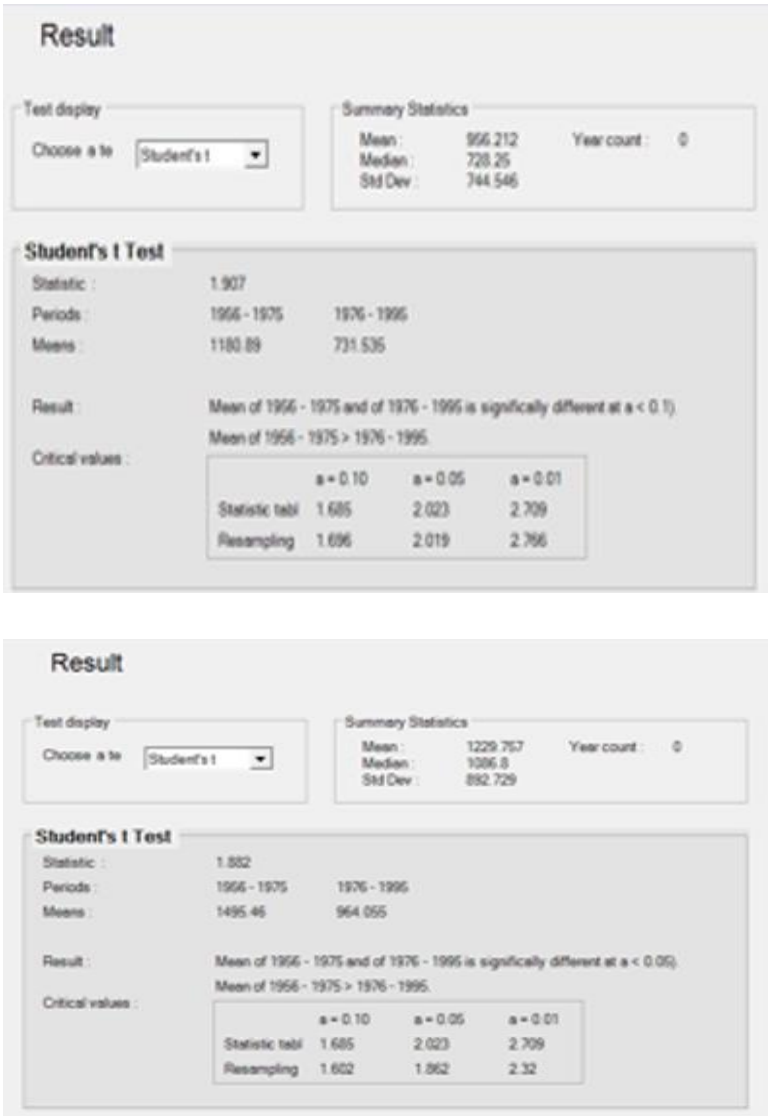

Nyando 1GD07 MAM

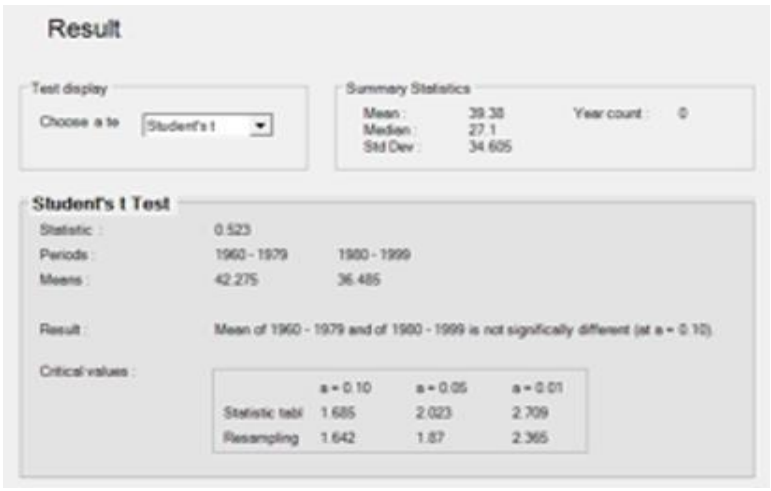

Nyando 1GD07 JJA

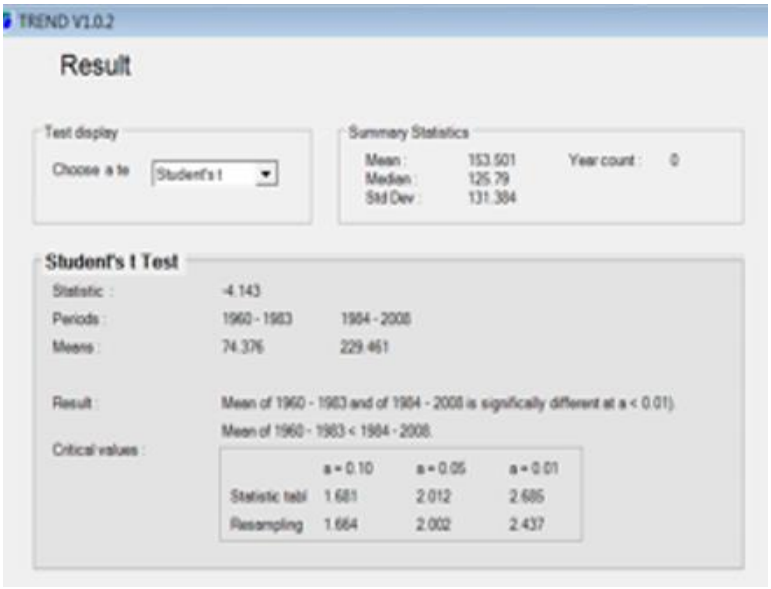

Nyando 1GD04 MAM

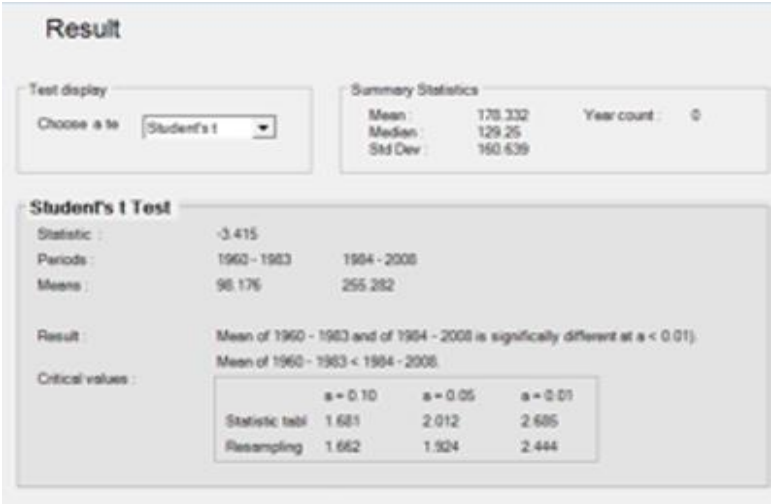

Nyando 1GD04 JJA

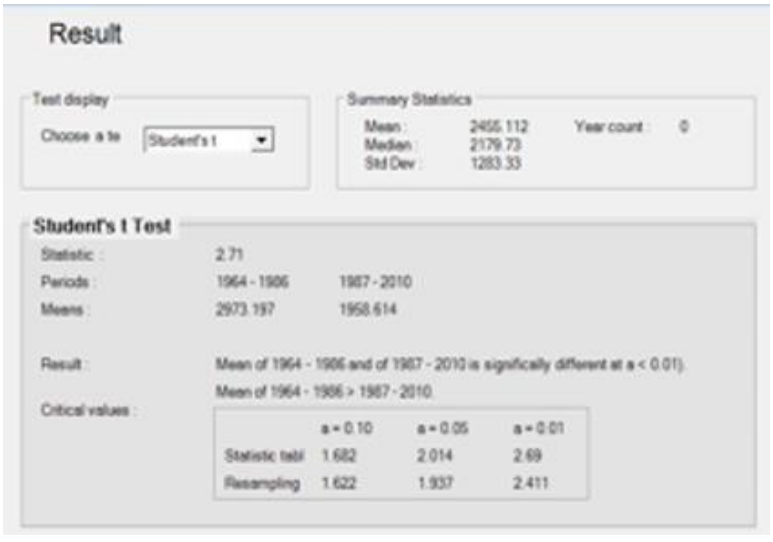

Ainamotua JJA

Ainopsiwa JJA

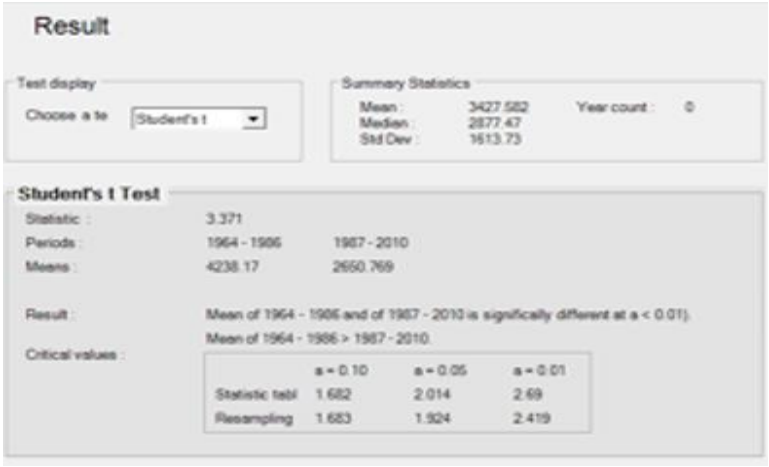

Masaita MAM

Masaita JJA

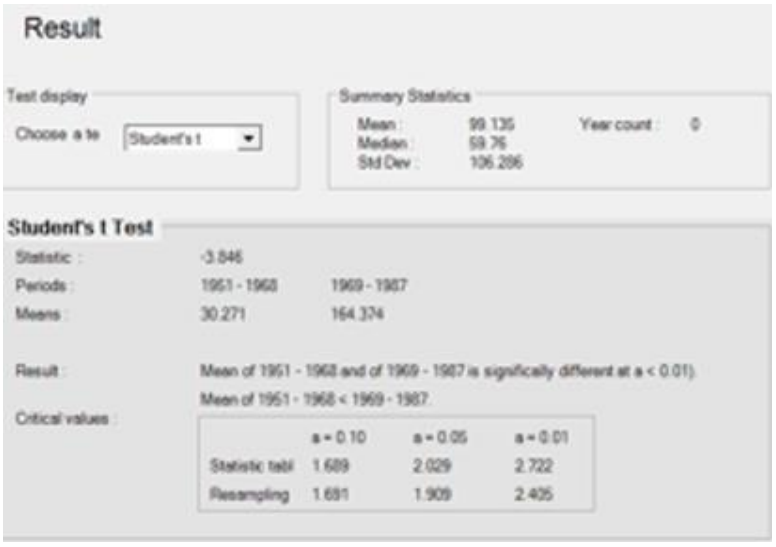

Mbogo MAM

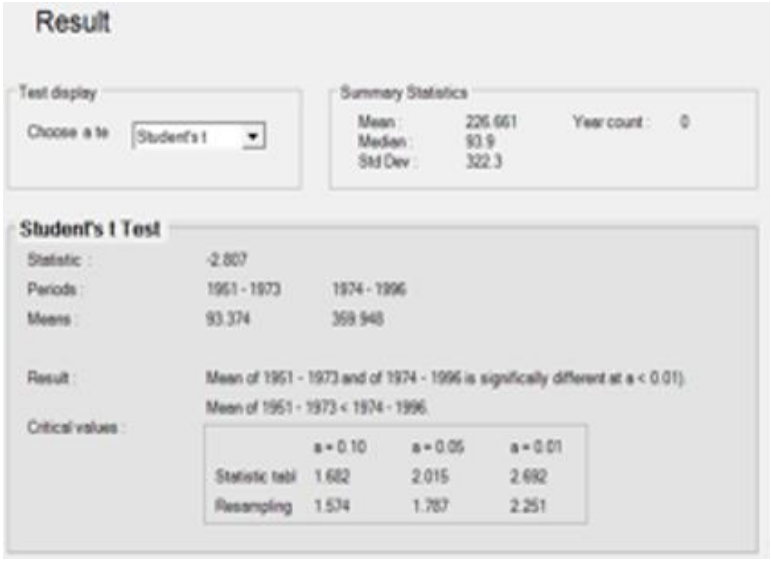

Mbogo JJA

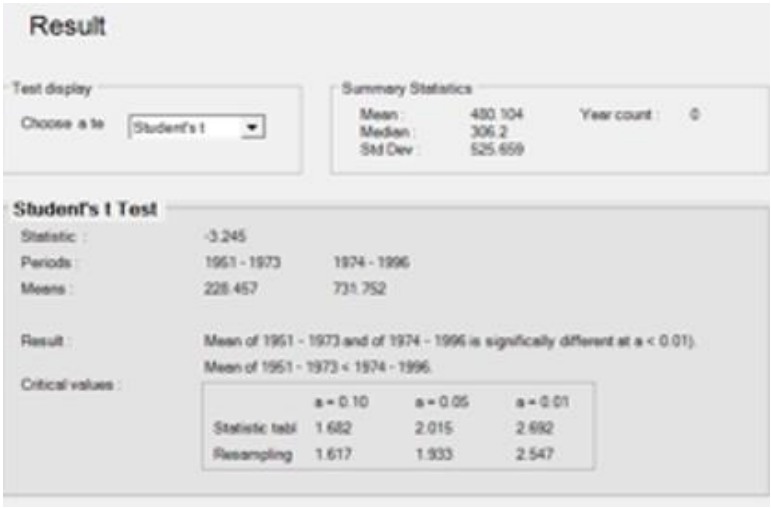

Namuting MAM

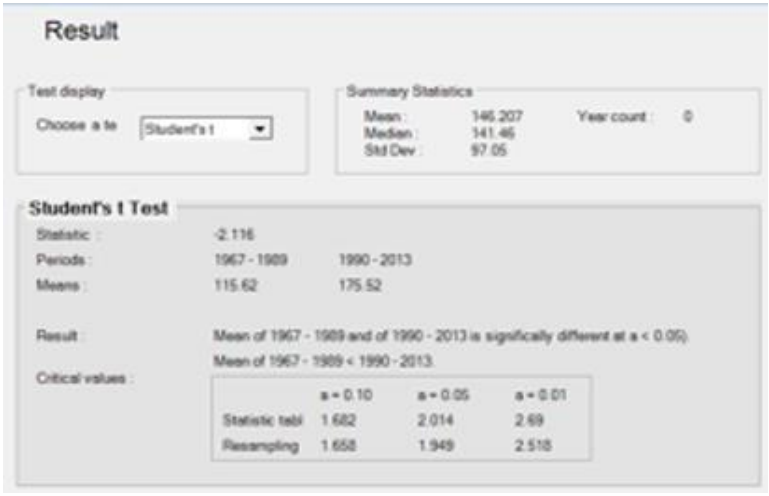

Namuting JJA

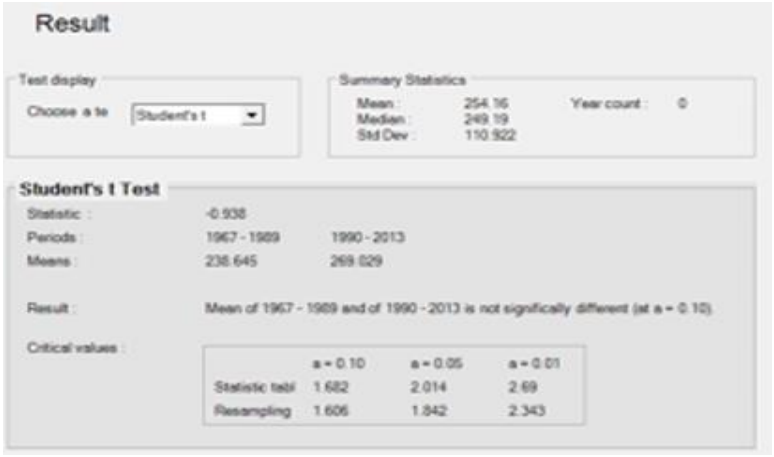

Nyando 1GC06 MAM

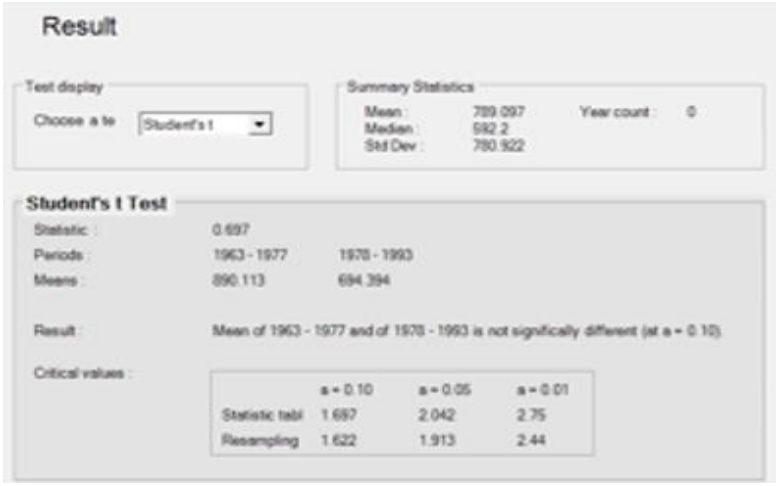

Nyando 1GC06 JJA

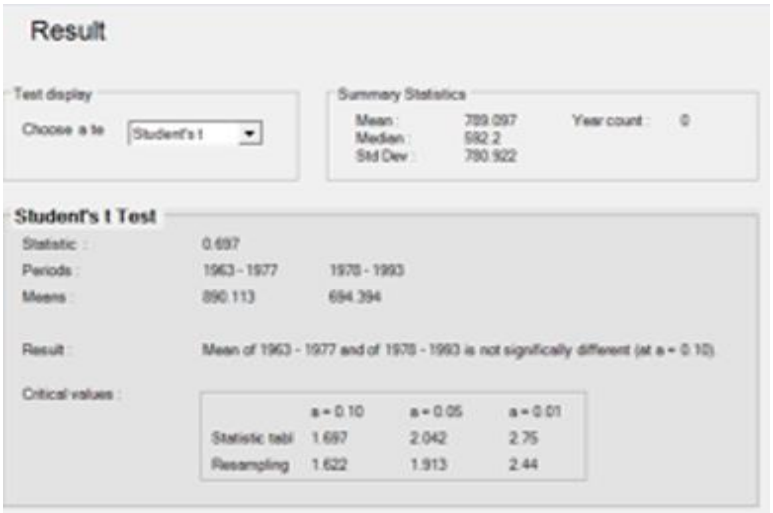

Nyando 1GD07 MAM

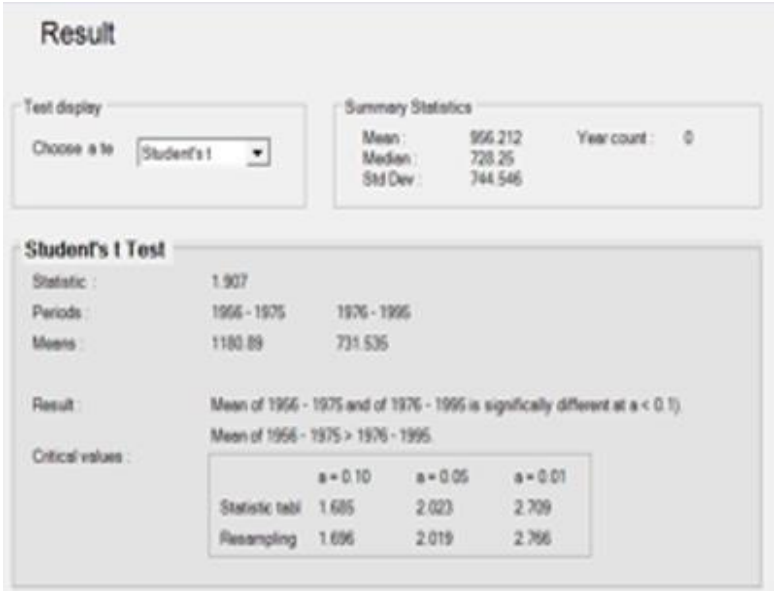

Nyando 1GD07 JJA

Nyando 1GD04 MAM

Appendix 5A: Normality Test Results

Appendix 5B: Rainfall normality test results

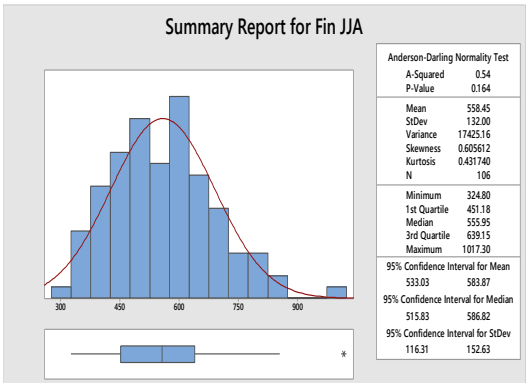

Finlay JJA

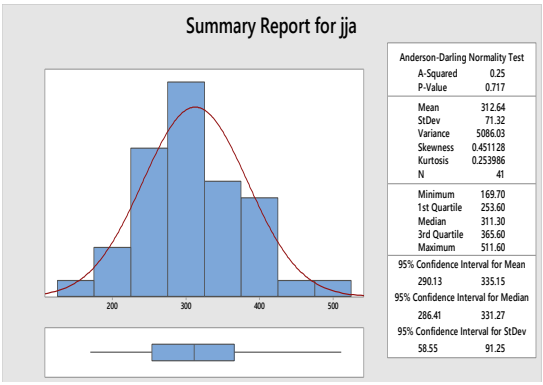

Chemelil JJA

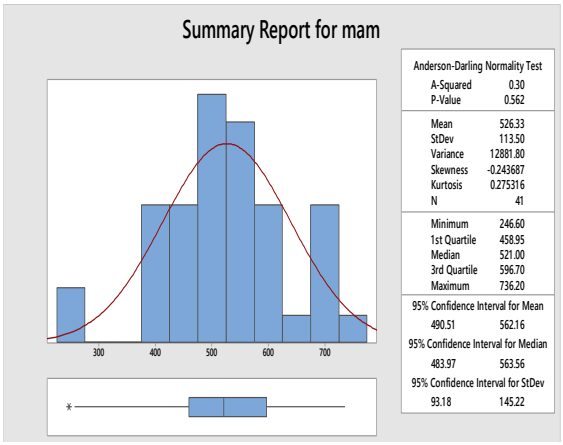

Kericho Met MAM

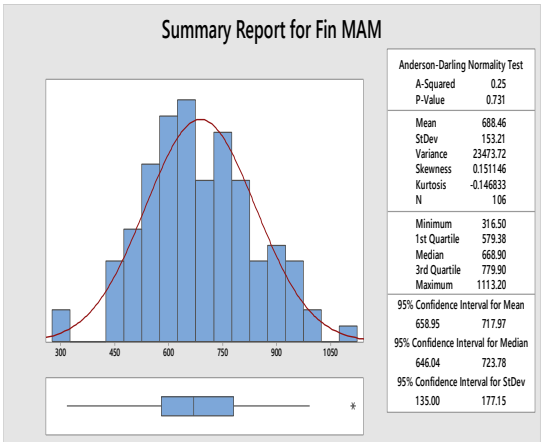

Finlay MAM

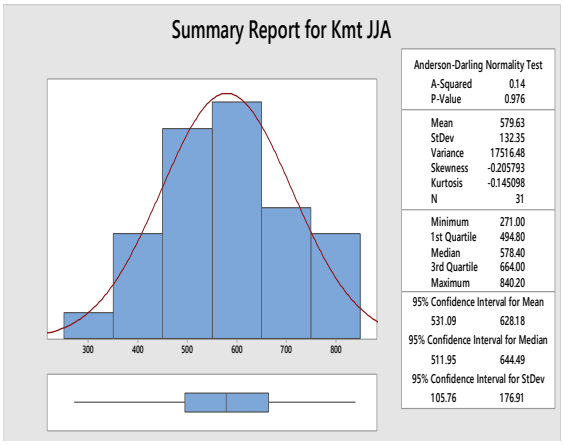

Kericho Met JJA

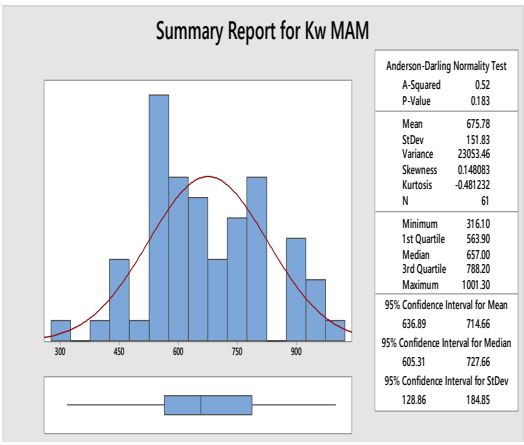

Kericho Water MAM

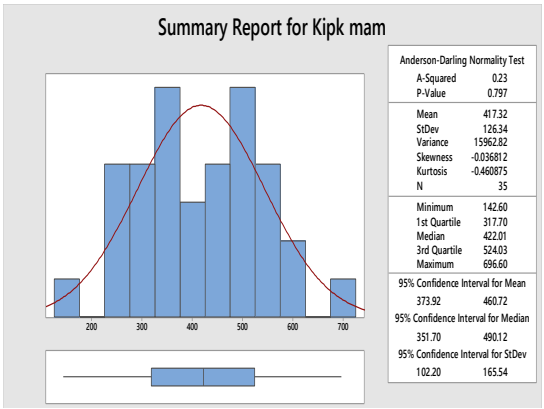

Kipkelion MAM

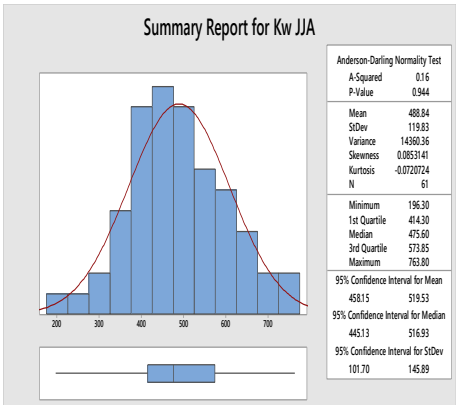

Kericho Water JJA

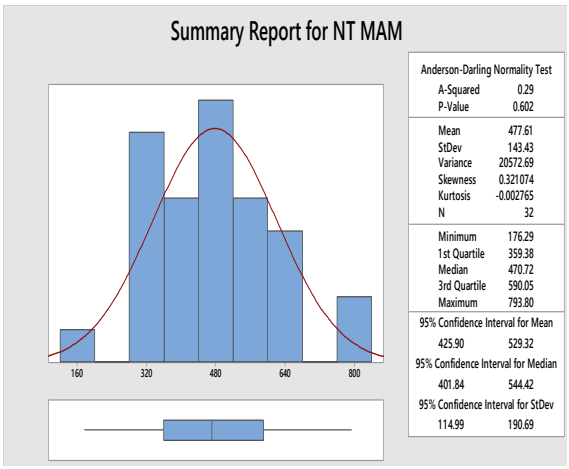

Nandi Tea MAM

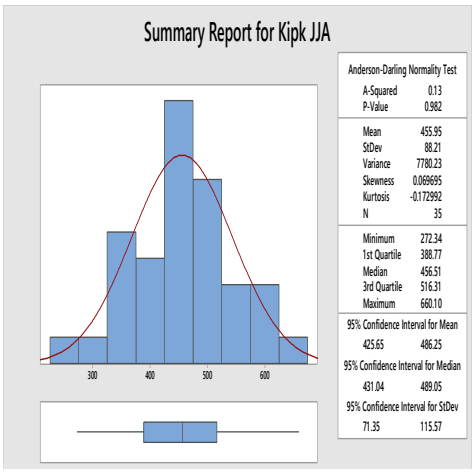

Kipkelion JJA

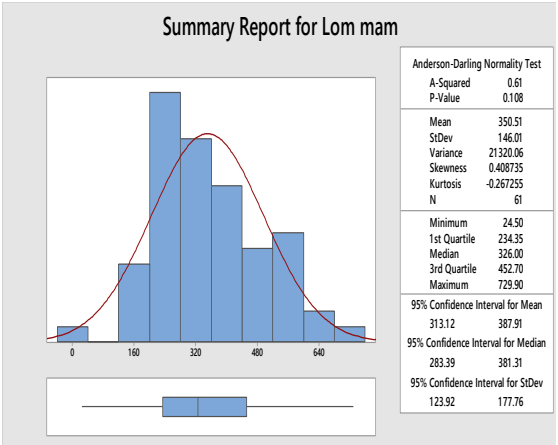

Londiani MAM

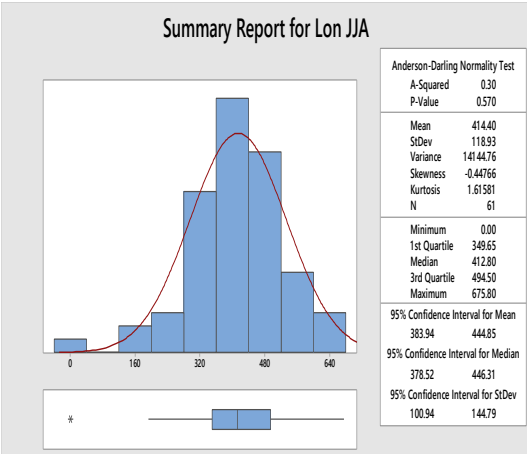

Londiani JJA

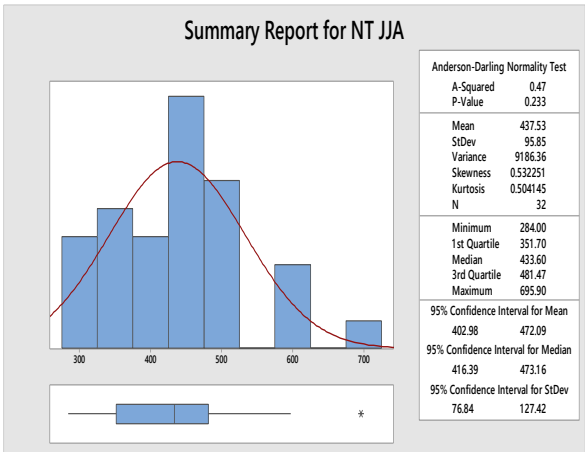

Nandi Tea JJA

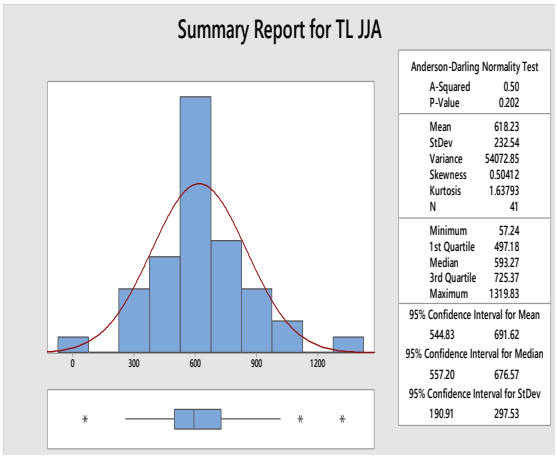

Timbilil JJA

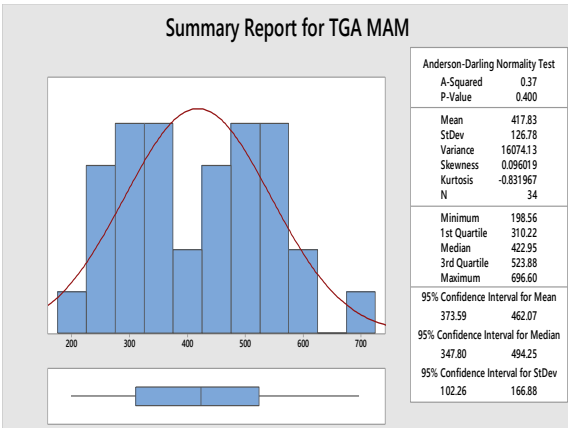

Tinga MAM

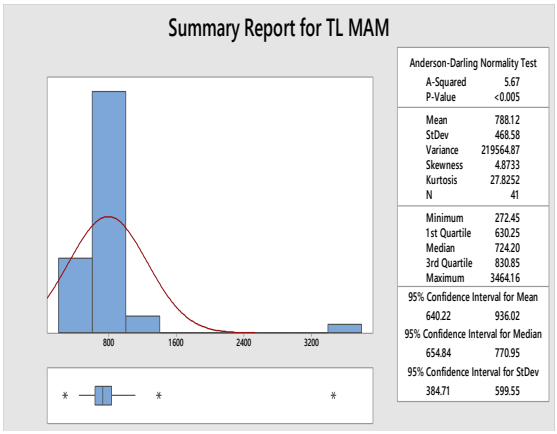

Timbilil MAM

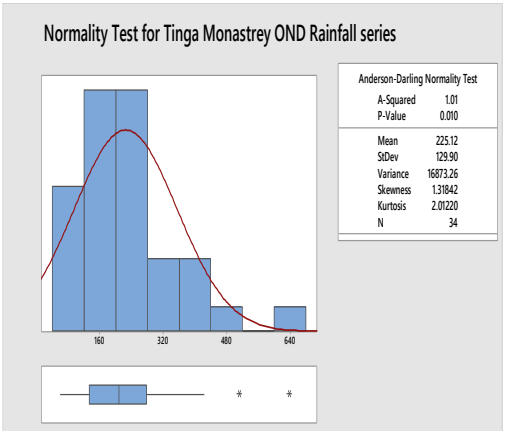

Tinga OND

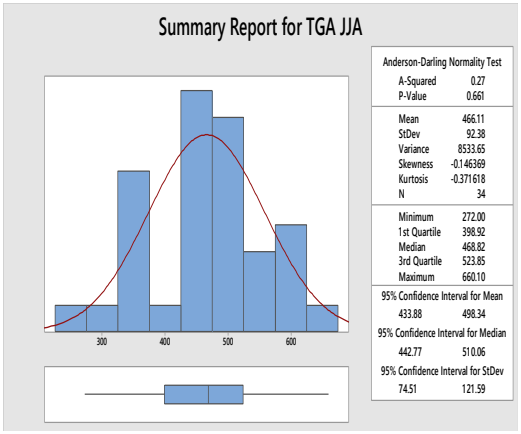

Tinga JJA

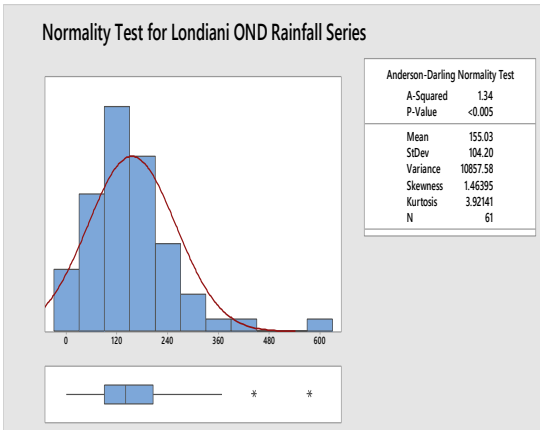

Londiani OND

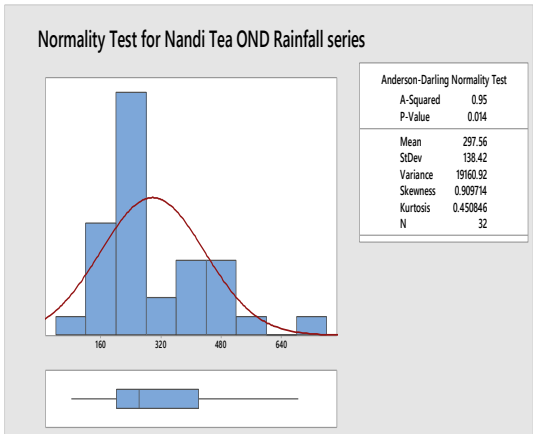

Nandi Tea OND

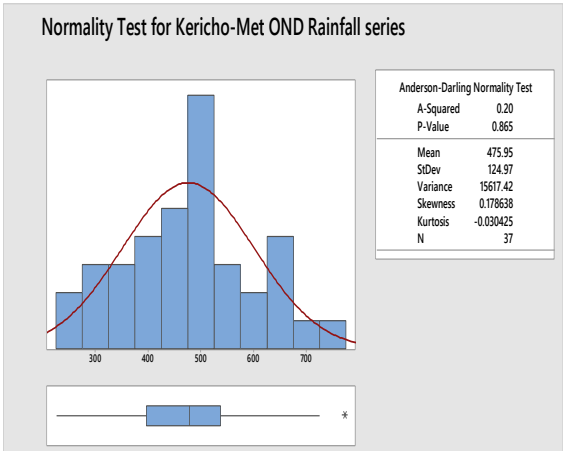

Kericho Met OND

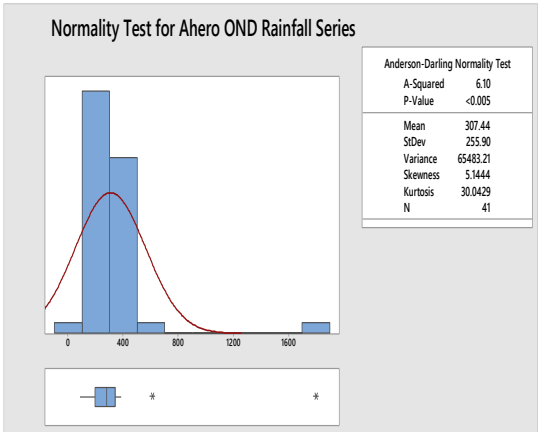

Ahero OND

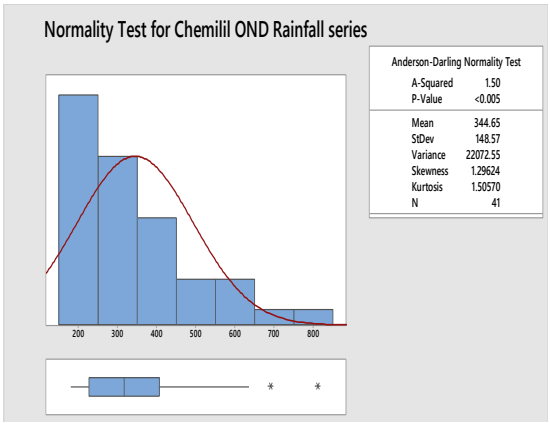

Chemelil OND

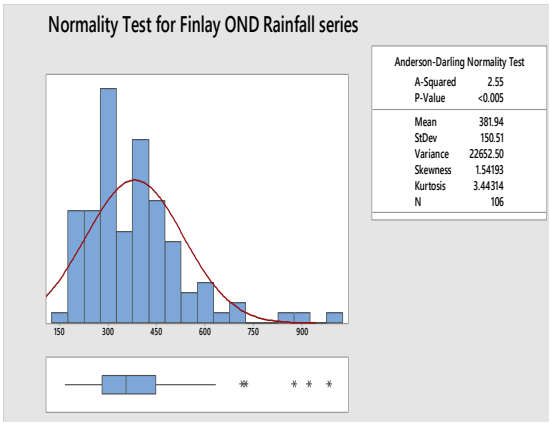

Finlay OND

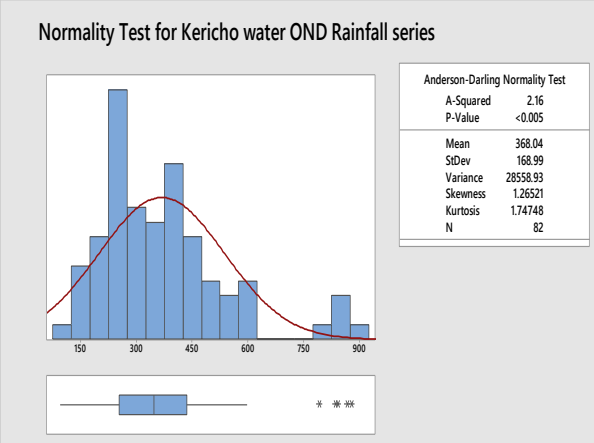

Kericho Water OND

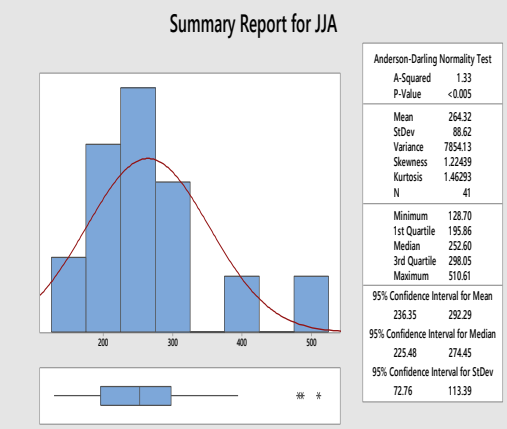

Ahero JJA

Appendix 5B: Streamflow normality test results

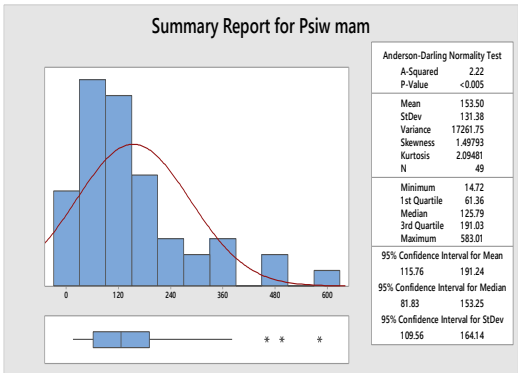

Ainopsiwa MAM

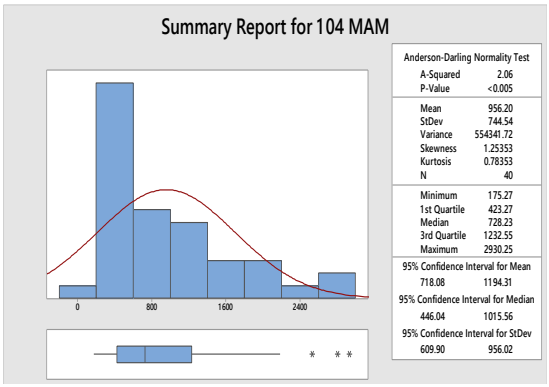

Nyando 104 MAM

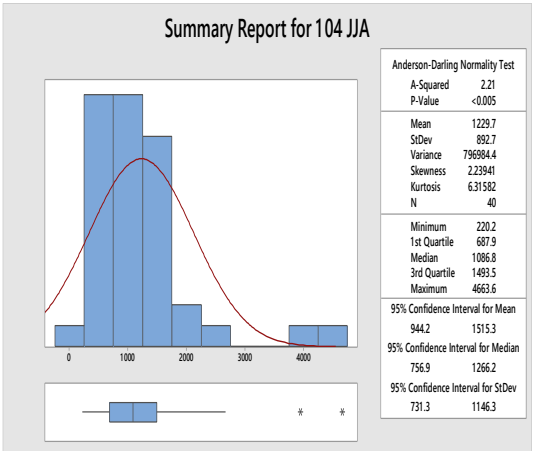

Nyando 104 MAM

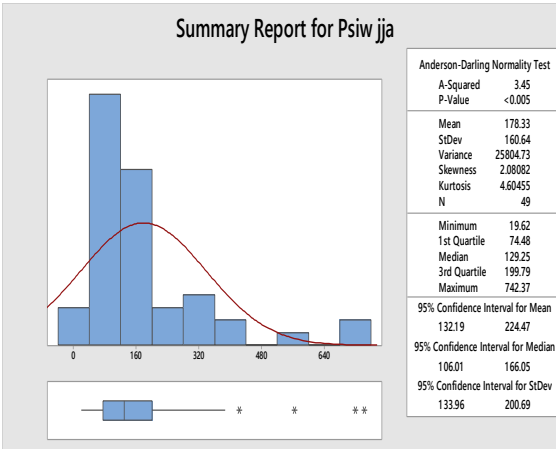

Ainopsiwa JJA

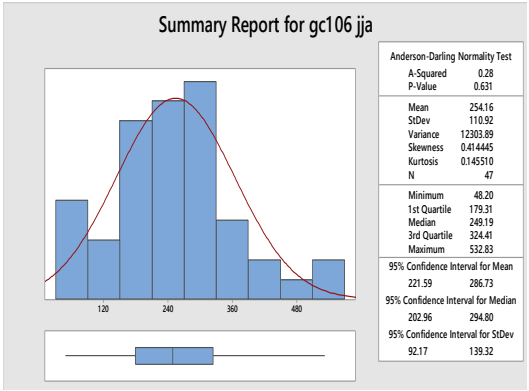

Nyando Kericho JJA

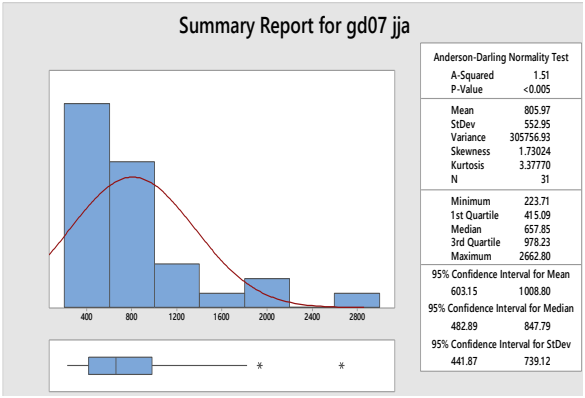

Nyando Kisumu JJA

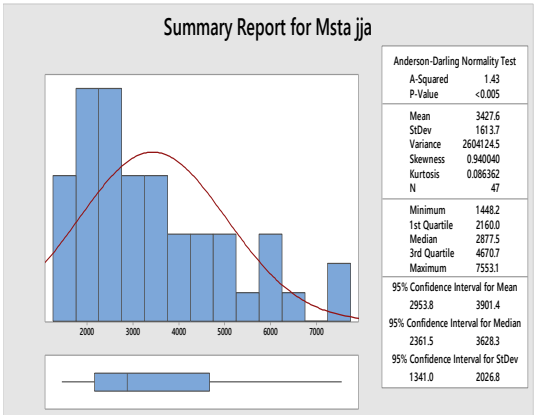

Masaita JJA

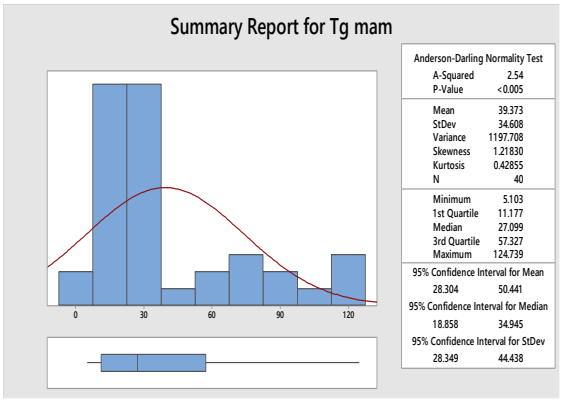

Tugenon MAM

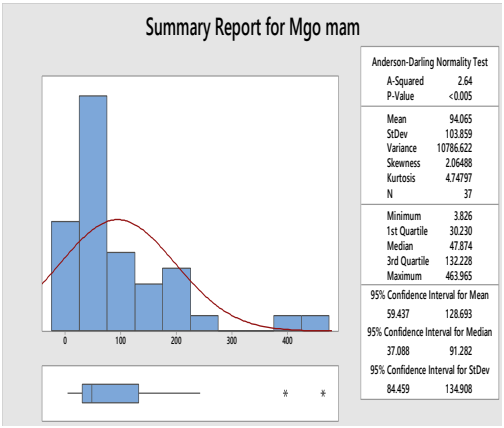

Mbogo MAM

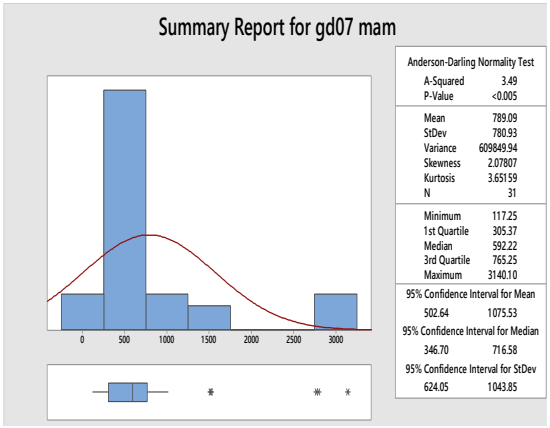

Nyando Kericho MAM

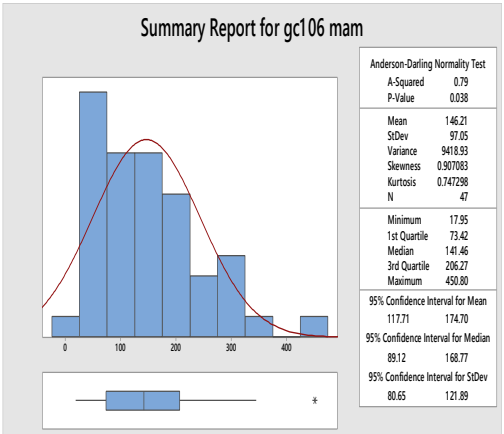

Nyando Kericho MAM

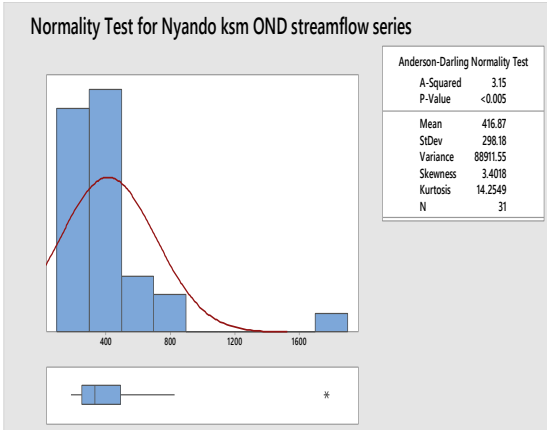

Nyando Kisumu OND

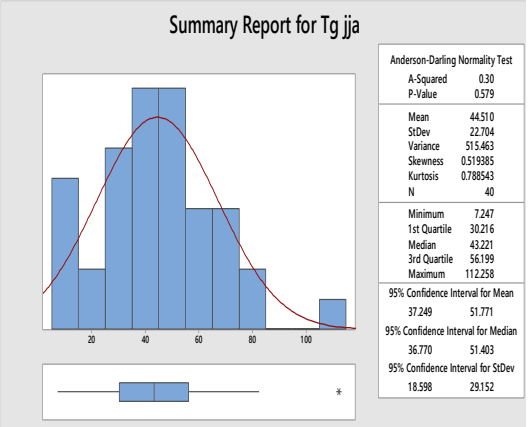

Tugenon JJA

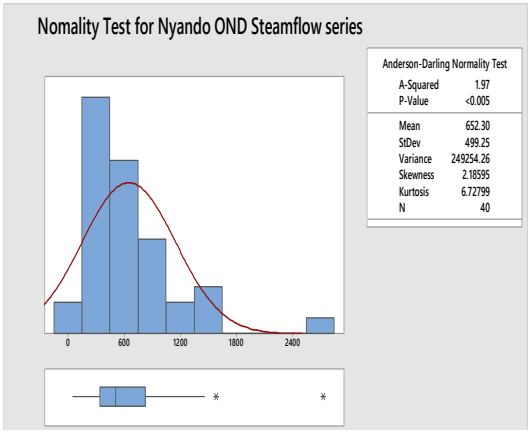

Nyando 1GD04 OND

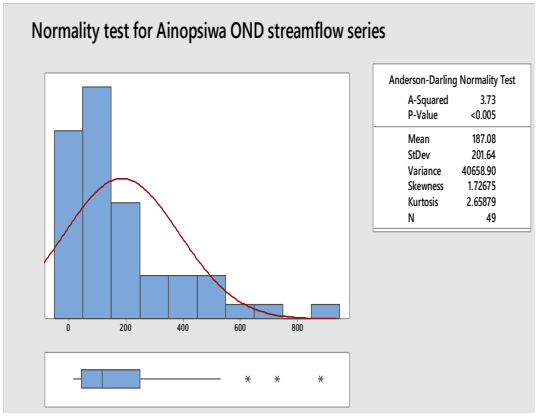

Ainopsiwa OND

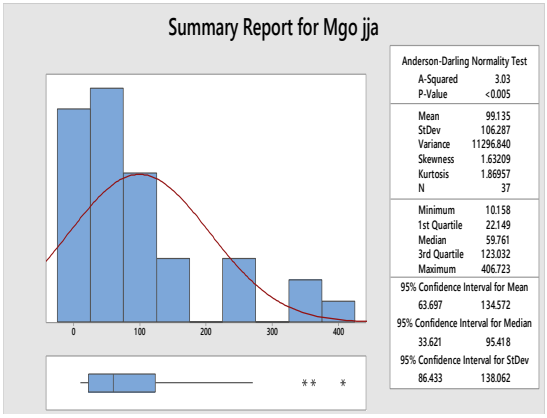

Mbogo JJA

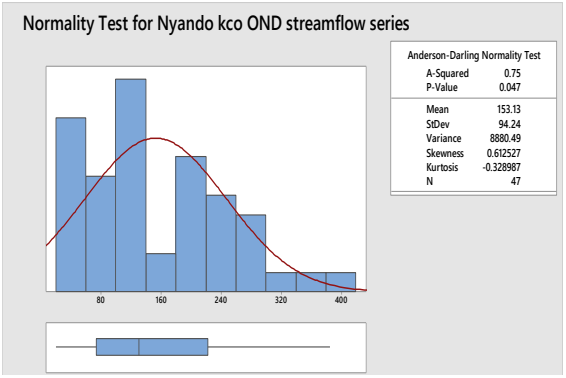

Nyando Kericho OND

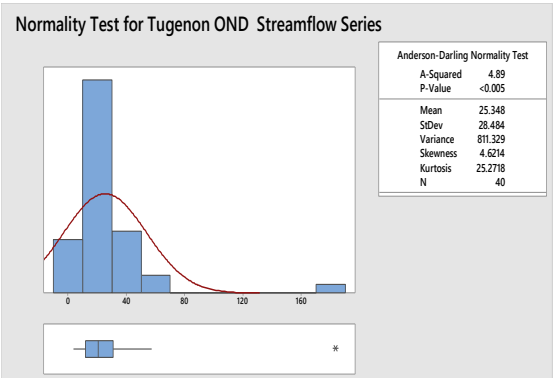

Tugenon OND

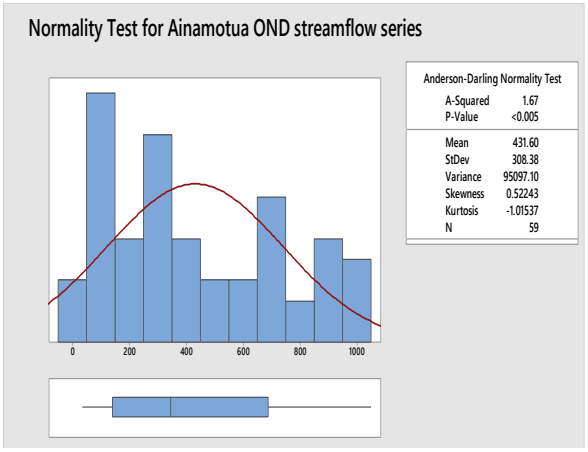

Ainamotua OND

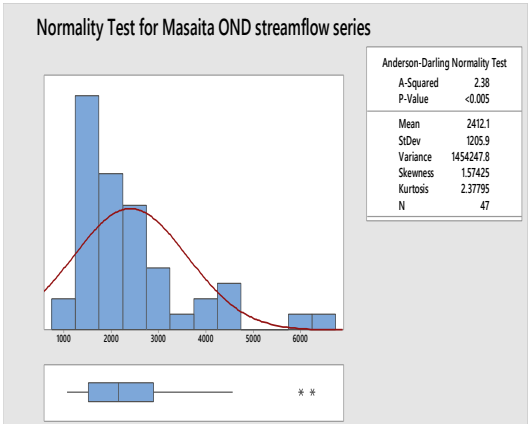

Masaita OND

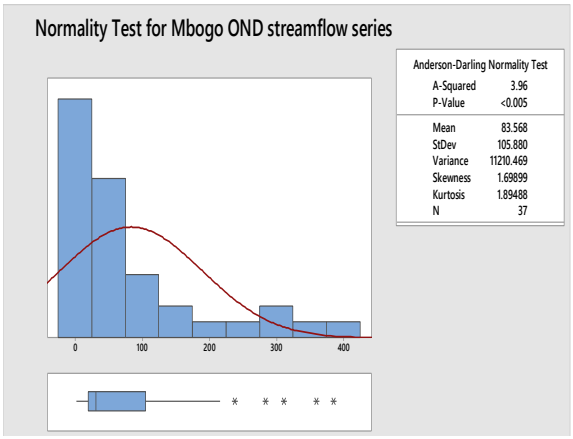

Mbogo OND

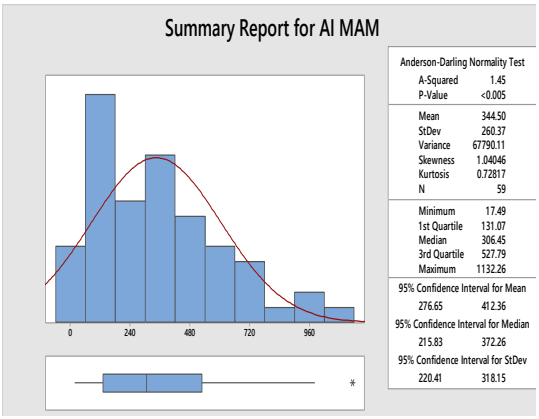

Ainamotua MAM

Appendix 6A: M-K Results for split rainfall series

Data file: Ahero MAM Set 2. result								
	Test statistic	Critical values			Critical values			Result
		(Statistical table)			(Resampling)			
		a=0.1	a=0.05	a=0.01	a=0.1	a=0.05	a=0.01	
M-K	-0.488	0.987	1.176	1.546	1.586	1.769	2.44	NS
Data file: Ahero MAM Set 3.csv								
	Test statistic	Critical values			Critical values			Result
		(Statistical table)			(Resampling)			
		a=0.1	a=0.05	a=0.01	a=0.1	a=0.05	a=0.01	
M-K	0.476	1.645	1.96	2.576	1.734	2.074	2.651	NS
Data file: Ahero MAM Set 4.csv								
	Test statistic	Critical values			Critical values			Result
		(Statistical table)			(Resampling)			
		a=0.1	a=0.05	a=0.01	a=0.1	a=0.05	a=0.01	
M-K	-0.358	0.74	0.882	1.159	1.521	1.878	2.415	NS
Data file: Chemelil MAM Set 3.csv								
	Test statistic	Critical values			Critical values			Result
		(Statistical table)			(Resampling)			
		a=0.1	a=0.05	a=0.01	a=0.1	a=0.05	a=0.01	
M-K	1.632	1.645	1.96	2.576	1.683	2.006	2.634	NS
Data file: Chemelil MAM Set 4.csv								
	Test statistic	Critical values			Critical values			Result
		(Statistical table)			(Resampling)			
		a=0.1	a=0.05	a=0.01	a=0.1	a=0.05	a=0.01	
M-K	1.355	0.658	0.784	1.03	1.46	1.877	2.294	NS
Data file: Finlay MAM Set 1.csv								
	Test statistic	Critical values			Critical values			Result
		(Statistical table)			(Resampling)			
		a=0.1	a=0.05	a=0.01	a=0.1	a=0.05	a=0.01	
M-K	0.068	1.645	1.96	2.576	1.666	1.972	2.838	NS
Data file: Finlay MAM Set 2.csv								
	Test statistic	Critical values			Critical values			Result
		(Statistical table)			(Resampling)			
		a=0.1	a=0.05	a=0.01	a=0.1	a=0.05	a=0.01	
M-K	0.285	1.645	1.96	2.576	1.641	1.963	2.48	NS
Data file: Finlay MAM Set 3.csv								
	Test statistic	Critical values			Critical values			Result
		(Statistical table)			(Resampling)			
		a=0.1	a=0.05	a=0.01	a=0.1	a=0.05	a=0.01	
M-K	0.089	1.645	1.96	2.576	1.588	1.855	2.498	NS
Data file: Finlay MAM Set 4.csv								
	Test statistic	Critical values			Critical values			Result

		(Statistical table)			(Resampling)			
		a=0.1	a=0.05	a=0.01	a=0.1	a=0.05	a=0.01	
M-K	1.525	0.987	1.176	1.546	1.647	1.891	2.379	NS
Data file: Kericho Met MAM Set 3.csv								
	Test statistic	Critical values			Critical values			Result
		(Statistical table)			(Resampling)			
		a=0.1	a=0.05	a=0.01	a=0.1	a=0.05	a=0.01	
M-K	-2.059	1.645	1.96	2.576	1.612	1.86	2.381	S (0.05)
Data file: Kericho Met MAM Set 4.csv								
	Test statistic	Critical values			Critical values			Result
		(Statistical table)			(Resampling)			
		a=0.1	a=0.05	a=0.01	a=0.1	a=0.05	a=0.01	
M-K	1.769	0.987	1.176	1.546	1.586	1.891	2.379	S (0.1)
Data file: Kericho water MAM Set 1 cvs.csv								
	Test statistic	Critical values			Critical values			Result
		(Statistical table)			(Resampling)			
		a=0.1	a=0.05	a=0.01	a=0.1	a=0.05	a=0.01	
M-K	-1.09	0.822	0.98	1.288	1.479	1.791	2.258	NS
Data file: Kericho water MAM Set 2 cvs.csv								
	Test statistic	Critical values			Critical values			Result
		(Statistical table)			(Resampling)			
		a=0.1	a=0.05	a=0.01	a=0.1	a=0.05	a=0.01	
M-K	-0.292	1.563	1.862	2.447	1.557	1.849	2.693	NS
Data file: Kericho water MAM Set 3 cvs.csv								
	Test statistic	Critical values			Critical values			Result
		(Statistical table)			(Resampling)			
		a=0.1	a=0.05	a=0.01	a=0.1	a=0.05	a=0.01	
M-K	-0.225	1.645	1.96	2.576	1.696	1.988	2.561	NS
Data file: Kericho water MAM Set 4 cvs.csv								
	Test statistic	Critical values			Critical values			Result
		(Statistical table)			(Resampling)			
		a=0.1	a=0.05	a=0.01	a=0.1	a=0.05	a=0.01	
M-K	0.894	0.74	0.882	1.159	1.61	1.789	2.415	NS
Data file: Kipkelion MAM Set 2.csv								
	Test statistic	Critical values			Critical values			Result
		(Statistical table)			(Resampling)			
		a=0.1	a=0.05	a=0.01	a=0.1	a=0.05	a=0.01	
M-K	0.537	0.74	0.882	1.159	1.521	1.789	2.236	NS
Data file: Londiani MAM Set 1 cvs.csv								
	Test statistic	Critical values			Critical values			Result
		(Statistical table)			(Resampling)			
		a=0.1	a=0.05	a=0.01	a=0.1	a=0.05	a=0.01	
Mann-Kendall	0	0.822	0.98	1.288	1.557	1.791	2.258	NS
Data file: Londiani MAM Set 2.csv								

	Test statistic	Critical values			Critical values			Result
		(Statistical table)			(Resampling)			
		a=0.1	a=0.05	a=0.01	a=0.1	a=0.05	a=0.01	
M-K	-0.952	1.645	1.96	2.576	1.632	1.972	2.464	NS
Data file: Londiani MAM Set 3.csv								
	Test statistic	Critical values			Critical values			Result
		(Statistical table)			(Resampling)			
		a=0.1	a=0.05	a=0.01	a=0.1	a=0.05	a=0.01	
M-K	-1.038	1.563	1.862	2.447	1.492	1.817	2.368	NS
Add Kericho Met set 3 result								
Data file: Nandi MAM Set 2.csv								
	Test statistic	Critical values			Critical values			Result
		(Statistical table)			(Resampling)			
		a=0.1	a=0.05	a=0.01	a=0.1	a=0.05	a=0.01	
M-K	0.894	0.74	0.882	1.159	1.521	1.789	2.326	NS
Data file: Nandi MAM Set 3.csv								
	Test statistic	Critical values			Critical values			Result
		(Statistical table)			(Resampling)			
		a=0.1	a=0.05	a=0.01	a=0.1	a=0.05	a=0.01	
M-K	0.564	1.645	1.96	2.576	1.607	1.889	2.34	NS
Data file: Timbilil MAM Set 2cvs.csv								
	Test statistic	Critical values			Critical values			Result
		(Statistical table)			(Resampling)			
		a=0.1	a=0.05	a=0.01	a=0.1	a=0.05	a=0.01	
M-K	0	0.74	0.882	1.159	1.521	1.878	2.326	NS
Data file: Timbilil MAM Set 3cvs.csv								
	Test statistic	Critical values			Critical values			Result
		(Statistical table)			(Resampling)			
		a=0.1	a=0.05	a=0.01	a=0.1	a=0.05	a=0.01	
M-K	-0.612	1.645	1.96	2.576	1.632	2.023	2.566	NS
Data file: Timbilil MAM Set 4cvs.csv								
	Test statistic	Critical values			Critical values			Result
		(Statistical table)			(Resampling)			
		a=0.1	a=0.05	a=0.01	a=0.1	a=0.05	a=0.01	
M-K	-0.716	0.74	0.882	1.159	1.521	1.789	2.326	NS
Data file: Tinga MAM Set 2cvs.csv								
	Test statistic	Critical values			Critical values			Result
		(Statistical table)			(Resampling)			
		a=0.1	a=0.05	a=0.01	a=0.1	a=0.05	a=0.01	
Mann-Kendall	1.252	0.74	0.882	1.159	1.521	1.789	2.326	NS
Data file: Tinga MAM Set 3.csv								
	Test statistic	Critical values			Critical values			Result

		(Statistical table)			(Resampling)			
		a=0.1	a=0.05	a=0.01	a=0.1	a=0.05	a=0.01	
M-K	0.631	1.645	1.96	2.576	1.611	1.915	2.522	NS
Data file: Ahero JJA Set 2								
	Test statistic	Critical values			Critical values			Result
		(Statistical table)			(Resampling)			
		a=0.1	a=0.05	a=0.01	a=0.1	a=0.05	a=0.01	
M-K	-1.147	0.658	0.784	1.03	1.564	1.877	2.398	NS
Data file: Ahero JJA Set 4 cvs.csv								
	Test statistic	Critical values			Critical values			Result
		(Statistical table)			(Resampling)			
		a=0.1	a=0.05	a=0.01	a=0.1	a=0.05	a=0.01	
M-K	-0.537	0.74	0.882	1.159	1.521	1.789	2.236	NS
Data file: Ahero JJA Set 3 cvs.csv								
	Test statistic	Critical values			Critical values			Result
		(Statistical table)			(Resampling)			
		a=0.1	a=0.05	a=0.01	a=0.1	a=0.05	a=0.01	
M-K	0.749	1.645	1.96	2.576	1.695	1.98	2.623	NS
Data file: Chemelil JJA Set 3 cvs.csv								
	Test statistic	Critical values			Critical values			Result
		(Statistical table)			(Resampling)			
		a=0.1	a=0.05	a=0.01	a=0.1	a=0.05	a=0.01	
M-K	-0.924	1.645	1.96	2.576	1.638	1.978	2.676	NS
Data file: Chemelil JJA Set 4 cvs.csv								
	Test statistic	Critical values			Critical values			Result
		(Statistical table)			(Resampling)			
		a=0.1	a=0.05	a=0.01	a=0.1	a=0.05	a=0.01	
M-K	-1.431	0.74	0.882	1.159	1.431	1.789	2.326	S (0.1)
Data file: Finlay JJA Set 1 cvs.csv								
	Test statistic	Critical values			Critical values			Result
		(Statistical table)			(Resampling)			
		a=0.1	a=0.05	a=0.01	a=0.1	a=0.05	a=0.01	
M-K	0.952	1.645	1.96	2.576	1.666	1.938	2.481	NS
Data file: Finlay JJA Set 2 cvs.csv								
	Test statistic	Critical values			Critical values			Result
		(Statistical table)			(Resampling)			
		a=0.1	a=0.05	a=0.01	a=0.1	a=0.05	a=0.01	
M-K	0	1.645	1.96	2.576	1.598	1.938	2.515	NS
Data file: Finlay JJA Set 3 cvs.csv								

	Test statistic	Critical values			Critical values			Result
		(Statistical table)			(Resampling)			
		a=0.1	a=0.05	a=0.01	a=0.1	a=0.05	a=0.01	
M-K	-1.8	1.645	1.96	2.576	1.638	1.978	2.611	S (0.1)
Data file: Finlay JJA Set 4cvs.csv								
	Test statistic	Critical values			Critical values			Result
		(Statistical table)			(Resampling)			
		a=0.1	a=0.05	a=0.01	a=0.1	a=0.05	a=0.01	
M-K	-0.671	0.987	1.176	1.546	1.525	1.83	2.318	NS
Data file: Kericho Met JJA set 3 cvs.csv								
	Test statistic	Critical values			Critical values			Result
		(Statistical table)			(Resampling)			
		a=0.1	a=0.05	a=0.01	a=0.1	a=0.05	a=0.01	
M-K	-1.373	1.645	1.96	2.576	1.664	1.954	2.403	NS
Data file: Kericho Met JJA set 4 cvs.csv								
	Test statistic	Critical values			Critical values			Result
		(Statistical table)			(Resampling)			
		a=0.1	a=0.05	a=0.01	a=0.1	a=0.05	a=0.01	
M-K	-0.547	1.069	1.274	1.674	1.478	1.807	2.299	NS
Data file: Kericho water JJA set 1.csv								
	Test statistic	Critical values			Critical values			Result
		(Statistical table)			(Resampling)			
		a=0.1	a=0.05	a=0.01	a=0.1	a=0.05	a=0.01	
M-K	1.431	0.74	0.882	1.159	1.521	1.878	2.683	NS
Data file: Kericho water JJA set 2 cvs.csv								
	Test statistic	Critical values			Critical values			Result
		(Statistical table)			(Resampling)			
		a=0.1	a=0.05	a=0.01	a=0.1	a=0.05	a=0.01	
M-K	-2.906	1.645	1.96	2.576	1.581	1.87	2.413	S (0.01)
Data file: Kericho water JJA set 4 cvs.csv								
	Test statistic	Critical values			Critical values			Result
		(Statistical table)			(Resampling)			
		a=0.1	a=0.05	a=0.01	a=0.1	a=0.05	a=0.01	
M-K	1.252	0.74	0.882	1.159	1.521	1.878	2.326	NS

Data file: Kipkelion JJA Set 2cvs.csv								
	Test statistic	Critical values			Critical values			Result
		(Statistical table)			(Resampling)			
		a=0.1	a=0.05	a=0.01	a=0.1	a=0.05	a=0.01	
M-K	0.716	0.74	0.882	1.159	1.521	1.789	2.326	NS
Data file: Kipkelion JJA Set 3 cvs.csv								
	Test statistic	Critical values			Critical values			Result

		(Statistical table)			(Resampling)			
		a=0.1	a=0.05	a=0.01	a=0.1	a=0.05	a=0.01	
M-K	-0.631	1.645	1.96	2.576	1.611	1.915	2.592	NS
Data file: Londiani JJA Set 1cvs.csv								
	Test statistic	Critical values			Critical values			Result
		(Statistical table)			(Resampling)			
		a=0.1	a=0.05	a=0.01	a=0.1	a=0.05	a=0.01	
M-K	0.894	0.74	0.882	1.159	1.521	1.789	2.236	NS
Data file: Londiani JJA Set 2 cvs.csv								
	Test statistic	Critical values			Critical values			Result
		(Statistical table)			(Resampling)			
		a=0.1	a=0.05	a=0.01	a=0.1	a=0.05	a=0.01	
M-K	-1.088	1.645	1.96	2.576	1.649	1.887	2.447	NS
Data file: Nandi JJA Set 2cvs.csv								
	Test statistic	Critical values			Critical values			Result
		(Statistical table)			(Resampling)			
		a=0.1	a=0.05	a=0.01	a=0.1	a=0.05	a=0.01	
M-K	0.537	0.74	0.882	1.159	1.61	1.878	2.326	NS
Data file: Nandi JJA Set 3cvs.csv: mm								
	Test statistic	Critical values			Critical values			Result
		(Statistical table)			(Resampling)			
		a=0.1	a=0.05	a=0.01	a=0.1	a=0.05	a=0.01	
M-K	-0.451	1.645	1.96	2.576	1.635	1.917	2.453	NS
Data file: Timbilil JJA Set 2cvs.csv								
	Test statistic	Critical values			Critical values			Result
		(Statistical table)			(Resampling)			
		a=0.1	a=0.05	a=0.01	a=0.1	a=0.05	a=0.01	
M-K	1.252	0.74	0.882	1.159	1.521	1.968	2.415	NS
Data file: Timbilil JJA Set 3cvs.csv								
	Test statistic	Critical values			Critical values			Result
		(Statistical table)			(Resampling)			
		a=0.1	a=0.05	a=0.01	a=0.1	a=0.05	a=0.01	
M-K	-1.394	1.645	1.96	2.576	1.615	1.955	2.566	NS
Data file: Timbilil JJA Set 4cvs.csv								
	Test statistic	Critical values			Critical values			Result
		(Statistical table)			(Resampling)			
		a=0.1	a=0.05	a=0.01	a=0.1	a=0.05	a=0.01	
M-K	-1.166	0.905	1.078	1.417	1.509	1.714	2.263	NS
Data file: Tinga JJA Set 2cvs.csv								
	Test statistic	Critical values			Critical values			Result

		(Statistical table)			(Resampling)			
		a=0.1	a=0.05	a=0.01	a=0.1	a=0.05	a=0.01	
M-K	0.179	0.74	0.882	1.159	1.521	1.878	2.415	NS
Data file: Tinga JJA Set 3 cvs.csv								
	Test statistic	Critical values			Critical values			Result
		(Statistical table)			(Resampling)			
		a=0.1	a=0.05	a=0.01	a=0.1	a=0.05	a=0.01	
M-K	-0.444	1.645	1.96	2.576	1.611	1.962	2.569	NS

Data file: Ahero OND Set 2cvs.csv								
	Test statistic	Critical values			Critical values			Result
		(Statistical table)			(Resampling)			
		a=0.1	a=0.05	a=0.01	a=0.1	a=0.05	a=0.01	
M-K	-0.104	0.658	0.784	1.03	1.46	1.772	2.398	NS
Data file: Ahero OND Set 3cvs.csv								
	Test statistic	Critical values			Critical values			Result
		(Statistical table)			(Resampling)			
		a=0.1	a=0.05	a=0.01	a=0.1	a=0.05	a=0.01	
M-K	1.802	1.645	1.96	2.576	1.615	1.938	2.447	S (0.1)
Data file: Ahero OND Set 4cvs.csv								
	Test statistic	Critical values			Critical values			Result
		(Statistical table)			(Resampling)			
		a=0.1	a=0.05	a=0.01	a=0.1	a=0.05	a=0.01	
M-K	0.358	0.74	0.882	1.159	1.431	1.699	2.236	NS
Data file: Chemelil OND set 3cvs.csv								
	Test statistic	Critical values			Critical values			Result
		(Statistical table)			(Resampling)			
		a=0.1	a=0.05	a=0.01	a=0.1	a=0.05	a=0.01	
M-K	-0.016	1.645	1.96	2.576	1.589	1.849	2.546	NS
Data file: Chemelil OND Set 4cvs.csv								
	Test statistic	Critical values			Critical values			Result
		(Statistical table)			(Resampling)			
		a=0.1	a=0.05	a=0.01	a=0.1	a=0.05	a=0.01	
M-K	0.313	0.658	0.784	1.03	1.46	1.772	2.294	NS
Data file: Finlay OND Set 1cvs.csv								
	Test statistic	Critical values			Critical values			Result
		(Statistical table)			(Resampling)			
		a=0.1	a=0.05	a=0.01	a=0.1	a=0.05	a=0.01	
M-K	0.068	1.645	1.96	2.576	1.581	1.904	2.6	NS
Data file: Finlay OND Set 2cvs.csv: mm								
	Test statistic	Critical values			Critical values			Result
		(Statistical table)			(Resampling)			

		a=0.1	a=0.05	a=0.01	a=0.1	a=0.05	a=0.01	
M-K	0	0.74	0.882	1.159	1.521	1.789	2.326	NS

Data file: Kericho water OND Set 4cvs.csv: mm								
	Test statistic	Critical values			Critical values			Result
		(Statistical table)			(Resampling)			
		a=0.1	a=0.05	a=0.01	a=0.1	a=0.05	a=0.01	
M-K	-0.358	0.74	0.882	1.159	1.521	1.878	2.326	NS
Data file: Kipkelion OND Set 2cvs.csv: mm								
	Test statistic	Critical values			Critical values			Result
		(Statistical table)			(Resampling)			
		a=0.1	a=0.05	a=0.01	a=0.1	a=0.05	a=0.01	
M-K	-0.179	0.74	0.882	1.159	1.521	1.878	2.236	NS
Data file: Kipkelion OND Set 3cvs.csv: mm								
	Test statistic	Critical values			Critical values			Result
		(Statistical table)			(Resampling)			
		a=0.1	a=0.05	a=0.01	a=0.1	a=0.05	a=0.01	
M-K	-1.051	1.645	1.96	2.576	1.611	1.962	2.756	NS
Data file: Londiani OND Set 1cvs.csv: mm								
	Test statistic	Critical values			Critical values			Result
		(Statistical table)			(Resampling)			
		a=0.1	a=0.05	a=0.01	a=0.1	a=0.05	a=0.01	
M-K	-0.716	0.74	0.882	1.159	1.431	1.699	2.236	NS
Data file: Londiani OND Set 2cvs.csv: mm								
	Test statistic	Critical values			Critical values			Result
		(Statistical table)			(Resampling)			
		a=0.1	a=0.05	a=0.01	a=0.1	a=0.05	a=0.01	
M-K	1.7	1.645	1.96	2.576	1.581	1.87	2.566	S (0.1)
Data file: Londiani OND Set 3cvs.csv: mm								
	Test statistic	Critical values			Critical values			Result
		(Statistical table)			(Resampling)			
		a=0.1	a=0.05	a=0.01	a=0.1	a=0.05	a=0.01	
Mann-Kendall	-1.006	1.563	1.862	2.447	1.622	1.947	2.531	NS
Data file: Nandi OND Set 2cvs.csv: mm								
	Test statistic	Critical values			Critical values			Result
		(Statistical table)			(Resampling)			
		a=0.1	a=0.05	a=0.01	a=0.1	a=0.05	a=0.01	
M-K	0	0.74	0.882	1.159	1.521	1.789	2.326	NS

Data file: Nandi OND Set 3 cvs.csv: mm								
	Test statistic	Critical values			Critical values			Result
		(Statistical table)			(Resampling)			
		a=0.1	a=0.05	a=0.01	a=0.1	a=0.05	a=0.01	
M-K	-1.015	1.645	1.96	2.576	1.635	1.917	2.538	NS
Data file: Tinga OND Set 2 cvs.csv: OND								
	Test statistic	Critical values			Critical values			Result
		(Statistical table)			(Resampling)			
		a=0.1	a=0.05	a=0.01	a=0.1	a=0.05	a=0.01	
M-K	-0.156	0.822	0.98	1.288	1.479	1.791	2.335	NS
Data file: Tinga OND Set 3.csv: mm								

Appendix 6B: M-K Results for split streamflow series

Data file: Ainamotua MAM set 1.csv								
	Test statistic	Critical values			Critical values			Result
		(Statistical table)			(Resampling)			
		a=0.1	a=0.05	a=0.01	a=0.1	a=0.05	a=0.01	
M-K	2.583	1.645	1.96	2.576	1.615	1.938	2.6	S (0.05)
Data file: Ainamotua MAM set 2.csv								
	Test statistic	Critical values			Critical values			Result
		(Statistical table)			(Resampling)			
		a=0.1	a=0.05	a=0.01	a=0.1	a=0.05	a=0.01	
M-K	0.929	1.645	1.96	2.576	1.64	1.995	2.687	NS
Data file: Ainopsiwa MAM set 1.csv								
	Test statistic	Critical values			Critical values			Result
		(Statistical table)			(Resampling)			
		a=0.1	a=0.05	a=0.01	a=0.1	a=0.05	a=0.01	
M-K	-1.241	1.645	1.96	2.576	1.664	1.946	2.34	NS
Data file: Ainopsiwa MAM set 2.csv								
	Test statistic	Critical values			Critical values			Result
		(Statistical table)			(Resampling)			
		a=0.1	a=0.05	a=0.01	a=0.1	a=0.05	a=0.01	
M-K	2.877	1.645	1.96	2.576	1.73	2.064	2.543	S (0.01)
Data file: Masaita MAM set 1.csv								
	Test statistic	Critical values			Critical values			Result
		(Statistical table)			(Resampling)			
		a=0.1	a=0.05	a=0.01	a=0.1	a=0.05	a=0.01	
M-K	0.682	1.398	1.666	2.19	1.591	1.856	2.576	NS
Data file: Masaita MAM set 2.csv								
	Test statistic	Critical values			Critical values			Result
		(Statistical table)			(Resampling)			
		a=0.1	a=0.05	a=0.01	a=0.1	a=0.05	a=0.01	
M-K	-0.807	1.645	1.96	2.576	1.613	1.876	2.551	NS
Data file: Mbogo MAM set 1.csv								
	Test statistic	Critical values			Critical values			Result
		(Statistical table)			(Resampling)			
		a=0.1	a=0.05	a=0.01	a=0.1	a=0.05	a=0.01	
M-K	3.892	1.645	1.96	2.576	1.581	1.836	2.515	S (0.01)
Data file: Mbogo MAM set 2.csv								
	Test statistic	Critical values			Critical values			Result
		(Statistical table)			(Resampling)			
		a=0.1	a=0.05	a=0.01	a=0.1	a=0.05	a=0.01	

M-K	1.073	0.74	0.882	1.159	1.521	1.699	2.415	NS
Data file: Nyando Kericho MAM set 1.csv								
	Test statistic	Critical values			Critical values			Result
		(Statistical table)			(Resampling)			
		a=0.1	a=0.05	a=0.01	a=0.1	a=0.05	a=0.01	
M-K	0.693	1.152	1.372	1.803	1.534	1.831	2.375	NS
Data file: Nyando Kericho MAM set 2.csv								
	Test statistic	Critical values			Critical values			Result
		(Statistical table)			(Resampling)			
		a=0.1	a=0.05	a=0.01	a=0.1	a=0.05	a=0.01	
M-K	1.508	1.645	1.96	2.576	1.622	1.93	2.416	NS
Data file: Nyando Kisumu MAM set 1.csv								
	Test statistic	Critical values			Critical values			Result
		(Statistical table)			(Resampling)			
		a=0.1	a=0.05	a=0.01	a=0.1	a=0.05	a=0.01	
M-K	0.28	1.481	1.764	2.318	1.539	1.854	2.519	NS
Data file: Nyando Kisumu MAM set 2.csv								
	Test statistic	Critical values			Critical values			Result
		(Statistical table)			(Resampling)			
		a=0.1	a=0.05	a=0.01	a=0.1	a=0.05	a=0.01	
M-K	0.754	0.905	1.078	1.417	1.577	1.851	2.331	NS
Data file: Nyando MAM set 1.csv								
	Test statistic	Critical values			Critical values			Result
		(Statistical table)			(Resampling)			
		a=0.1	a=0.05	a=0.01	a=0.1	a=0.05	a=0.01	
M-K	-1.851	1.645	1.96	2.576	1.565	1.829	2.689	S (0.05)
Data file: Nyando MAM set 2.csv								
	Test statistic	Critical values			Critical values			Result
		(Statistical table)			(Resampling)			
		a=0.1	a=0.05	a=0.01	a=0.1	a=0.05	a=0.01	
M-K	0.109	1.069	1.274	1.674	1.642	1.861	2.354	NS
Data file: Tugenon MAM set 1.csv								
	Test statistic	Critical values			Critical values			Result
		(Statistical table)			(Resampling)			
		a=0.1	a=0.05	a=0.01	a=0.1	a=0.05	a=0.01	
M-K	0.169	1.645	1.96	2.576	1.635	2.03	2.566	NS
Data file: Tugenon MAM set 2.csv: mam								
	Test statistic	Critical values			Critical values			Result

		(Statistical table)			(Resampling)			
		a=0.1	a=0.05	a=0.01	a=0.1	a=0.05	a=0.01	
M-K	-0.606	1.645	1.96	2.576	1.619	1.922	2.447	NS
Data file: AINAMOTUA MAM CVS Complete Series								
	Test statistic	Critical values			Critical values			Result
		(Statistical table)			(Resampling)			
		a=0.1	a=0.05	a=0.01	a=0.1	a=0.05	a=0.01	
M-K	5.284	1.645	1.96	2.576	1.602	1.844	2.335	S (0.01)
Data file: AINOPSIWA MAM CVS.csv								
	Test statistic	Critical values			Critical values			Result
		(Statistical table)			(Resampling)			
		a=0.1	a=0.05	a=0.01	a=0.1	a=0.05	a=0.01	
M-K	4.663	1.645	1.96	2.576	1.664	1.991	2.534	S (0.01)
Data file: MASAITA MAM CVS.csv								
	Test statistic	Critical values			Critical values			Result
		(Statistical table)			(Resampling)			
		a=0.1	a=0.05	a=0.01	a=0.1	a=0.05	a=0.01	
M-K	-3.008	1.645	1.96	2.576	1.632	1.871	2.485	S (0.01)
Data file: MBOGO MAM CVS.csv								
	Test statistic	Critical values			Critical values			Result
		(Statistical table)			(Resampling)			
		a=0.1	a=0.05	a=0.01	a=0.1	a=0.05	a=0.01	
M-K	5.258	1.645	1.96	2.576	1.648	1.936	2.433	S (0.01)
Data file: NYANDO KERICHO MAM CVS.csv								
	Test statistic	Critical values			Critical values			Result
		(Statistical table)			(Resampling)			
		a=0.1	a=0.05	a=0.01	a=0.1	a=0.05	a=0.01	
M-K	2.494	1.645	1.96	2.576	1.697	2.082	2.769	S (0.05)
Data file: Ainamotua JJA set 1.csv								
	Test statistic	Critical values			Critical values			Result
		(Statistical table)			(Resampling)			
		a=0.1	a=0.05	a=0.01	a=0.1	a=0.05	a=0.01	
M-K	3.433	1.645	1.96	2.576	1.683	1.955	2.668	S (0.01)
Data file: Ainamotua JJA set 2.csv								
	Test statistic	Critical values			Critical values			Result
		(Statistical table)			(Resampling)			
		a=0.1	a=0.05	a=0.01	a=0.1	a=0.05	a=0.01	
M-K	1.877	1.645	1.96	2.576	1.561	1.936	2.667	S (0.1)
Data file: Ainopsiwa JJA set 1.csv								
	Test statistic	Critical values			Critical values			Result

		(Statistical table)			(Resampling)			
		a=0.1	a=0.05	a=0.01	a=0.1	a=0.05	a=0.01	
M-K	0.902	1.645	1.96	2.576	1.579	1.889	2.397	NS
Data file: Ainopsiwa JJA set 2.csv								
	Test statistic	Critical values			Critical values			Result
		(Statistical table)			(Resampling)			
		a=0.1	a=0.05	a=0.01	a=0.1	a=0.05	a=0.01	
M-K	3.586	1.645	1.96	2.576	1.584	1.876	2.439	S (0.01)
Data file: Masaita JJA set 1.csv								
	Test statistic	Critical values			Critical values			Result
		(Statistical table)			(Resampling)			
		a=0.1	a=0.05	a=0.01	a=0.1	a=0.05	a=0.01	
M-K	0	1.398	1.666	2.19	1.629	1.894	2.538	NS
Data file: Masaita JJA set 2.csv								
	Test statistic	Critical values			Critical values			Result
		(Statistical table)			(Resampling)			

		a=0.1	a=0.05	a=0.01	a=0.1	a=0.05	a=0.01	
M-K	0.319	1.645	1.96	2.576	1.632	2.026	2.664	NS
Data file: Mbogo JJA set 1.csv								
	Test statistic	Critical values			Critical values			Result
		(Statistical table)			(Resampling)			
		a=0.1	a=0.05	a=0.01	a=0.1	a=0.05	a=0.01	
M-K	5.167	1.645	1.96	2.576	1.615	1.87	2.515	S (0.01)
Data file: Mbogo JJA set 2.csv								
	Test statistic	Critical values			Critical values			Result
		(Statistical table)			(Resampling)			
		a=0.1	a=0.05	a=0.01	a=0.1	a=0.05	a=0.01	
M-K	2.326	0.74	0.882	1.159	1.61	1.878	2.326	S (0.05)
Data file: Nyando JJA set 1.csv								
	Test statistic	Critical values			Critical values			Result
		(Statistical table)			(Resampling)			
		a=0.1	a=0.05	a=0.01	a=0.1	a=0.05	a=0.01	
M-K	-1.322	1.645	1.96	2.576	1.609	1.874	2.469	NS

Data file: Nyando JJA set 2.csv								
	Test statistic	Critical values			Critical values			Result
		(Statistical table)			(Resampling)			
		a=0.1	a=0.05	a=0.01	a=0.1	a=0.05	a=0.01	
M-K	1.752	1.069	1.274	1.674	1.533	1.861	2.573	S (0.1)
Data file: Nyando Kericho JJA set 1.csv								
	Test statistic	Critical values			Critical values			Result
		(Statistical table)			(Resampling)			
		a=0.1	a=0.05	a=0.01	a=0.1	a=0.05	a=0.01	
M-K	1.287	1.152	1.372	1.803	1.584	1.881	2.425	NS
Data file: Nyando Kericho JJA set 2.csv								
	Test statistic	Critical values			Critical values			Result
		(Statistical table)			(Resampling)			
		a=0.1	a=0.05	a=0.01	a=0.1	a=0.05	a=0.01	
M-K	0.47	1.645	1.96	2.576	1.67	1.995	2.659	NS
Data file: Nyando Kisumu JJA set 1.csv								
	Test statistic	Critical values			Critical values			Result
		(Statistical table)			(Resampling)			
		a=0.1	a=0.05	a=0.01	a=0.1	a=0.05	a=0.01	
M-K	0.14	1.481	1.764	2.318	1.679	1.959	2.554	NS

Data file: Tugenon JJA set 1.csv								
	Test statistic	Critical values			Critical values			Result
		(Statistical table)			(Resampling)			
		a=0.1	a=0.05	a=0.01	a=0.1	a=0.05	a=0.01	
M-K	-0.113	1.645	1.96	2.576	1.607	1.889	2.425	NS
Data file: Tugenon JJA set 2.csv								
	Test statistic	Critical values			Critical values			Result
		(Statistical table)			(Resampling)			
		a=0.1	a=0.05	a=0.01	a=0.1	a=0.05	a=0.01	
M-K	-0.076	1.398	1.666	2.19	1.591	1.856	2.538	NS
Data file: AINAMOTUA JJA CVS.csv Complete series								

	Test statistic	Critical values			Critical values			Result
		(Statistical table)			(Resampling)			
		a=0.1	a=0.05	a=0.01	a=0.1	a=0.05	a=0.01	
M-K	6.605	1.645	1.96	2.576	1.589	1.877	2.681	S (0.01)
Data file: AINOPSIWA JJA CVS.csv								
	Test statistic	Critical values			Critical values			Result
		(Statistical table)			(Resampling)			
		a=0.1	a=0.05	a=0.01	a=0.1	a=0.05	a=0.01	
M-K	5.56	1.645	1.96	2.576	1.681	2.026	2.732	S (0.01)
Data file: MASAITA JJA CVS.csv								
	Test statistic	Critical values			Critical values			Result
		(Statistical table)			(Resampling)			
		a=0.1	a=0.05	a=0.01	a=0.1	a=0.05	a=0.01	
M-K	-2.824	1.645	1.96	2.576	1.687	2.027	2.577	S (0.01)
Data file: MBOGO JJA CVS.csv								
	Test statistic	Critical values			Critical values			Result
		(Statistical table)			(Resampling)			
		a=0.1	a=0.05	a=0.01	a=0.1	a=0.05	a=0.01	
M-K	6.422	1.645	1.96	2.576	1.622	1.91	2.472	S (0.01)
Data file: NYANDO JJA CVS.csv								
	Test statistic	Critical values			Critical values			Result
		(Statistical table)			(Resampling)			
		a=0.1	a=0.05	a=0.01	a=0.1	a=0.05	a=0.01	
M-K	-1.666	1.645	1.96	2.576	1.643	1.992	2.633	S (0.1)
Data file: NYANDO KERICHO JJA CVS.csv								
	Test statistic	Critical values			Critical values			Result
		(Statistical table)			(Resampling)			
		a=0.1	a=0.05	a=0.01	a=0.1	a=0.05	a=0.01	
M-K	1.064	1.645	1.96	2.576	1.614	1.862	2.614	NS
Data file: NYANDO KSM JJA CVS.csv								
	Test statistic	Critical values			Critical values			Result
		(Statistical table)			(Resampling)			
		a=0.1	a=0.05	a=0.01	a=0.1	a=0.05	a=0.01	
M-K	-0.306	1.645	1.96	2.576	1.649	1.887	2.532	NS
Data file: TUGENON JJA CVS.csv								
	Test statistic	Critical values			Critical values			Result
		(Statistical table)			(Resampling)			
		a=0.1	a=0.05	a=0.01	a=0.1	a=0.05	a=0.01	

M-K	0.384	1.645	1.96	2.576	1.678	2.109	2.61	NS
Data file: Ainamotua OND set 1.csv								
	Test statistic	Critical values			Critical values			Result
		(Statistical table)			(Resampling)			
		a=0.1	a=0.05	a=0.01	a=0.1	a=0.05	a=0.01	
M-K	2.21	1.645	1.96	2.576	1.615	1.938	2.549	S (0.05)
Data file: Ainamotua OND set 2.csv								
	Test statistic	Critical values			Critical values			Result
		(Statistical table)			(Resampling)			
		a=0.1	a=0.05	a=0.01	a=0.1	a=0.05	a=0.01	
M-K	2.667	1.645	1.96	2.576	1.581	1.916	2.45	S (0.01)
Data file: Ainopsiwa OND set 1.csv								
	Test statistic	Critical values			Critical values			Result
		(Statistical table)			(Resampling)			
		a=0.1	a=0.05	a=0.01	a=0.1	a=0.05	a=0.01	
M-K	-0.395	1.645	1.96	2.576	1.664	1.917	2.538	NS
Data file: Ainopsiwa OND set 2.csv								
	Test statistic	Critical values			Critical values			Result
		(Statistical table)			(Resampling)			
		a=0.1	a=0.05	a=0.01	a=0.1	a=0.05	a=0.01	
M-K	3.294	1.645	1.96	2.576	1.668	1.918	2.606	S (0.01)
Data file: Masaita OND set 1.csv								
	Test statistic	Critical values			Critical values			Result
		(Statistical table)			(Resampling)			
		a=0.1	a=0.05	a=0.01	a=0.1	a=0.05	a=0.01	
M-K	1.212	1.398	1.666	2.19	1.629	2.008	2.765	NS
Data file: Masaita OND set 2.csv								
	Test statistic	Critical values			Critical values			Result
		(Statistical table)			(Resampling)			
		a=0.1	a=0.05	a=0.01	a=0.1	a=0.05	a=0.01	
M-K	0.506	1.645	1.96	2.576	1.632	1.951	2.551	NS
Data file: Mbogo OND set 1.csv								
	Test statistic	Critical values			Critical values			Result
		(Statistical table)			(Resampling)			
		a=0.1	a=0.05	a=0.01	a=0.1	a=0.05	a=0.01	
M-K	3.637	1.645	1.96	2.576	1.547	1.853	2.464	S (0.01)
Data file: Mbogo OND set 2.csv								
	Test statistic	Critical values			Critical values			Result
		(Statistical table)			(Resampling)			

		a=0.1	a=0.05	a=0.01	a=0.1	a=0.05	a=0.01	
M-K	1.61	0.74	0.882	1.159	1.521	1.878	2.326	S (0.1)
Data file: Nyando Kericho OND set 1.csv								
	Test statistic	Critical values			Critical values			Result
		(Statistical table)			(Resampling)			
		a=0.1	a=0.05	a=0.01	a=0.1	a=0.05	a=0.01	
M-K	0.099	1.152	1.372	1.803	1.534	1.782	2.326	NS
Data file: Nyando Ksm OND set 1.csv								
	Test statistic	Critical values			Critical values			Result
		(Statistical table)			(Resampling)			
		a=0.1	a=0.05	a=0.01	a=0.1	a=0.05	a=0.01	
M-K	0.35	1.481	1.764	2.318	1.574	1.854	2.414	NS
Data file: Nyando Ksm OND set 2.csv								
	Test statistic	Critical values			Critical values			Result
		(Statistical table)			(Resampling)			
		a=0.1	a=0.05	a=0.01	a=0.1	a=0.05	a=0.01	
M-K	0.754	0.905	1.078	1.417	1.509	1.851	2.4	NS
Data file: Nyando OND set 1.csv								
	Test statistic	Critical values			Critical values			Result
		(Statistical table)			(Resampling)			
		a=0.1	a=0.05	a=0.01	a=0.1	a=0.05	a=0.01	
M-K	-1.014	1.645	1.96	2.576	1.609	1.962	2.601	NS
Data file: Nyando OND set 2.csv								
	Test statistic	Critical values			Critical values			Result
		(Statistical table)			(Resampling)			
		a=0.1	a=0.05	a=0.01	a=0.1	a=0.05	a=0.01	
M-K	-0.438	1.069	1.274	1.674	1.588	1.861	2.245	NS
Data file: Tugenon OND set 1.csv								
	Test statistic	Critical values			Critical values			Result
		(Statistical table)			(Resampling)			
		a=0.1	a=0.05	a=0.01	a=0.1	a=0.05	a=0.01	

Appendix 7A: Wavelet trend results for rainfall

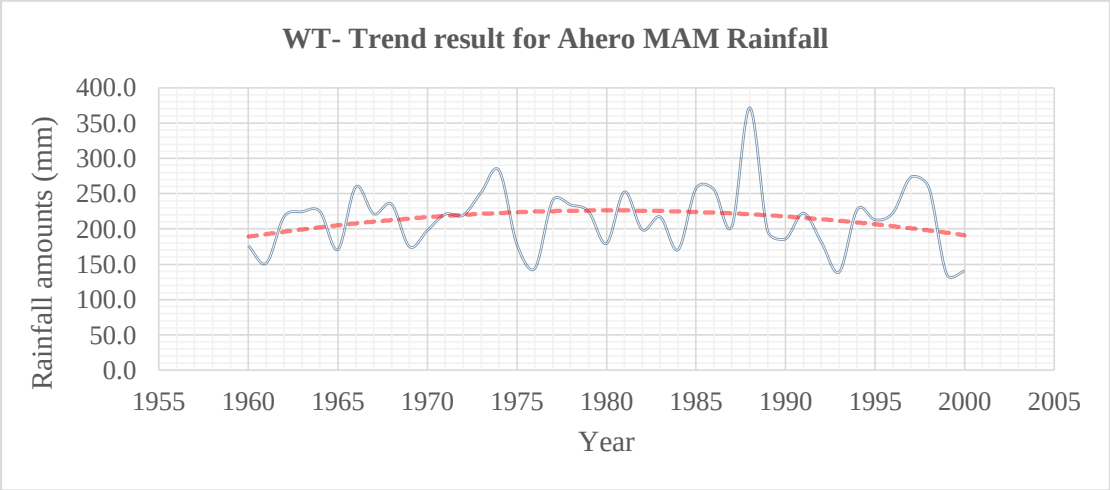

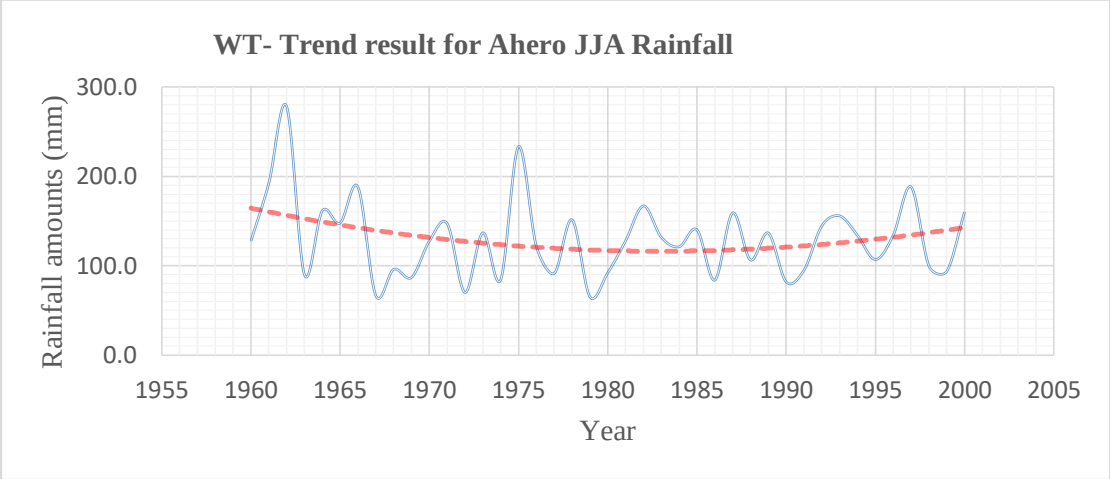

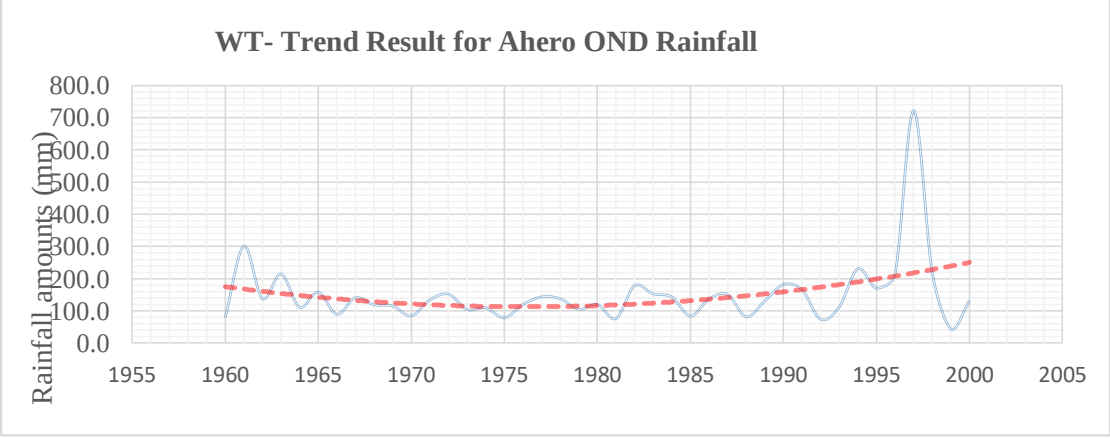

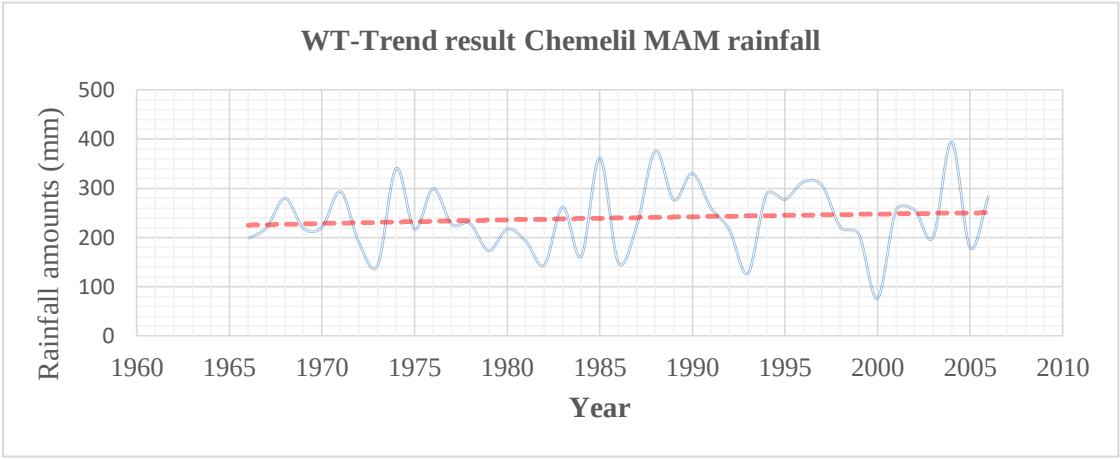
WT-Trend result Chemelil MAM rainfall
Rainfall amounts (mm)
500
400
300
200
100
0
1960
1965
1970
1975
1980
1985
1990
1995
2000
2005
2010
Year

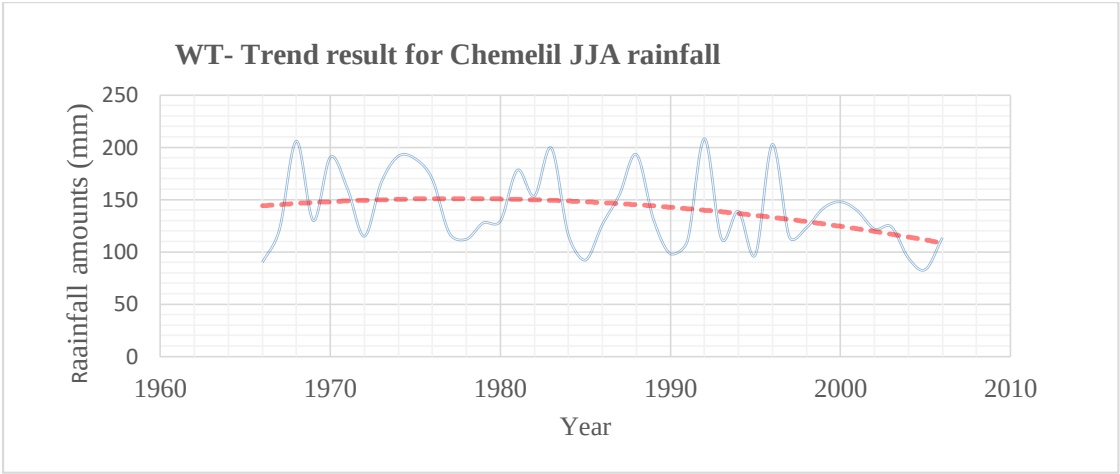
WT- Trend result for Chemelil JJA rainfall
Raainfall amounts (mm)
250
200
150
100
50
0
1960
1970
1980
1990
2000
2010
Year

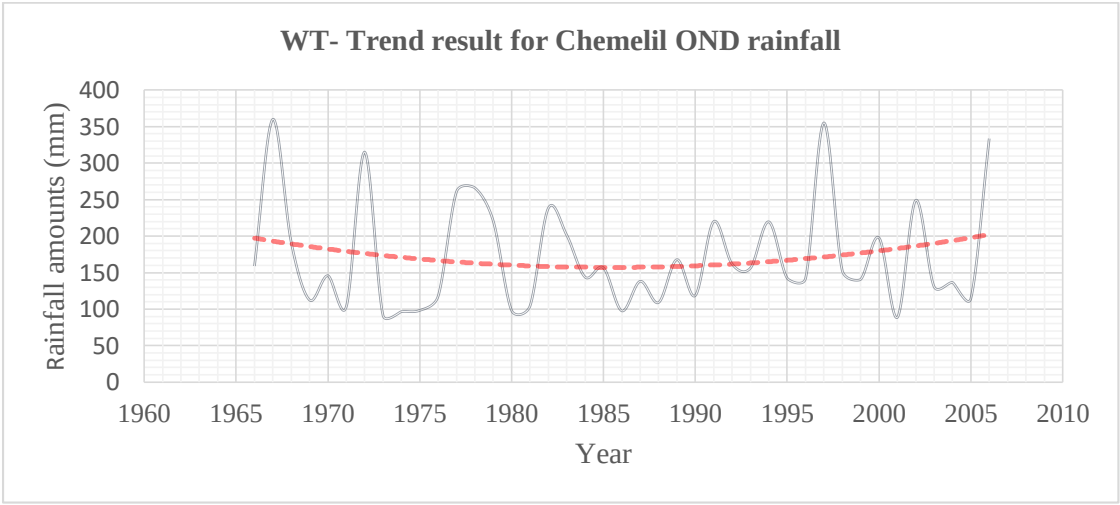
WT- Trend result for Chemelil OND rainfall
Rainfall amounts (mm)
400
350
300
250
200
150
100
50
0
1960
1965
1970
1975
1980
1985
1990
1995
2000
2005
2010
Year

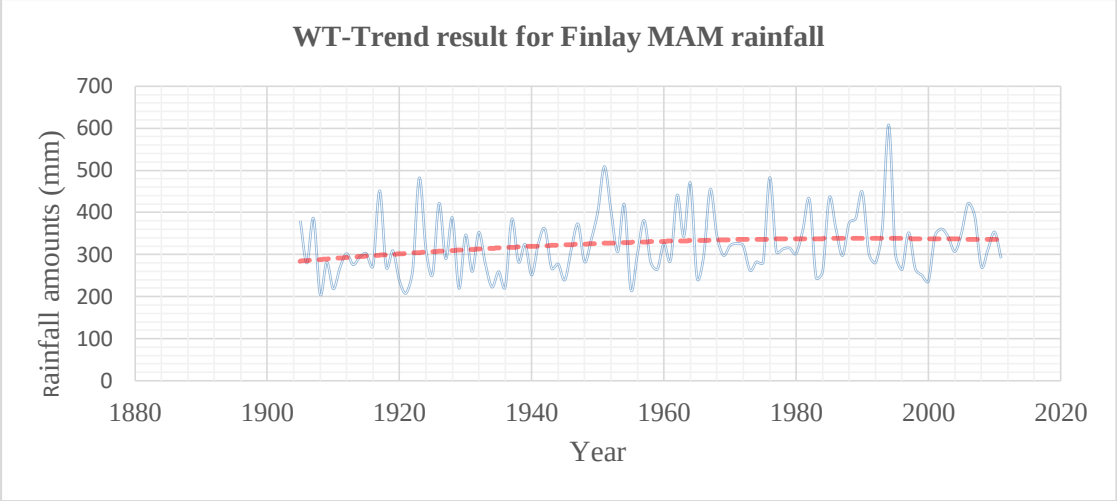
WT-Trend result for Finlay MAM rainfall
Rainfall amounts (mm)
700
600
500
400
300
200
100
0
1880
1900
1920
1940
1960
1980
2000
2020
Year

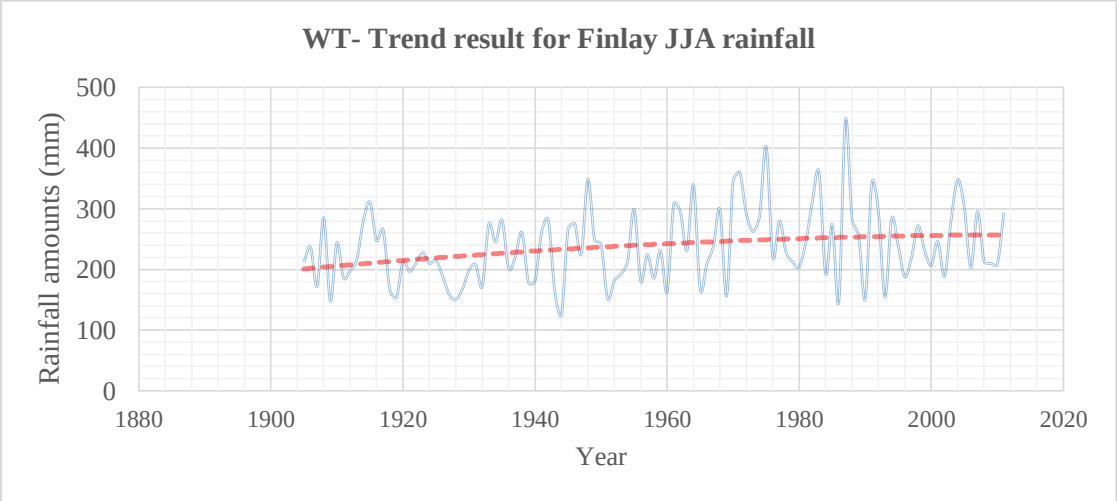
WT- Trend result for Finlay JJA rainfall
Rainfall amounts (mm)
500
400
300
200
100
0
1880
1900
1920
1940
1960
1980
2000
2020
Year

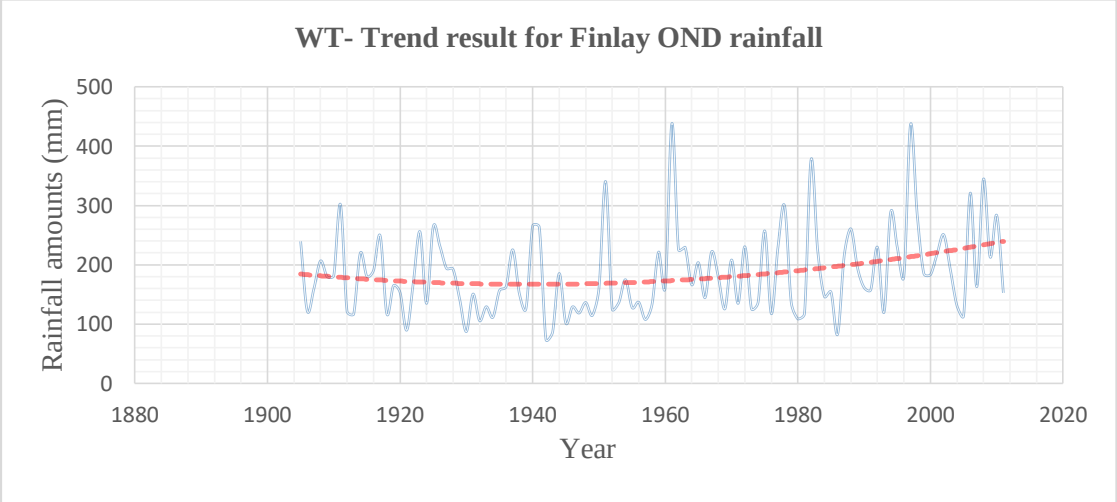
WT- Trend result for Finlay OND rainfall
Rainfall amounts (mm)
500
400
300
200
100
0
1880
1900
1920
1940
1960
1980
2000
2020
Year

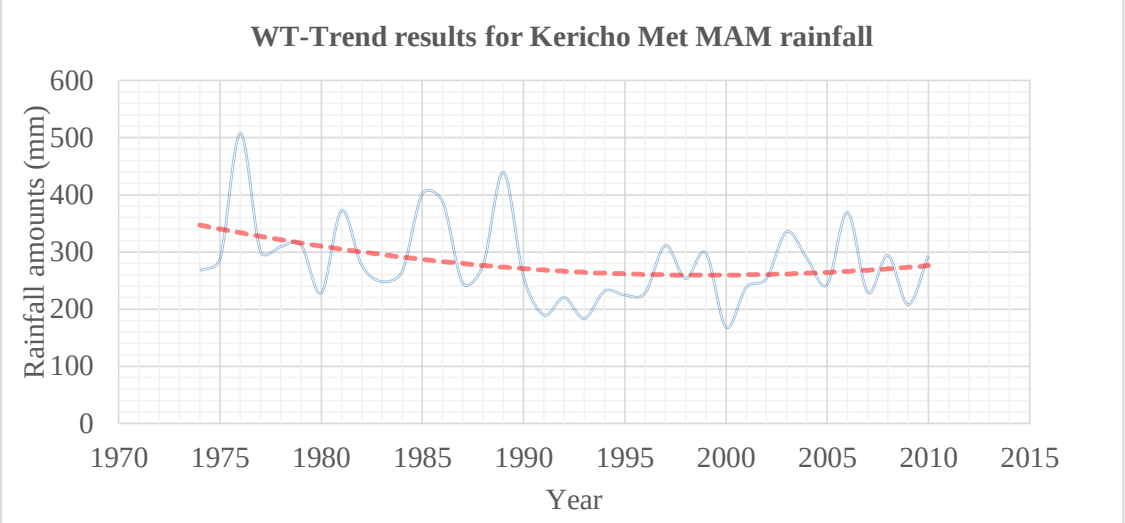
WT-Trend results for Kericho Met MAM rainfall
Rainfall amounts (mm)
600
500
400
300
200
100
0
1970
1975
1980
1985
1990
1995
2000
2005
2010
2015
Year

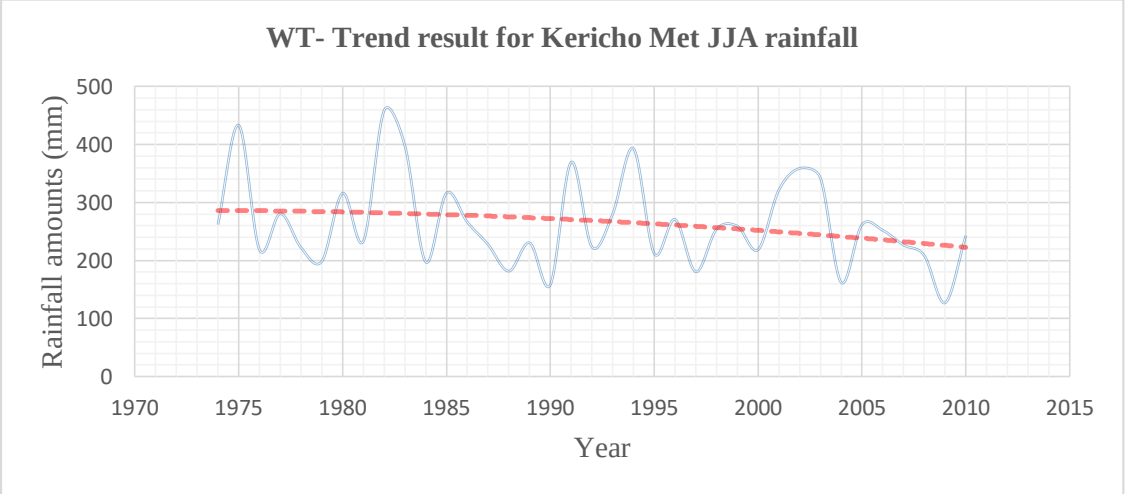
WT- Trend result for Kericho Met JJA rainfall
Rainfall amounts (mm)
500
400
300
200
100
0
1970
1975
1980
1985
1990
1995
2000
2005
2010
2015
Year

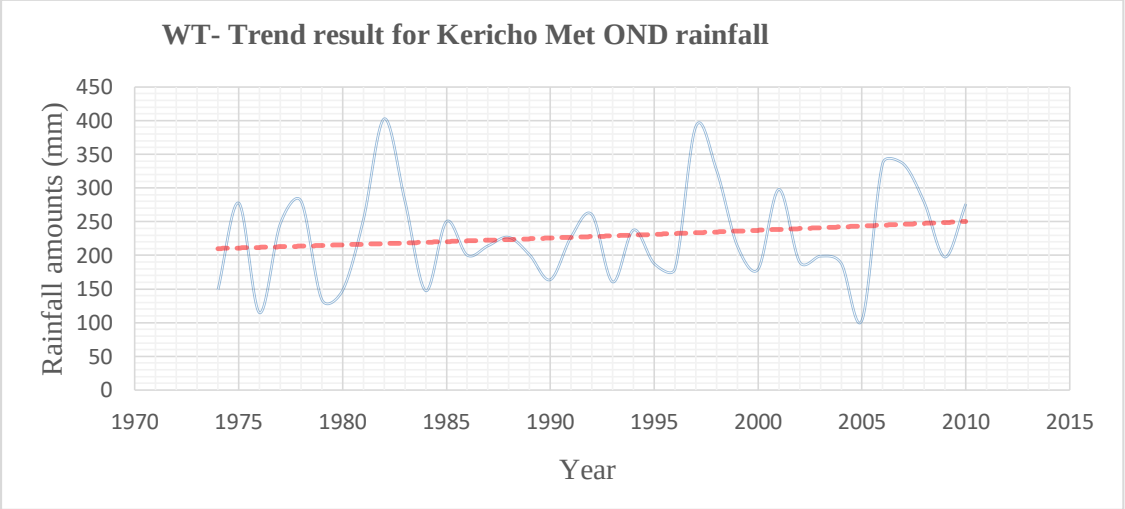
WT- Trend result for Kericho Met OND rainfall
Rainfall amounts (mm)
450
400
350
300
250
200
150
100
50
0
1970
1975
1980
1985
1990
1995
2000
2005
2010
2015
Year

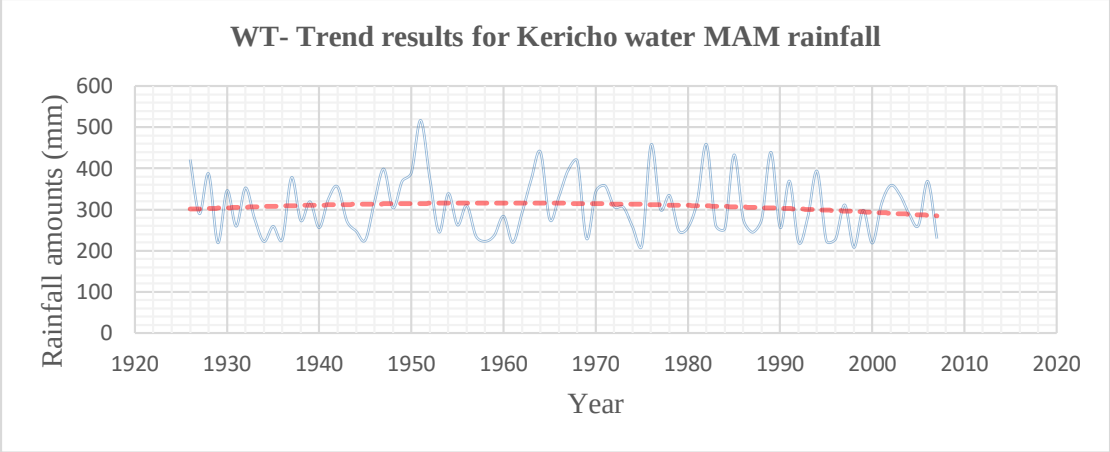
WT- Trend results for Kericho water MAM rainfall
Rainfall amounts (mm)
600
500
400
300
200
100
0
1920
1930
1940
1950
1960
1970
1980
1990
2000
2010
2020
Year

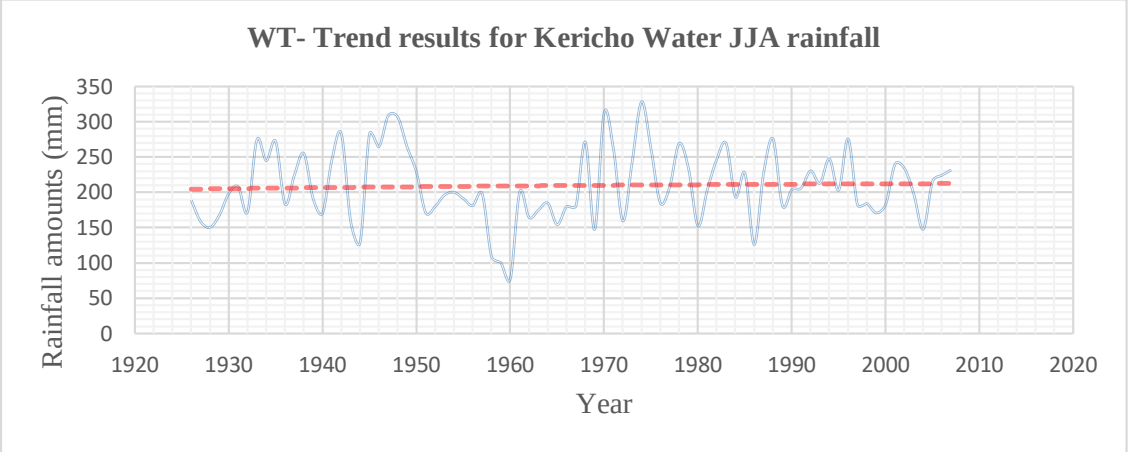
WT- Trend results for Kericho Water JJA rainfall
Rainfall amounts (mm)
350
300
250
200
150
100
50
0
1920
1930
1940
1950
1960
1970
1980
1990
2000
2010
2020
Year

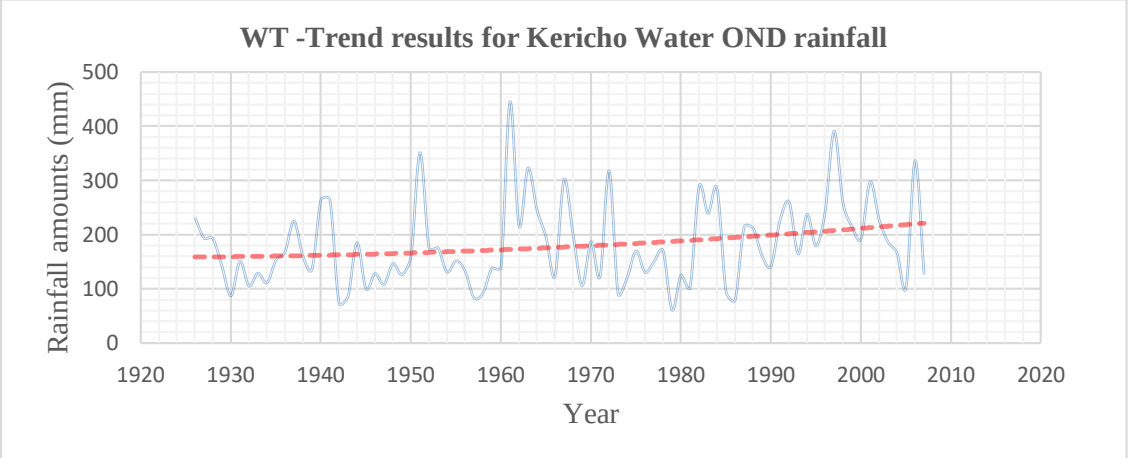
WT -Trend results for Kericho Water OND rainfall
Rainfall amounts (mm)
500
400
300
200
100
0
1920
1930
1940
1950
1960
1970
1980
1990
2000
2010
2020
Year

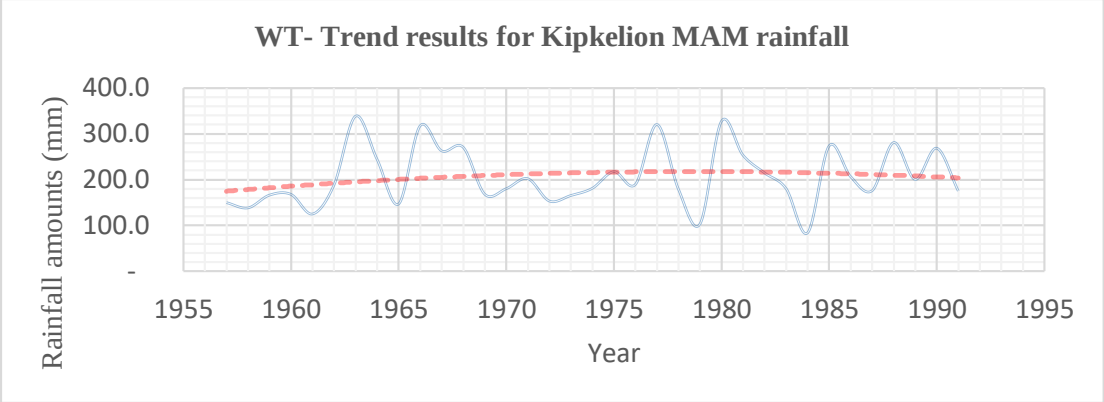
WT- Trend results for Kipkelion MAM rainfall
Rainfall amounts (mm)
400.0
300.0
200.0
100.0
-
1955
1960
1965
1970
1975
1980
1985
1990
1995
Year

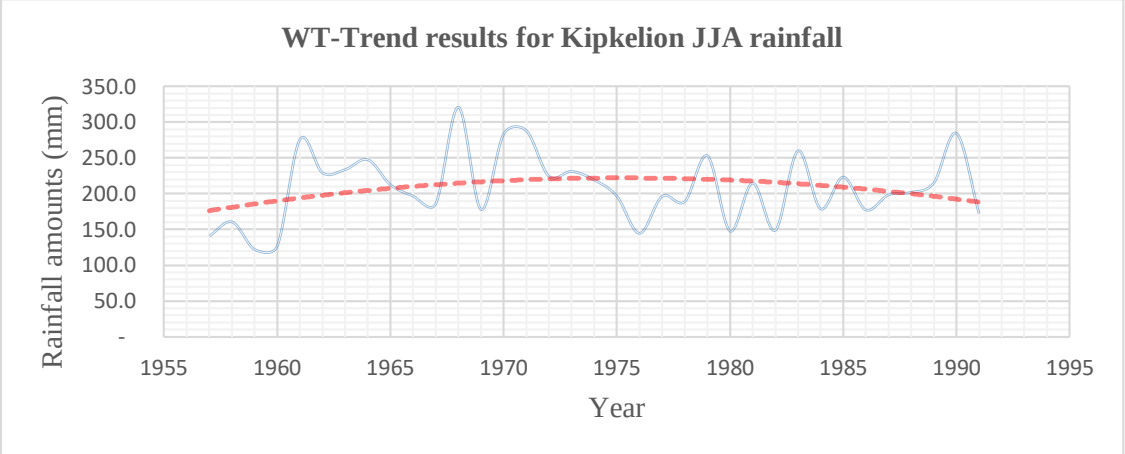
WT-Trend results for Kipkelion JJA rainfall
Rainfall amounts (mm)
350.0
300.0
250.0
200.0
150.0
100.0
50.0
-
1955
1960
1965
1970
1975
1980
1985
1990
1995
Year

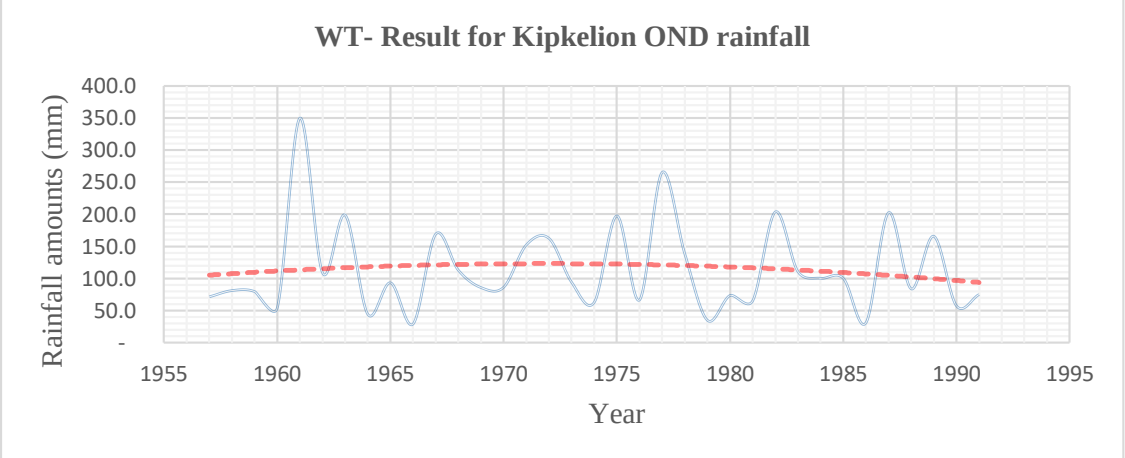
WT- Result for Kipkelion OND rainfall
Rainfall amounts (mm)
400.0
350.0
300.0
250.0
200.0
150.0
100.0
50.0
-
1955
1960
1965
1970
1975
1980
1985
1990
1995
Year

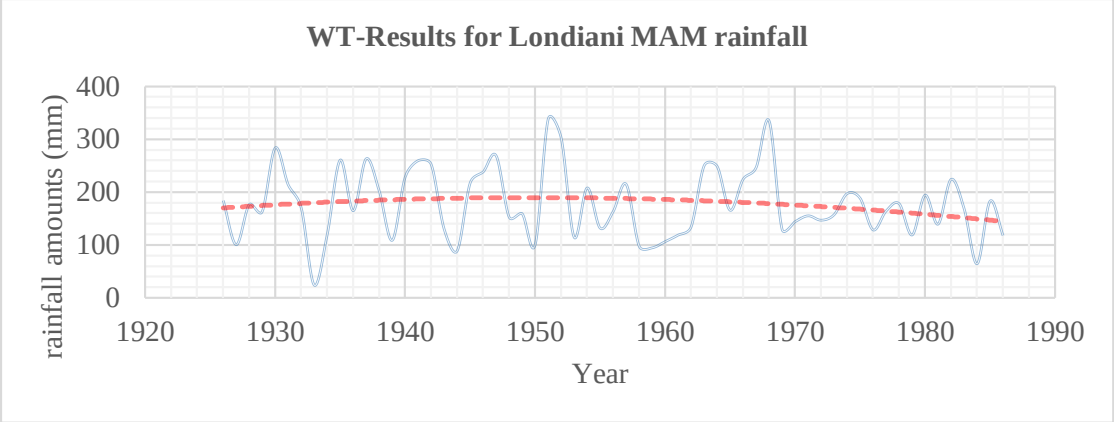
WT-Results for Londiani MAM rainfall
rainfall amounts (mm)
400
300
200
100
0
1920
1930
1940
1950
1960
1970
1980
1990
Year

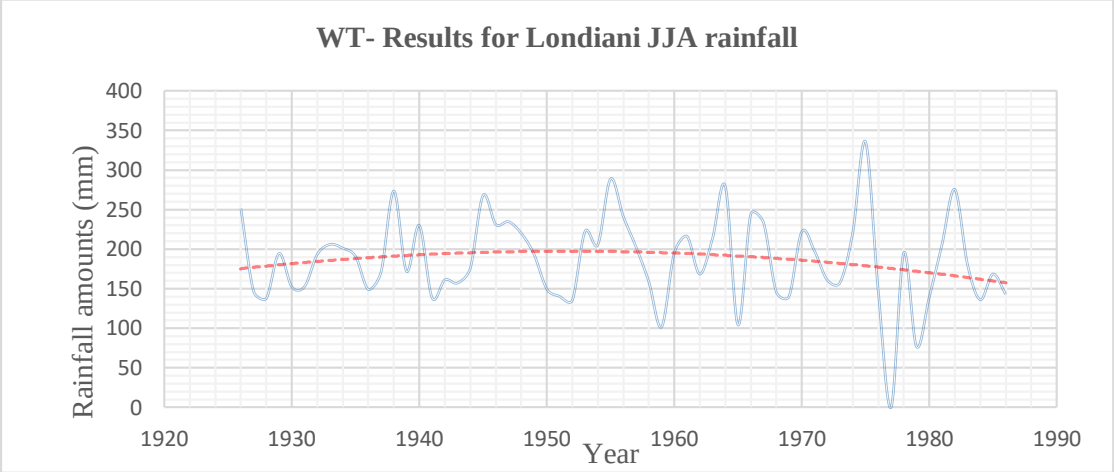
WT- Results for Londiani JJA rainfall
Rainfall amounts (mm)
400
350
300
250
200
150
100
50
0
1920
1930
1940
1950
1960
1970
1980
1990
Year

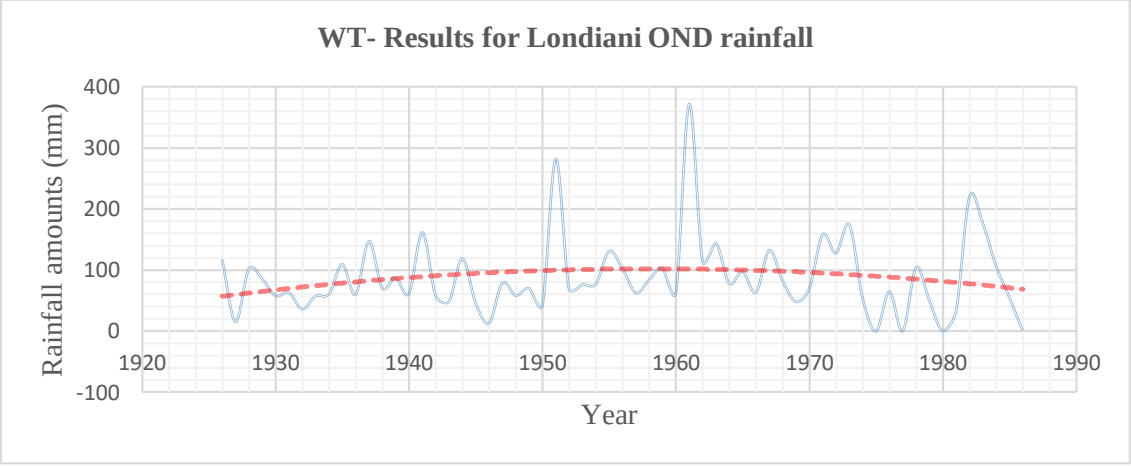
WT- Results for Londiani OND rainfall
Rainfall amounts (mm)
400
300
200
100
0
-100
1920
1930
1940
1950
1960
1970
1980
1990
Year

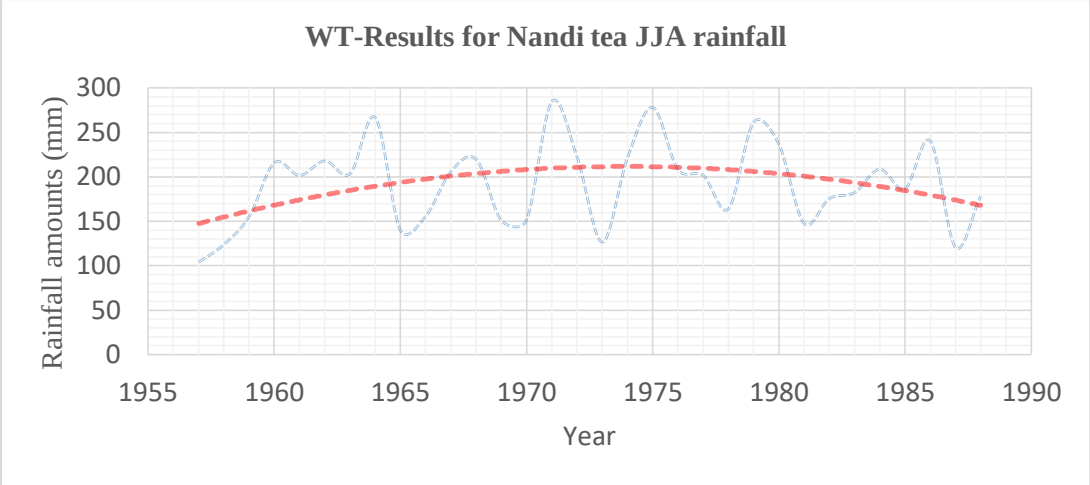
WT-Results for Nandi tea JJA rainfall
Rainfall amounts (mm)
300
250
200
150
100
50
0
1955
1960
1965
1970
1975
1980
1985
1990
Year

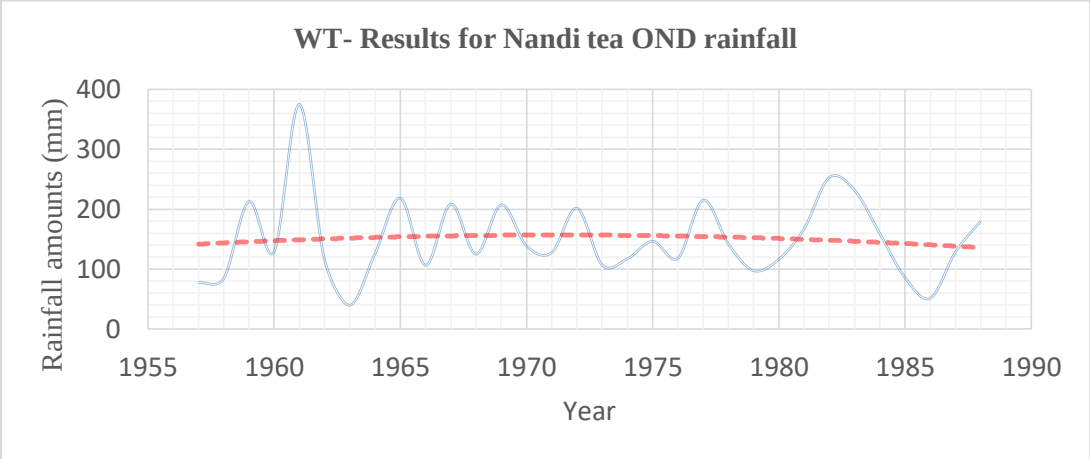
WT- Results for Nandi tea OND rainfall
Rainfall amounts (mm)
400
300
200
100
0
1955
1960
1965
1970
1975
1980
1985
1990
Year

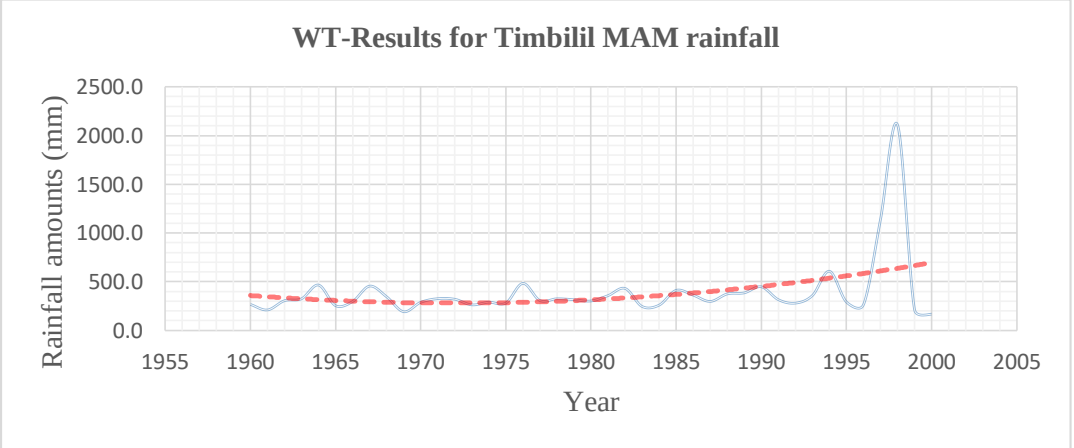
WT-Results for Timbilil MAM rainfall
Rainfall amounts (mm)
2500.0
2000.0
1500.0
1000.0
500.0
0.0
1955
1960
1965
1970
1975
1980
1985
1990
1995
2000
2005
Year

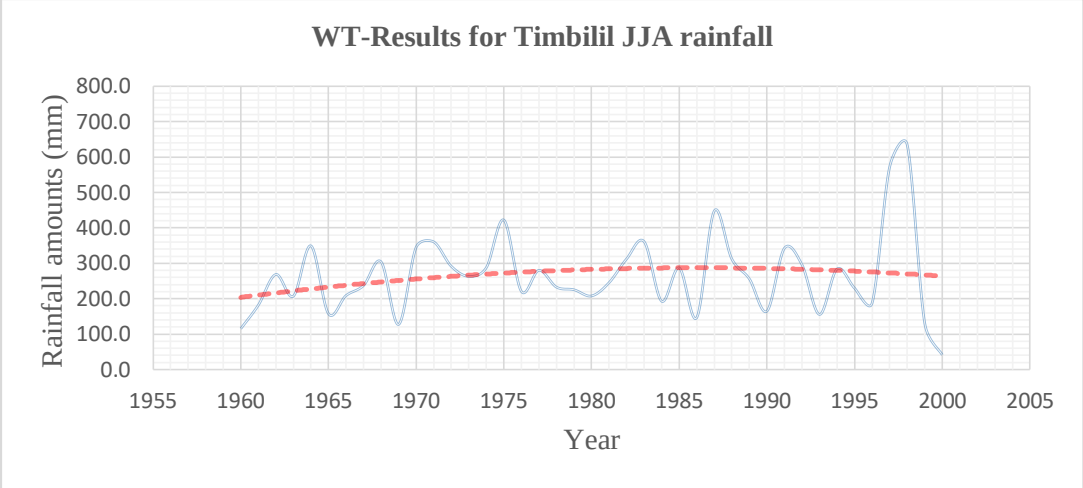
WT-Results for Timbilil JJA rainfall
Rainfall amounts (mm)
800.0
700.0
600.0
500.0
400.0
300.0
200.0
100.0
0.0
1955
1960
1965
1970
1975
1980
1985
1990
1995
2000
2005
Year

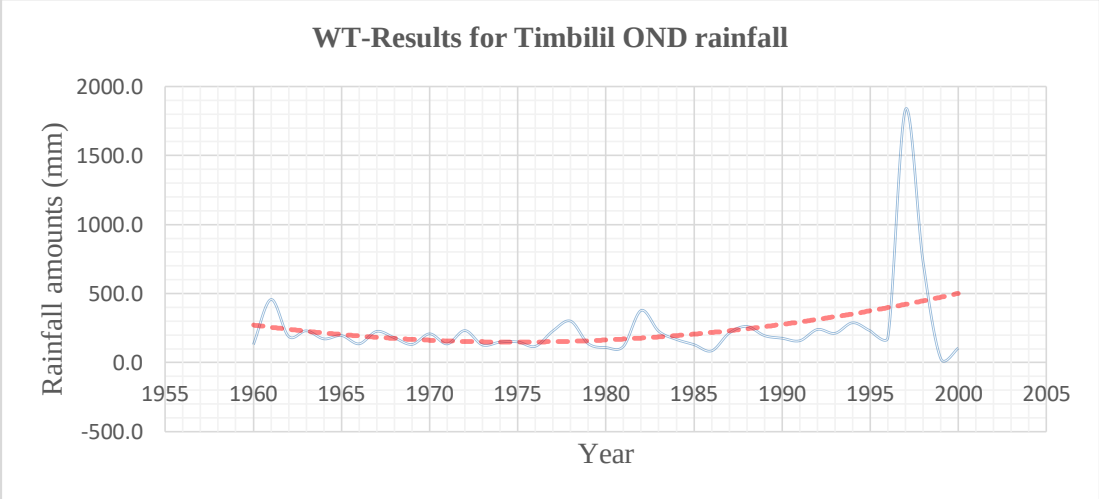
WT-Results for Timbilil OND rainfall
Rainfall amounts (mm)
2000.0
1500.0
1000.0
500.0
0.0
-500.0
1955
1960
1965
1970
1975
1980
1985
1990
1995
2000
2005
Year

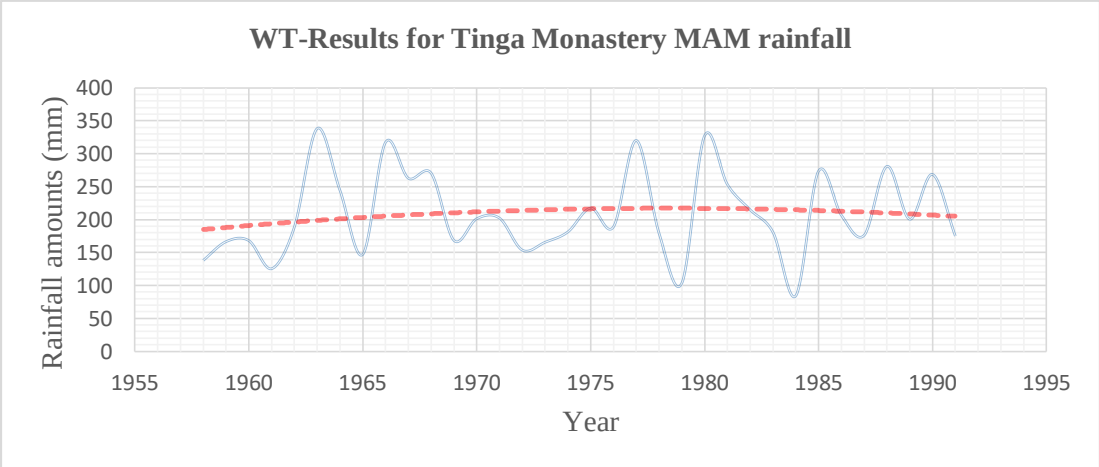
WT-Results for Tinga Monastery MAM rainfall
Rainfall amounts (mm)
400
350
300
250
200
150
100
50
0
1955
1960
1965
1970
1975
1980
1985
1990
1995
Year

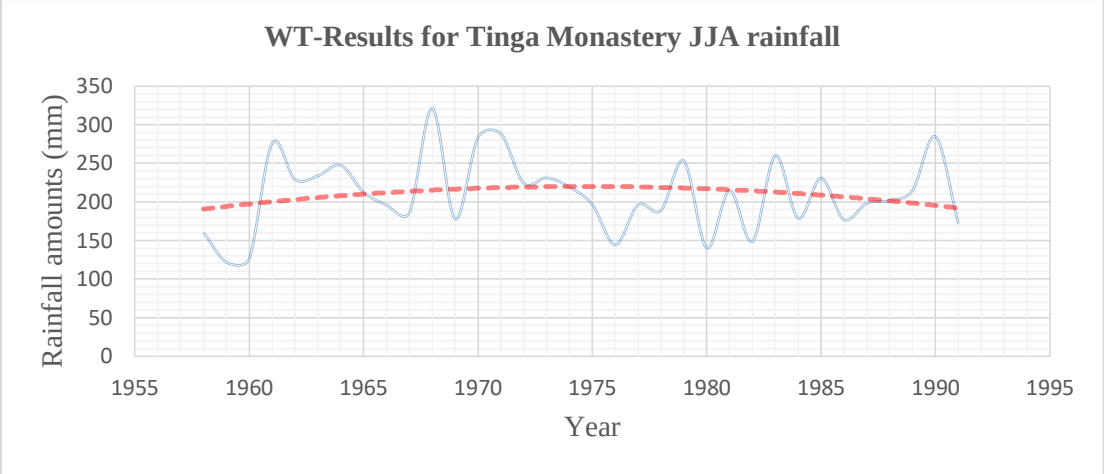
WT-Results for Tinga Monastery JJA rainfall
Rainfall amounts (mm)
350
300
250
200
150
100
50
0
1955
1960
1965
1970
1975
1980
1985
1990
1995
Year

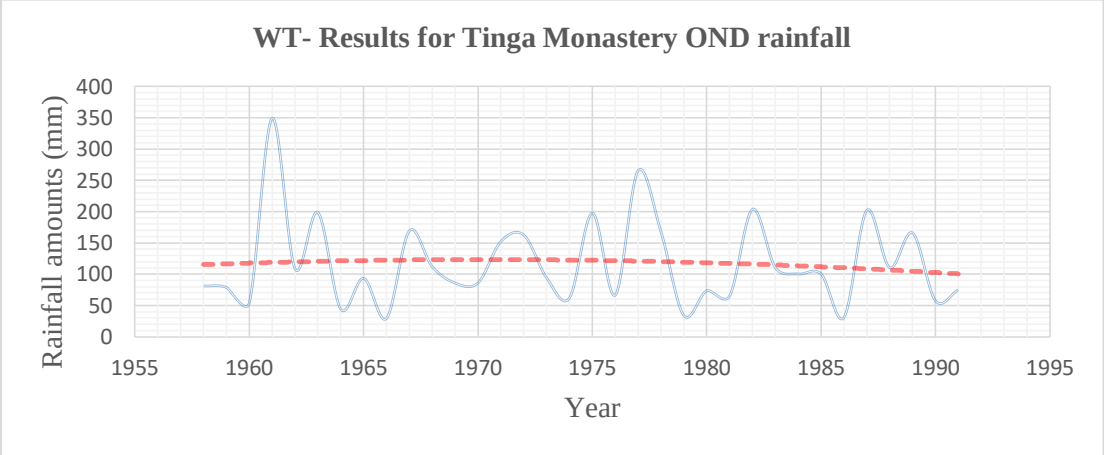
WT- Results for Tinga Monastery OND rainfall
Rainfall amounts (mm)
400
350
300
250
200
150
100
50
0
1955
1960
1965
1970
1975
1980
1985
1990
1995
Year

Appendix 7B-Wavelet trend results for streamflow

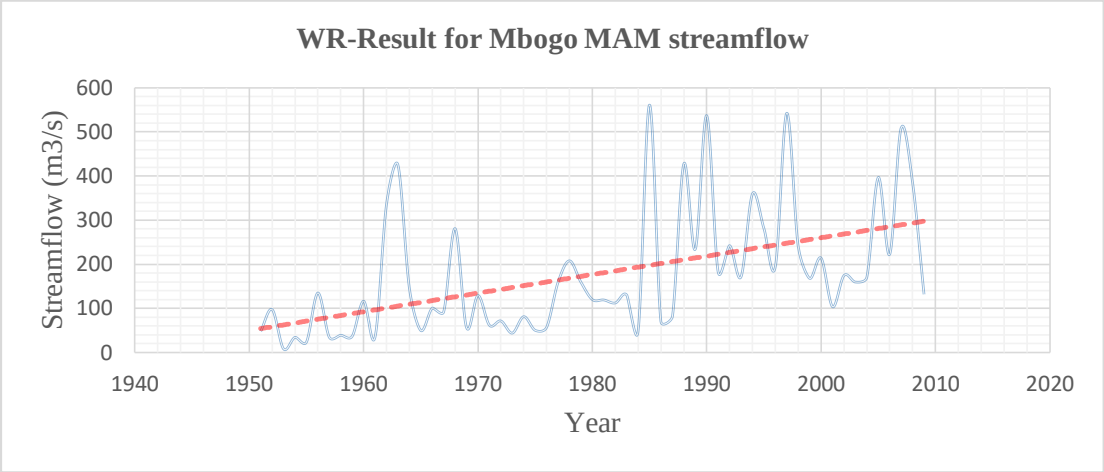

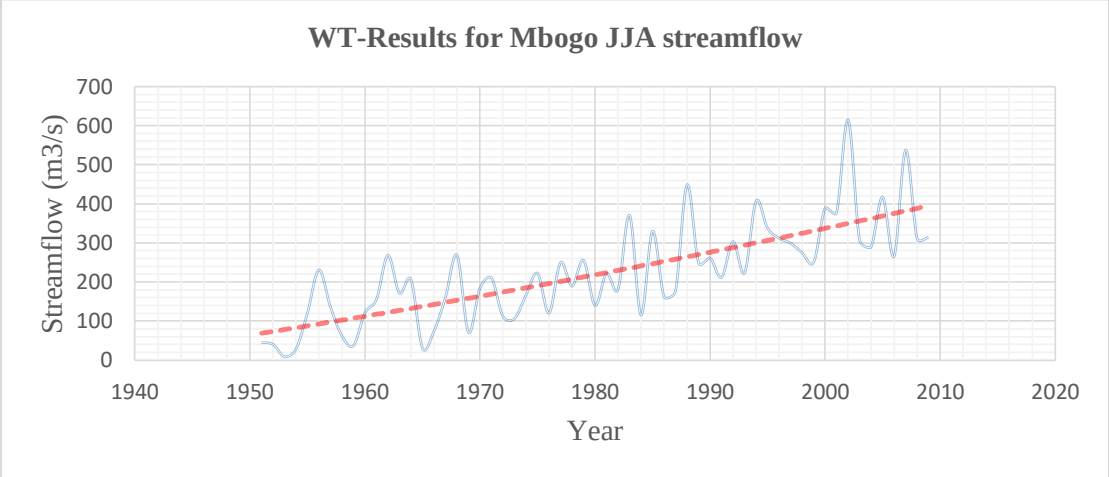

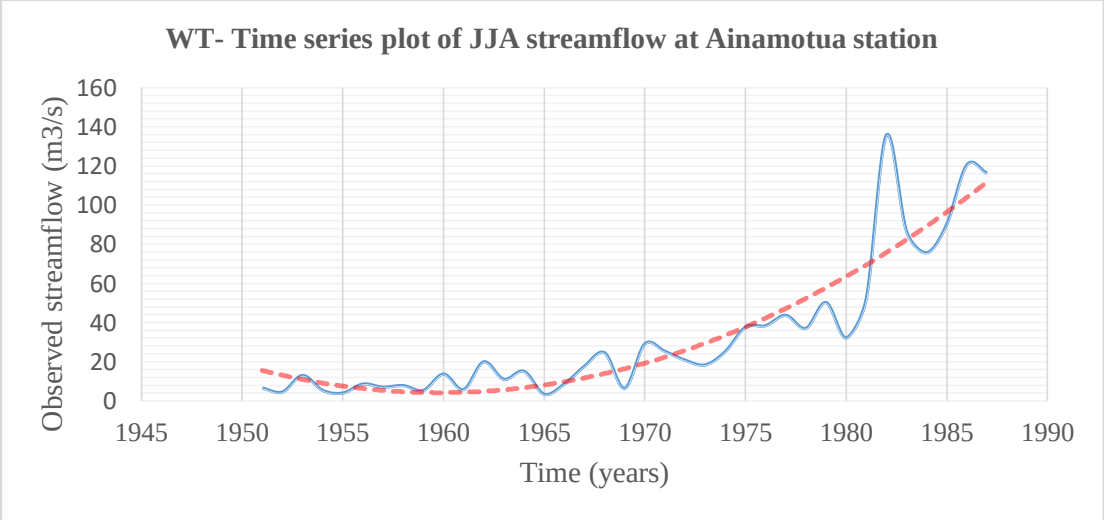

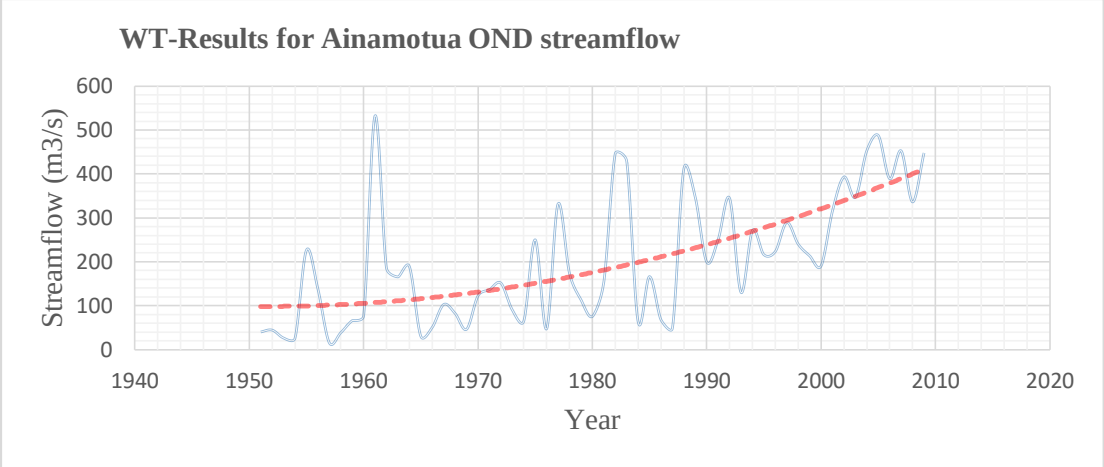
WT-Results for Ainamotua OND streamflow
Streamflow (m3/s)
600
500
400
300
200
100
0
1940
1950
1960
1970
1980
1990
2000
2010
2020
Year

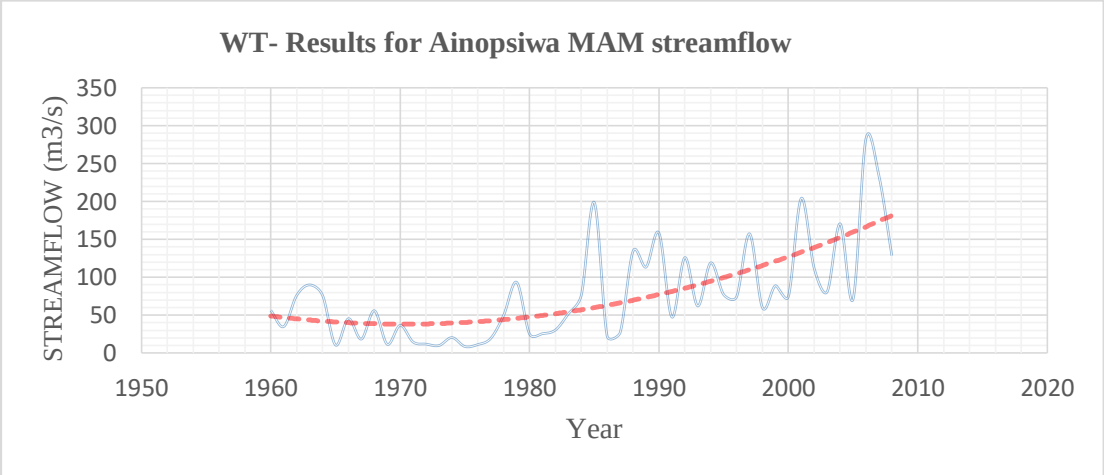
WT- Results for Ainopsiwa MAM streamflow
STREAMFLOW (m3/s)
350
300
250
200
150
100
50
0
1950
1960
1970
1980
1990
2000
2010
2020
Year

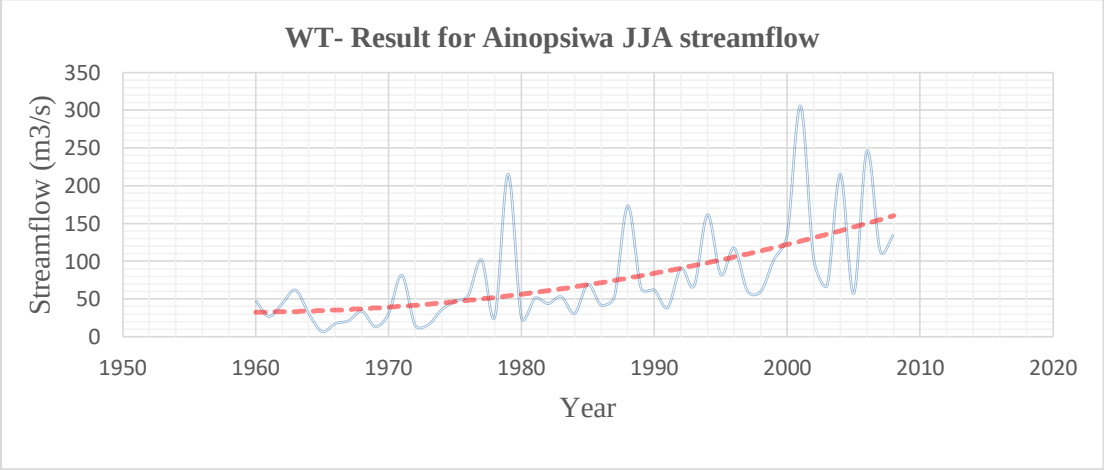
WT- Result for Ainopsiwa JJA streamflow
Streamflow (m3/s)
350
300
250
200
150
100
50
0
1950
1960
1970
1980
1990
2000
2010
2020
Year

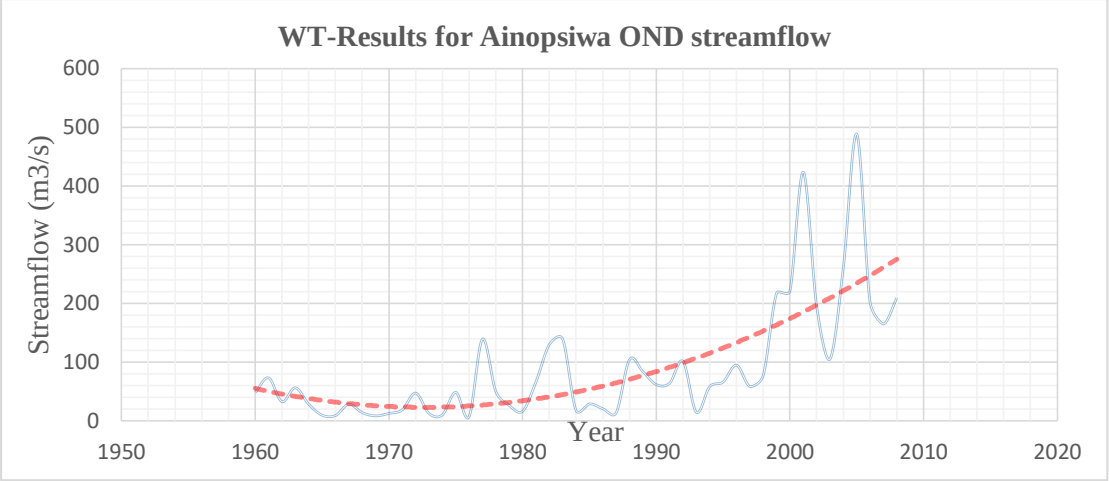
WT-Results for Ainopsiwa OND streamflow
Streamflow (m3/s)
600
500
400
300
200
100
0
1950
1960
1970
1980
1990
2000
2010
2020
Year

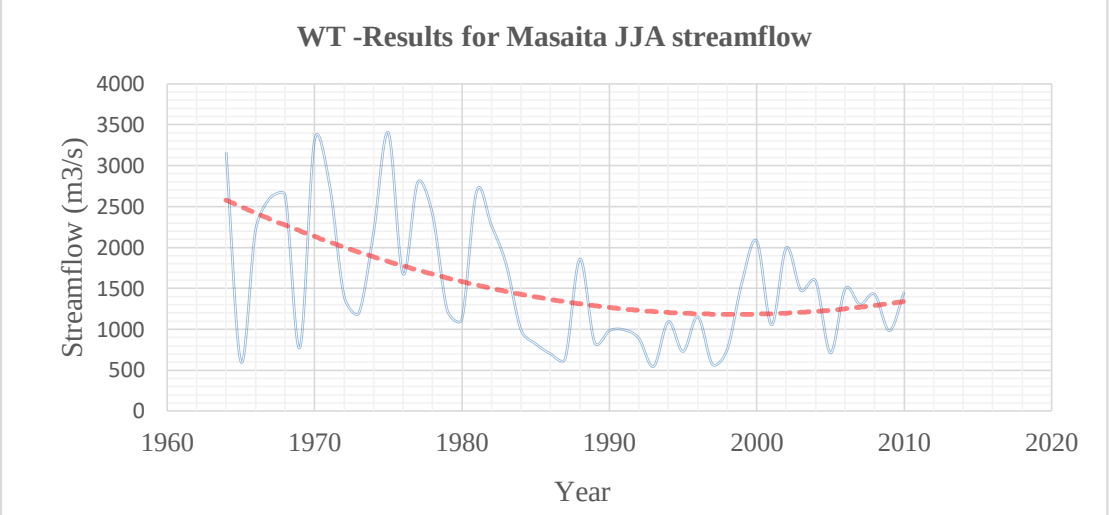
WT -Results for Masaita JJA streamflow
Streamflow (m3/s)
4000
3500
3000
2500
2000
1500
1000
500
0
1960
1970
1980
1990
2000
2010
2020
Year

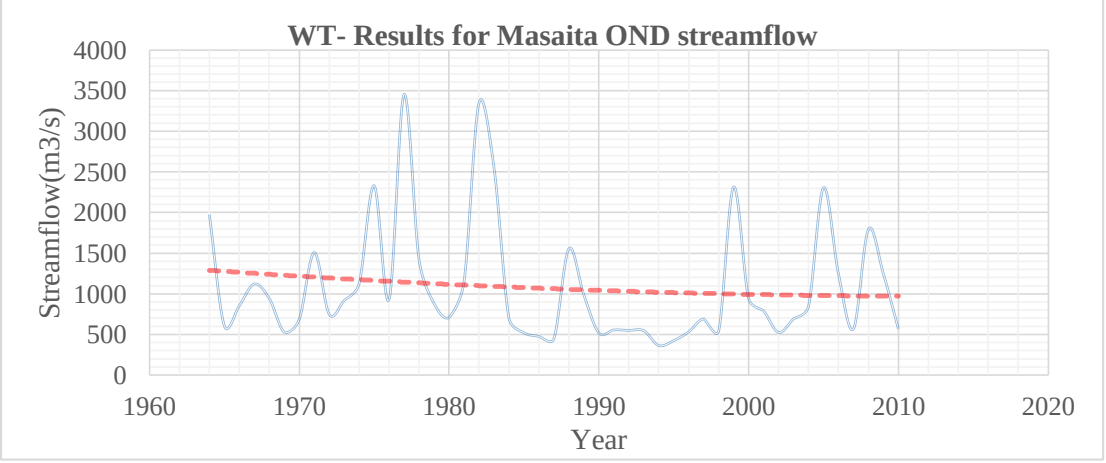
WT- Results for Masaita OND streamflow
Streamflow(m3/s)
4000
3500
3000
2500
2000
1500
1000
500
0
1960
1970
1980
1990
2000
2010
2020
Year

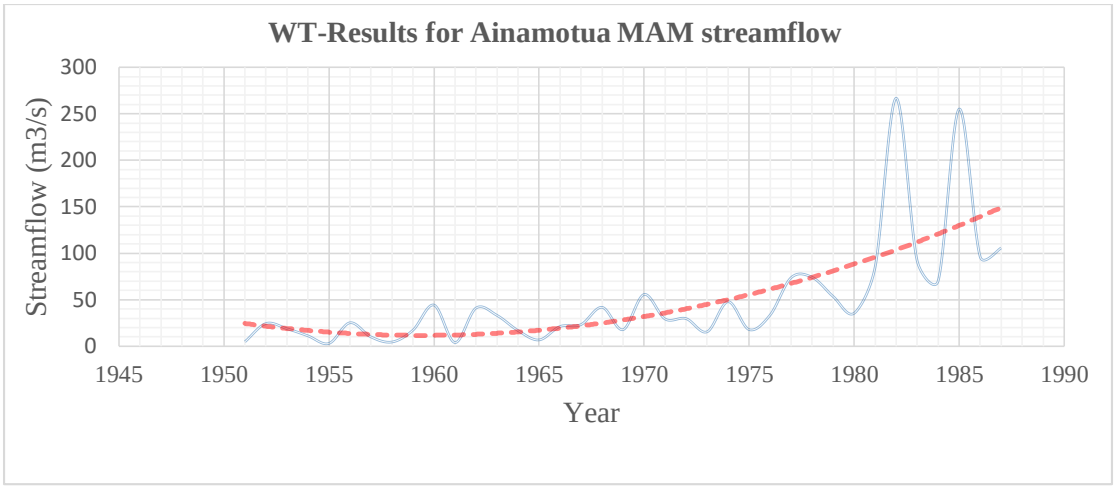
WT-Results for Ainamotua MAM streamflow
Streamflow (m3/s)
300
250
200
150
100
50
0
1945
1950
1955
1960
1965
1970
1975
1980
1985
1990
Year

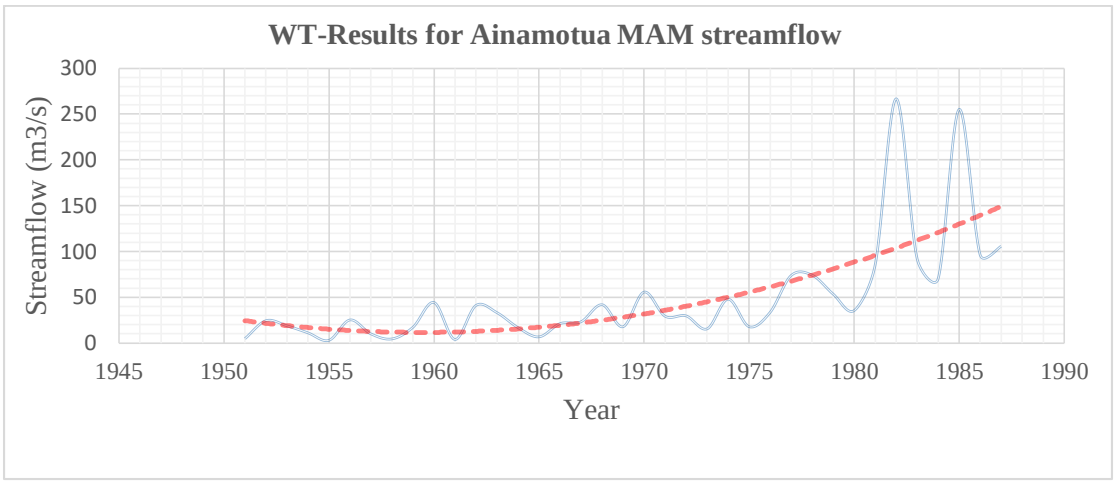
WT-Results for Ainamotua MAM streamflow
Streamflow (m3/s)
300
250
200
150
100
50
0
1945
1950
1955
1960
1965
1970
1975
1980
1985
1990
Year

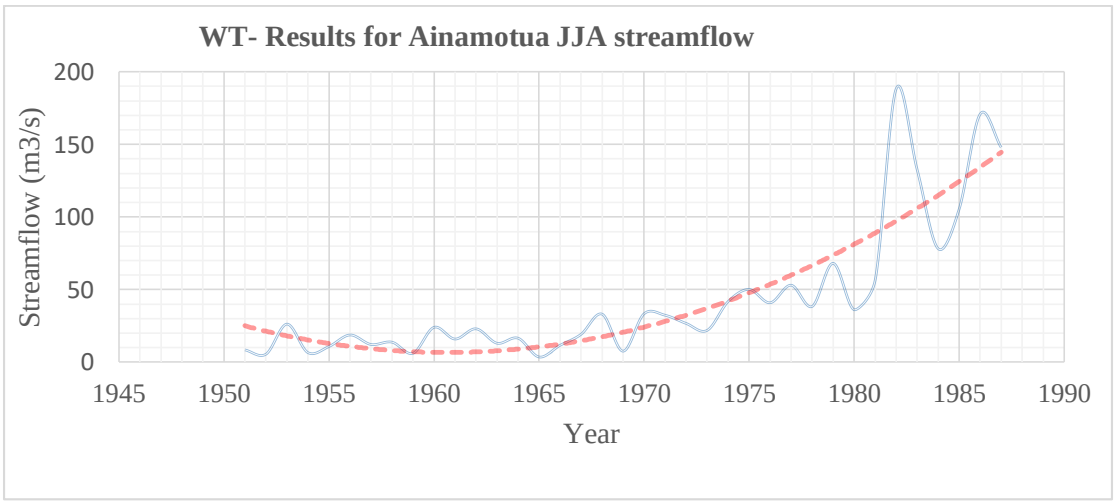
WT- Results for Ainamotua JJA streamflow
Streamflow (m3/s)
200
150
100
50
0
1945
1950
1955
1960
1965
1970
1975
1980
1985
1990
Year

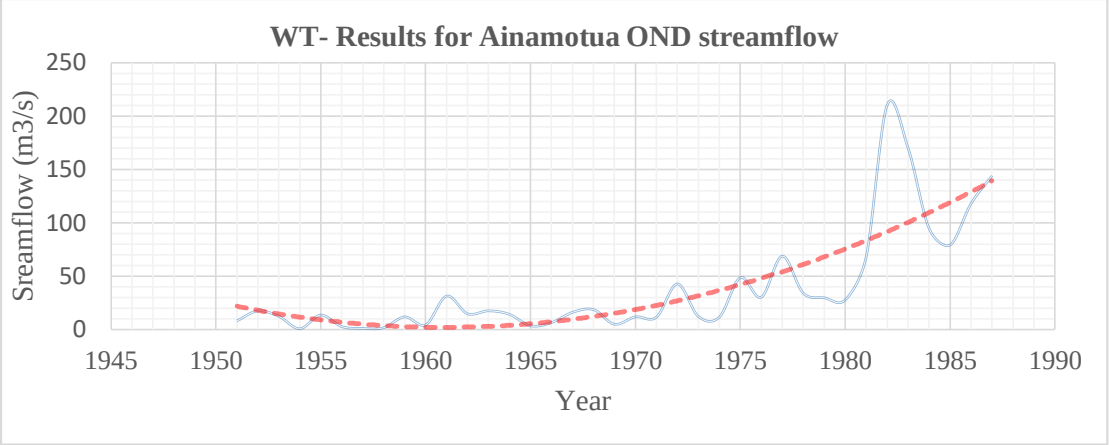
WT- Results for Ainamotua OND streamflow
Sreamflow (m3/s)
250
200
150
100
50
0
1945
1950
1955
1960
1965
1970
1975
1980
1985
1990
Year

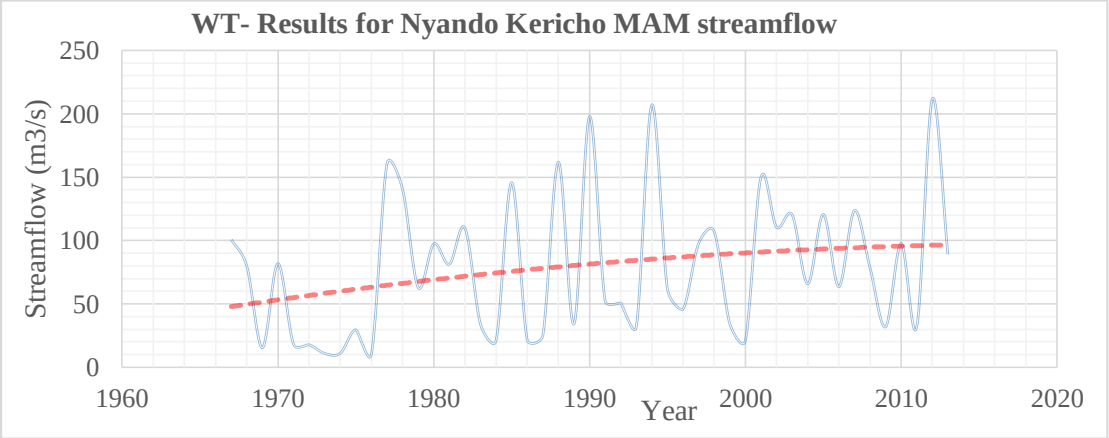
WT- Results for Nyando Kericho MAM streamflow
Streamflow (m3/s)
250
200
150
100
50
0
1960
1970
1980
1990
2000
2010
2020
Year

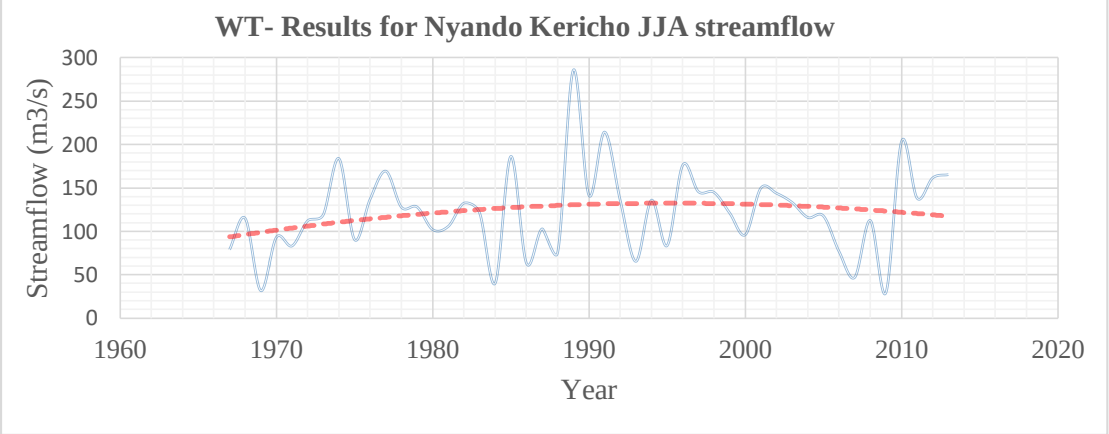
WT- Results for Nyando Kericho JJA streamflow
Streamflow (m3/s)
300
250
200
150
100
50
0
1960
1970
1980
1990
2000
2010
2020
Year

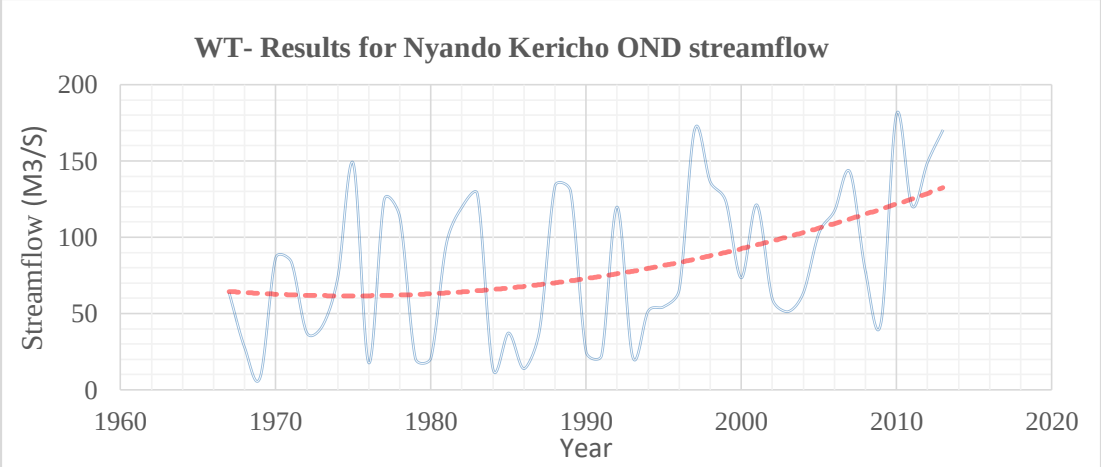
WT- Results for Nyando Kericho OND streamflow
Streamflow (M3/S)
200
150
100
50
0
1960
1970
1980
1990
2000
2010
2020
Year

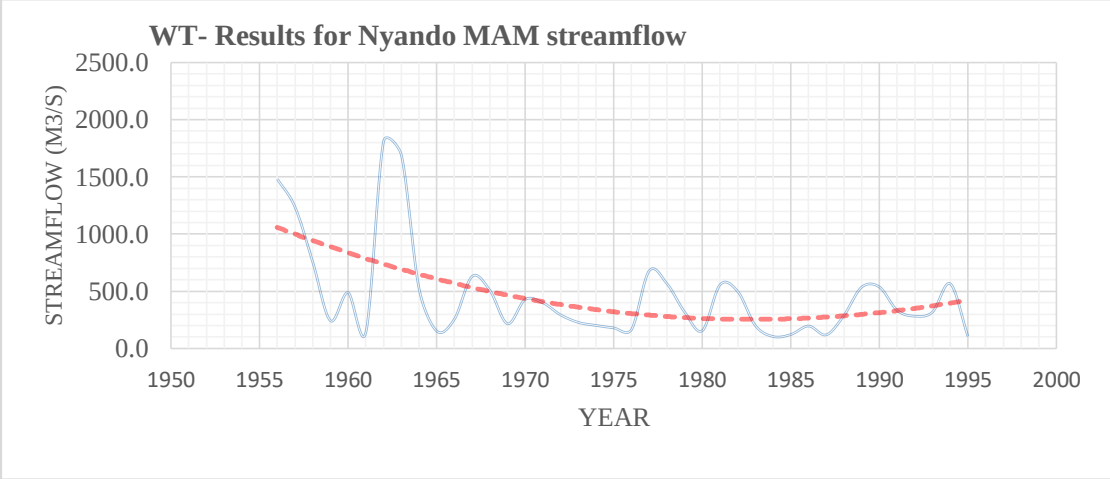
WT- Results for Nyando MAM streamflow
STREAMFLOW (M3/S)
2500.0
2000.0
1500.0
1000.0
500.0
0.0
1950
1955
1960
1965
1970
1975
1980
1985
1990
1995
2000
YEAR

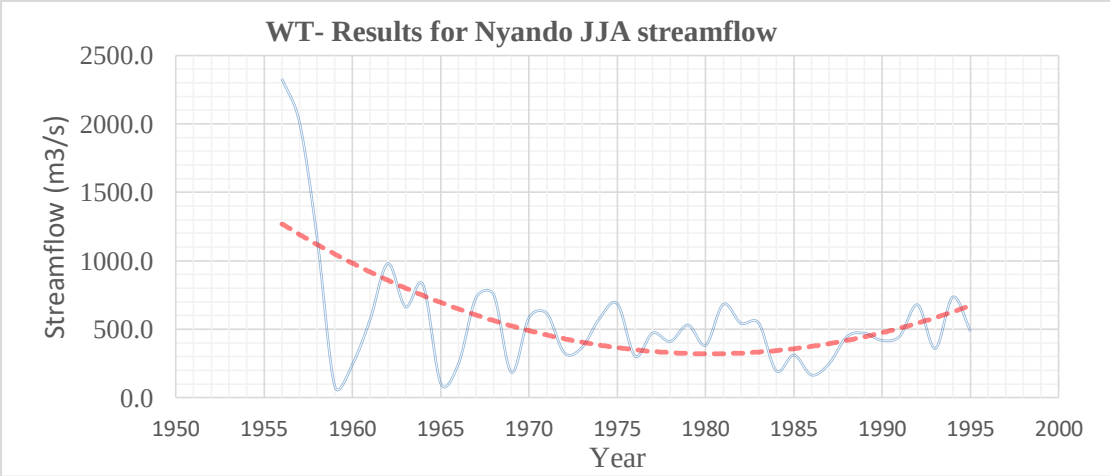
WT- Results for Nyando JJA streamflow
Streamflow (m3/s)
2500.0
2000.0
1500.0
1000.0
500.0
0.0
1950
1955
1960
1965
1970
1975
1980
1985
1990
1995
2000
Year

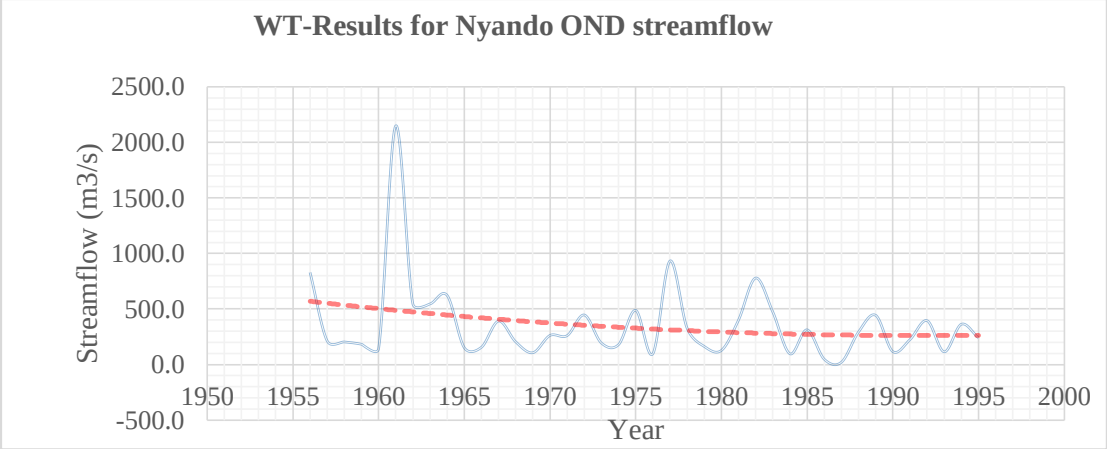
WT-Results for Nyando OND streamflow
Streamflow (m3/s)
2500.0
2000.0
1500.0
1000.0
500.0
0.0
-500.0
1950
1955
1960
1965
1970
1975
1980
1985
1990
1995
2000
Year

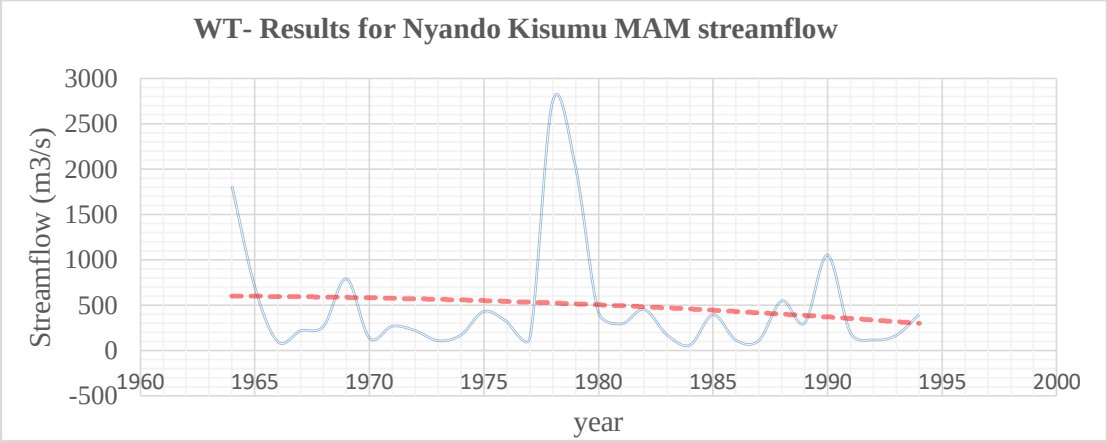
WT- Results for Nyando Kisumu MAM streamflow
Streamflow (m3/s)
3000
2500
2000
1500
1000
500
0
-500
1960
1965
1970
1975
1980
1985
1990
1995
2000
year

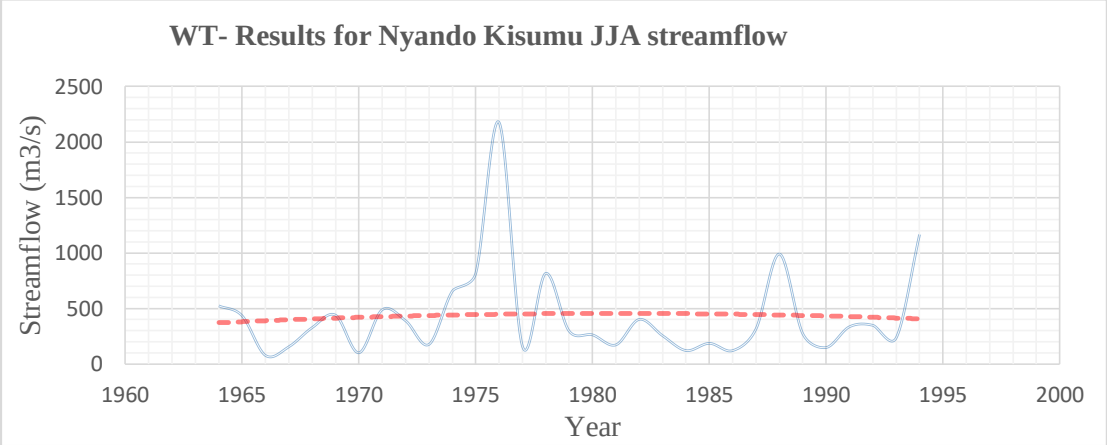
WT- Results for Nyando Kisumu JJA streamflow
Streamflow (m3/s)
2500
2000
1500
1000
500
0
1960
1965
1970
1975
1980
1985
1990
1995
2000
Year

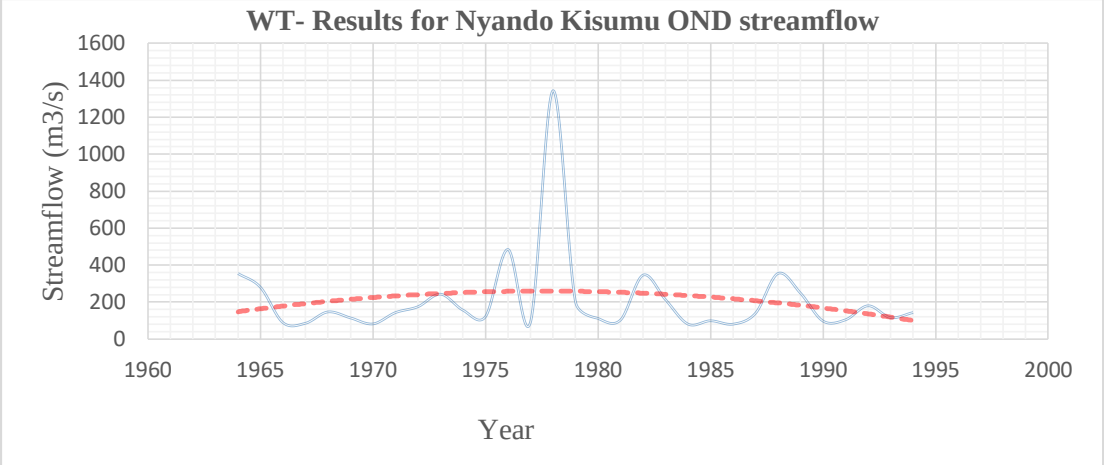
WT- Results for Nyando Kisumu OND streamflow
Streamflow (m3/s)
1600
1400
1200
1000
800
600
400
200
0
1960
1965
1970
1975
1980
1985
1990
1995
2000
Year

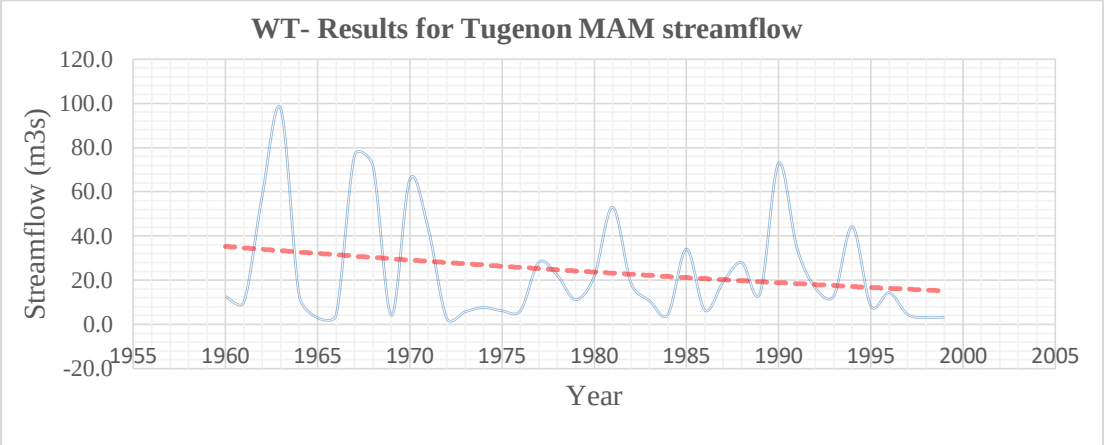
WT- Results for Tugenon MAM streamflow
Streamflow (m3s)
120.0
100.0
80.0
60.0
40.0
20.0
0.0
-20.0
1955
1960
1965
1970
1975
1980
1985
1990
1995
2000
2005
Year

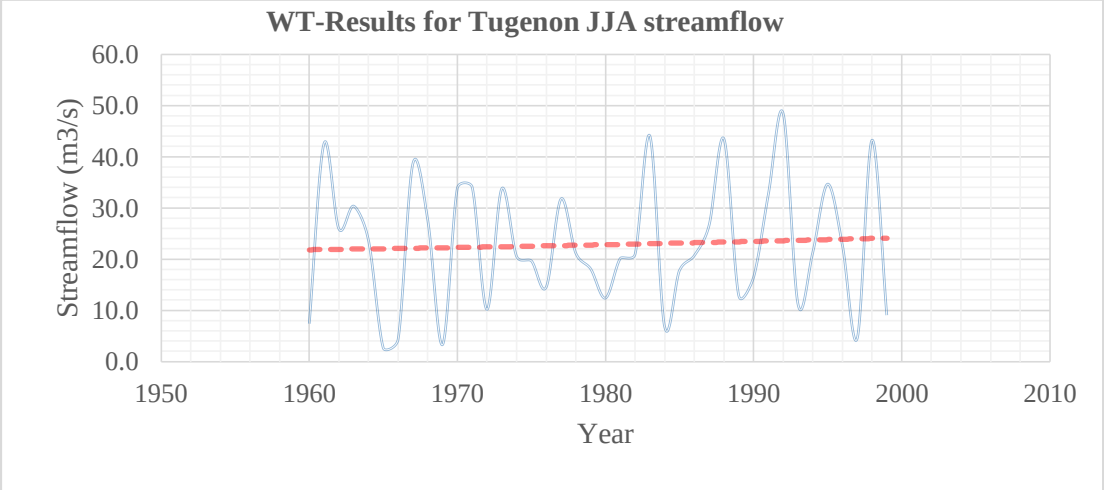
WT-Results for Tugenon JJA streamflow
Streamflow (m3/s)
60.0
50.0
40.0
30.0
20.0
10.0
0.0
1950
1960
1970
1980
1990
2000
2010
Year

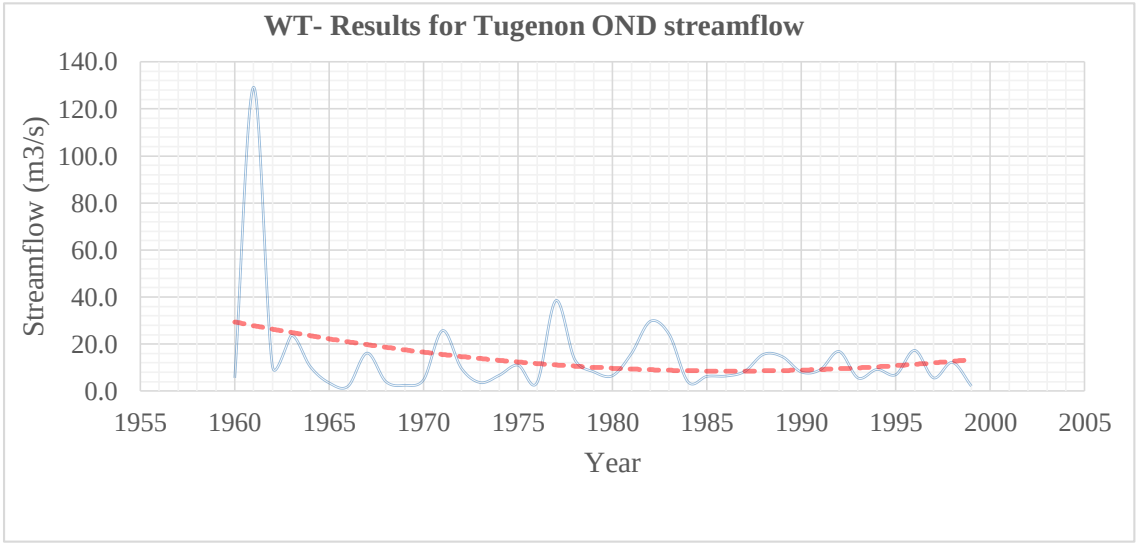
WT- Results for Tugenon OND streamflow
Streamflow (m3/s)
140.0
120.0
100.0
80.0
60.0
40.0
20.0
0.0
1955
1960
1965
1970
1975
1980
1985
1990
1995
2000
2005
Year

Appendix 8A: Rainfall Spectral Analysis Results

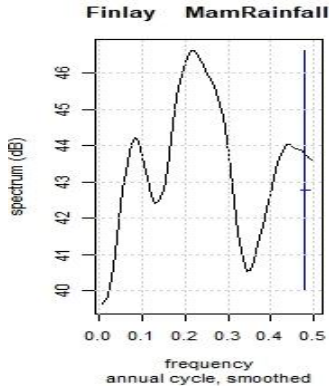

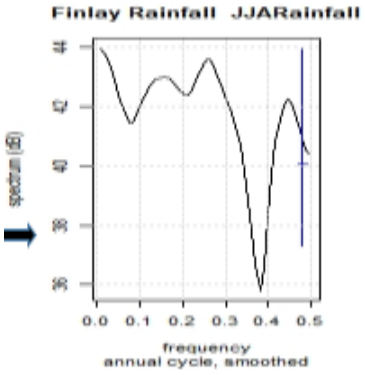

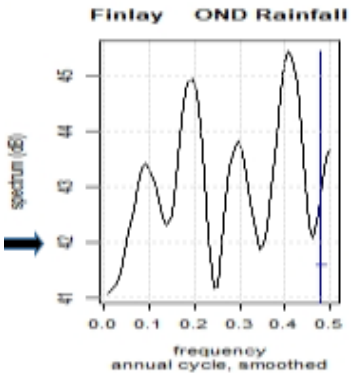

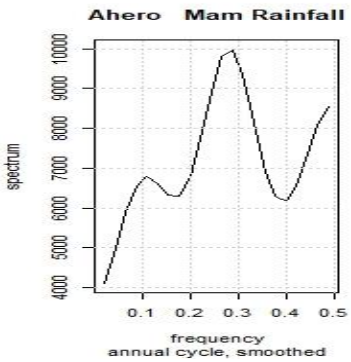

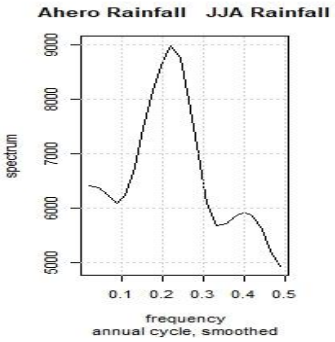

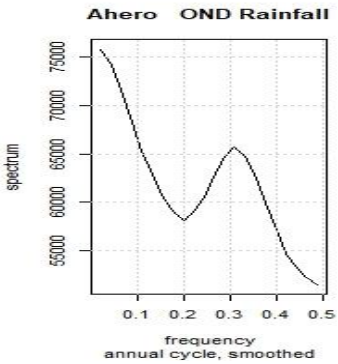

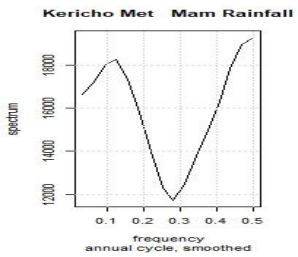

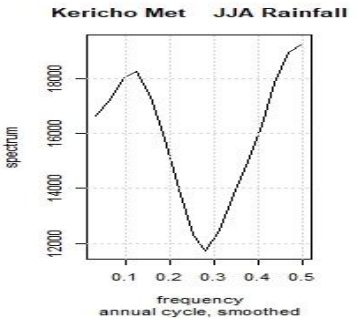

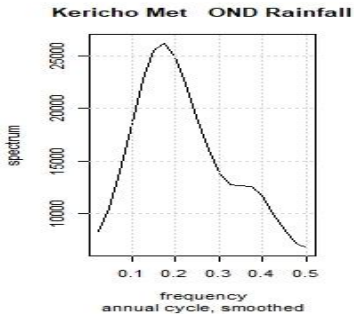

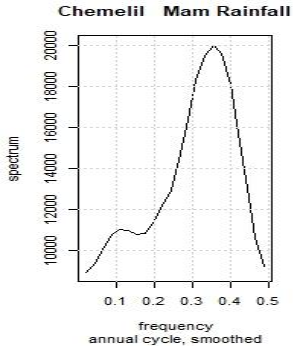

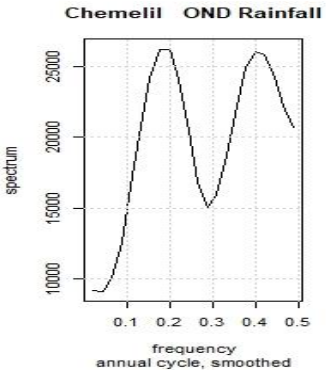

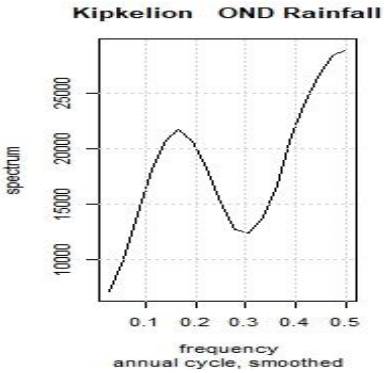

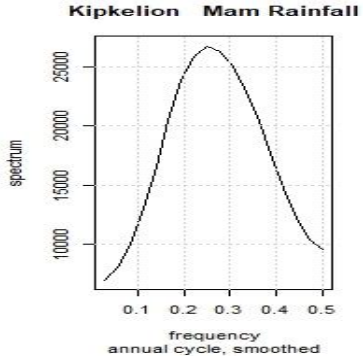
Kipkelion Mam Rainfall
spectrum
frequency
annual cycle, smoothed

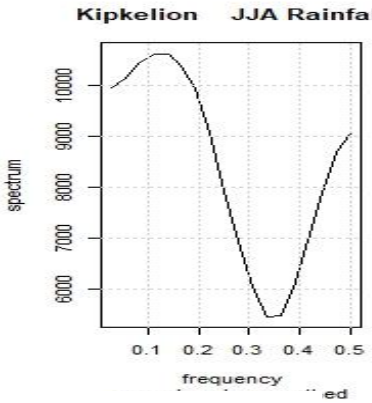
Kipkelion JJA Rainfall
spectrum
frequency

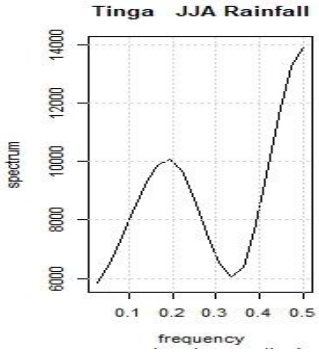
Tinga JJA Rainfall
spectrum
frequency

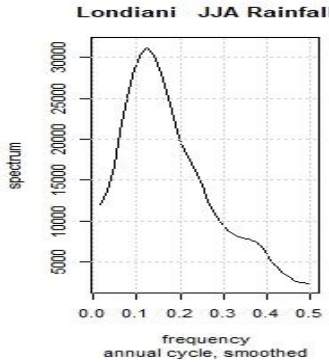
Londiani JJA Rainfall
spectrum
frequency
annual cycle, smoothed

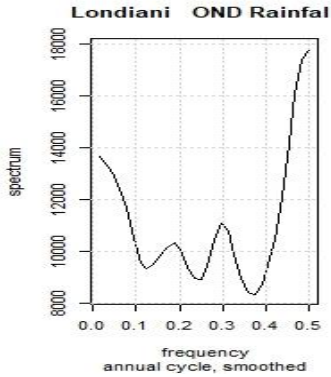
Londiani OND Rainfall
spectrum
frequency
annual cycle, smoothed

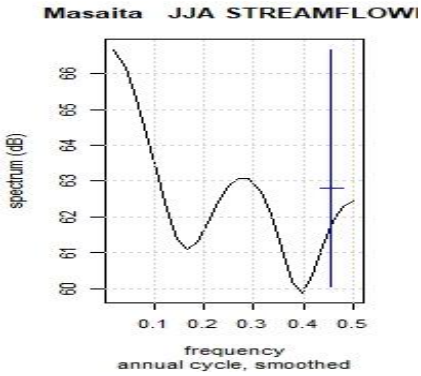
Masaita JJA STREAMFLOW
spectrum (dB)
frequency
annual cycle, smoothed

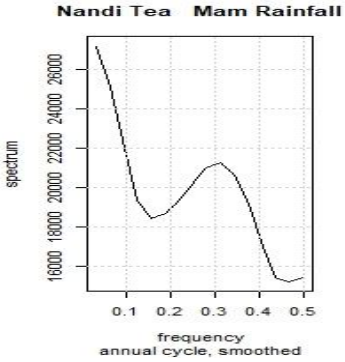
Nandi Tea Mam Rainfall
spectrum
frequency
annual cycle, smoothed

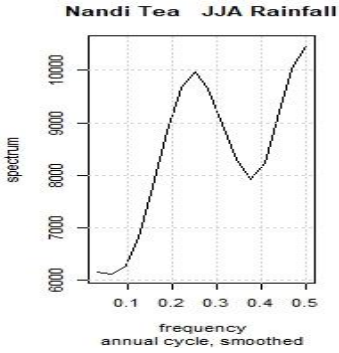
Nandi Tea JJA Rainfall
spectrum
frequency
annual cycle, smoothed

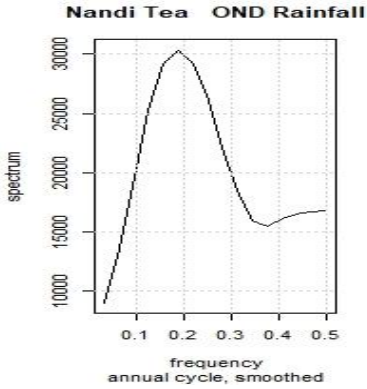
Nandi Tea OND Rainfall
spectrum
frequency
annual cycle, smoothed

Appendix 8B: Streamflow spectral analysis results (periodograms)

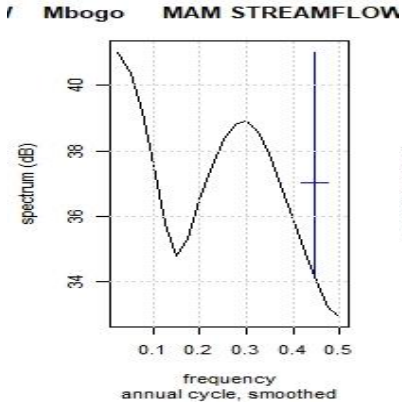

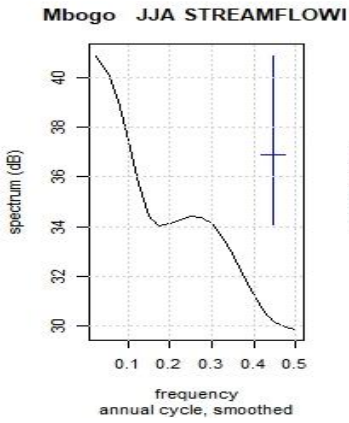

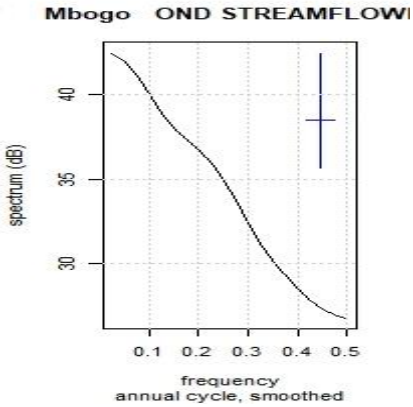

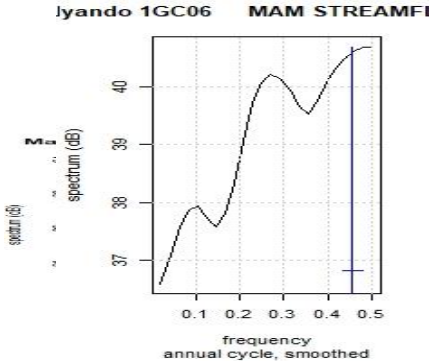

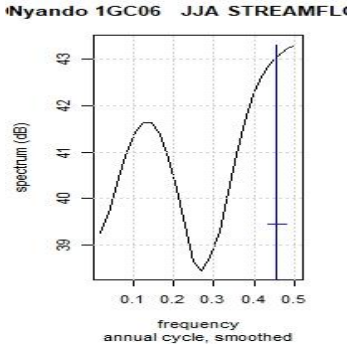

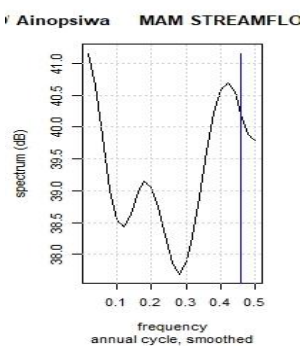

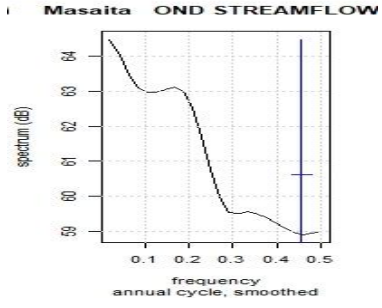

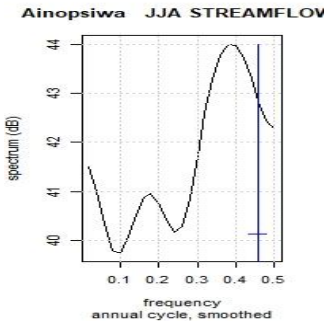

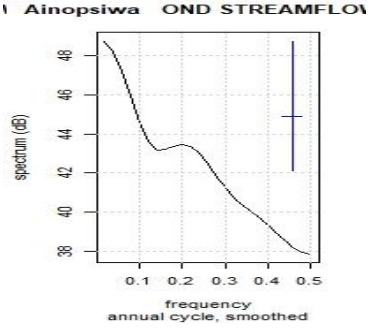

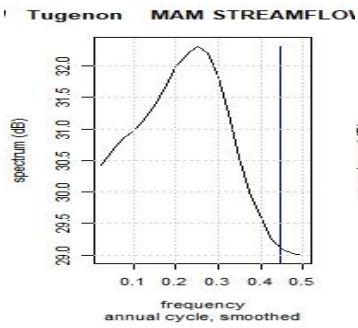

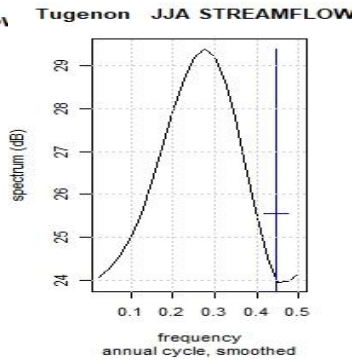

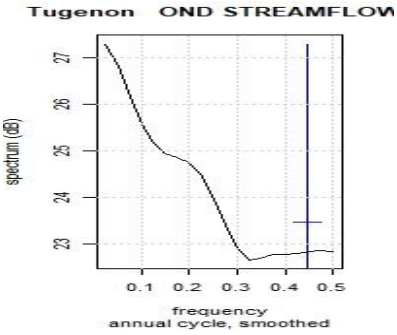

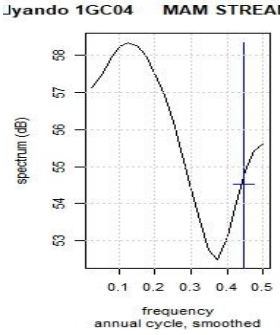
Nyando 1GC04 MAM STREAMFI
spectrum (dB)
frequency
annual cycle, smoothed

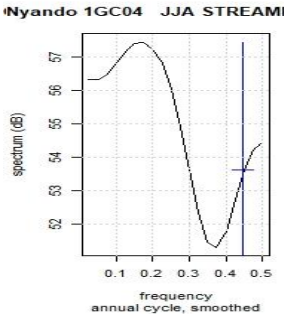
Nyando 1GC04 JJA STREAMFL
spectrum (dB)
frequency
annual cycle, smoothed

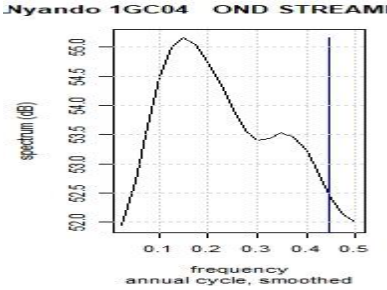
Nyando 1GC04 OND STREAMFL
spectrum (dB)
frequency
annual cycle, smoothed

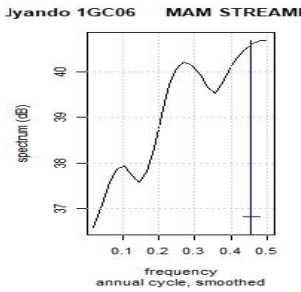
Nyando 1GC06 MAM STREAMFI
spectrum (dB)
frequency
annual cycle, smoothed

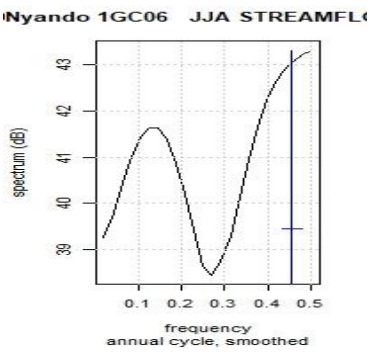
Nyando 1GC06 JJA STREAMFL
spectrum (dB)
frequency
annual cycle, smoothed

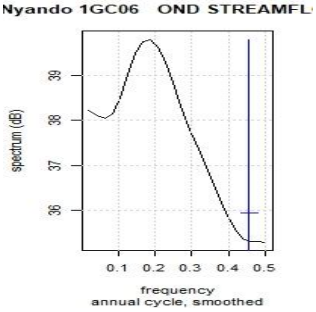
Nyando 1GC06 OND STREAMFL
spectrum (dB)
frequency
annual cycle, smoothed

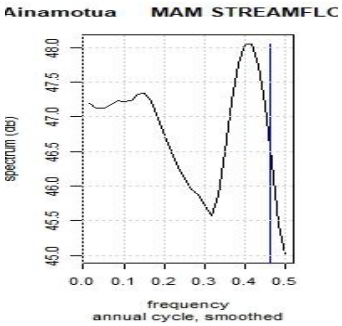
Ainamotua MAM STREAMFLC
spectrum (dB)
frequency
annual cycle, smoothed

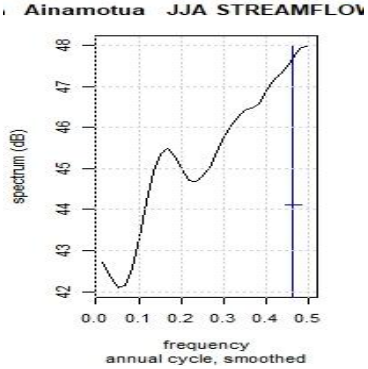
Ainamotua JJA STREAMFLOW
spectrum (dB)
frequency
annual cycle, smoothed

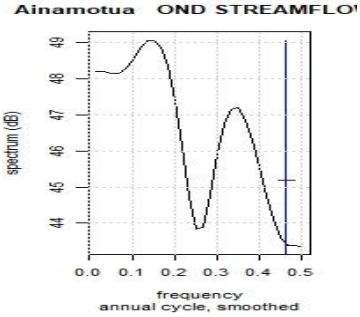
Ainamotua OND STREAMFLOW
spectrum (dB)
frequency
annual cycle, smoothed

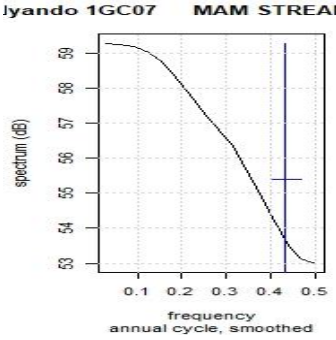
Nyando 1GC07 MAM STREAMFI
spectrum (dB)
frequency
annual cycle, smoothed

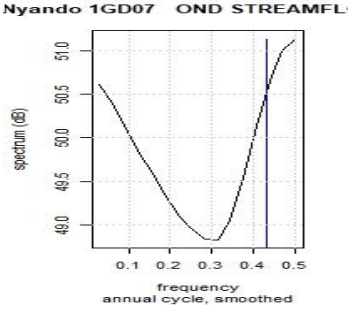
Nyando 1GD07 OND STREAMFL
spectrum (dB)
frequency
annual cycle, smoothed

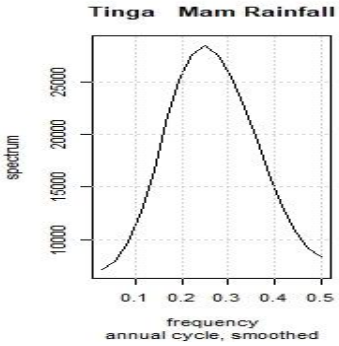
Tinga Mam Rainfall
spectrum
frequency
annual cycle, smoothed

Appendix 9A: Wavelet rainfall periodicity results

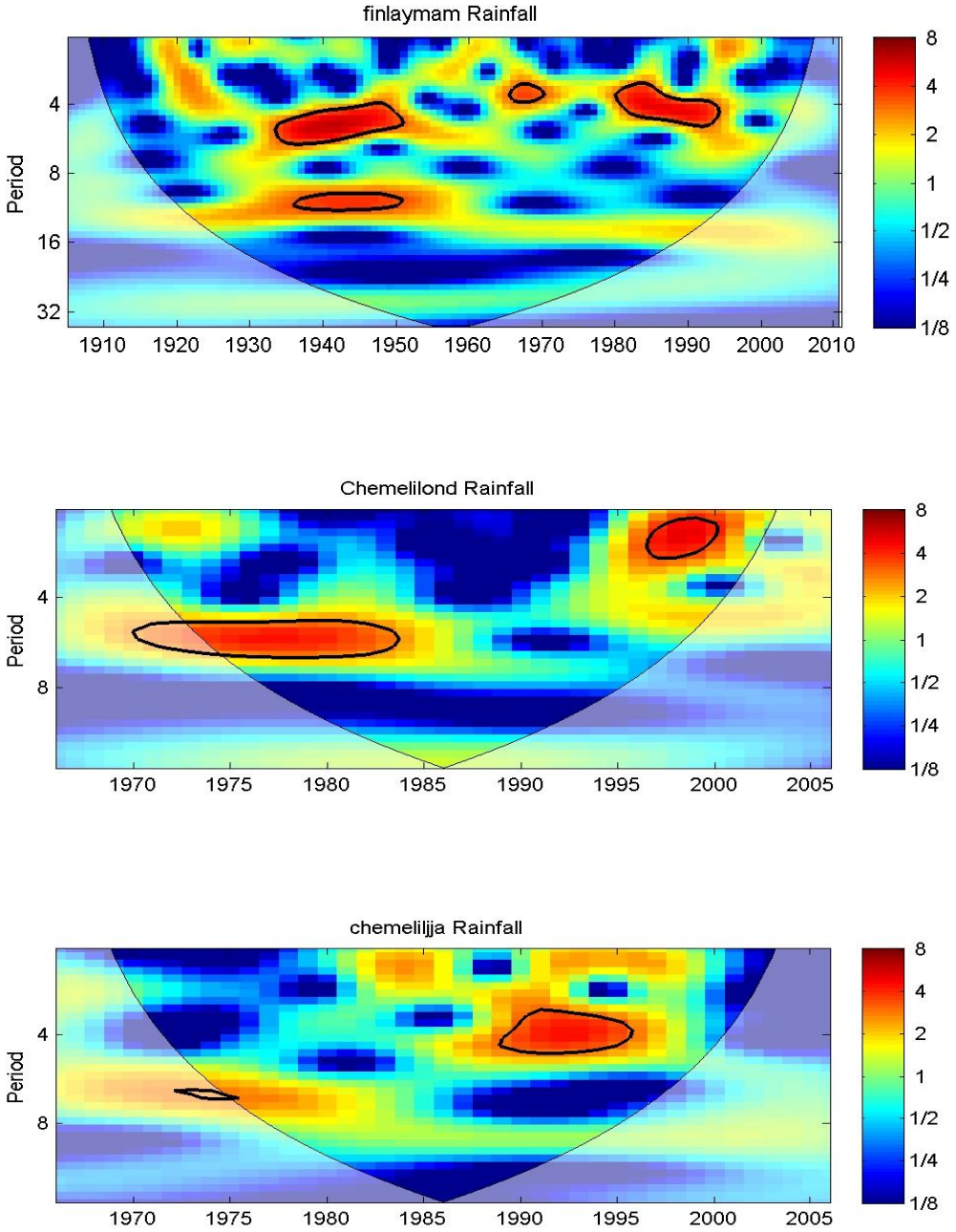

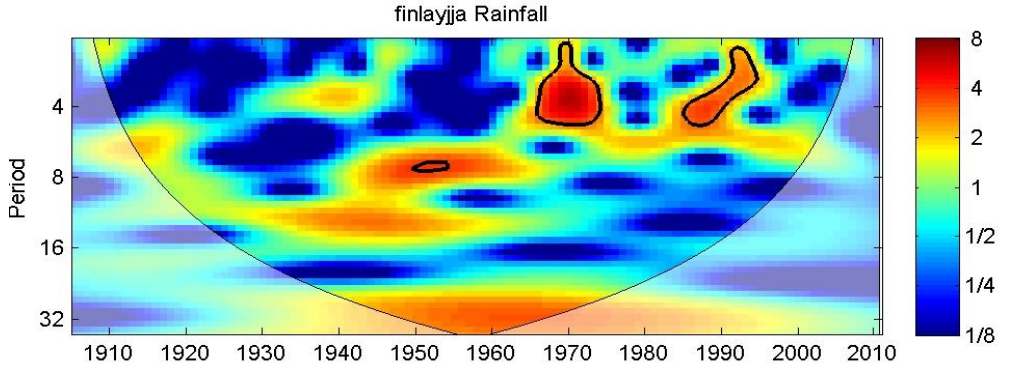
finlayjja Rainfall
Period
4
8
16
32
1910
1920
1930
1940
1950
1960
1970
1980
1990
2000
2010
8
4
2
1
1/2
1/4
1/8

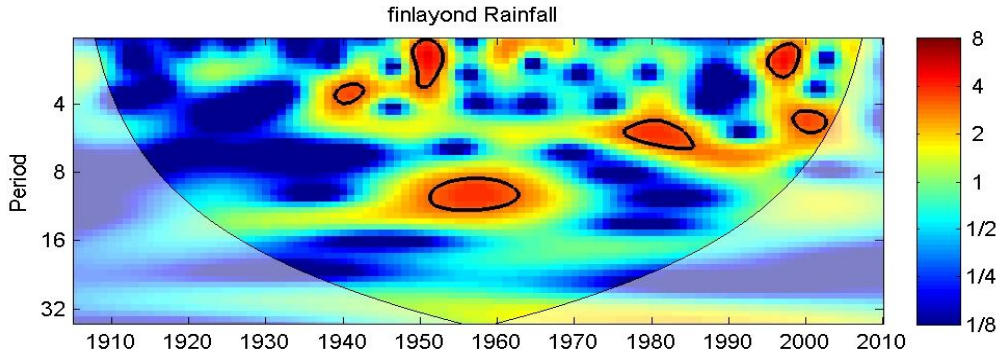
finlayond Rainfall
Period
4
8
16
32
1910
1920
1930
1940
1950
1960
1970
1980
1990
2000
2010
8
4
2
1
1/2
1/4
1/8

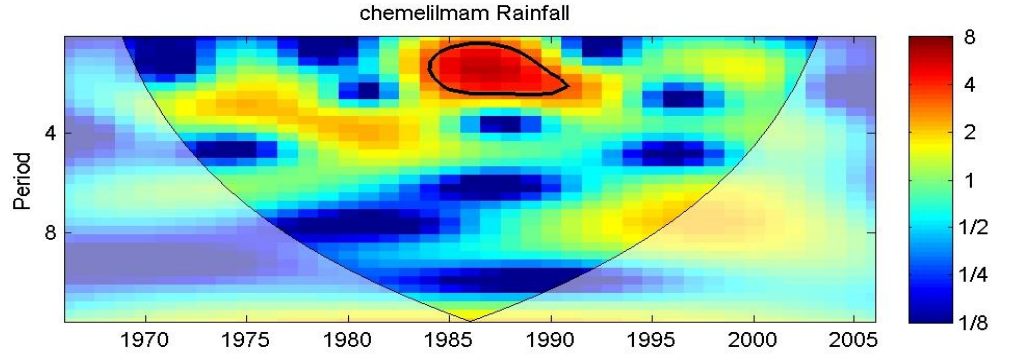
chemelilmam Rainfall
Period
4
8
1970
1975
1980
1985
1990
1995
2000
2005
8
4
2
1
1/2
1/4
1/8

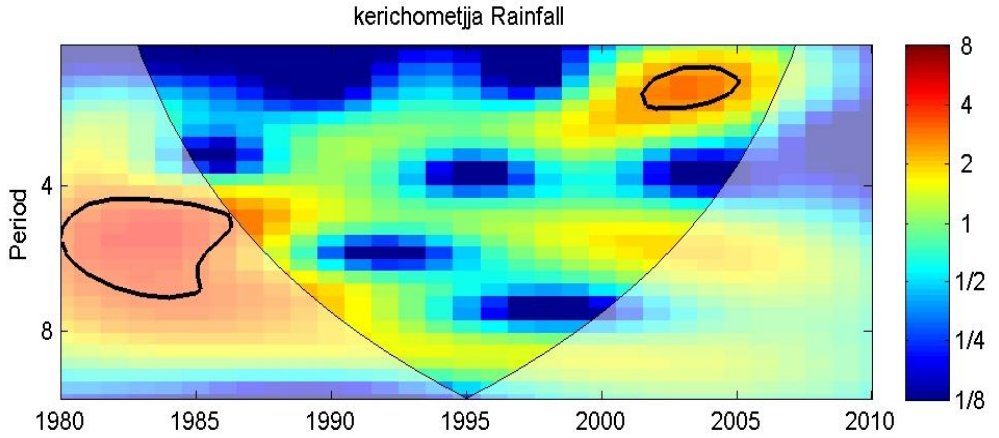
kerichometjja Rainfall
Period
4
8
1980
1985
1990
1995
2000
2005
2010
8
4
2
1
1/2
1/4
1/8

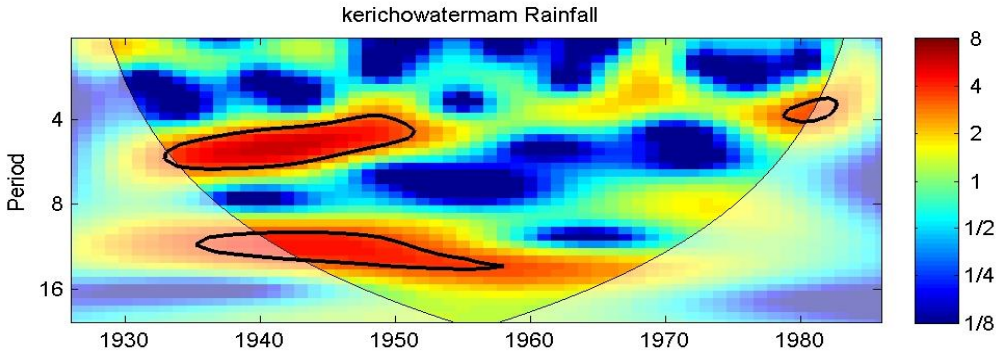
kerichowatermam Rainfall
Period
4
8
16
1930
1940
1950
1960
1970
1980
8
4
2
1
1/2
1/4
1/8

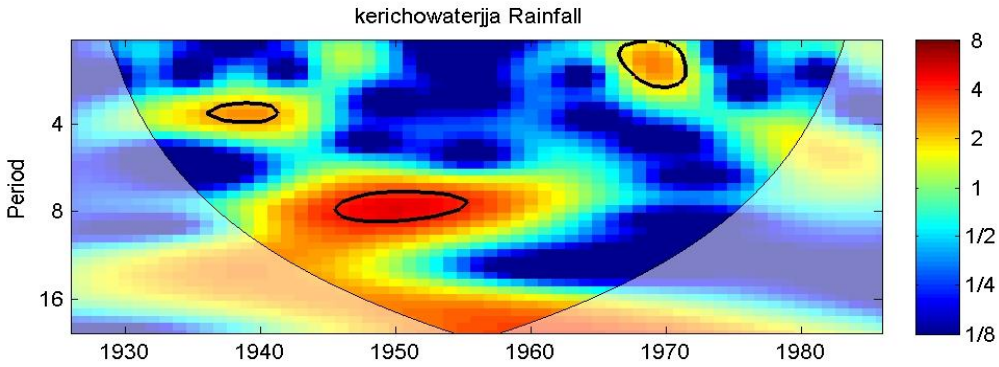
kerichowaterjja Rainfall
Period
4
8
16
1930
1940
1950
1960
1970
1980
8
4
2
1
1/2
1/4
1/8

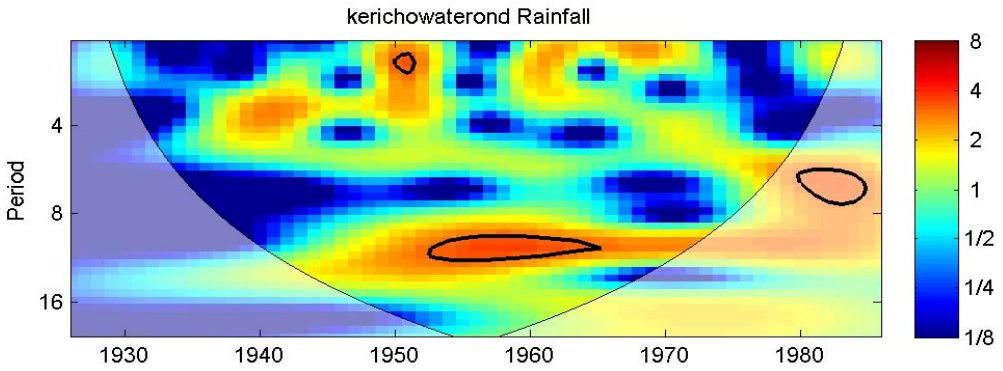
kerichowaterond Rainfall
Period
4
8
16
1930
1940
1950
1960
1970
1980
8
4
2
1
1/2
1/4
1/8

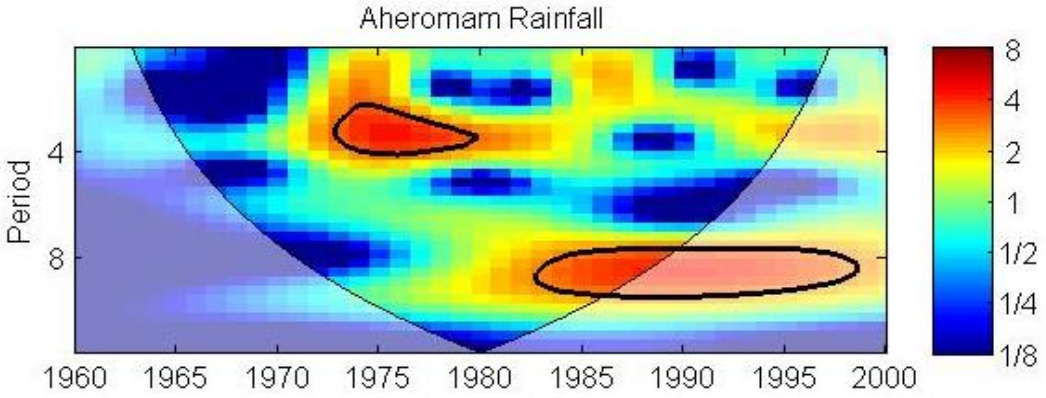
Aheromam Rainfall
Period
4
8
1960
1965
1970
1975
1980
1985
1990
1995
2000
8
4
2
1
1/2
1/4
1/8

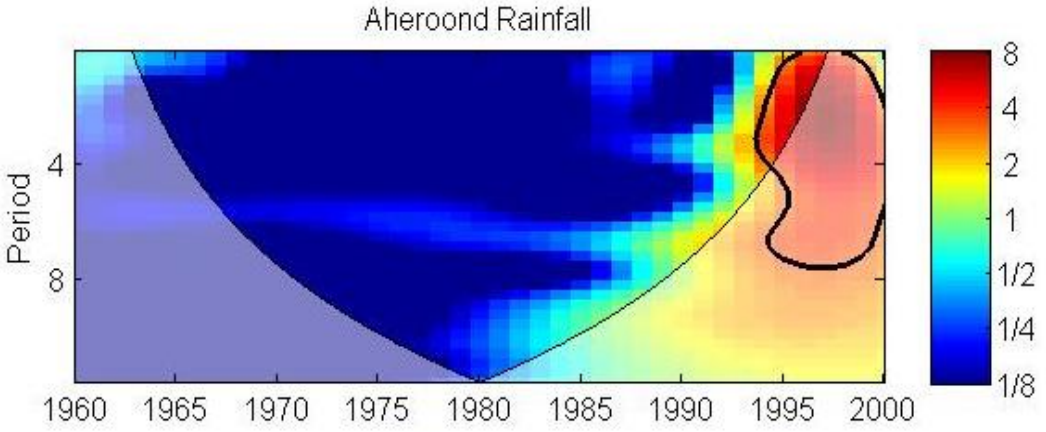
Aheroond Rainfall
Period
4
8
1960
1965
1970
1975
1980
1985
1990
1995
2000
8
4
2
1
1/2
1/4
1/8

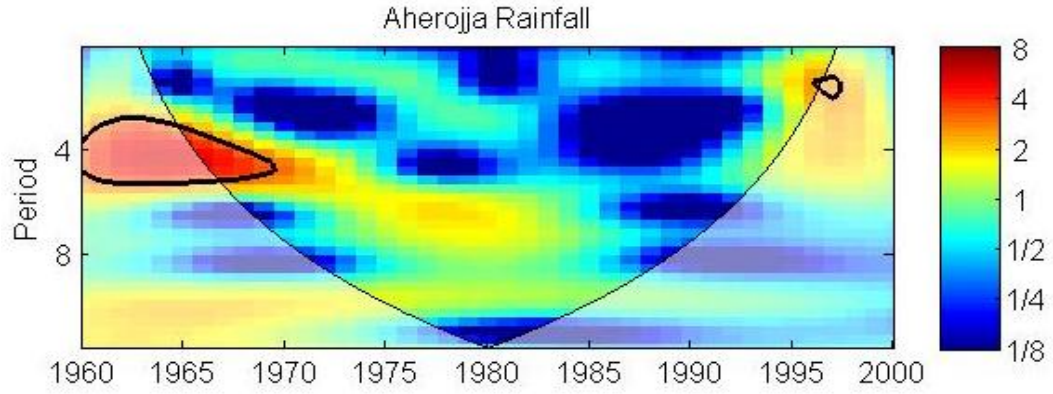
Aherojja Rainfall
Period
4
8
1960
1965
1970
1975
1980
1985
1990
1995
2000
8
4
2
1
1/2
1/4
1/8

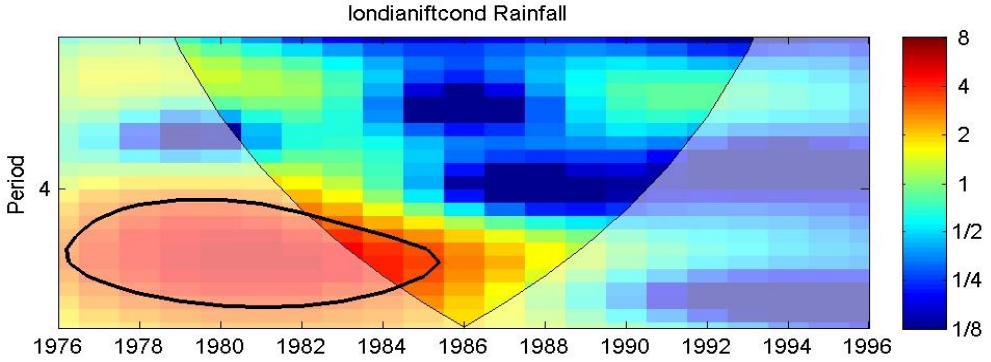
londianiftcond Rainfall
Period
4
1976
1978
1980
1982
1984
1986
1988
1990
1992
1994
1996
8
4
2
1
1/2
1/4
1/8

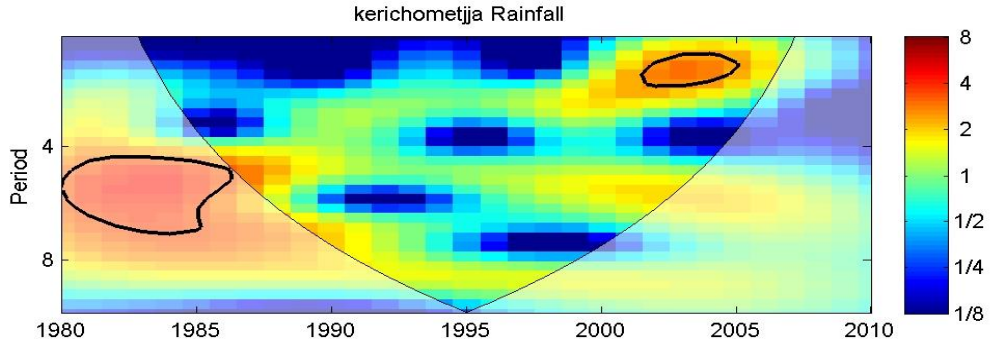
kerichometjja Rainfall
Period
4
8
1980
1985
1990
1995
2000
2005
2010
8
4
2
1
1/2
1/4
1/8

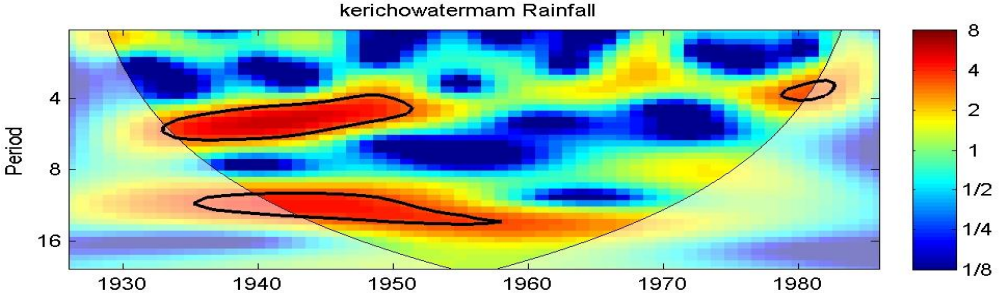
kerichowatermam Rainfall
Period
4
8
16
1930
1940
1950
1960
1970
1980
8
4
2
1
1/2
1/4
1/8

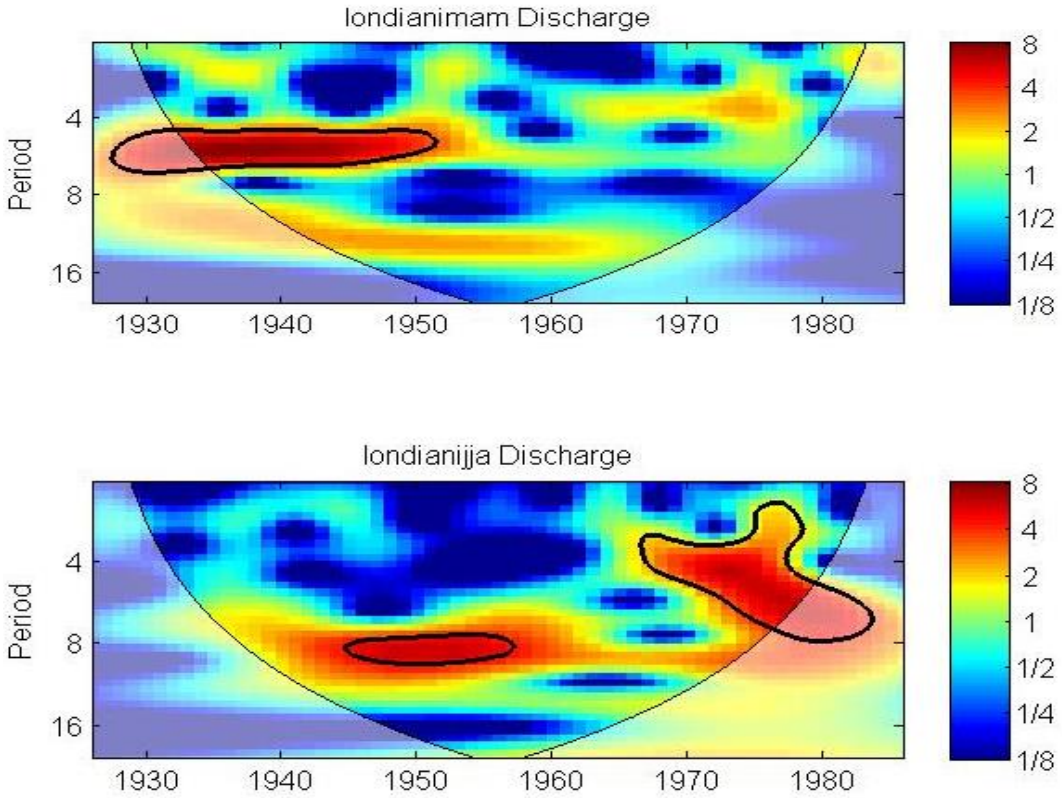
Iondianimam Discharge
Period
4
8
16
1930
1940
1950
1960
1970
1980
8
4
2
1
1/2
1/4
1/8
Iondianijja Discharge
Period
4
8
16
1930
1940
1950
1960
1970
1980
8
4
2
1
1/2
1/4
1/8

Appendix 9B: Streamflow wavelet spectral results

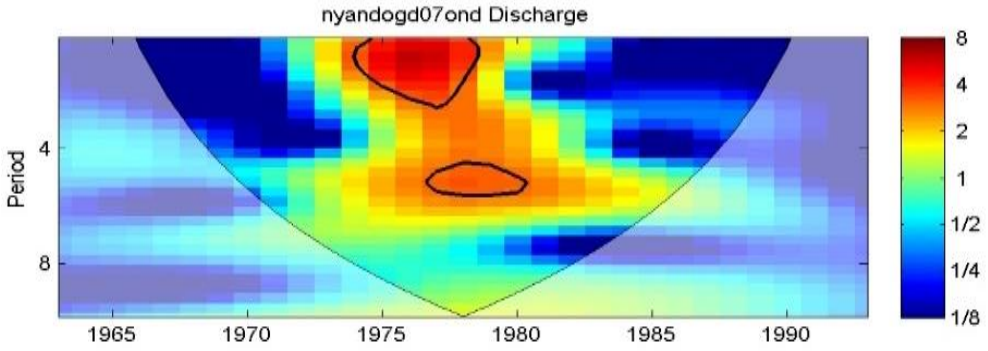

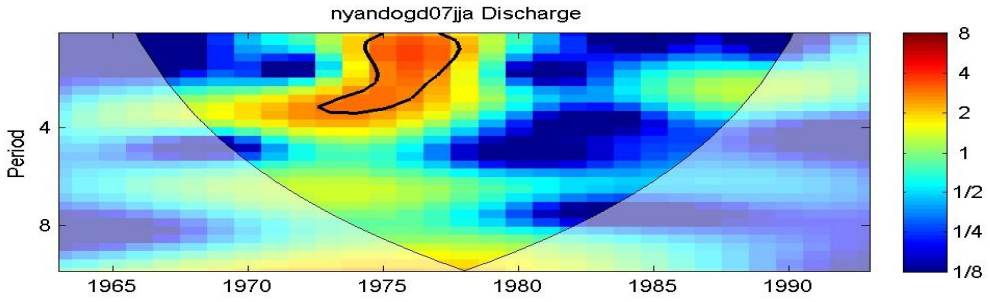

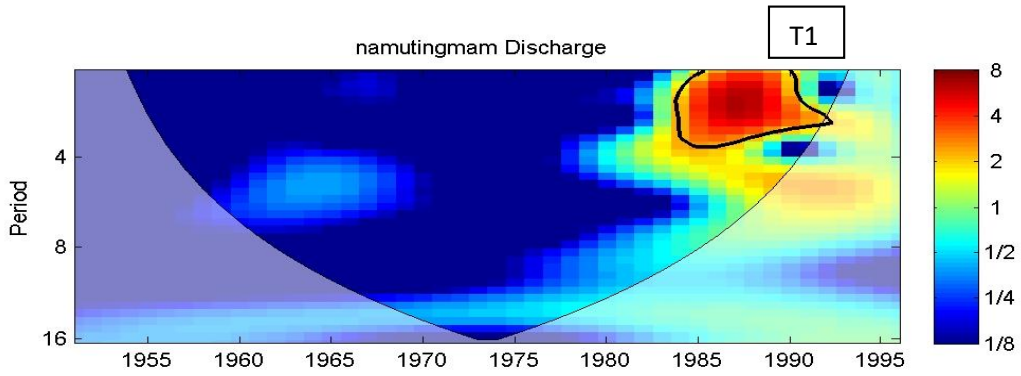

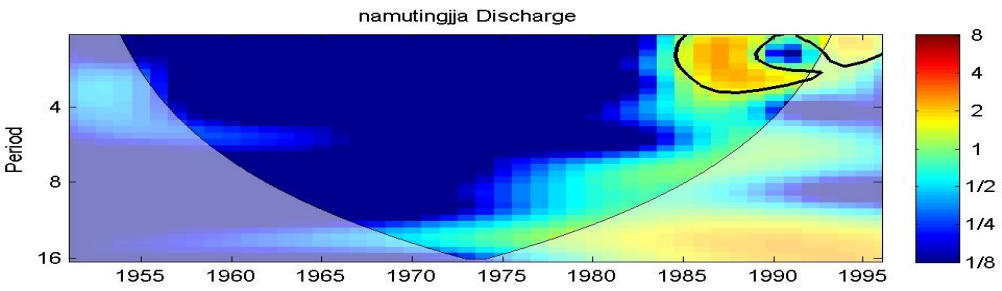

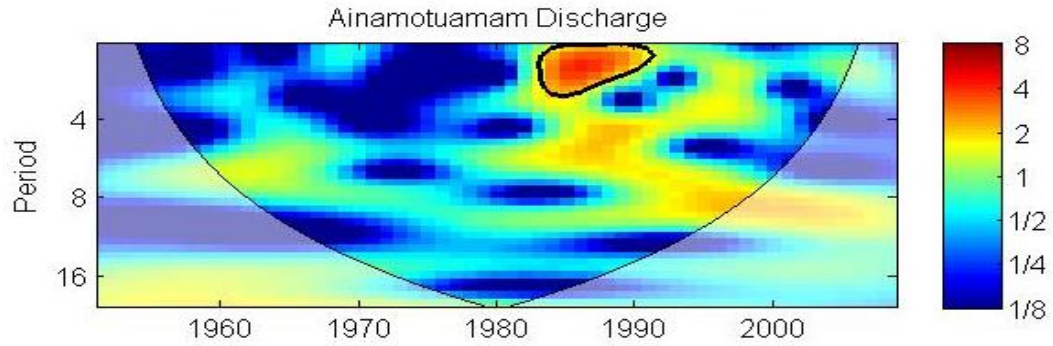
Ainamotuamam Discharge
Period
4
8
16
1960
1970
1980
1990
2000
8
4
2
1
1/2
1/4
1/8

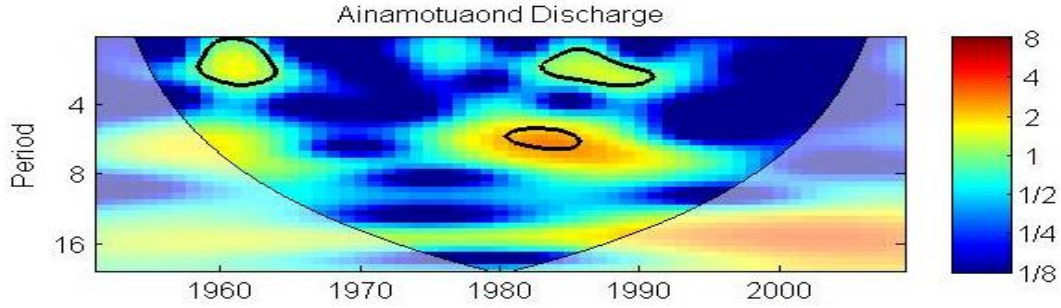
Ainamotuaond Discharge
Period
4
8
16
1960
1970
1980
1990
2000
8
4
2
1
1/2
1/4
1/8

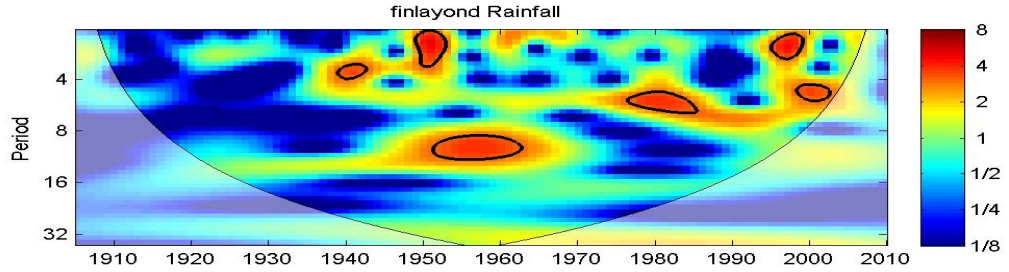
finlayond Rainfall
Period
4
8
16
32
1910
1920
1930
1940
1950
1960
1970
1980
1990
2000
2010
8
4
2
1
1/2
1/4
1/8

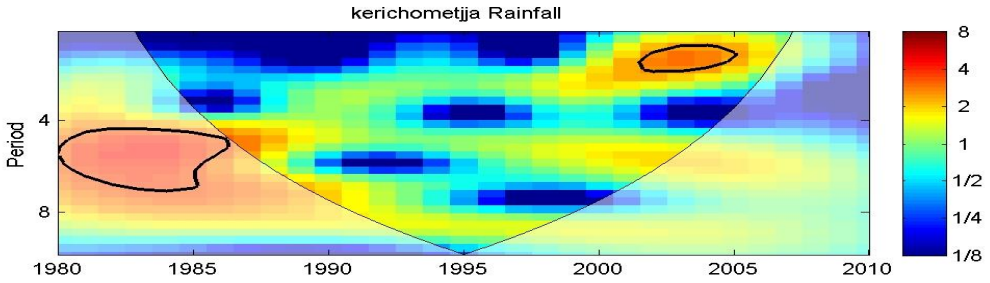
kerichometjja Rainfall
Period
4
8
1980
1985
1990
1995
2000
2005
2010
8
4
2
1
1/2
1/4
1/8

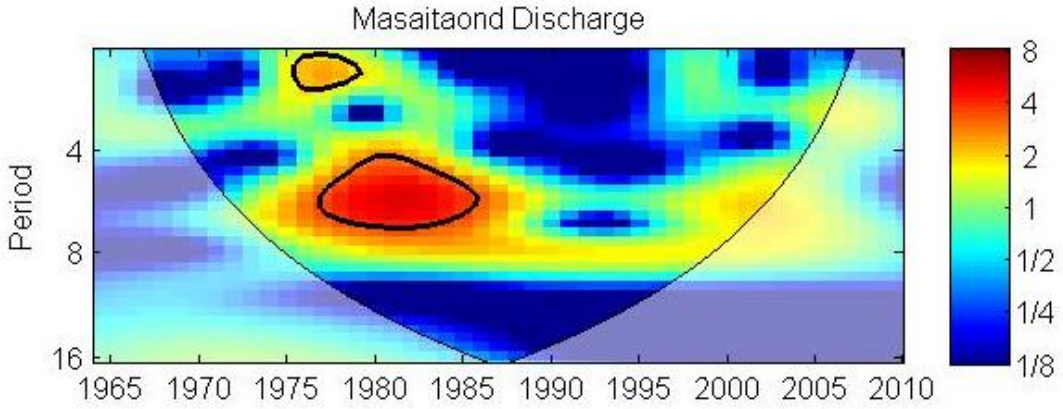
Masaitaond Discharge
Period
4
8
16
1965
1970
1975
1980
1985
1990
1995
2000
2005
2010
8
4
2
1
1/2
1/4
1/8

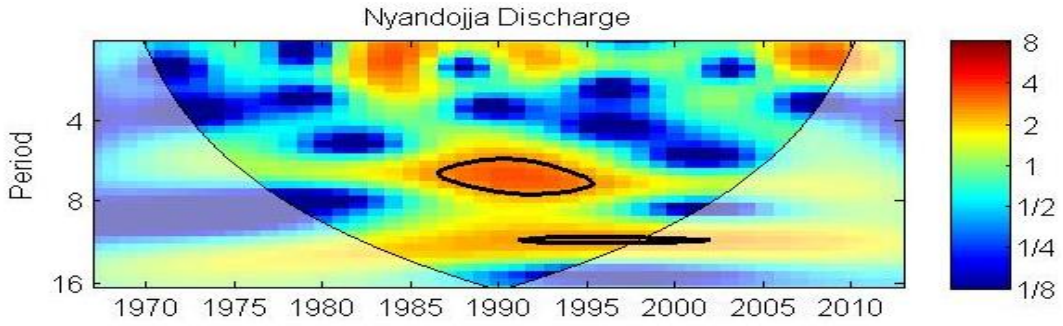
Nyandojja Discharge
Period
4
8
16
1970
1975
1980
1985
1990
1995
2000
2005
2010
8
4
2
1
1/2
1/4
1/8

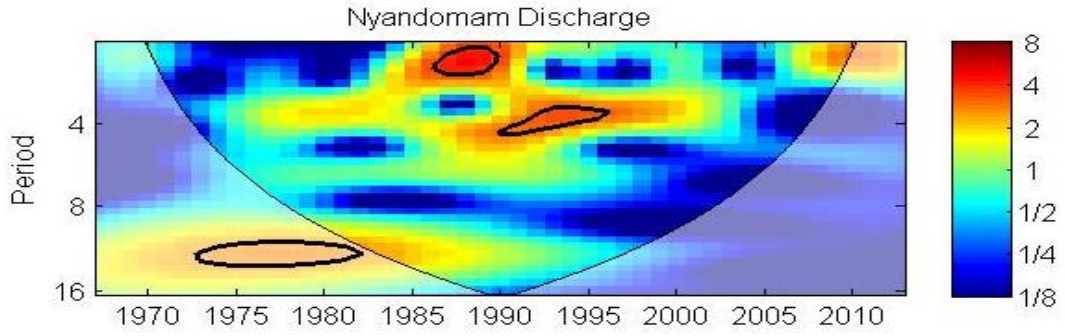
Nyandomam Discharge
Period
4
8
16
1970 1975 1980 1985 1990 1995 2000 2005 2010
8
4
2
1
1/2
1/4
1/8

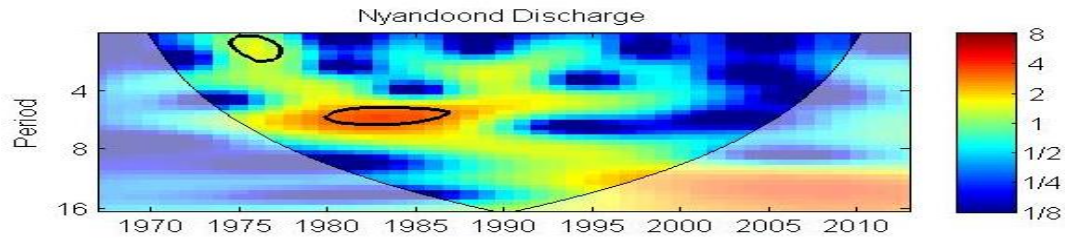
Nyandoond Discharge
Period
4
8
16
1970 1975 1980 1985 1990 1995 2000 2005 2010
8
4
2
1
1/2
1/4
1/8

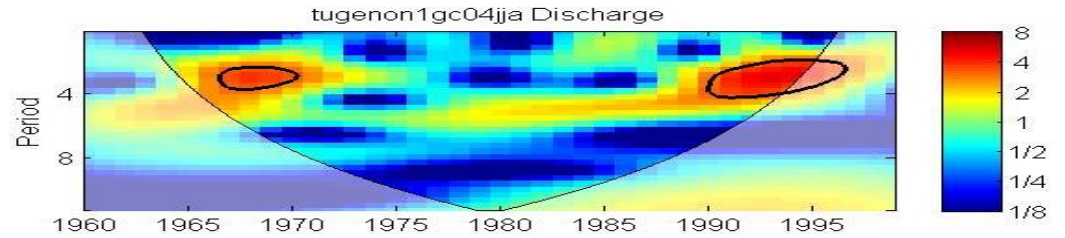
tugenon1gc04jja Discharge
Period
4
8
1960 1965 1970 1975 1980 1985 1990 1995
8
4
2
1
1/2
1/4
1/8

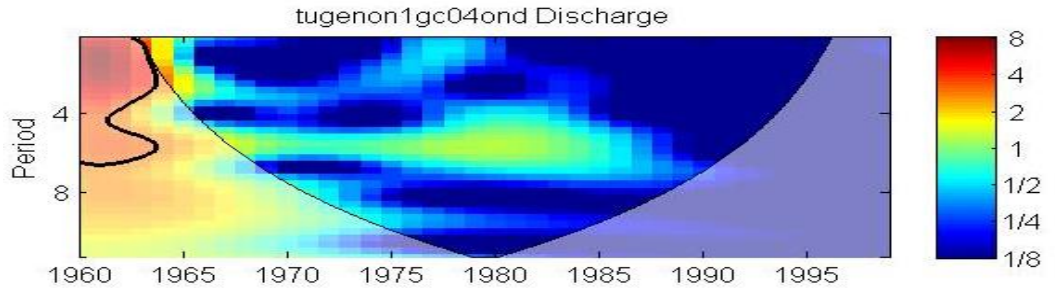
tugenon1gc04ond Discharge
Period
4
8
1960 1965 1970 1975 1980 1985 1990 1995
8
4
2
1
1/2
1/4
1/8

Appendix 9C: Cross wavelet results

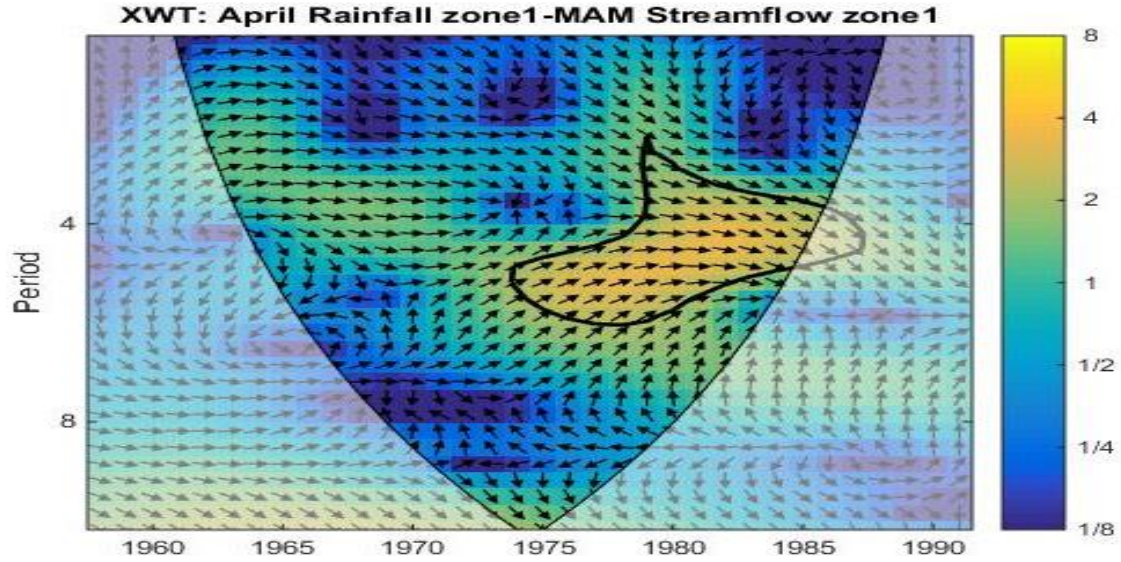

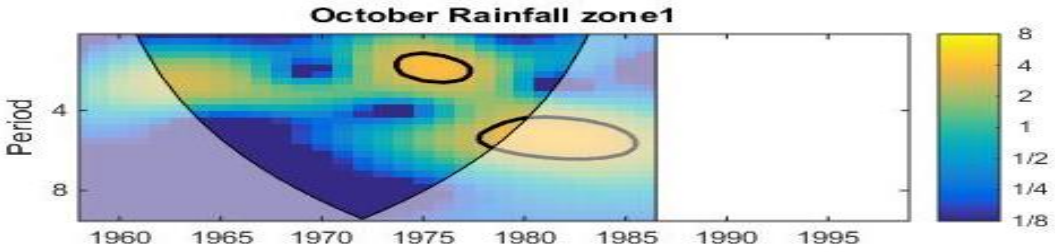

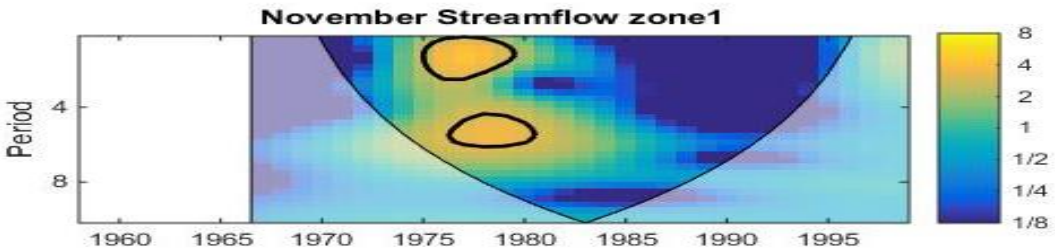

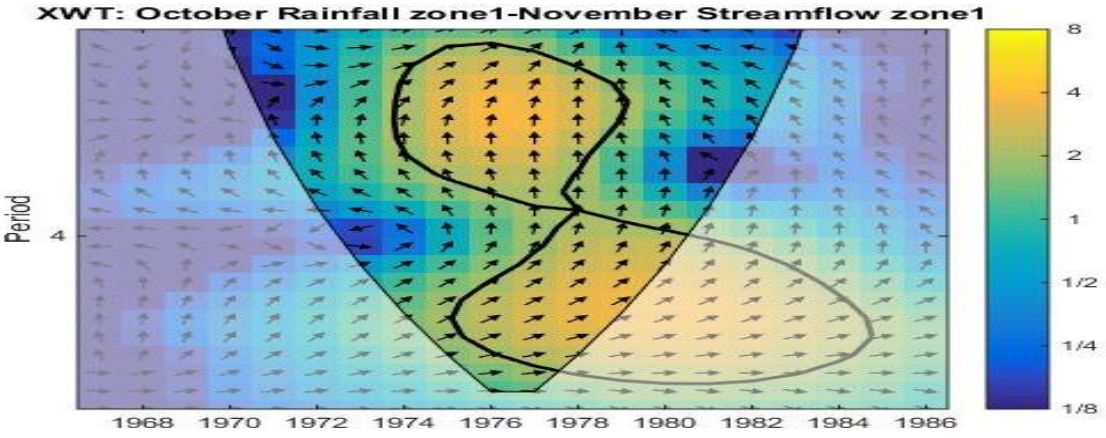

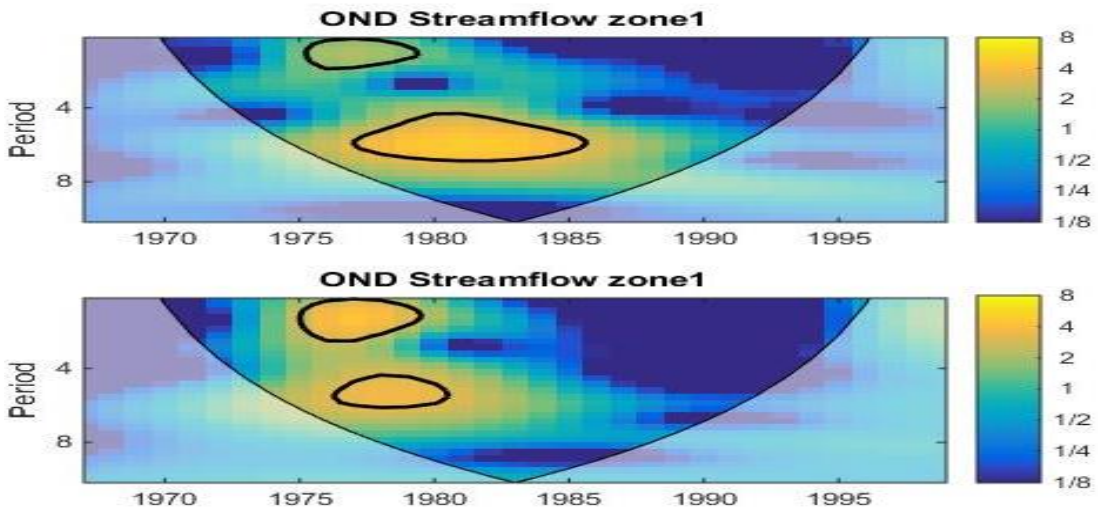
OND Streamflow zone1
Period
4
8
1970
1975
1980
1985
1990
1995
8
4
2
1
1/2
1/4
1/8
OND Streamflow zone1
Period
4
8
1970
1975
1980
1985
1990
1995
8
4
2
1
1/2
1/4
1/8

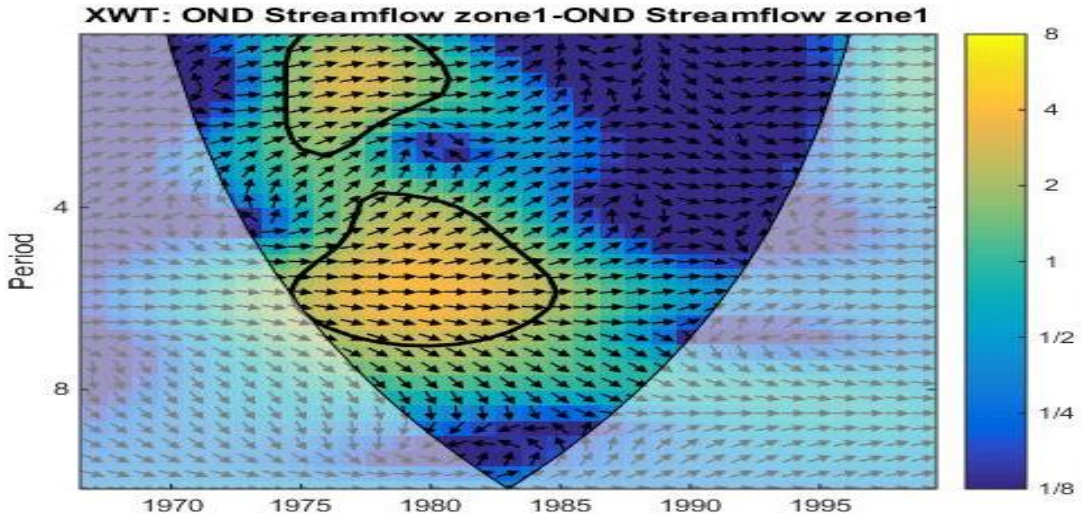
XWT: OND Streamflow zone1-OND Streamflow zone1
Period
4
8
1970
1975
1980
1985
1990
1995
8
4
2
1
1/2
1/4
1/8

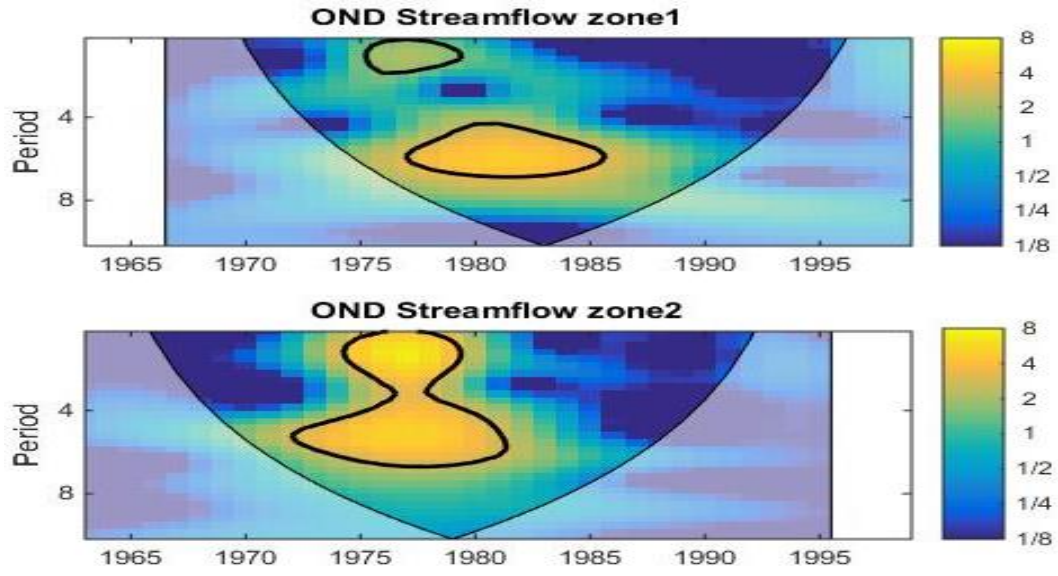
OND Streamflow zone1
Period
4
8
1965
1970
1975
1980
1985
1990
1995
8
4
2
1
1/2
1/4
1/8
OND Streamflow zone2
Period
4
8
1965
1970
1975
1980
1985
1990
1995
8
4
2
1
1/2
1/4
1/8

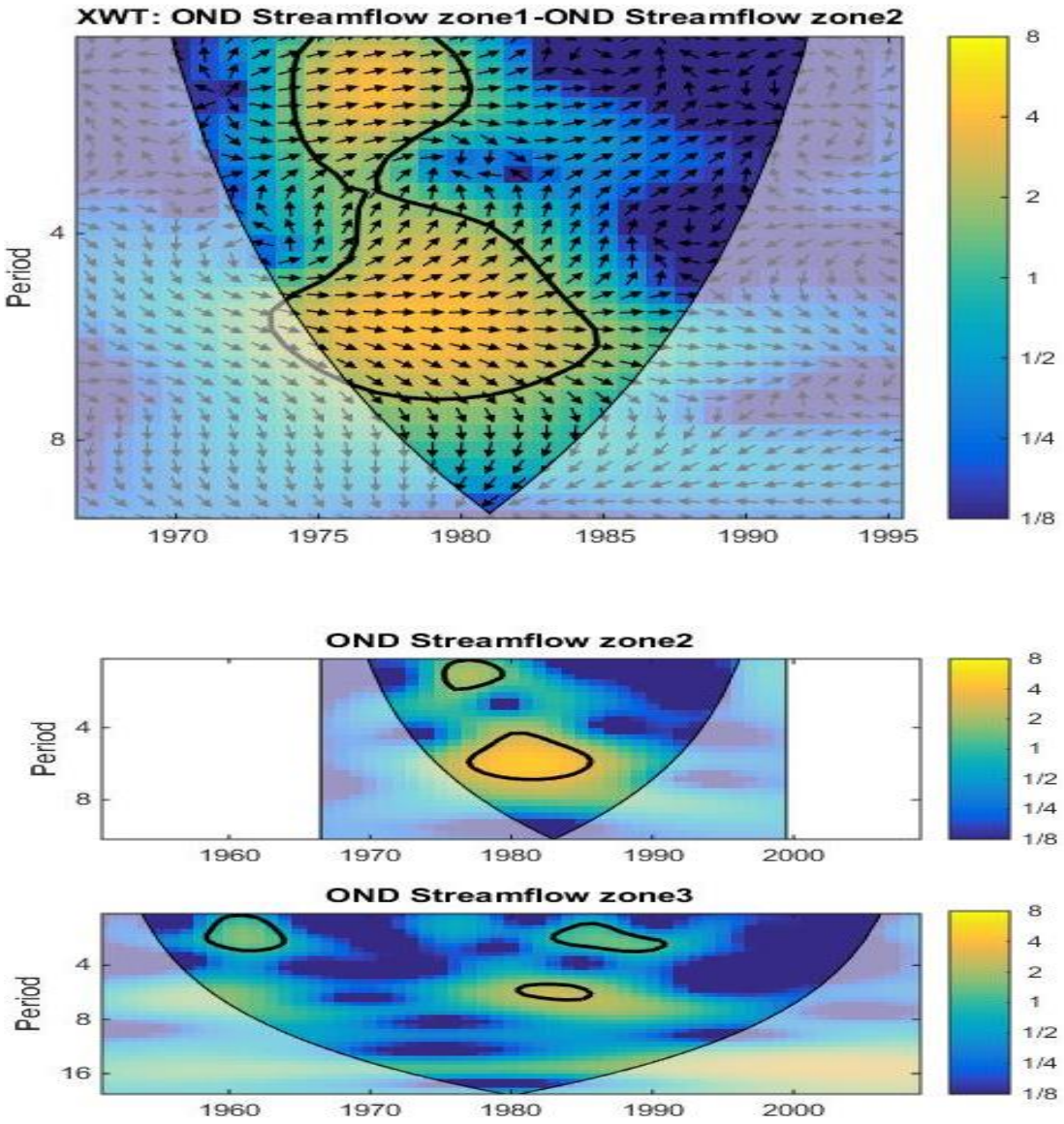
XWT: OND Streamflow zone1-OND Streamflow zone2
Period
4
8
1970
1975
1980
1985
1990
1995
8
4
2
1
1/2
1/4
1/8
OND Streamflow zone2
Period
4
8
1960
1970
1980
1990
2000
8
4
2
1
1/2
1/4
1/8
OND Streamflow zone3
Period
4
8
16
1960
1970
1980
1990
2000
8
4
2
1
1/2
1/4
1/8

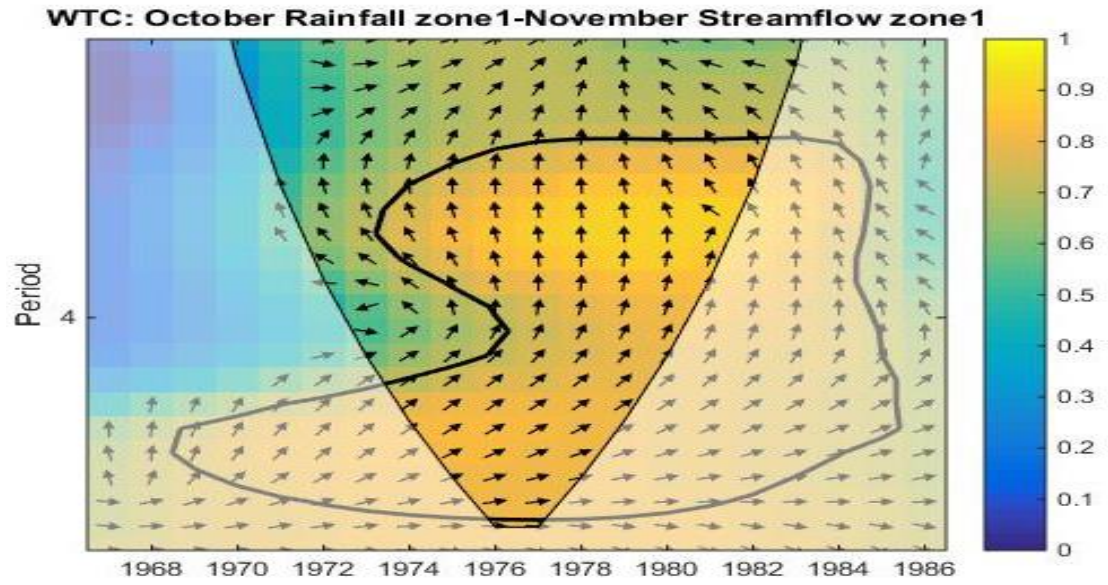
WTC: October Rainfall zone1-November Streamflow zone1
Period
4
1968 1970 1972 1974 1976 1978 1980 1982 1984 1986
1
0.9
0.8
0.7
0.6
0.5
0.4
0.3
0.2
0.1
0

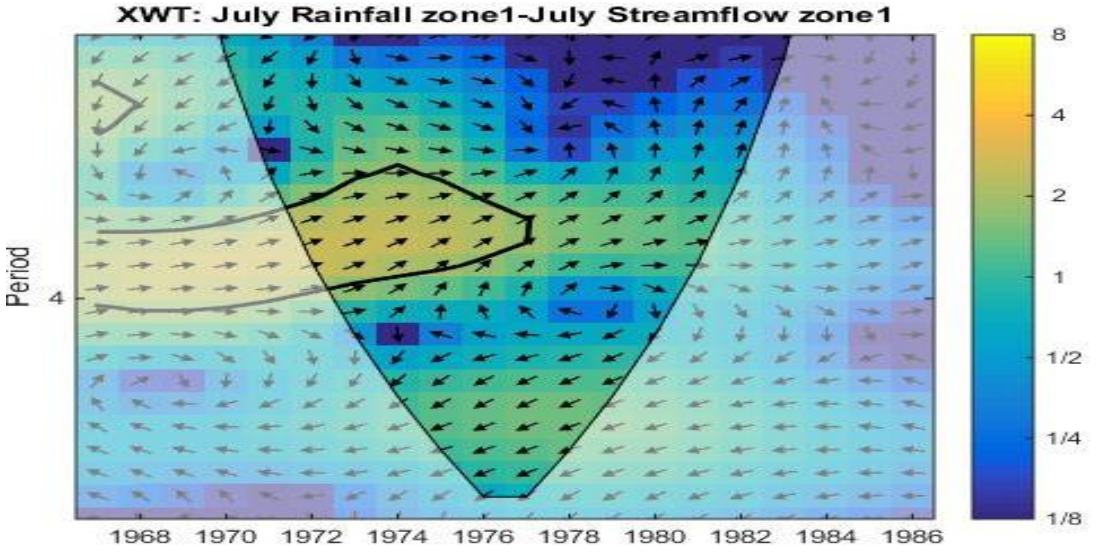
XWT: July Rainfall zone1-July Streamflow zone1
Period
4
1968 1970 1972 1974 1976 1978 1980 1982 1984 1986
8
4
2
1
1/2
1/4
1/8

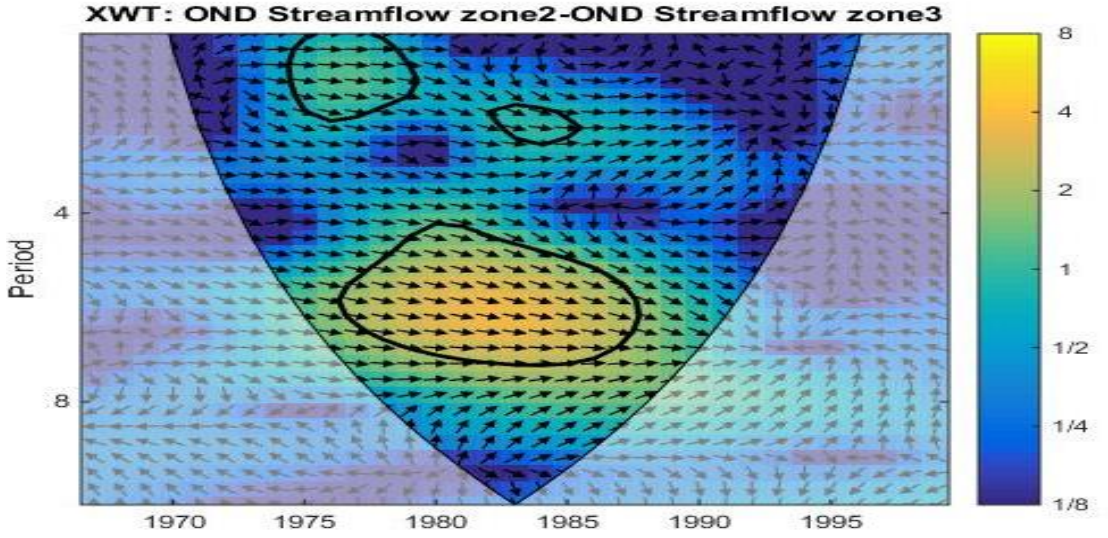
XWT: OND Streamflow zone2-OND Streamflow zone3
Period
4
8
1970 1975 1980 1985 1990 1995
8
4
2
1
1/2
1/4
1/8

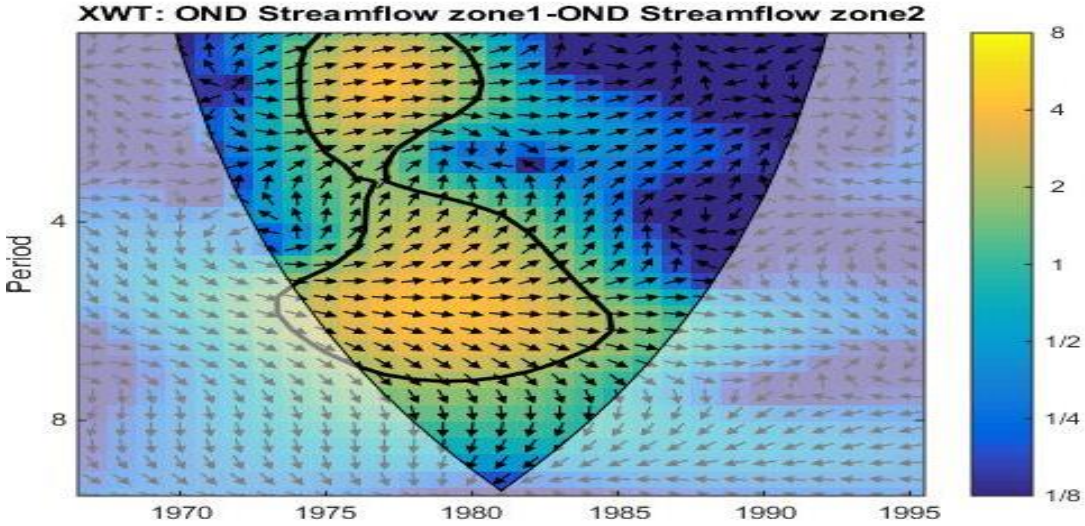
XWT: OND Streamflow zone1-OND Streamflow zone2
Period
4
8
1970
1975
1980
1985
1990
1995
8
4
2
1
1/2
1/4
1/8

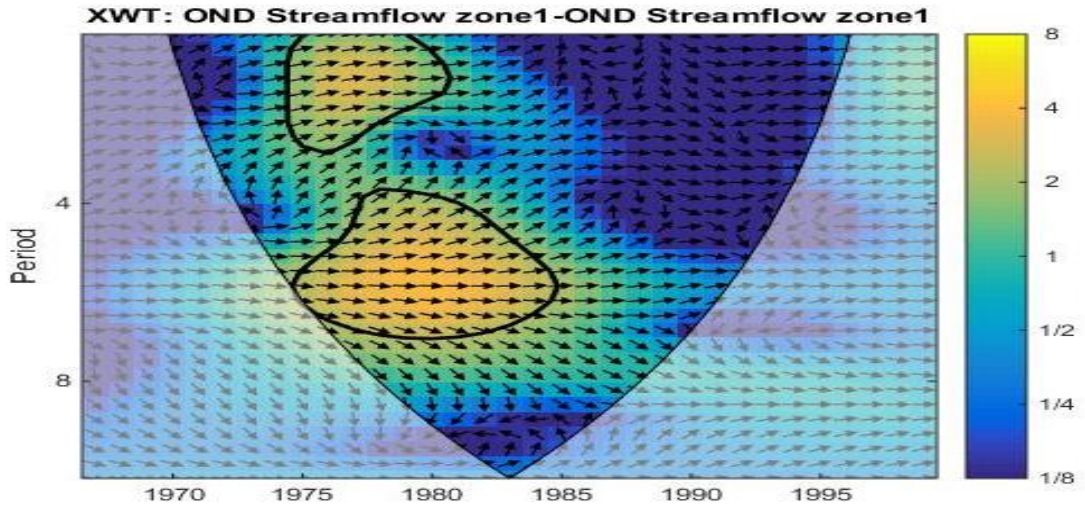
XWT: OND Streamflow zone1-OND Streamflow zone1
Period
4
8
1970
1975
1980
1985
1990
1995
8
4
2
1
1/2
1/4
1/8

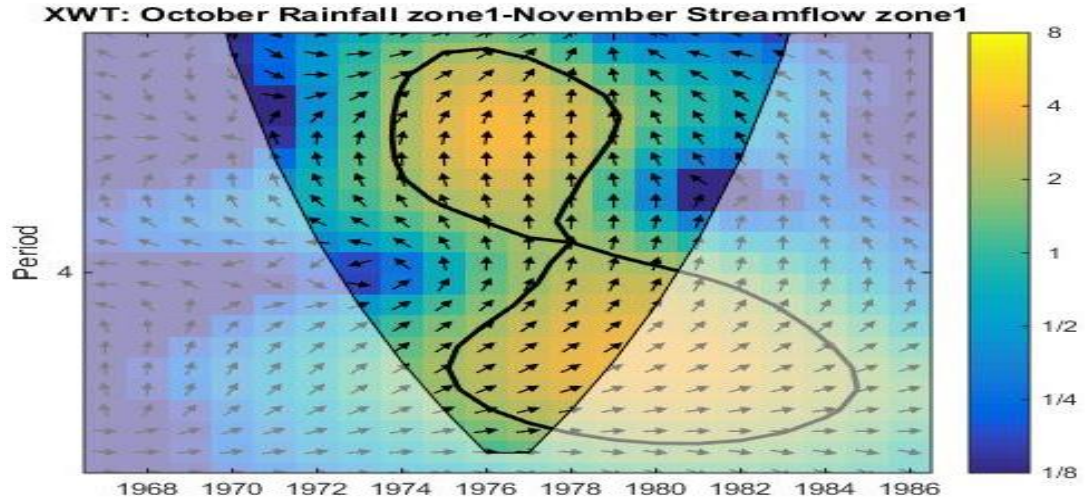
XWT: October Rainfall zone1-November Streamflow zone1
Period
4
1968
1970
1972
1974
1976
1978
1980
1982
1984
1986
8
4
2
1
1/2
1/4
1/8

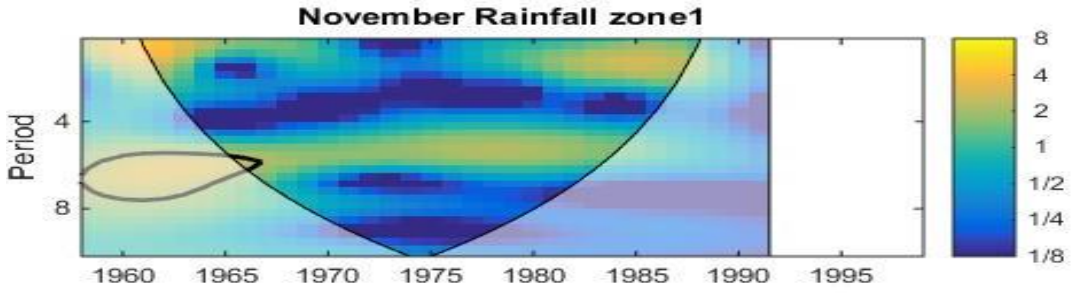
November Rainfall zone1
Period
4
8
1960
1965
1970
1975
1980
1985
1990
1995
8
4
2
1
1/2
1/4
1/8

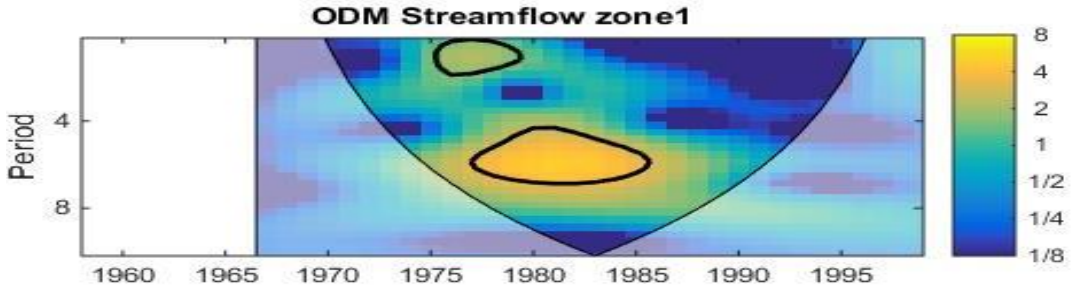
ODM Streamflow zone1
Period
4
8
1960
1965
1970
1975
1980
1985
1990
1995
8
4
2
1
1/2
1/4
1/8

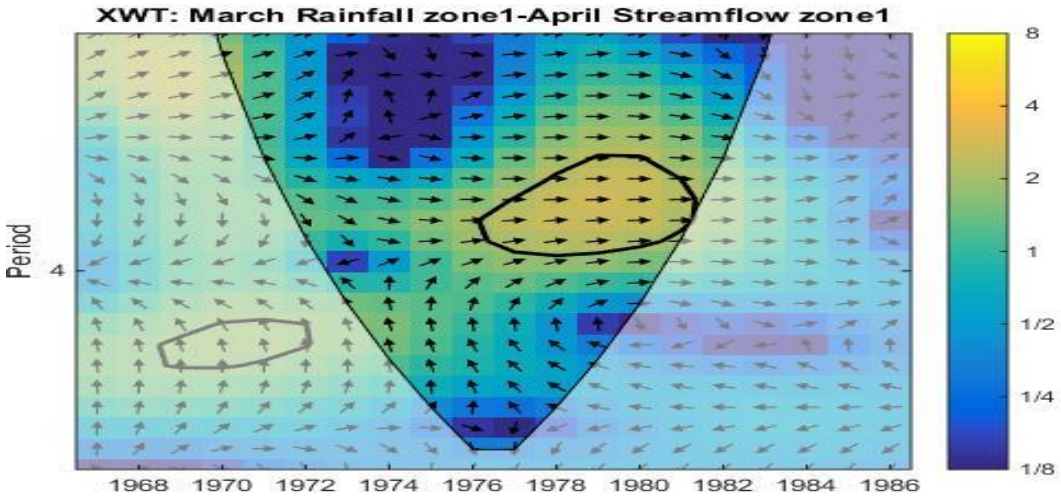
XWT: March Rainfall zone1-April Streamflow zone1
Period
4
1968
1970
1972
1974
1976
1978
1980
1982
1984
1986
8
4
2
1
1/2
1/4
1/8

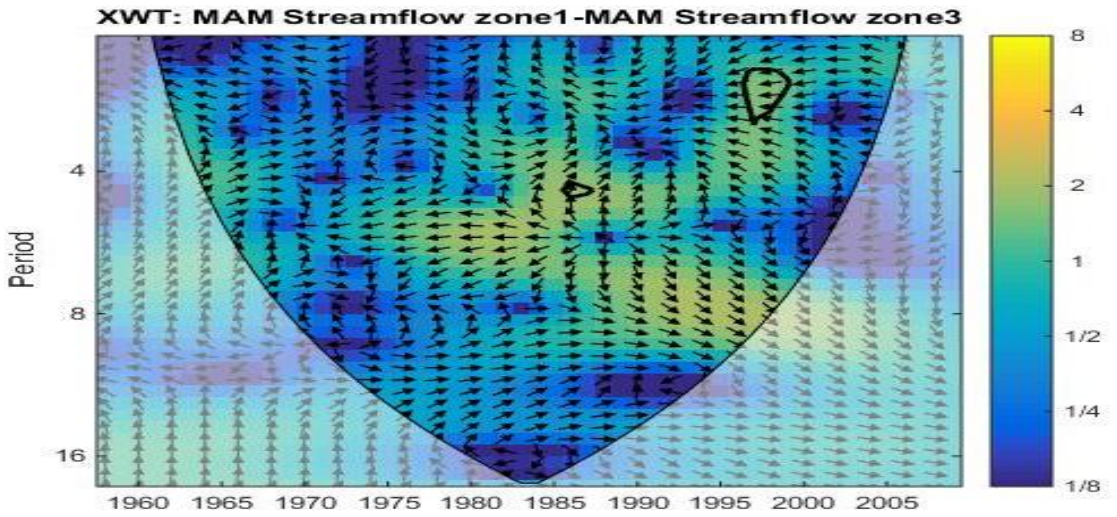

Appendix 9D: Wavelet Coherence

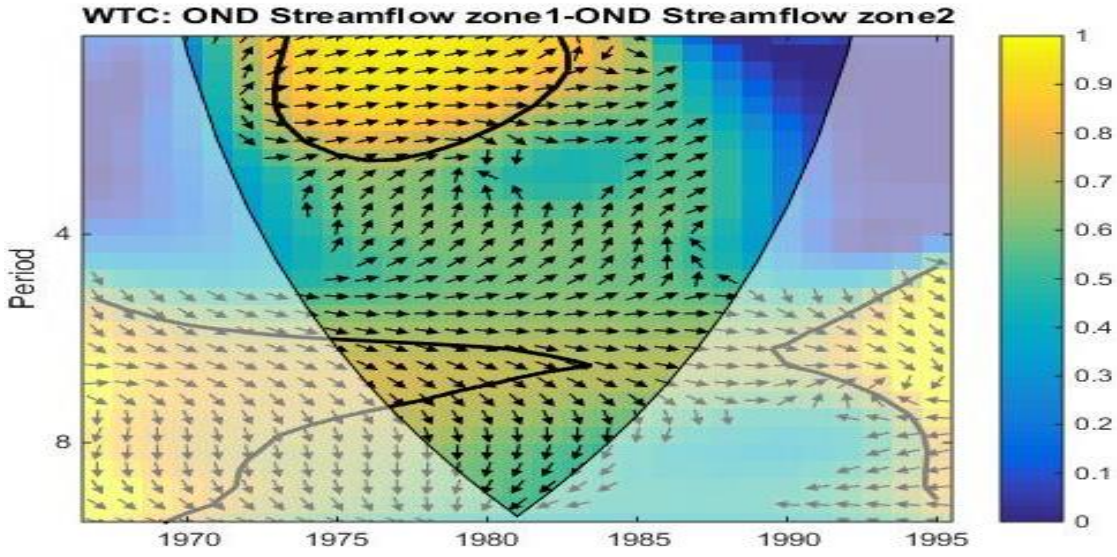

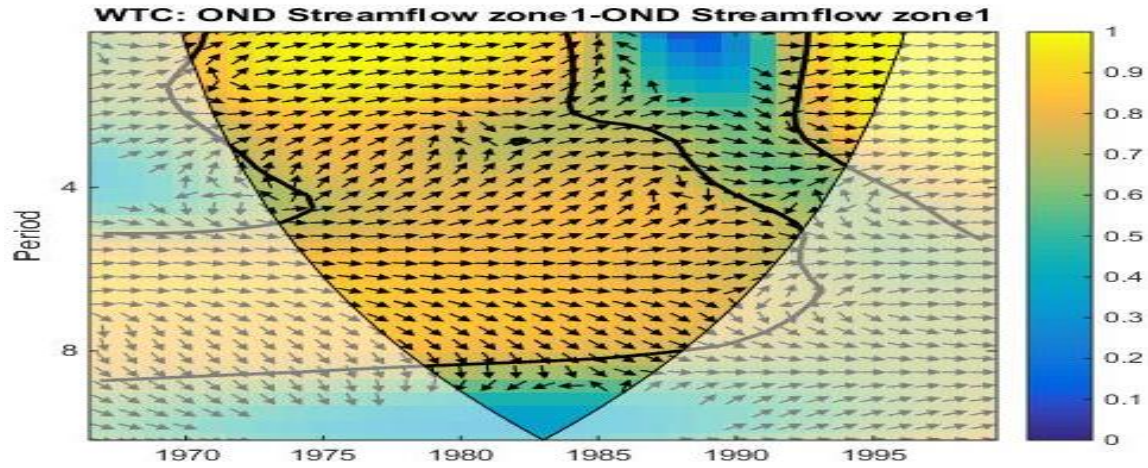

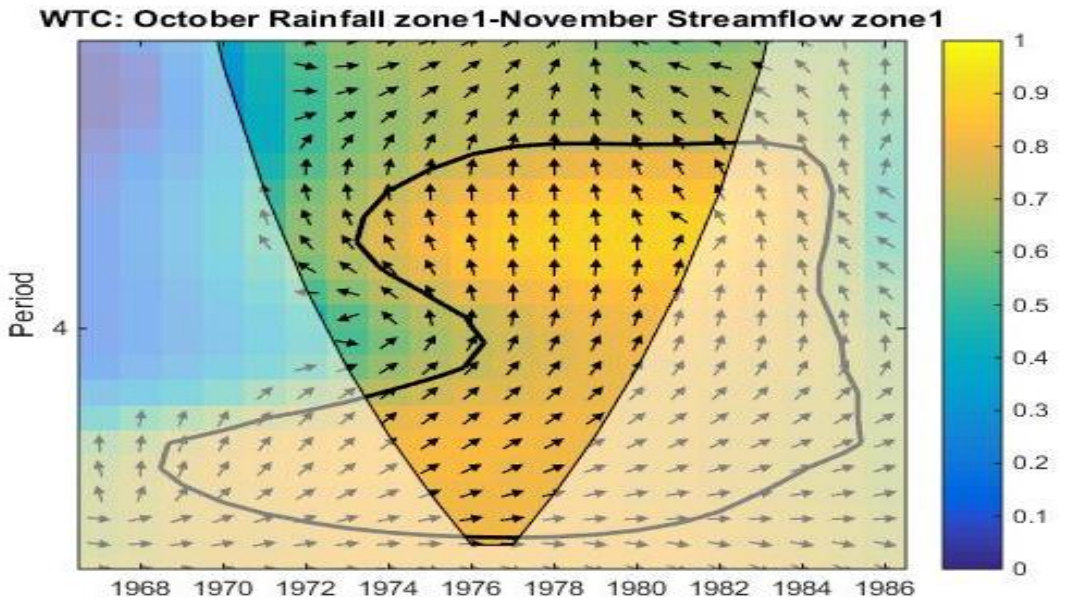
WTC: October Rainfall zone1-November Streamflow zone1
Period
4
1968 1970 1972 1974 1976 1978 1980 1982 1984 1986
1 0.9 0.8 0.7 0.6 0.5 0.4 0.3 0.2 0.1 0

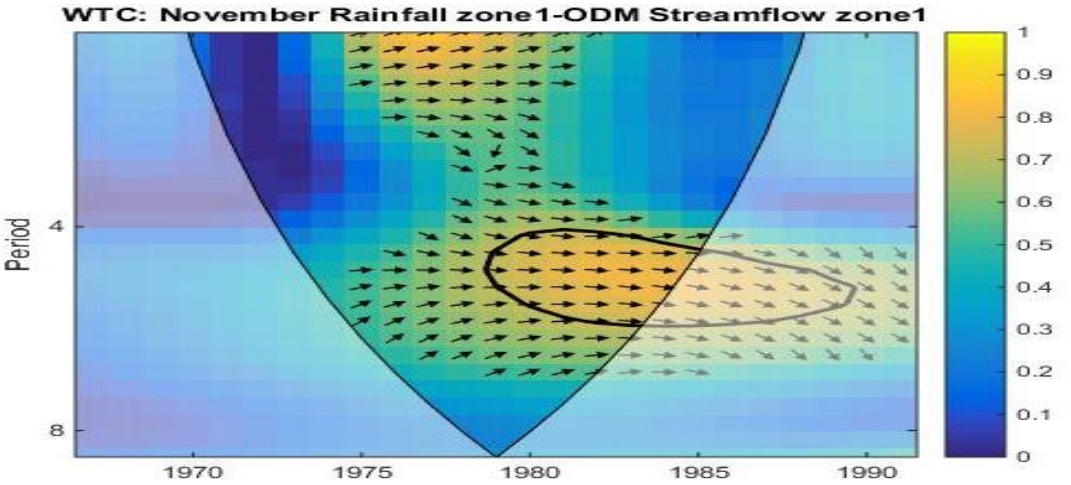
WTC: November Rainfall zone1-ODM Streamflow zone1
Period
4
8
1970 1975 1980 1985 1990
1 0.9 0.8 0.7 0.6 0.5 0.4 0.3 0.2 0.1 0

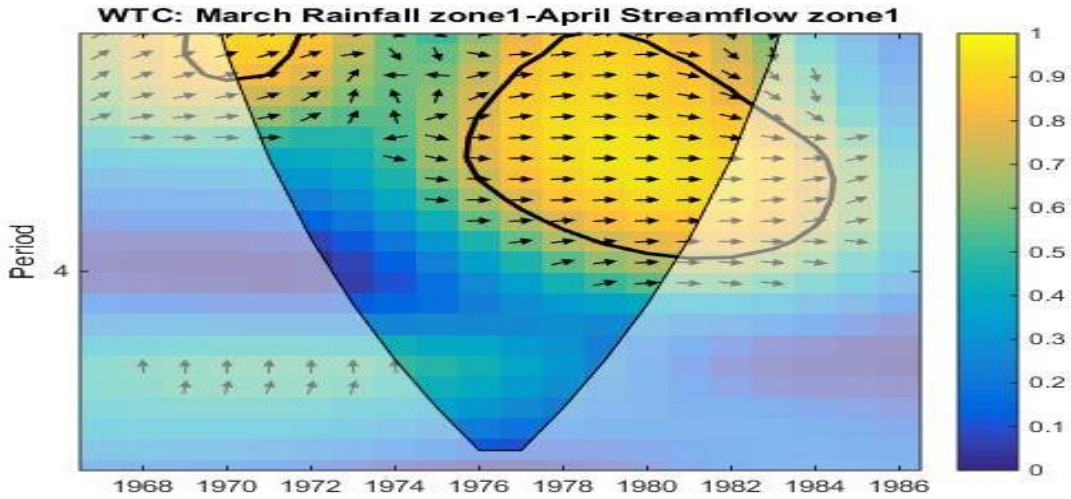
WTC: March Rainfall zone1-April Streamflow zone1
Period
4
1968 1970 1972 1974 1976 1978 1980 1982 1984 1986
1 0.9 0.8 0.7 0.6 0.5 0.4 0.3 0.2 0.1 0

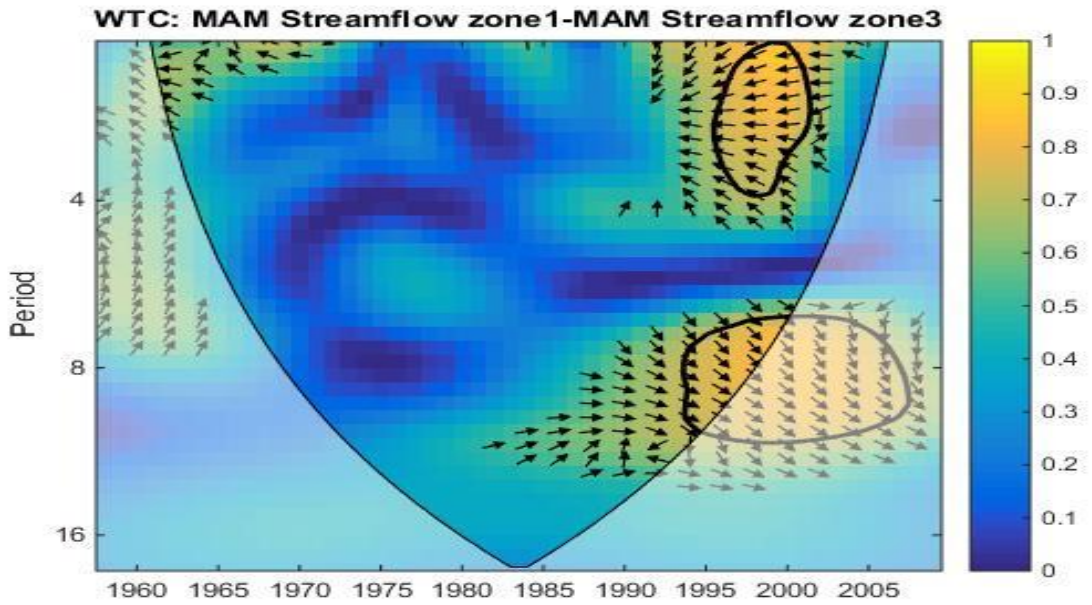
WTC: MAM Streamflow zone1-MAM Streamflow zone3
Period
4
8
16
1960 1965 1970 1975 1980 1985 1990 1995 2000 2005
1 0.9 0.8 0.7 0.6 0.5 0.4 0.3 0.2 0.1 0

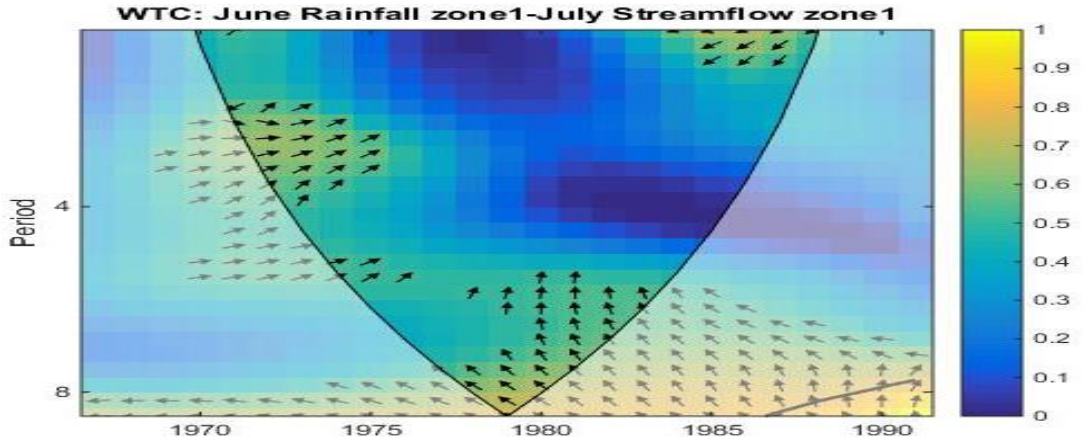
WTC: June Rainfall zone1-July Streamflow zone1
Period
4
8
1970 1975 1980 1985 1990
1 0.9 0.8 0.7 0.6 0.5 0.4 0.3 0.2 0.1 0

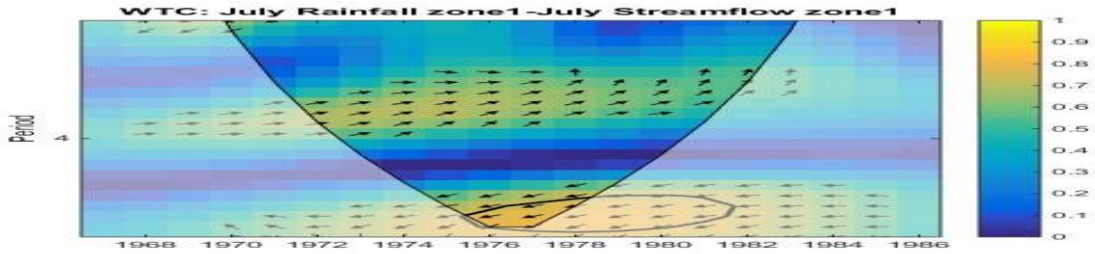
WTC: July Rainfall zone1-July Streamflow zone1
Period
4
1968 1970 1972 1974 1976 1978 1980 1982 1984 1986
1 0.9 0.8 0.7 0.6 0.5 0.4 0.3 0.2 0.1 0

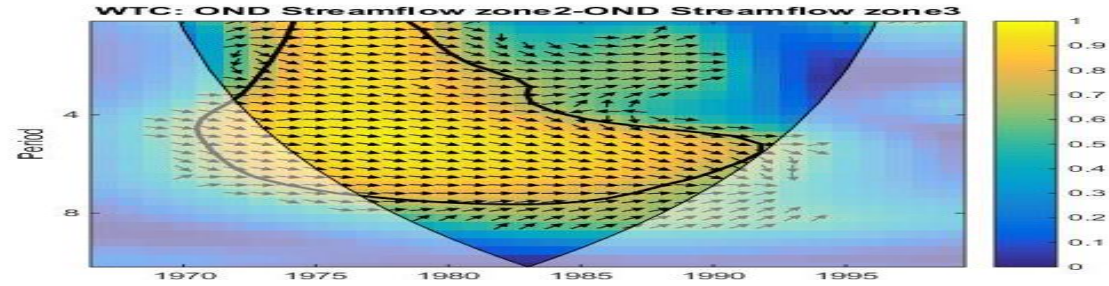
WTC: OND Streamflow zone2-OND Streamflow zone3
Period
4
8
1970 1975 1980 1985 1990 1995
1 0.9 0.8 0.7 0.6 0.5 0.4 0.3 0.2 0.1 0

Appendix 10A: Rainfall annual maximum series

Year	Chem	Finlay	K. Met	K. Water	LOND	Nandi	Kip	Ahero	Tinga	Timbilil
1960		414.6		283.8	195.3	341.4	168.1	176.4	168.1	267.1
1961		438.0		444.6	371.6	374.9	349.6	300.7	349.0	456.6
1962		441.0		291.9	168.6	262.3	277.8	278.3	277.8	305.3
1963		342.8		373.9	249.9	398.1	338.3	224.4	338.3	324.6
1964		469.7		439.7	279.8	299.6	247.5	224.7	247.5	465.9
1965		244.9		276.3	165.8	218.3	212.5	170.9	212.5	254.1
1966	198.1	295.3		331.5	244.3	233.2	317.3	259.7	317.3	296.6
1967	359.9	454.8		395.9	246.4	352.5	262.7	221.4	262.7	455.0
1968	289.8	345.2		417.4	334.4	278.9	321.1	235.0	321.1	345.2
1969	325.9	298.0		229.4	140.5	207.3	177.9	174.8	177.9	192.0
1970	221.3	345.2		343.8	222.2	282.8	283.4	221.8	283.4	345.2
1971	293.3	360.5		358.0	197.8	284.6	288.3	221.0	288.3	360.5
1972	314.9	320.4		317.9	161.1	222.2	224.3	219.6	224.3	320.4
1973	251.5	262.9		305.7	201.5	257.9	231.1	251.8	231.1	262.9
1974	340.4	287.6	267.8	328.5	221.3	221.5	219.1	282.9	219.1	289.8
1975	217.3	402.6	433.1	261.5	335.9	277.9	217.5	233.1	217.5	422.1
1976	299.3	482.7	507.6	457.8	147.0	208.1	189.7	144.1	189.0	482.8
1977	275.1	306.4	300.6	301.5	164.3	223.4	320.1	240.7	320.1	306.4
1978	266.0	313.2	309.5	334.3	195.4	243.3	188.9	234.1	188.9	325.2
1979	292.2	315.3	312.4	248.5	169.9	266.5	252.9	224.8	252.9	315.3
1980	217.2	302.5	316.1	256.4	194.2	280.2	327.3	179.5	327.3	302.5
1981	208.9	357.8	372.2	320.3	206.1	224.7	253.2	252.5	253.2	357.3
1982	238.3	430.9	458.6	458.5	275.7	252.9	214.8	198.9	214.8	430.9
1983	262.1	359.8	397.7	269.2	180.8	231.7	259.9	217.1	259.9	360.9
1984	183.0	259.6	266.2	284.6	136.2	208.4	178.7	170.6	178.7	259.6
1985	361.8	434.5	401.9	433.2	183.0	245.2	273.5	257.5	273.5	411.5
1986	170.5	362.1	387.7	276.2	143.0	240.3	206.6	255.8	234.4	362.1
1987	223.9	446.9	244.8	244.8		275.5	202.3	203.6	202.0	447.7
1988	376.2	374.8	362.0	362.0		295.4	280.8	371.5	280.8	374.8
1989	276.4	385.5	439.4	439.4			215.1	197.3	215.1	385.5
1990	330.3	447.9	255.9	256.5			284.5	185.9	284.5	447.9
1991	260.6	342.6	369.4	369.4			175.5	222.4	175.0	342.6
1992	215.7	294.3	260.5	260.5				181.3		295.9
1993	249.1	357.9	280.2	282.2				155.7		357.9
1994	287.7	607.5	393.1	393.3				230.6		607.5
1995	277.4	301.6	224.6	224.6				212.9		291.6
1996	313.1	264.0	270.8	275.7				222.9		264.0
1997	355.0	436.5	391.1	391.1				721.3		1834.0
1998	226.9	285.5	326.9	276.9				314.9		2108.5
1999	206.0	250.9	298.4	298.4				234.4		211.1
2000	197.7	237.0	218.6	218.6				160.3		166.5
2001	290.6	345.5	445.4	452.5						
2002	256.0	360.7	358.9	358.9						
2003	200.4	341.6	342.4	335.5						
2004	394.2	347.9	288.6	288.6						
2005	204.3	351.0	261.8	261.8						
2006	333.7	421.4	369.3	368.7						
2007		391.0	335.6	335.6						
2008		344.5	294.0							
2009		311.9	301.1							

Year	Chem	Finlay	K. Met	K. Water	LOND	Nandi	Kip	Ahero	Tinga	Timbilil
2010		353.1	293.5							

Appendix 10B: Streamflow annual maximum series

Year	Ainamotua	1GD04	Ainopsiwa	MASAITA	Mbogo	1GD07	1GC06	Tugenon
1951	0.79				0.14			
1952	1.57				0.39			
1953	0.43				0.42			
1954	1.54				0.17			
1955	4.73				0.21			
1956	4.60	23.88			0.41			
1957	2.26	33.48			0.20			
1958	1.00	18.73			0.22			
1959	1.18	3.91			0.27			
1960	2.39	8.13	0.91		0.72			0.21
1961	8.86	35.79	1.21		0.50			2.15
1962	6.69	29.19	1.43		0.66			0.94
1963	6.85	27.30	1.45		0.53	29.21		1.57
1964	3.63	22.35	1.22	51.35	0.28	11.64		0.43
1965	0.80	2.53	0.17	17.42	0.11	1.542		0.05
1966	2.51	8.52	0.75	35.97	0.35	4.33		0.17
1967	2.59	11.79	0.45	42.09	0.37	5.27	1.75	1.23
1968	4.52	12.11	0.90	75.52	0.67	13.15	1.91	1.19
1969	1.22	4.81	0.27	12.52	0.30	2.17	0.97	0.15
1970	3.65	9.45	0.61	53.32	0.92	7.87	2.11	1.09
1971	4.21	9.93	1.31	44.88	0.52	6.27	1.92	0.72
1972	2.52	7.44	0.78	22.67	0.71	4.04	1.81	0.16
1973	2.12	6.38	0.27	35.75	0.36	11.64	1.92	0.54
1974	2.68	9.38	0.57	35.16	0.79	13.57	2.96	0.48
1975	5.84	14.37	1.28	54.85	1.16	35.09	2.39	0.39
1976	1.94	4.91	0.88	27.06	0.65	2.58	2.21	0.23
1977	5.51	15.53	2.24	57.52	1.18	44.28	2.89	0.64
1978	3.73	9.61	0.82	38.84	1.195	32.59	2.38	0.35
1979	5.50	17.08	7.81	25.32	1.15	12.96	2.64	0.45
1980	2.26	6.19	0.73	26.46	0.60	4.71	1.64	0.34
1981	3.57	12.60	1.09	43.37	1.42	7.51	2.38	0.88
1982	7.19	12.56	2.15	53.93	4.30	4.10	2.13	0.47
1983	6.92	10.45	2.24	41.21	2.73	1.94	3.05	0.71
1984	1.86	3.21	1.27	16.79	1.57	6.33	0.67	0.11
1985	9.04	5.20	3.20	15.44	4.11	1.99	3.00	0.54
1986	2.61	3.16	0.67	11.30	2.93	5.26	1.01	0.34
1987	2.95	4.17	0.88	10.67	2.99	15.97	1.71	0.44
1988	7.23	7.19	2.79	29.95		4.87	2.60	0.70
1989	5.59	8.64	1.82	15.92		17.46	4.60	0.23
1990	8.94	19.34	2.63	21.56		5.58	3.29	1.21
1991	4.04	7.51	1.029	16.03		6.19	3.45	0.55
1992	5.55	10.94	2.09	18.35		3.79	2.18	0.81
1993	3.72	5.99	1.12	9.109		18.80	1.57	0.21
1994	6.85	11.86	2.69	22.35			3.33	0.71
1995	5.44	7.82	1.32	11.76			1.79	0.55
1996	5.20		1.95	18.58			2.84	0.36
1997	8.74		2.53	11.130			2.75	0.25
1998	5.62		1.82	13.45			2.61	0.69
1999	4.16		4.34	38.53			2.018	0.15
2000	7.97		3.56	33.51			1.65	
2001	6.08		14.30	17.02			2.49	
2002	9.91		3.14	34.17			2.31	
2003	5.67		1.69	23.80			2.14	
2004	7.31		4.21	46.12			1.86	
2005	8.77		7.86	37.16			1.96	
2006	6.48		4.72	54.37			2.08	
2007	9.18		3.77	21.05			2.34	
2008	7.07		3.37	29.89			1.81	
2009	7.22			52.67			0.75	

Year	Ainamotua	1GD04	Ainopsiwa	MASAITA	Mbogo	1GD07	1GC06	Tugenon
2010				32.85			3.28	
2011							2.22	
2012							3.41	
2013							2.7	

Appendix 11A: Rainfall growth curves

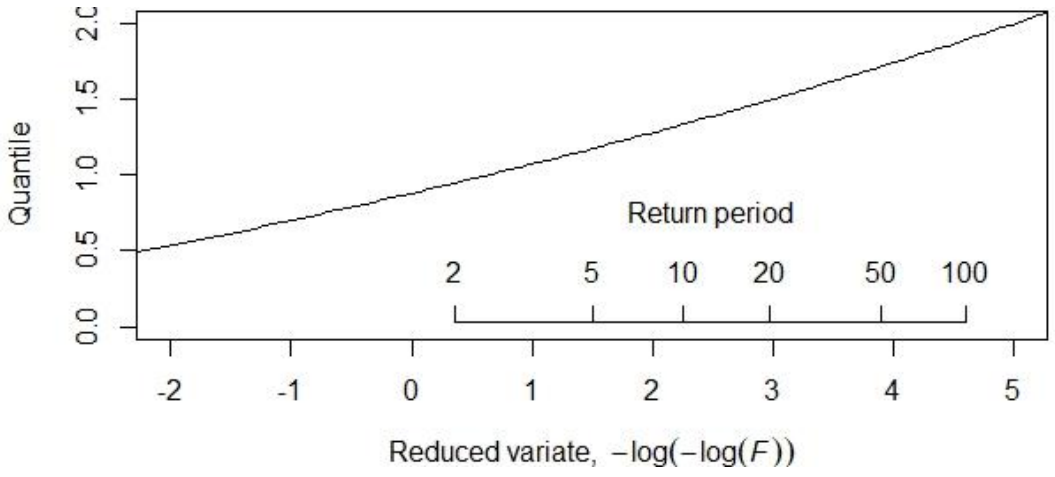

(i): Rainfall growth curve for cluster I

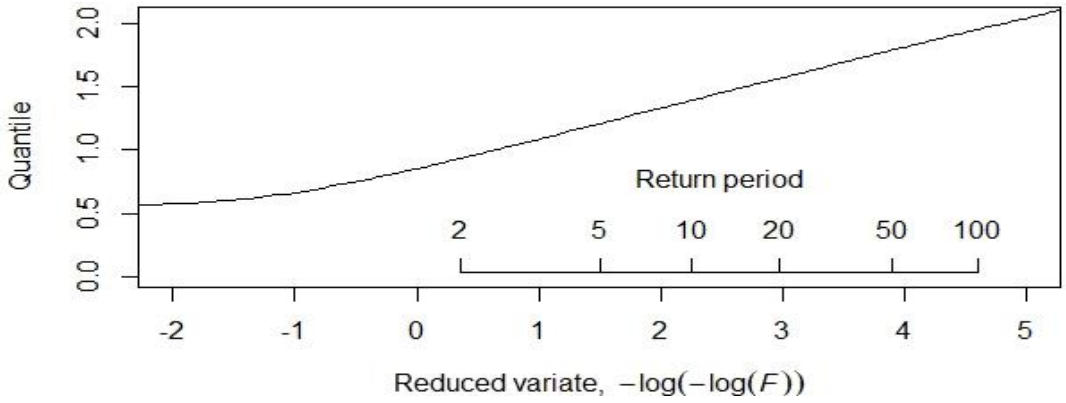

(ii): Rainfall growth curve for cluster II

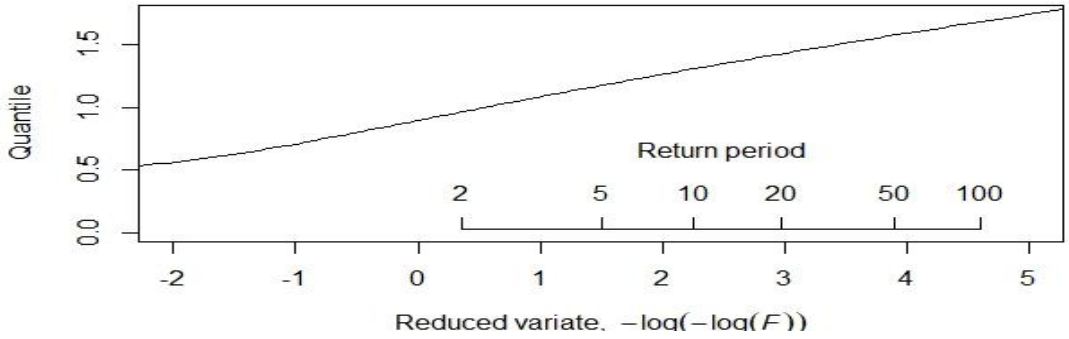

(iii): Rainfall growth curve for cluster III

Appendix 11B: Streamflow growth curves

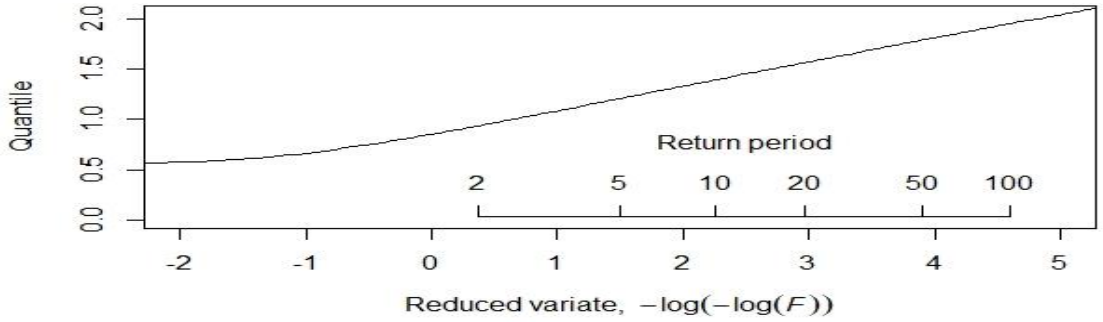

(i) Streamflow growth curve for cluster I

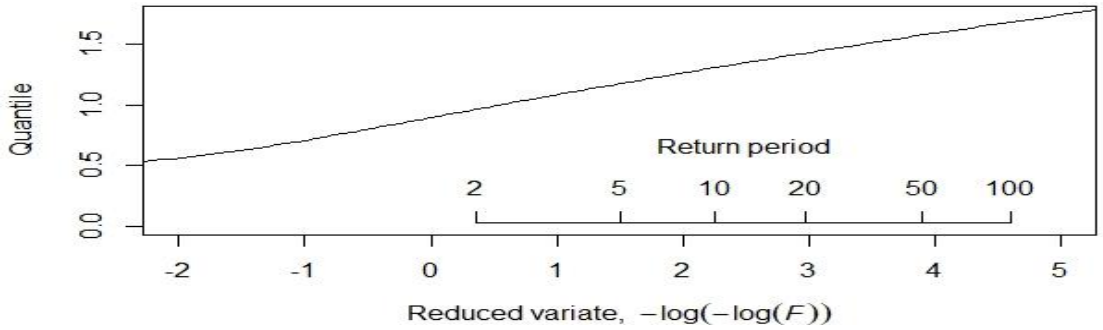

(ii) Streamflow growth curve for cluster II

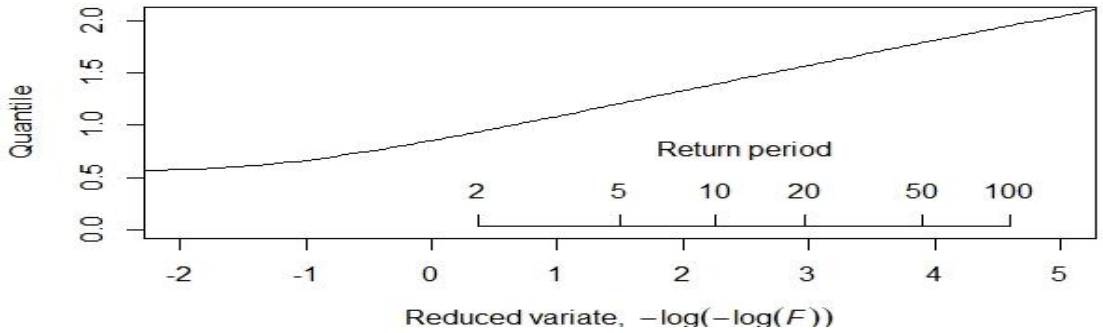

(iii) Streamflow growth curve for cluster III

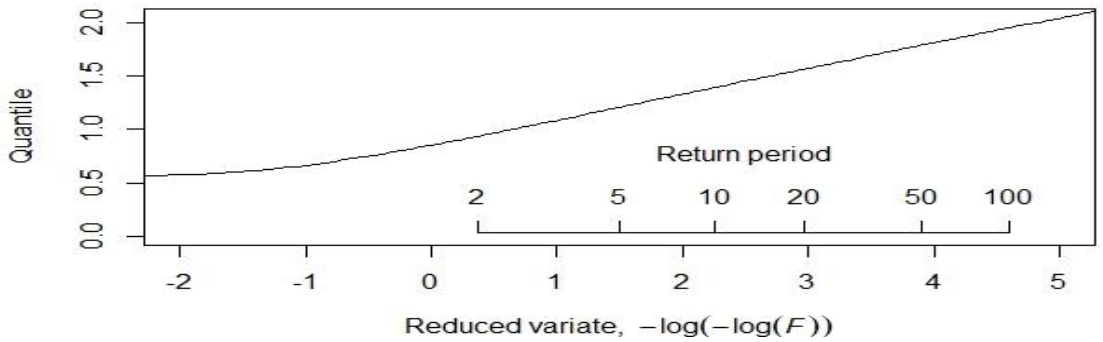

(iii) Streamflow growth curve for cluster IV

Appendix 12: Plagiarism checker certificate

SR030

EDU 999 THESIS WRITING COURSE

PLAGIARISM AWARENESS CERTIFICATE

This certificate is awarded to

JOHN ODONGO SARANGA

TEC/PGCS/08/11

In recognition for passing the University's plagiarism

Awareness test with a similarity index of 07% and

Striving to maintain academic integrity

Awarded by:

Prof. John Changách, CERM-ESA Project Leader Date: 20th/12/2021